Generation of Metal Nanoparticles in the Presence of Oligoproline Derivatives

Inauguraldissertation

zur

Erlangung der Würde eines Doktors der Philosophie

vorgelegt der

Philosophisch-Naturwissenschaftlichen Fakultät

der Universität Basel

von

Pia Feinäugle

aus Pfullendorf (Deutschland)

Freiburg, 2014

Namensnennung-Keine kommerzielle Nutzung-Keine Bearbeitung 3.0 Schweiz
(CC BY-NC-ND 3.0 CH)

Sie dürfen: **Teilen** — den Inhalt kopieren, verbreiten und zugänglich machen

Unter den folgenden Bedingungen:

Namensnennung — Sie müssen den Namen des Autors/Rechteinhabers in der von ihm festgelegten Weise nennen.

Keine kommerzielle Nutzung — Sie dürfen diesen Inhalt nicht für kommerzielle Zwecke nutzen.

Keine Bearbeitung erlaubt — Sie dürfen diesen Inhalt nicht bearbeiten, abwandeln oder in anderer Weise verändern.

Wobei gilt:

- **Verzichtserklärung —** Jede der vorgenannten Bedingungen kann **aufgehoben** werden, sofern Sie die ausdrückliche Einwilligung des Rechteinhabers dazu erhalten.
- **Public Domain (gemeinfreie oder nicht-schützbare Inhalte) —** Soweit das Werk, der Inhalt oder irgendein Teil davon zur Public Domain der jeweiligen Rechtsordnung gehört, wird dieser Status von der Lizenz in keiner Weise berührt.
- **Sonstige Rechte —** Die Lizenz hat keinerlei Einfluss auf die folgenden Rechte:
    - Die Rechte, die jedermann wegen der Schranken des Urheberrechts oder aufgrund gesetzlicher Erlaubnisse zustehen (in einigen Ländern als grundsätzliche Doktrin des **fair use** bekannt);
    - Die **Persönlichkeitsrechte** des Urhebers;
    - Rechte anderer Personen, entweder am Lizenzgegenstand selber oder bezüglich seiner Verwendung, zum Beispiel für **Werbung** oder Privatsphärenschutz.
- **Hinweis —** Bei jeder Nutzung oder Verbreitung müssen Sie anderen alle Lizenzbedingungen mitteilen, die für diesen Inhalt gelten. Am einfachsten ist es, an entsprechender Stelle einen Link auf diese Seite einzubinden.

Quelle: http://creativecommons.org/licenses/by-nc-nd/3.0/ch/ Datum: 12.11.2013

Genehmigt von der Philosophisch-Naturwissenschaftlichen Fakultät auf Antrag von:

Prof. Dr. Helma Wennemers

Prof. Dr. Marcel Mayor

Basel, den 12.11.2013

Prof. Dr. Jörg Schibler

Dekan

Abstract

The generation of metal nanoparticles has raised tremendous interest in recent years. They offer a huge variety of possible applications, due to their unique properties which strongly depend on their morphology. The controlled formation of nanoparticles of desired, monodisperse sizes and shapes still remains a challenge.

Herein we present the design and investigation of novel peptidic additives in the formation of different metal nanoparticles. Oligoprolines in different lengths were functionalized with guanidine, imidazole, primary amine, carboxylic acid, indole and pyrrolidinyl groups on the backbone. All of the peptides adopt the well-defined polyproline type II (PPII) helix which was not disturbed by the functionalization on the backbone. The formation reaction was carried out with and without an external reducing agent.

The additives were first investigated in the formation reaction of silver nanoparticles (AgNPs). The peptides bearing guanidine and imidazole groups were able to stabilize monodisperse and spherical nanoparticles using an external reducing agent in different sizes. Applying the additives without external reducing agents led in the case of guanidine- and indole-functionalized peptides also to the formation of monodisperse and spherical AgNPs.
In the presence of amine-functionalized peptides using ascorbic acid as external reducing agents non-spherical shapes were obtained and with pyrrolidinyl-functionalized peptides rods formed, next to spherical nanoparticles.
It was found that not only the functional group that was attached, but also the defined secondary structure was necessary for the peptides to act as additive in the formation reaction to stabilize nanoparticles in defined sizes and shapes.

In the formation of gold nanoparticles (AuNPs), guanidine- and imidazole-functionalized peptides were able to act as additives resulting in monodisperse nanoparticles when an external reducing agent was used. In contrast to the investigations for the formation of AgNPs also with amine-functionalized peptides monodisperse AuNPs were obtained. Without external reducing agent only polydisperse AuNPs were formed.

In the attempt to test the variability of the designed additives, first tests, evaluating the imidazole-functionalized peptides in the formation of platinum nanoparticles (PtNPs) was carried out. This resulted as well in monodisperse nanoparticles.

Furthermore a novel additive was designed inspired by a tripeptide, indentified in studies earlier carried out in our group. Using this peptide bearing two different functional groups it was possible to use it as additive in the formation of AgNPs using weak and strong reducing agents as well as visible light.

These results demonstrate the potential of these peptidic additives in the formation of metal nanoparticles in defined sizes and shapes.

The following dissertation was carried out under the supervision of Prof. Dr. Helma Wennemers at the University of Basel from March 2009 until November 2011 and at ETH Zurich from December 2011 until December 2013.

Parts of this work were published:

Feinäugle, P., Wennemers, H., Generation of silver nanoparticles in the presence of the oligoproline derivatives, *Proceedings of the 32nd European Peptide Symposium*, **2012**, 224

Parts of this work were presented in Posters at the following conferences:

Swiss Nano Convention, **2013**, Basel, Switzerland

Fall meeting of the Swiss Chemical Society, **2012**, ETH Zurich, Switzerland

32. European Peptide Symposium, **2012**, Athen, Greece

Fall meeting of the Swiss Chemical Society, **2011**, University of Lausanne, Switzerland

31. Regio Symposium, **2011**, Centre de Sornetan, Switzerland

10th International Conference of Material Chemistry, **2011**, Manchester, UK

Acknowledgment

First of all I would like to thank my supervisor Prof. Dr. Helma Wennemers for giving me the opportunity to work on this great topic in her group. I also would like to thank for her advice as well as the freedom and trust that she put in me. I am additionally thankful for the opportunity and financial support which she provided, that enabled me to attend national and international conferences.
I am grateful to Prof. Dr. Marcel Mayor for accepting the co-reference of this thesis.

I want to thank all the past and present members from the Wennemers group who helped and supported me and made it a great time. Especially I would like to thank the people from room 101, respectively H312 for their support and friendship. Special thanks I would like to express to my friends Dr. Yukihiro Arakawa, Dr. Jian Gao, Dr. Rolf Kramer, Alexander Käslin, Valentina Volic, Gabriel Schäfer, Claudio Grünenfelder, Dr. Gururaj Joshi and Ludmila Ziegler. And of course Annette Bahlinger, who especially in the last month helped and motivated me.

In addition, I am very thankful to Dr. Rolf Kramer and Dr. Bartosz Lewandowski for their help in proof-reading my thesis.

I am very thankful to the ability to use the TEM facilities at the ZMB at the University of Basel, the EMEZ at the ETHZ and the ZMB at the University of Zürich. Especially I would like to thank Vesna Olivieri and Ursula Sauder (ZMB, University of Basel), Peter Tittmann (EMEZ, ETHZ) and Gery Barmettler (ZMB, University of Zürich).

My special thanks go to my friend Natalie Rykena who is my cheerleader since school time. I cannot imagine my life without her constant support and love.
Big thanks go also to Christiane Klotz who was and is my companion, supporter and friend.
Furthermore I want to thank Dr. Mathias Hill for everything that he did and is and who is always there for me.

Und nicht zuletzt danke ich meiner Familie für die konstante Unterstützung in den Jahren meines Studium und der Doktorarbeit.

Table of Content

1. Introduction

1.1. Noble Metal Nanoparticles

1.1.1. History

The first documented usage of nanoparticles comes from the 4th century and the fabrication of the Lycurgus Cup. This cup possesses dichroic glass with gold and silver nanoparticles embedded into it. They make the glass look opaque green from the outside, but when the cup is held with its interior facing the light source, it appears translucent red (Figure 1).[1]

Figure 1: Lycurgus Cup (Rome) from the 4th century AD; **a)** light shining from the outside results in a green coloration; **b)** light shining from the inside results in a red coloration.

From the 9th to the 17th century nanoparticles were used by artisans to generate a metallic luster on ceramics.[2-3] This effect was due to the presence of silver, gold or copper nanoparticles in the glaze, which were introduced by a special technique. The pottery was heated up to 600°C which allowed the nanoparticles to form from the metal salts and to migrate into the glaze were they were stabilized and can be seen until today, if the ceramics survived the centuries.[2, 4-5] Starting from the 6th to the 15th century gold and silver nanoparticles were also employed to stain glass windows in European cathedrals.[6] From the 13th to the 16th century, carbon nanotubes found their application in the manufacturing of Damascus sabre blades which are famous for their particular strength and resilience.[7-8]

The first contribution to the laboratory-based research on this topic was made by Michael Faraday.[9] In his paper from 1857 he described the synthesis of gold nanoparticles and their interaction with light. However a more significant progress and development of this research area required for

particular, advanced analytical techniques to be developed first. Transmission electron microscopy (TEM) and scanning electron microscopy (SEM) made it possible to gain deeper understanding of this growing field.

A significant milestone was the famous speech delivered by Richard Feynman in 1959 where he declared: “there is plenty of room at the bottom”.[10] This speech was often recognized as the birth point of nanotechnology, as it provided the scientific community with visionary ideas of what could be achieved and which challenges need to be tackled in the future.

1.1.2. Properties

IUPAC defines nanoparticles as particles of any shape with a size between 1 and 100 nm.[11] However tubes and fibers with only two dimensions in this size range are also referred as nanoparticles.[11]

When considering nanoparticles, the relatively high percentage of atoms present on the surface becomes relevant as it results in a large surface to volume ratio. Therefore nanoparticles possess distinctively different properties compared to those of bulk materials. They also strongly depend on the size and shape of the particles.[12] The ability to influence the properties of such nanostructures by controlling their geometry made this field very attractive and was one of the main reasons why the number of research projects focused around this topic was dramatically increased within the last decades. Especially gold and silver nanoparticles have attracted much attention due to their possible applications in electronics,[13] catalysis,[14-15] imaging[16-18] and medicine.[19-21]

All metal nanoparticles display surface plasmon resonance (SPR).[12, 22] The surface plasmon resonance originates from the interaction of light with the nanoparticles which are smaller in diameter than the wavelength of the radiation. At a certain wavelength the photons resonate with the free electrons on the metal particle surface which causes them to oscillate locally around the particle. This phenomenon is defined as the localized surface plasmon resonance (LSPR, Figure 2).[23]

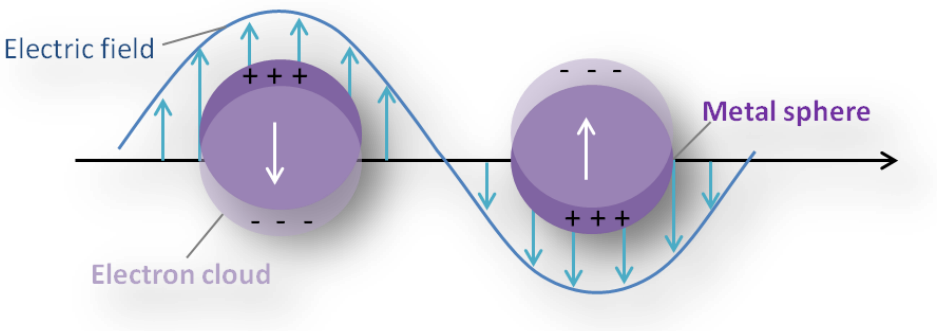

Figure 2: Schematic diagram of a localized surface plasmon resonance (LSPR).

The resonance conditions are depending on the dielectric constant of the metal and the surrounding material as well as the size and shape of the nanoparticles.[18]

The SPR of nanoparticles can be observed in UV-Vis spectroscopy and for copper, silver and gold nanoparticles it appears in the visible region of the spectrum (Figure 3). These nanoparticles are therefore colored which qualifies them for application in imaging.

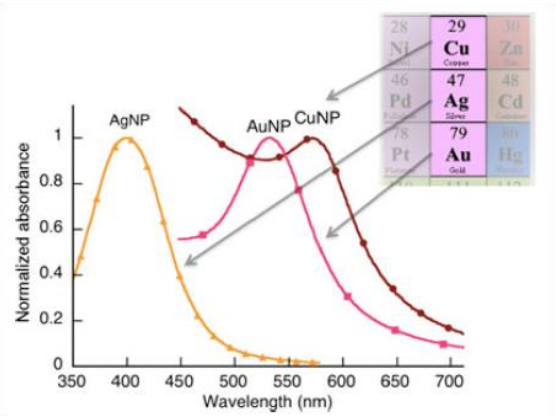

Figure 3: Representative visible absorption spectra of spherical copper, silver and gold nanoparticles in solutions.[24]

1.2. Silver Nanoparticles (AgNPs)

AgNPs are among the most researched noble metal nanoparticles. As already mentioned above, they offer many possibilities for applications in imaging, catalysis, as antimicrobial agents and in electronics. Some examples are highlighted in the following chapter 1.2.1. In the course of the research carried out in the field, many different ways of generating AgNPs were found. Different approaches are presented in chapter 1.2.2.

1.2.1. Applications of AgNPs

1.2.1.1. AgNPs Used in Imaging

Immobilization of biomolecules on nanoparticle surface was shown to be an efficient new approach towards biosensors, taking advantage of different properties like localized surface plasmon resonance (LSPR), surface enhanced Raman spectroscopy (SERS) and surface enhanced fluorescence (SEF) for sensitive detection.[25] The group of Van Duyne developed an optical biosensor using triangular AgNPs.[26] The system was tested for the binding of the antigen ADDL, a putative Alzheimer's disease pathogen and anti-ADDL antibodies. Anti-ADDL antibodies were covalently bound to the nanoparticle surface *via* a sulfur bond and the antigen ADDL was incubated using different concentrations. The next step was incubation with a fixed concentration of free anti-ADDL antibody that was binding to the previously attached antigen ADDL (Figure 4). This was monitored using transmission UV-Vis spectroscopy, where a shift in the absorbance was observed upon binding. The assay format provided quantitative binding information about the antigen and the second antibody detection. This allowed to obtain the concentration, the binding constants and investigate the aggregation mechanisms under physiologically relevant concentrations, offering a new perspective for the understanding and potential diagnosis of Alzheimer's disease.[26]

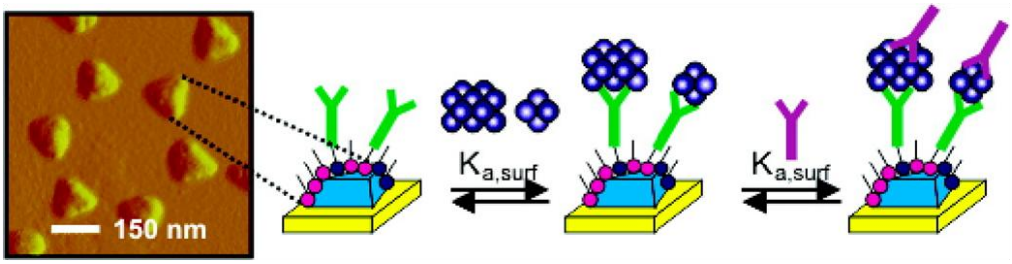

Figure 4: Experimental setup for the LSPR biosensor for the ADDL detection and surface chemistry.[26]

The group of Wang used AgNPs for sensing in an enzymatic assay.[27] The enzymatic activity of calf intestine alkaline phosphatase (CIAP), dephosphorylating adenosine triphosphate (ATP) and of protein kinase A (PKA), phosphorylating a peptide, was investigated. In the conditions applied ATP prevented AgNPs from aggregating. However it was also consumed in both studied reactions. Therefore as soon as the reaction took place, the AgNPs started to aggregate, which resulted in an absorbance shift and with this, a visible change in color (Figure 5). Using this method, not only the activity of enzymes but also of added inhibitors could be determined. On top of that detection of the activity in complex biological fluids was achieved.[27]

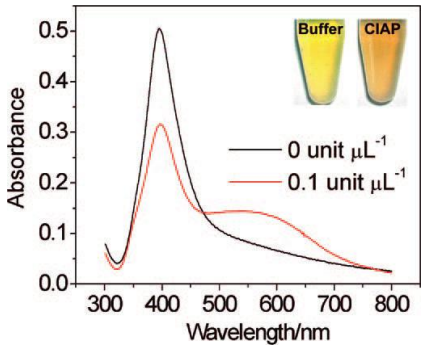

Figure 5: UV-Vis spectra of AgNPs used in the study of Wang *et al.*[27] in presence of 0.5 mM ATP without (black line) and with (red line) 0.1 unit/ µL CIAP.

1.2.1.2. AgNPs Used for Catalysis

Application of nanoparticles in catalysis is a rapidly growing field of research.[28] AgNPs are employed in many different reactions like C-C bond formation,[29-30] reduction of nitroarenes [31-32] and Diels-Alder cycloadditions.[14, 33]

An example of catalysis with AgNPs is the work of Chattopadhyay *et al*.[30] They used chitosan-supported AgNPs for the oxidative coupling of phenols. The reaction took place in the presence of iodine as an oxidant. The iodine was incorporated into the phenol, followed by an oxidative C-C coupling to obtain a biphenyl (Figure 6). When unsubstituted phenol was used as a substrate, the yield of 75% was achieved (Figure 6a). The reaction was highly regioselective as, with α-naphtol only the 2,2' coupled product and with *β*-naphtol the 3,3' coupled one were obtained (Figure 6b,c). The outcome observed for *β*-naphtol was different than the typical selectivity described in literature for homogeneous catalysts.[34-36] Furthermore low catalyst loading and mild reaction conditions could be applied. Preliminary mechanistic investigations suggested that this is a radical process taking place after chemisorption of the reactants on the AgNP surface.[30]

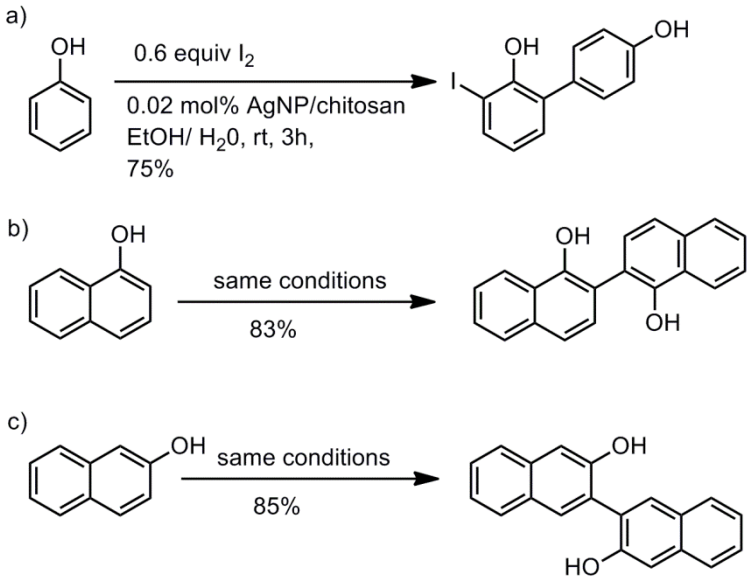

Figure 6: AgNP catalyzed oxidative coupling of phenolic compounds; **a)** phenol, **b)** *α*-naphtol, **c)** *β*-naphtol.[30]

1.2.1.3. AgNPs Used as Antimicrobial Agents

Silver in its different forms has been used as a disinfectant for thousands of years.[5, 37-38] The first documented report came from Herodotus, an ancient Greek historian who lived in the fifth century BC. He described that water was stored in silver containers to keep it fresh for years.[37] Hippocrates, the father of modern medicine, described the use of silver powders in wound healing.[37] Silver was extensively used in medicine, until the first half of the 20th century. Electric colloids were the main tool in antimicrobial therapy until the development of antibiotics in 1942.[37] After this, the use of silver and silver salts for such purposes decreased, but it still found its application in different medical fields, especially in burn treatment.[39-40]

Nowadays, as there are more and more multidrug-resistant bacteria strains developing, there is a high demand for new antibiotics.[41] Therefore silver becomes attractive again, as a possible drug candidate.

AgNPs were also investigated for this purpose,[38, 42-44] as by using them, some drawbacks arising during therapy with silver ions, like deactivation upon reaction with biomaterial can be overcome. They are also more reactive due to the large surface to volume ratio compared to bulk silver.[42]

A representative example of AgNPs application as antibacterial agent is the work of Sharma *et al.*[45] They synthesized nanoparticles of different sizes (25-50 nm) and tested their behavior against a broad spectrum of gram-negative and gram-positive bacteria, including some multi-drug resistant

strains. They have demonstrated that the AgNPs had an antibacterial effect towards all tested bacterial strains, including the multi-drug resistant strain, even at very low nanoparticle concentrations (≤ 2 µg/ mL AgNPs). Furthermore they found that the smallest nanoparticles, with a diameter of 25 nm, displayed the highest activity.[45]

The mechanisms of how AgNPs act against the bacteria are not fully understood, but several possible pathways are currently being discussed (Figure 7).[46]

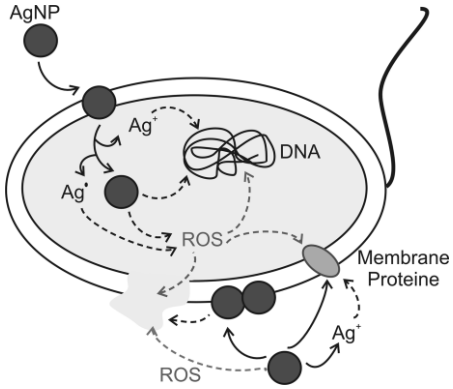

Figure 7: Possible pathways of interaction between AgNPs and bacteria cells: interaction with the cell wall, with the DNA, with membrane proteins and formation of reactive oxygen species (ROS).[46]

It is assumed that the nanoparticles attach to the cell membrane, disturbing its permeability and respiration functions.[47-48] They also penetrate into the cell.[49] The AgNPs interact with sulfur-containing proteins as well as with phosphorus-containing molecules, like the DNA. Additional possible reaction pathways are the release of Ag^+ ions leading to their interaction with proteins and DNA[44] and the silver induced formation of reactive oxygen species (ROS) that can damage the cell.[46]

1.2.1.4. AgNPs Used in Electronics

Due to their high electric and thermal conductivity, AgNPs find application in various electronic devices.[13, 50-51] They are utilized, for example in the printing of electronic circuits,[50, 52] as well as for construction of organic field-effect transistors (OFETs).[51]

In the ink-jet printing methodology, an AgNP suspension is printed on a substrate. The nanoparticles show a dramatically lowered melting point compared to the melting point of the bulk material, due to the increase of surface energy.[53-54] The printed nanoparticle suspension can be used as microjunctions after sintering at low temperatures.[55]

Lewis *et al.* have demonstrated the patterning of silver microelectrodes by omnidirectional printing of AgNPs on different substrates.[50] Using this technique they formed microelectrodes which are resistant against bending and stretching of the substrate and therefore suitable for fragile, three

dimensional devices, as well as for spanning interconnects for example for solar cell and light emitting diode arrays.[50]

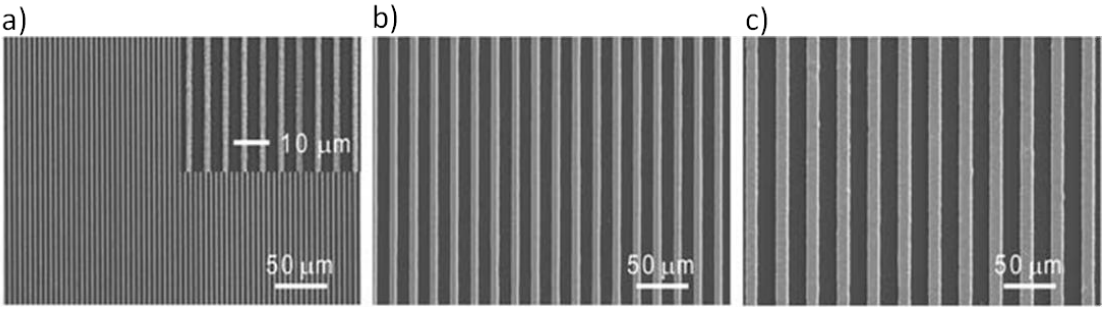

Figure 8: SEM image of planar arrays of silver microelectrodes patterned with: **a)** 1 µm nozzle, **b)** 5 µm nozzle, **c)** 10 µm nozzle.[50]

Uniform and high aspect ratio motifs were achieved and their width and height are defined only by the diameter of the nozzle and the number of the printed layers (Figure 8). After a very short sintering time of less than 30 min the microelectrodes had an electrical resistance of $5.2 * 10^{-5}$ ohm * cm, which is almost the value of 10^{-6} ohm * cm that can be reached with bulk silver.[50]

1.2.2. AgNP Generation

As the properties of nanoparticles depend strongly on the preparation method, it is important to find appropriate synthetic conditions to control their morphology and through it also their properties.[12, 56-58] Even though many different approaches have already been developed, controlled synthesis allowing to obtain nanoparticles of defined sizes and shapes still remains a challenge.

There are two main approaches towards the generation of AgNPs, the top-down and the bottom-up approach.

1.2.2.1. AgNP Generation Using the Top-Down Strategy

In the top-down approach the nanostructure is obtained by miniaturization of the bulk silver using different techniques. Typically this is done by mechanical grinding, lithography, chemical vapour deposition or laser ablation and subsequent stabilization of the resulting nano-sized metal particles by additives.[59-60] Nanoparticles with diameters from 10 nm to 100 nm can be obtained in this way.

One of the main drawbacks of the top-down approach, are the defects of the nanoparticle surface that arise during the synthesis[60] and influence the properties. For example in nanowires used in electronics, such imperfections would lead to a reduced conductivity and due to inelastic surface

scattering to the generation of excessive heat which would complicate the potential applicability of these nanodevices.[60] A selection of techniques mentioned above will be described in the following paragraphs.

1.2.2.1.1. AgNP Generation Using Laser Ablation

In 1993, laser ablation was introduced as a new methodology for nanoparticle generation by Henglein *et al.* without any stabilizer as additive.[61]

The generation of AgNPs using this technique, followed a four step procedure.[62] First the ablation step was applied. A laser pulse (1064 nm, 310 mJ per pulse) was used to irradiate a silver foil in an aqueous solution to produce an Ag hydrosol. The next three steps involved irradiation of the hydrosol to reduce its mean size, first with laser pulses of the same wavelength, then with a wavelength of 532 nm (170 mJ per pulse) and again with the original wavelength.[62] The experimental setup is depicted in Figure 9.

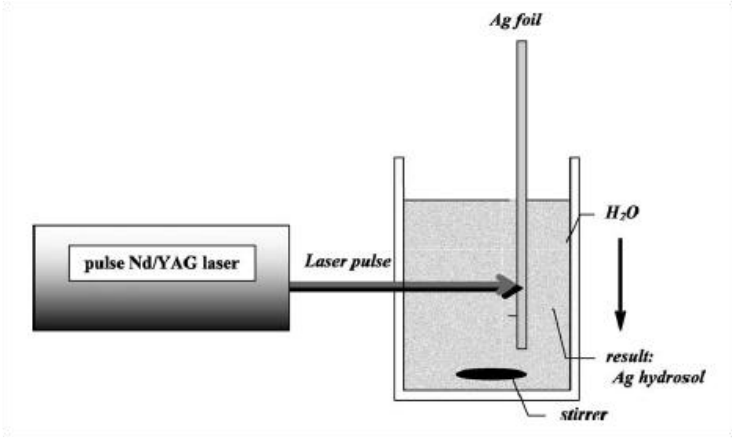

Figure 9: Schematic setup for laser ablation to generate AgNPs.[62]

After the ablation step, the resulting particles were polydisperse with diameters around 100 m. After fragmentation the polydispersity of nanoparticles had decreased and diameters of about 30 nm were reached.[62]

Other groups tried to improve this approach by using stabilizing additives like polyvinyl pyrrolidone (PVP)[63] and sodium dodecylsulfate (SDS).[64] The usage of stabilizing additives increased the efficiency of the laser ablation as well as stabilized the resulting nanoparticles.

1.2.2.1.2. AgNP Generation Using Chemical Vapour Deposition

Chemical vapour deposition (CVD) is a technique used for the application of a substrate onto a matrix.

Pal *et al.* described deposition of AgNPs in a diamond-like carbon (DLC) film using capacitively coupled plasma (CCP) CVD technique.[65] They used different methane and argon gas mixtures to test their influence on the deposition process on a glass substrate. The silver concentration was controlled by the argon concentration in the starting mixture. The size of the resulting AgNPs increased with increased silver concentration in the vapor from 11 nm to 36 nm.

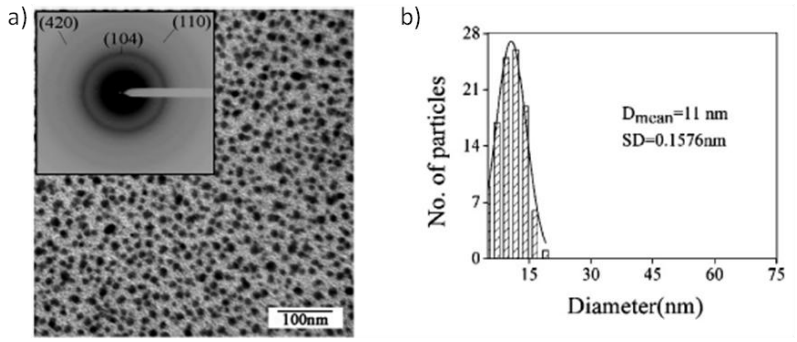

Figure 10: a) TEM image of nAg-DLC film deposited with a methane to argon mixture of 1:1, b) histogram.[65]

1.2.2.2. AgNP Generation Using the Bottom-Up Strategy

In the bottom-up approach the nanoparticles are obtained by assembling basic building blocks (atoms) one by one to end up with a nano-sized structure. In synthetic chemistry a similar approach is also used to generate more complex molecules. This is the method of choice when the size of the desired structure lies in the lower nanometer range (1-10 nm), which is not possible to obtain by the top-down strategy.[60] Also bigger particles of up to 100 nm are often generated using this strategy. The advantages of the bottom-up approach are the possibility to generate nanostructures with less defects and their more homogeneous chemical composition. This is due to the fact that through the assembly of the building blocks, a decrease of the Gibbs free energy is achieved, thus a state closer to a thermodynamic equilibrium is reached.[60] Another advantage of the method is the tunability of the building blocks used for the generation of nanoparticles allowing to obtain ones possessing the desired properties.[60]

Typically the generation is performed by reduction of a silver salt in the presence of an additive to guide the nucleation and stabilize the resulting nanoparticles. The reduction is either done by irradiation of silver ions with visible light or by using a chemical reducing agent. There are many parameters which can be varied in the process to improve its outcome, like the silver salt, the reducing agent or the additives. The most common additives are polymers, like polyvinyl pyrrolidone (PVP)[66-69] or polyvinyl alcohol (PVA)[70], surfactants, like sodium dodecylsulfate (SDS)[71-72] or

cetyltrimethylammonium bromide (CTAB),[73] dendrimers,[74] and biomolecules like, DNA,[75] sugars,[43] proteins,[76] peptides[46, 77-78] and amino acids.[79]

1.2.2.2.1. AgNP Generation Using the Photochemical Method

Using the photochemical method for the generation of AgNPs offers some advantages like good spatial and temporal control, avoiding additional reducing agents.[80] The position of the light irradiation, as well as the irradiation time can be controlled. The nanoparticles are formed either by direct photoreduction of a metal source or by reduction *via* photochemically generated intermediates, like excited molecules and radicals.[81] It is very important to stabilize the nanoparticles obtained using this method to prevent their aggregation.

In a study of Pal *et al*., ascorbic acid was used as a photoactive molecule in the generation of AgNPs.[82] The formation of nanoparticles, using $AgNO_3$ with surfactant Triton X-100 as stabilizing additive, in the presence of ascorbic acid, was complete after 4 min of irradiation with a 15 W UV-lamp. TEM studies revealed that the resulting AgNPs were polydisperse with diameters of 15 – 60 nm and some larger aggregates also present. In later studies, the same authors managed to demonstrate SERS activity of the nanoparticles.[82]

The variability of the photochemical approach towards nanoparticle generation was shown by Scaiano *et al.*.[80] They first generated small AgNP seeds by irradiation of an aqueous solution of the photoinitiator I-2959, $AgNO_3$ and citrate with UV light (Figure 11). The growth of the particles stopped at a diameter of about 3 nm and a spherical shape due to the citrate binding to the nanoparticle surface.

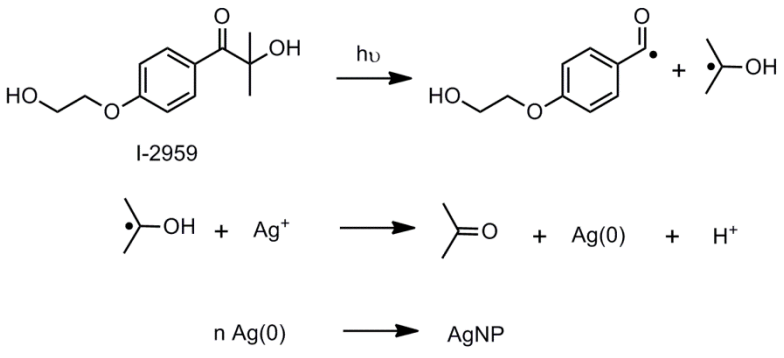

Figure 11: AgNP seed formation after irradiation of the reaction mixture with UV light.[80]

The formed seeds were then irradiated with different wavelengths using narrow band LEDs. Depending on the wavelength, the spherical particles changed their morphology to various forms (Figure 12). For example at the wavelength of 405 nm, spherical AgNPs with an average diameter of

25 nm were obtained, whereas irradiation with 455 nm LED led to transformation into dodecahedral AgNPs.

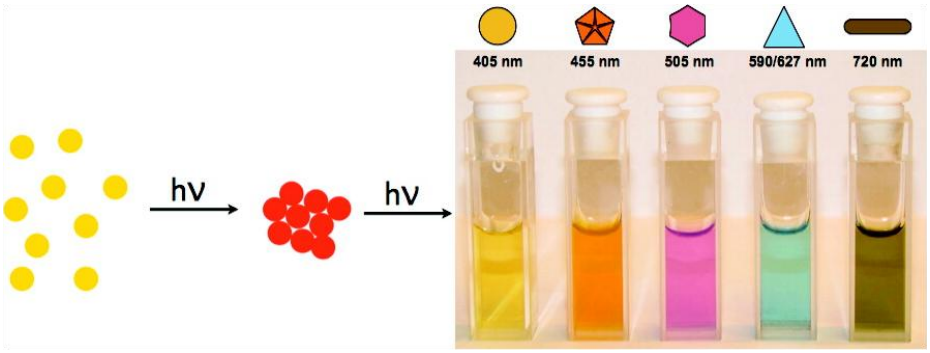

Figure 12: Schematic representation of the formation of AgNPs, the different solutions generated under LED irradiation at the indicated wavelength (in nm) and the corresponding shape that was found in TEM studies. Yellow spheres representing Ag (0) seeds, red spheres representing intermediate aggregates of Ag (0) that form during irradiation.[80]

The reason for such outcome of the described process was the aggregation of the AgNP seeds in an intermediate step before they were influenced by the varied excitation wavelength and the induced electromagnetic field to grow into the respective morphologies (Figure 12).[80]

Another example of the photochemical based generation of AgNPs is the work of Mirkin *et al.*.[83-84] In their approach they also first synthesized small, spherical AgNPs with diameter below 10 nm, which were converted by irradiation with visible light to larger prism structures.[84] The spheres were synthesized using sodium borohydride as an external reducing agent, in the presence of sodium citrate and bis(*p*-sulphonatophenyl) phenylphosphine dehydrate dipotassium (BSSP) as stabilizing additives. Under irradiation with a narrowband light source (150 W xenon lamp with an optical bandpass filter (centre wavelength = 550 nm, width = 40 nm) for 50 h two types of particles were formed, nanoprisms with an average edge length of 70 nm ± 12 and bigger ones with an average edge length of 150 nm ± 16 (Figure 13). However the thickness of both types of species was almost the same (9.8 nm ± 1.0).

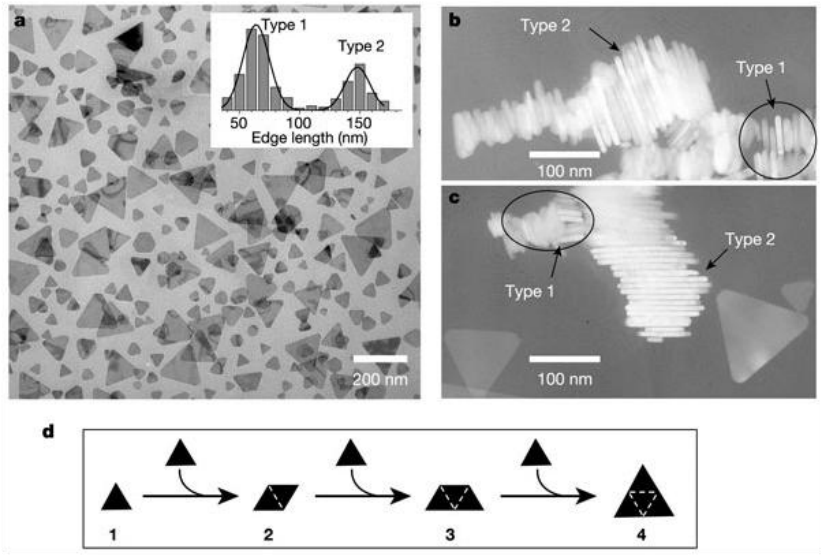

Figure 13: a) TEM image of Ag nanoprisms with two different sizes, b) - c) TEM images of stacks of nanoprisms, d) schematic representation of the proposed light-induced fusion growth. [84]

The authors proposed a light-induced edge-selective particle fusion mechanism where four of the smaller prisms fuse into a bigger prism, as shown in Figure 13d. When an additional light beam of an appropriate wavelength, exciting the quadrupole plasmon of the smaller nanoprism (340 nm) was used, the formation of the bigger prisms was suppressed. Such photo-cooperativity provides a way of controlling the prism size with light, by preventing particle fusion, and by varying the first wavelength.[84]

The photochemical method has been used quite successfully to control the size and shape, especially of anisotropic AgNPs. However the synthesis *via* such route is often time consuming and an expensive light source is required. Furthermore most of the techniques developed to date require a two step procedure. First smaller spherical nanoparticles need to be formed, which is often done by chemical reduction. It would be much more efficient if control over the morphology could already be achieved in the first step.

1.2.2.2.2. AgNP Generation by Chemical Reduction

Chemical reduction is the most frequently applied method for generation of AgNPs. Different approaches have been developed by many different groups yielding AgNPs of different sizes and shapes.[12, 56-57, 85] The synthesis of AgNPs by this approach is typically carried out using a metal precursor, a reducing agent and a stabilizing additive. The formation reaction consists of two stages which are nucleation and growth (Figure 14). The size and shape of the resulting nanoparticles depend on the relative rates of those two stages which can be controlled through careful adjustment

of the reaction parameters like concentration, pH and temperature.[5] Even though many approaches have been carried out so far it still remains a challenge to generate them in defined size and shapes.

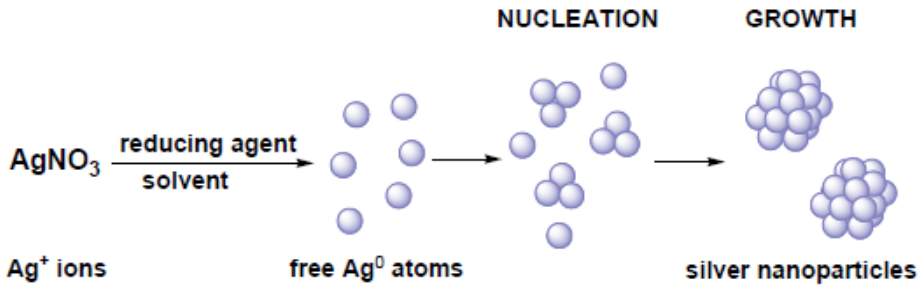

Figure 14: Mechanism of AgNP formation via chemical reduction starting from a solution of $AgNO_3$.[5]

In 1978 Creighton *et al.* described one of the first methods to generate AgNPs.[86] They were formed by reduction of $AgNO_3$ with an excess of ice-cold sodium borohydride. The resulting particles were spherical with diameters of 1 to 10 nm.[86] Then, in 1982 Lee and Meisel described a different method using sodium citrate as chemical reducing agent in a boiling aqueous solution.[87] Boiling of the solution was necessary for the reaction to proceed, because citrate is a much weaker reducing agent then sodium borohydride. The resulting nanoparticles were polydisperse, with diameters of 60 nm ± 200.[56] Citrate is not only the reducing agent, but it also stabilizes the resulting AgNPs by binding to the nanoparticle surface. However oxidation products of citrate anions can also bind to the nanoparticle surface and affect the growth in an unfavorable fashion.

These two reports mentioned above described the first two methods for the generation of AgNPs. Interestingly the two reducing agents used then are until now most frequently applied for such purpose.[85]

Third reducing agent, ascorbic acid, has also been quite commonly used in the generation reaction. It is a weaker reducing agent than sodium borohydride, but at the same time, stronger than citrate. Matijević *et al.* described a method where ascorbic acid was used as reducing agent for $AgNO_3$ resulting in nanoparticles with a mean diameter of about 26 nm.[88] They used Dadax 19, a sodium salt of a high-molecular-weight naphthalene sulfonate formaldehyde condensate, as a stabilizing additive. Ascorbic acid was also used as reducing agent in a study of van Blaaderen *et al*..[89] In this case gum arabicum was applied for the stabilization of big particles with diameter of about 100 nm.

Another popular method to obtain AgNPs is the Tollens reaction. In which, ammoniacal silver is reduced to elemental silver and an aldehyde is oxidized to a carboxylic acid. Xia *et al.* described that they were using ready-made silver-plating solution, containing ammonical silver and formaldehyde to generate AgNPs with diameters of 20 – 50 nm.[90]

Sugars, like glucose can also be used as reducing agents in the Tollens reaction. One example for such application was the study of Qiao *et al.*.[67] When PVP was used as an additive, AgNPs with a narrow size distribution were formed. The authors assumed that it was a result of the coordination of nitrogen atoms in the polymer structure to the silver and formation of a protective layer for nanoparticle growth. For bigger nanoparticles with diameters of 500 - 1000 nm, both the nitrogen and the oxygen in the polymer were expected to be coordinating to the silver.[67]

Carell *et al.* attached aldehyde moieties onto DNA bases incorporated into a DNA strain.[91] Using such platform in the Tollens reaction resulted in AgNP decorated DNA strains (Figure 15). The particles were stabilized by the carboxylic acid moieties formed by oxidation of the aldehyde residues during the reduction of the silver salt.

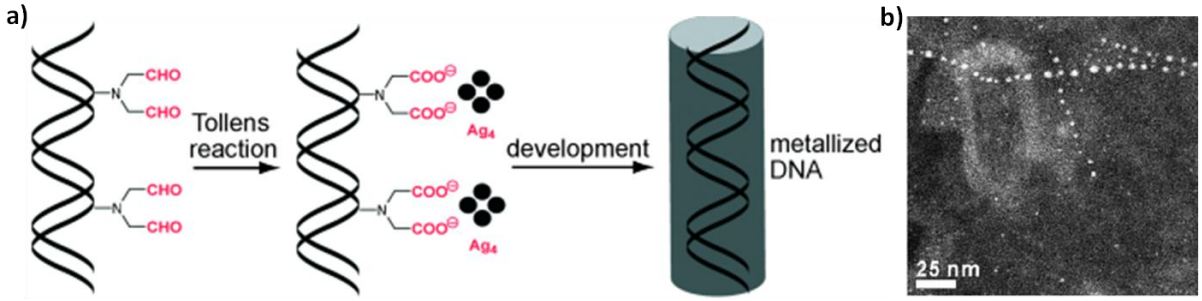

Figure 15: a) Schematic presentation of the Tollens reaction using decorated DNA strain resulting in AgNP formation, b) TEM image of AgNP decorated DNA strains.[91]

Wennemers *et al.* also used the Tollens reaction for the generation of AgNPs.[78] They attached aldehyde moieties to the backbone of oligoproline peptides, which adopt a defined secondary structure (chapter 1.4). Utilizing peptides of different lengths resulted in nanoparticles of various sizes. The size of the nanoparticles showed a linear correlation to the length of the used peptides. (Figure 16). Correlation of molecular dimension with the resulting nanoparticles morphology was observed for the first time.

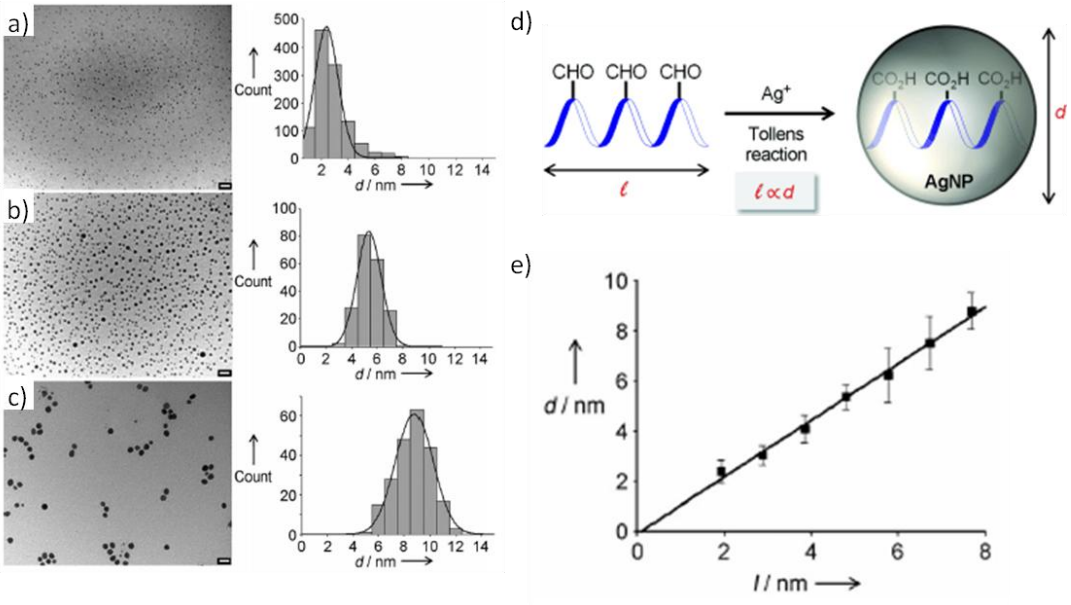

Figure 16: a) - c) TEM images of AgNPs generated with peptides of different length: a) 2 nm, b) 5 nm, c) 8 nm, d) schematic representation of the AgNP generation reaction, e) correlation of the lengths of oligoprolines with the average diameter of the corresponding AgNPs.[78]

A method often used for the generation of AgNPs is the polyol method. The Ag^+ reduction is carried out by poly-alcohols, under reflux conditions.[5] Xia *et al*. described the generation of AgNPs using ethylene glycol as reducing agent and polyvinyl pyrrolidone (PVP) as a stabilizing additive. The resulting AgNPs had a cubic shape which was assumed to be due to the selective adsorption of PVP on different crystallographic planes (Figure 17).[66]

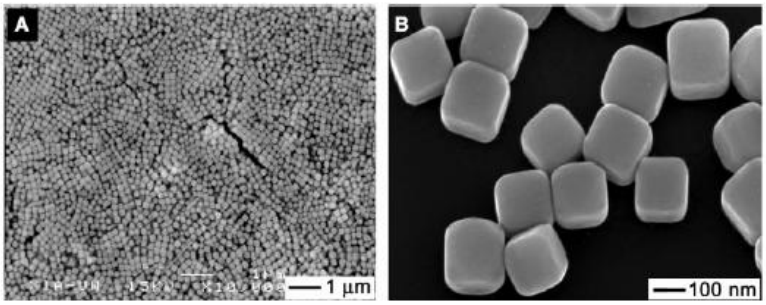

Figure 17: a)-b) SEM images of slightly truncated cubic AgNPs generated using ethylene glycol as reducing agent in presence of PVP as stabilising agent.[66]

1.2.2.2.3. Biosynthesis of AgNPs

There are many examples of biological systems capable of producing nanostructures, with high specificity and precision.[57, 92-93] Even though silver and silver nanoparticles show antimicrobial activity (1.2.1.3) it was discovered that some bacterial strains which were exposed to a high silver

concentration were still able to grow. One example is the silver resistant strain *Pseudomonas stutzeri* AG259 which was found in the soil of silver mines.[94] Granqvist *et al.* reported the accumulation of nanosized crystals of diverse size and shape in the periplasmic space of the bacteria cell (Figure 18).[95] It was reasoned that this accumulation protected the bacteria from the antibacterial effects of the silver ions.

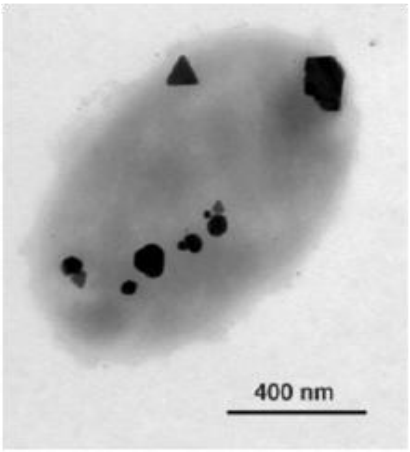

Figure 18: TEM image of *P. Stutzeri* AG259 showing AgNPs of various sizes.[95]

The resistance mechanism and how the nanoparticles are formed, is still poorly understood. It is assumed that proteins expressed from a unique plasmid (pKK1) which this bacteria strain possesses, are responsible for the resistance.[96] One of bacteria's genes, silE encodes for a 143 amino acid protein which binds to metal. It is structurally similar to a proposed copper binding protein found in a copper resistant *E.coli* strain. It lacks cysteine which is typically found in metal binding proteins.[96] Instead it has ten histidines which assumingly are binding to the metal.

Many natural proteins and peptides are capable of directing the growth of AgNPs.[57] This is why they attract more and more attention as potential additives for the generation of nanoparticles.

1.2.2.2.4. Generation of AgNPs with Peptides as Additives

Peptides are attractive candidates to be used in the generation of AgNPs which is clearly reflected in the increasing amount of publications devoted to this topic in recent years.[57-58, 77-78, 85] Peptides possess self-assembly and recognition properties which are useful for the binding and promotion of the AgNPs nucleation and growth processes. The identification of appropriate peptides for such purpose is one of the main challenges in this field.

Naik *et al.* identified peptides within a phage display library which bind to the surface of silver particles.[97] Three peptides AG3 (AYSSGAPPMPPF), AG4 (NPSSLFRYLPSD) and AG5 (SLATQPPRTPPV)

were able to reduce silver ions and direct the formation of AgNPs. An enrichment of proline and hydroxyl-containing amino acid residues was found in the hits from the library assay. Out of the found peptides, AG4 was the predominant sequence present. Using this peptide resulted in formation of AgNPs with diameters of 60 – 150 nm and hexagonal, spherical and triangular shapes (Figure 19). The authors stated that this peptide preferably binds to the Ag(111) surface which enhances the formation of polyhedral crystals with a face-centered-cubic (fcc) lattice structure.

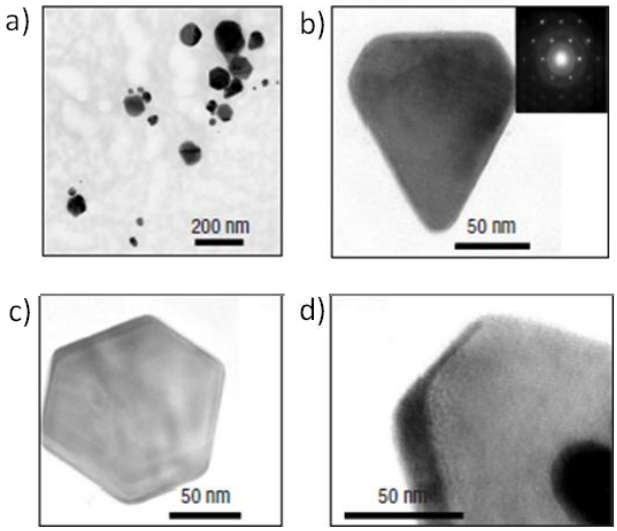

Figure 19: a)-c) TEM images of different morphologies that were obtained in the AgNP generation reaction using peptide AG4, d) TEM image of an edge of a truncated triangle, showing the plate thickness.[97]

The three-dimensional structure of the peptide was predicted to be chair-like with the help of NMR data.[98] The same method was used to assign the amino acids Leu5, Phe6 and Arg7 as the silver-interacting moieties as they showed the biggest signal shift upon addition of silver ions.[98]

Wennemers *et al.* identified different tripeptides within a split-and-mix library as additives for the generation of AgNPs.[77] The different sequences had a decisive influence on the size and shape of resulting nanoparticles. For example, AgNPs with diameter of about 50 nm were generated in presence of peptide His-Ahx-Asp bound on a Tentagel resin. Using resin-bound peptide Ser-Ahx-Tyr resulted in much smaller AgNPs of about 10 nm in diameter.[77] These studies clearly suggest that the peptide sequences, as well as the functional groups they bear, are crucial for the morphology of resulting AgNPs.

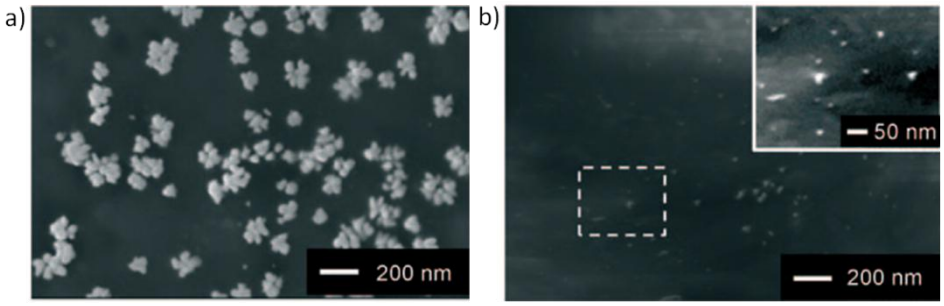

Figure 20: SEM images of AgNPs generated with peptides bound on Tentagel resin: a) peptide His-Ahx-Asp, b) peptide Ser-Ahx-Tyr.[77]

Wright *et al.* examined the influence of a histidine-rich peptide (HRE), on the stabilization of AgNPs.[99-100] This peptide with the sequence AHHAHHAAD, is an epitope of the histidine rich protein II, which was implicated in the biomineralization of heme, copper and/or zinc in different organisms. They were able to generate spherical nanoparticles with an average diameter of 11.2 nm (Figure 21). However the particles showed a rather broad size distribution

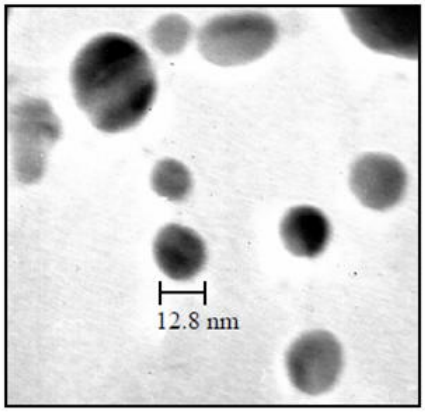

Figure 21: TEM image of AgNPs generated in the presence of the HRE peptide.[99]

In the study of Xie *et al.*, proteins from the green algae C. *Vulgaris* were used as additives for the generation of AgNPs.[101] The proteins were not only acting as stabilizing additives, but were also able to reduce the silver ions and therefore generate the AgNPs. The resulting nanoparticles had an average diameter of 44 nm and a plate-like shape (Figure 22a).

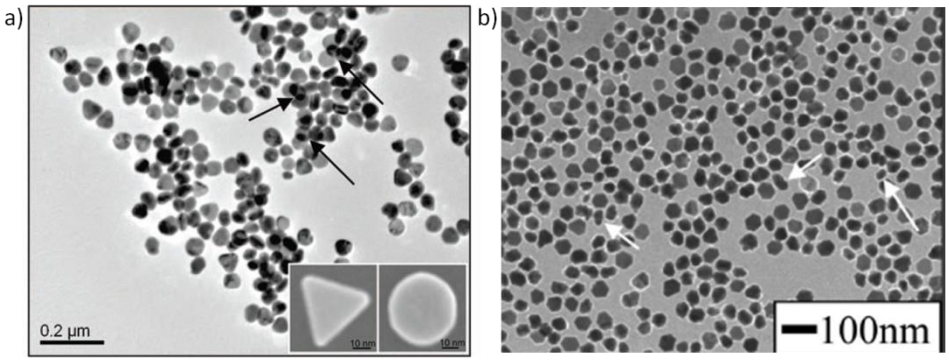

Figure 22: a) TEM image of AgNPs synthesized using the green algae C. *Vulgaris*. Arrows indicate overlapping particles, **b)** AgNPs generated using a rationally designed peptide DDY, arrows show truncated triangular silver nanoplates standing perpendicularly on the TEM grid.[101]

Through chemical modification of the protein the authors found that tyrosine residues were responsible for the reduction and the acidic functional groups for the anisotropic growth into the nanoplate-like shape.[101] Using this information they designed a simple tripeptide, bearing a DDY sequence, with which they were able to generate silver nanoplates with a narrow size distribution (Figure 22b).[101]

A study of Mandal *et al.* was also aimed at a rational design of peptides that can act as additives.[102] They synthesized the tripeptide H-Leu-Aib-Trp-OMe, containing tryptophan which was expected to act as a reducing moiety to form AgNPs. Using this peptide they were able to generate nanoparticles with an average diameter of 13.7 nm ± 2.0 (Figure 23).

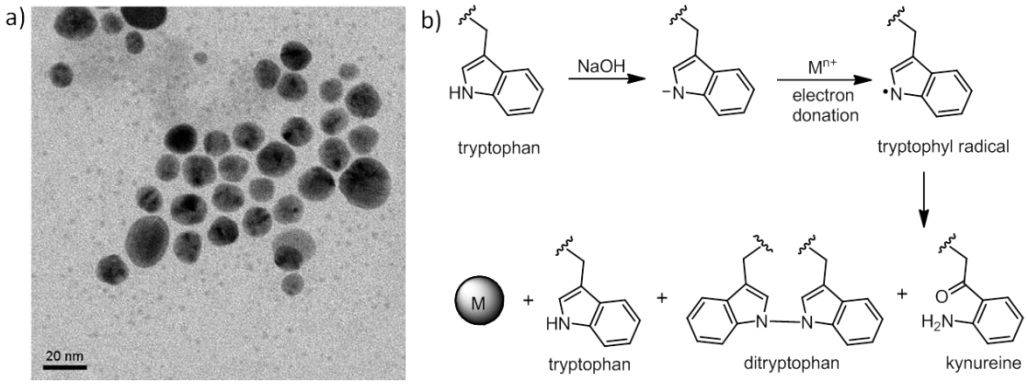

Figure 23: a) TEM image of AgNPs generated with the peptide H-Leu-Aib-Trp-OMe; b) Plausible oxidation pathway of tryptophan.[102]

An oxidation pathway for the tryptophan moiety, supported by IR measurements, was outlined as shown in Figure 23b - leading to tryptophan, ditryptophan and kynureine as reaction products.[102]

Zhang *et al.*, used a plant extract from *Capsicum annum L*. for AgNP generation.[103] They suggested that the reducing ability of the peptide contained in the extract comes from the amide groups. They

supported this hypothesis by IR and electrochemical data. They detected that after the reduction of silver ions the NH plane bending vibration signal disappeared from the IR spectrum which points to an oxidation of the amide group.[103] The amide groups of cyclic peptides curcacycline A and B were also associated with the reduction of silver ions for generation of AgNPs in the study of Misra *et al.*.[104-105]

However peptides are not only used as stabilizing and reducing agents, but sometimes also as structure determining scaffolds. For example Gazit *et al.* used the dipeptide Phe-Phe that is cable of assembling into nanotubes, as a scaffold for the generation of silver nanowires.[106] The silver ions were reduced using sodium citrate. After enzymatic degradation of the peptide, the silver nanowire was released (Figure 24).

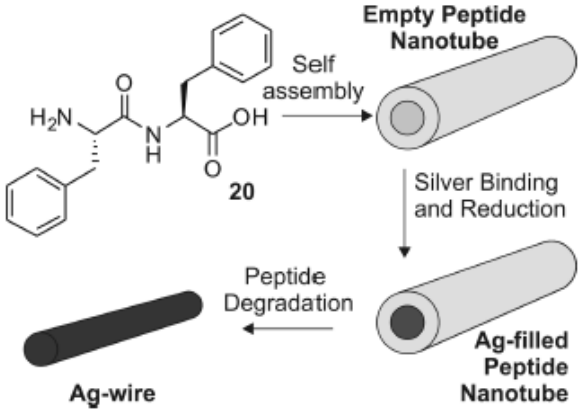

Figure 24: Schematic representation of formation of silver nanowires using self-assembled peptide nanotubes as scaffolds.[106]

Even though many studies were carried out, it is not yet fully understood how peptides act in the generation reaction. They typically possess different functional groups which influence their performance. The role of the individual functional groups is however also not clear, just as the influence of the secondary structure that the peptides provide.

1.3. Gold Nanoparticles (AuNPs)

As already mentioned in chapter 1.1., the first publication on nanoparticles, written by Michael Faraday concerned AuNPs.[9] From that moment on, the amount of research on AuNPs gradually increased with every decade. Today they are one of the most researched nanostructures. In the following chapter, some of their possible applications will be highlighted. Their most common generation pathways will then be introduced.

1.3.1. Applications of AuNPs

1.3.1.1. AuNPs used in Imaging

AuNPs show a LSPR, are easy modifiable on the surface and display a certain biocompatibility. This makes them excellent platforms for chemical and biological sensing.[107]

Mirkin *et al.* used AuNPs with a diameter of 13 nm for sensing of complementary DNA.[108-109] They attached through a thiol moiety, non-complementary DNA oligonucleotides on the AuNP surface. After addition of oligonucleotide duplexes with complementary 'sticky ends', aggregation of the AuNPs occurred. This process was shown to be thermally reversible. The color change upon aggregation could be used for sensing of specific DNA sequences (Figure 25).

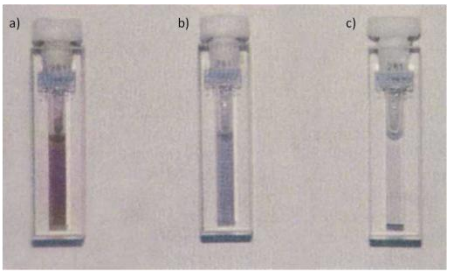

Figure 25: Cuvettes with AuNPs, a) at 80°C, DNA-modified nanoparticles, not aggregated; b) solution cooled to room temperature before aggregation; c) formed aggregates at the bottom of the cuvette. Heating of b) and c) results again in state of a).[108]

The first example of application of such a detection technique was presented by Leuvering *et al.*.[110-112] They developed sol particle immunoassays for molecules, like chorionic gonadotrophin, an indicator for pregnancy in urine and serum. Specific antibodies were bound to the surface of AuNPs. After detection and binding to the target molecule, the AuNPs aggregated which was indicated by a visible color change or could be detected with a spectrophotometer.

Like silver, gold is also able to enhance Raman signals for the purposes of SERS.[107, 113] Halas *et al.* used AuNPs to monitor the protonation and deprotonation of surface bound mercaptobenzoic acid

by SERS.[114] The system which they developed proved to be a highly sensitive nanoscale pH-meter with an accuracy of ± 0.10 pH units.

1.3.1.2. AuNPs used in Catalysis

The application of AuNPs in catalysis has gained increasing interest in recent years.[115-116] It represents a bridge between homogeneous and heterogeneous catalysis. Interestingly the catalytic ability is strongly size dependent and disappears completely when the particles become too big.[115] AuNPs show an intrinsic catalytic activity, for example for aerobic oxidation of alcohols, 1,2-diols and CO as well as borohydride reduction and carbon-carbon cross-couplings.[115-116]

A representative example for application of AuNPs in catalysis is the work of Tsukuda *et al.*.[117-119] They prepared monodisperse AuNPs with an average diameter of 1.3 nm, using PVP as a stabilizing additive and investigated their performance in the catalytic oxidation of benzylic alcohols in water at room temperature (Figure 26) The catalytic activity was considerably higher when smaller AuNPs (1.3 nm vs. 9.5 nm) were used.

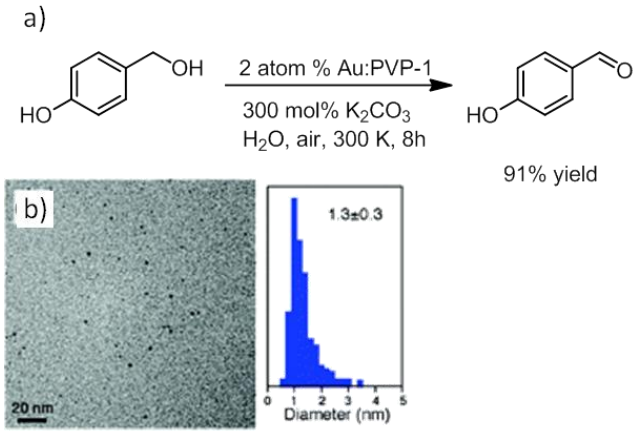

Figure 26: a) Oxidation reaction with an AuNP catalyst, b) TEM image and histogram of AuNPs stabilized with PVP.[117]

1.3.1.3. AuNPs used in Medicinal Applications

AuNPs have many possible applications for medicinal purposes, like cancer therapy, in imaging or drug delivery into cells. Some examples will be presented in this chapter.

El-Sayed *et al.* have demonstrated a system for nuclear targeting of AuNPs in cancer cells leading to cytokinesis arrest.[120] This resulted in an incomplete cell division and in the end in apoptosis. The researchers generated 30 nm AuNPs coated with polyethylene glycol that was conjugated with two peptides, RGD and a nuclear localization signal (NLS) peptide. After incubation of the AuNPs with

malignant epithelial cells HSC-3 and non-malignant epithelial cells HaCat, they were found to be specifically taken up into cancer cells, and exclusively cause the cytokinesis arrest in those cells (Figure 27).

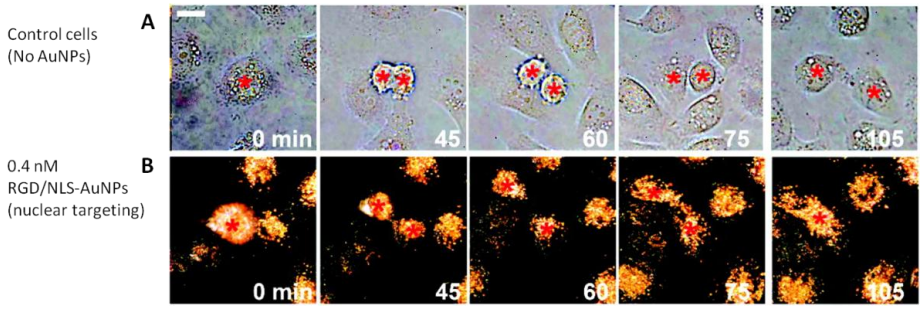

Figure 27: Real-time images of cell division of cancer cells. Upper pictures show the normal cell division cycle. In presence of AuNPs the cell division stopped at 75 min and a binucleate cell was formed. Scale bar: 10 µm.[120]

AuNPs can also be employed as non-toxic carriers for drug and gene-delivery. The gold core provides stability and the outer layer flexibility for tuning the properties to optimize the delivery conditions. One possibility for selective drug delivery is the glutathione-mediated (GSH) release of prodrugs. A methodology study was carried out by Rotello *et al.* where they delivered a hydrophobic dye into human Hep G2 cells.[121] Due to significantly increased intracellular concentration of GSH a thiol exchange is triggered and the surface bound dye is released inside the cell (Figure 28).

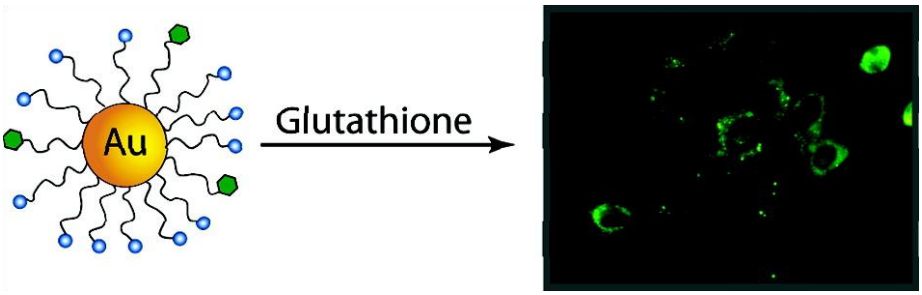

Figure 28: Schematic representation of the functionalized AuNPs and the GSH-mediated release. Microscopy image on the right side showing released fluorescence dye inside human Hep G2 cells.[121]

1.3.1.4. AuNPs used in Electronics

By decreasing the size of nanoparticles down to 2 nm and beyond and therefore also their capacitance it is possible to control single electron movements, even at room temperature. Using this property allows to design single electron devices.

In the work of Dadosh *et al.* the authors connected two AuNPs by dithiolated short organic molecules.[122] This system was electrostatically trapped between two metal electrodes which

allowed for studying the electrical conductance through organic molecules. 4,4-Biphenyldithiol (BDP), bis-(4-mercaptophenyl)-ether (BPE) and 1,4-benzenedimethanethiol (BDMT) were investigated (Figure 29). It was found that the oxygen in BPE and the methylene groups in BDMT suppress the electrical conductance of these compounds compared to that of BPD.

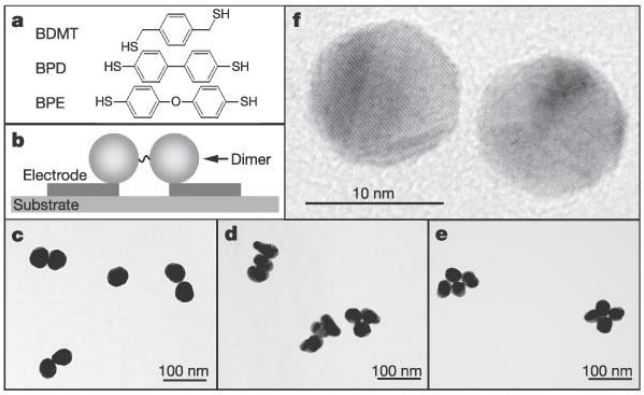

Figure 29: a) The structures of the investigated organic molecules, b) schematic representation of the connected AuNPs, c)-d) TEM images of BDMT dimer, trimer and tetramer structures with 50 nm particles f) Dimer consisting of 10 nm AuNPs connected with BDMT.[122]

1.3.2. AuNP Generation

Similarly to the generation of AgNPs, also in the AuNP generation one of the main challenges lies in controlling their morphology which can be achieved through establishing the optimal conditions for the formation reaction.[12, 123-124] Many different generation processes have been developed and some of them will be highlighted in this chapter, again divided in the top-down and the bottom-up approaches.

1.3.2.1. AuNP Generation Using the Top-Down Strategy

As explained before, the top-down strategy is based on the miniaturization of the bulk material by physical methods. For example Electron-Beam Lithography is used in the generation of multi-shaped nanostructures down to 10 nm in size.[125]

As described for the AgNP generation, laser ablation is also one of the most common techniques used for the preparation of AuNPs.[126] One example of laser ablation application was described by Meunier *et al.*.[127] They generated monodispersed and functionalized spherical AuNPs with diameter between 2 and 80 nm, depending on the gold to stabilizing additive ratio (Figure 30).

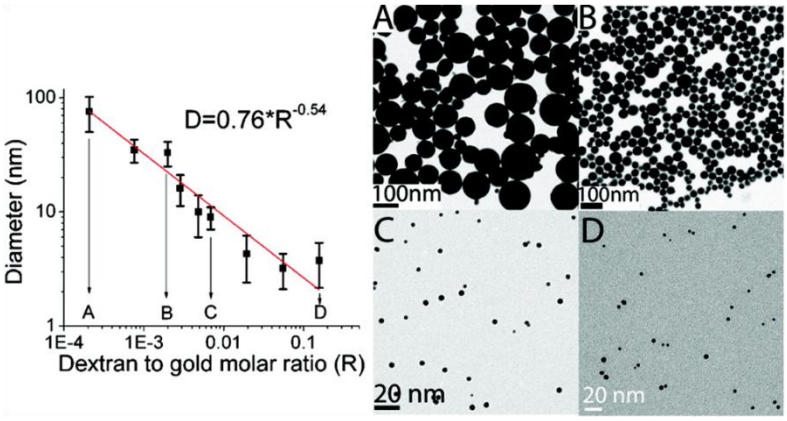

Figure 30: Correlation between the size of AuNPs and the dextran (40 kDa) to gold ratio, a)-d) TEM images of AuNPs.[127]

In the first step nanoparticle seeds were generated by femtosecond laser ablation of gold pellets, immersed in an aqueous dextran solution, which served as stabilizing additive. A second growth phase followed which was carried out under milder irradiation conditions.

1.3.2.2. AuNP Generation Using the Bottom-Up Strategy

The strategy for generation of AuNPs by the bottom-up approach typically involves the reduction of a gold salt in presence of a stabilizing additive. The reduction is carried out either by irradiation or by a chemical reducing agent. These methods are similar to those used in the bottom-up approach for the generation of AgNPs. Some examples of AuNPs formation using the bottom-up strategy will be highlighted in this chapter.

1.3.2.2.1. AuNP Generation Using the Photochemical Method

The photochemical reduction is often used for the generation of AuNPs, similarly to the photochemical generation of AgNPs.[81] In the work of Esumi *et al.* the AuNP formation was achieved by UV irradiation of a gold salt in the presence of the surfactant hexadexylpyridinium chloride (CPCl) as a stabilizing additive.[128] The resulting spherical nanoparticles were monodisperse with an average diameter of 9.3 nm (Figure 31). Other tested surfactants were not able to stabilize the AuNPs in a defined size and shape.

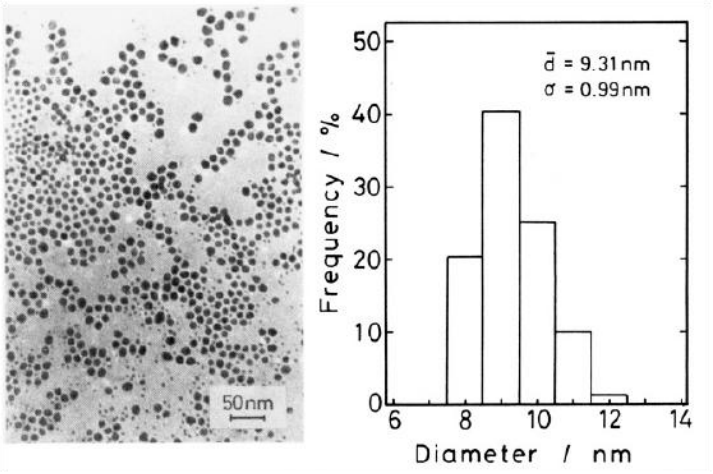

Figure 31: TEM image and the associated histogram of AuNPs generated in the presence of CPCl as a stabilizing additive by UV irradiation over 150 min..[128]

1.3.2.2.2. AuNP Generation Using the Turkevich Method

This method for AuNP formation was introduced in 1951 by Turkevich *et al.*.[129] The procedure involves using citrate both as a reducing agent and a stabilizing moiety. Citrate is quickly added, to a boiling aqueous $HAuCl_4$ solution resulting in formation of polydisperse AuNPs with an average diameter of 20 nm. The gold salt is reduced to elemental gold and at the same time the citrate is oxidized to dicarboxy acetone (Figure 32). The nanoparticle size could be adjusted by varying the citrate to gold salt ratio. The higher the citrate concentration, the smaller the generated nanoparticles.[130], This method was further optimized in many studies by adjusting other reaction parameters, like the temperature and pH.[124] The approach was later modified by Lee and Meisel for the generation of AgNPs (described in chapter 1.2.2.2.2).[87]

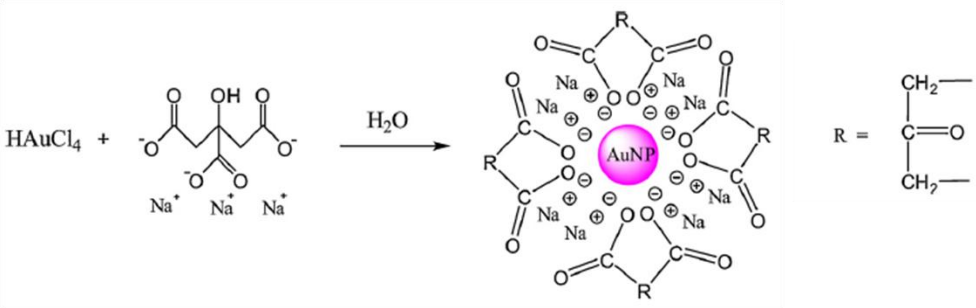

Figure 32: AuNP generation using the Turkevich method.[124]

1.3.2.2.3. AuNP Generation Using the Brust-Schiffrin Method

This is a two phase generation process where chlorauric acid in water and tetraoctylammonium bromide (TOAB) in toluene react with sodium borohydride as a reducing agent. The additive TOAB is

then exchanged by an alkanethiol which stabilizes the nanoparticles with diameters between 5 - 6 nm, low dispersity and cuboctahedral and icosahedral shapes. (Figure 33).[124, 131]

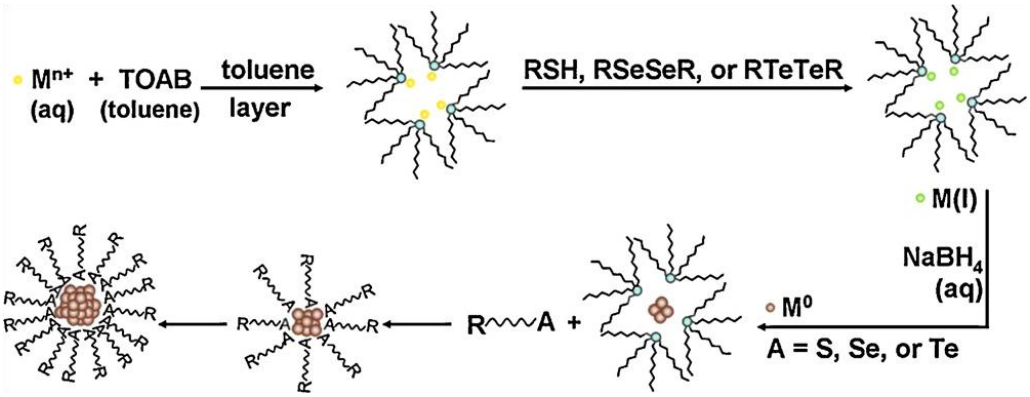

Figure 33: Mechanism for metal nanoparticle synthesis by the Brust-Schiffrin Method.[131]

This method has several advantages which also explains its extensive usage. It is a facile synthesis that can be carried out at room temperature, the resulting AuNPs are very stable and the additives can easily be substituted with their modified versions to functionalize the nanoparticles differently.[124, 131-132]

1.3.2.2.4. AuNP Generation Using the Seed-Mediated Growth Method

In this method small nanoparticle seeds are generated in the first step. In the second step these seeds are added into a solution containing chlorauric acid, stabilizing additives and a reducing agent. The second, growth stage is typically a slow process carried out with a mild reducing agent and which only occurs in presence of the AuNP seeds as catalysts. The growth therefore takes place only on the surface of the existing seeds and no new nanoparticles are formed. The resulting nanoparticles can have many different sizes and shapes, depending on the reducing agent, the additive and the reaction conditions.

One example of such approach is the work of Murphy *et al.*, in which they described the preparation of a huge variety of different structures depending on the experimental conditions.[133] The seeds were added to a growth solution, containing chlorauric acid, ascorbic acid as reducing agent and cetyltrimethylammonium bromide (CTAB) as stabilizing additive. The morphology of the resulting nanoparticles depended on the quantities of each of the reaction components and rods, hexagon-, cube-, triangle- and star-like shapes were identified.[133]

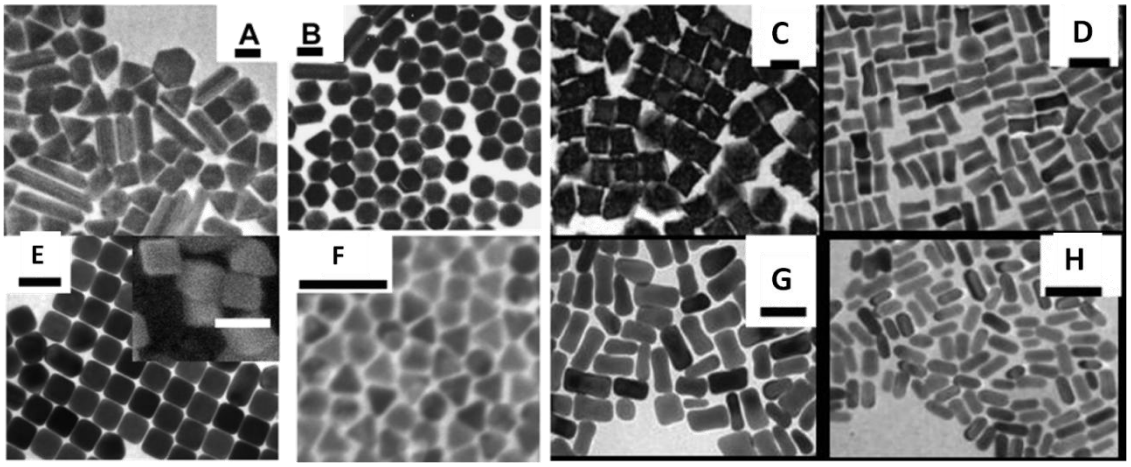

Figure 34: TEM images of AuNPs generated with the seed-mediated growth method by Murphy *et al.* with different shapes evolving depending on the reactant concentrations. Scale bar = 100 nm.[133]

1.3.2.2.5. Biosynthesis of AuNP

As in the case of AgNPs, also AuNPs can be generated by microbes.[134] For example Murray *et al.* have observed that the *Bacillus subtilis* were able to reduce Au^{3+} to Au(0) and generated AuNPs with diameters between 5 - 25 nm inside of the cell wall (Figure 35).[135]

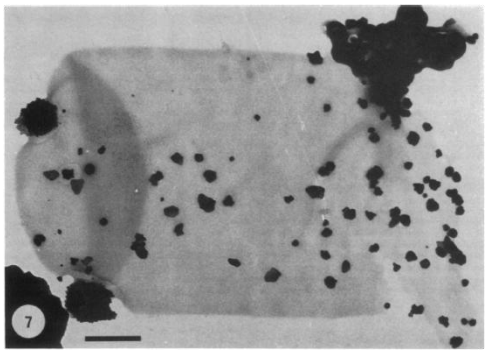

Figure 35: Cell wall of *Bacillus subtilis* with AuNPs. Scale bar = 100 nm.[135]

Wang *et al.,* used *E. coli* DH5α as a bionanofactory to reduce chloroauric acid and guide the nucleation of AuNPs.[136] They incubated the bacteria in a chloroauric acid solution and after a short time, AuNP generation was observed. TEM and SEM investigation proved the formation of nanoparticles that were bound to the cell surface. These bacteria were then used as a membrane surface-display system. By attaching hemoglobine together with the bacteria to a glassy carbon electrode the direct electron transfer between the protein and the electrodes could be investigated, to serve as a model to understand the electron-transfer mechanisms in the biological systems. [136]

1.3.2.2.6. Generation of AuNPs with Peptides as Additives

One of the first groups who investigated the possible applicability of peptides for the generation of AuNPs was the group of Brown.[137-138] They developed a method to screen a cell-surface-displayed peptide library on E. *coli* cells. The cells were incubated in a gold salt solution containing sodium ascorbate, used as a reducing agent. Three polypeptides that accelerated the AuNP growth by binding to the surface were identified. One of them was chosen by the group of Chen and was further investigated as additive for the generation of AuNPs.[139] It was found that the peptides's performance strongly depended on the reaction conditions such as the pH of the solution which needed to be adjusted carefully.

Peptide AG3 (AYSSGAPPMPPF), identified within a phage display library in the study of Naik *et al.* for binding to silver nanoparticles (chapter 1.2.2.2.4) was further investigated for the ability to act as an additive in the AuNP generation process.[97, 140] The peptide proved capable of reducing Au^{3+} and also stabilizing the resulting AuNPs with a diameter of around 12.8 nm (Figure 36). The functional group of the tryptophan amino acid in the peptide was presumed to act as a reducing agent in the process.

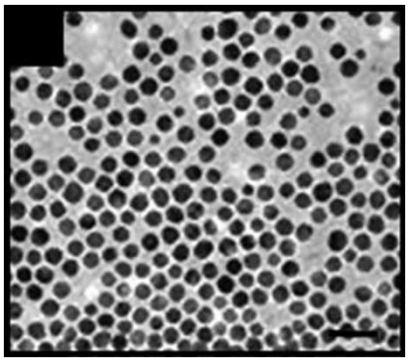

Figure 36: TEM images of AuNPs generated in the presence of peptide AG3, a) scale bar = 100 nm, b) scale bar = 20 nm.[140]

This study showed the intrinsic versatility of peptides in stabilization of metal nanoparticles, as the peptide selected for the stabilization of AgNPs also showed a clear ability to act as an additive in the generation of AuNPs.

Similar conclusions were drawn from the work of Wright *et al*. on the usage of peptides in the generation of metal nanoparticles.[99-100] As described before, they used the HRE peptide (chapter 1.2.2.2.4) to stabilize AgNPs. However in the course of their study they also found this peptide suitable for stabilization of AuNPs with an average size of 9.5 m which was smaller than the resulting diameter obtained by the formation of AgNPs (11.2 nm).

Serizawa *et al*. investigated the generation of AuNPs in the presence of a basic model peptide containing the sequence RPTR, previously identified as an essential motif that binds specifically to film surfaces composed of isotactic poly(methyl methacrylate).[141] This peptide was modified with a cysteine which was expected to bind to the gold surface and then used in the AuNP generation reaction. The reduction took place in the HEPES buffer and resulted in nanoparticles with an average diameter of 10 nm (Figure 37).

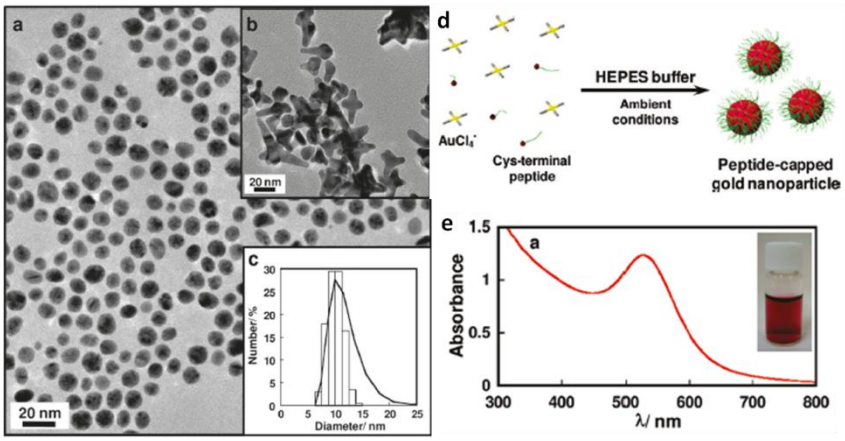

Figure 37: a) TEM image of AuNPs generated in the presence of CRPTR peptide, b) TEM image of AuNPs generated and stabilized by HEPES, c) histogram of AuNPs generated in the presence of CRPTR peptide, d) schematic representation of AuNP generation, e) UV-Vis spectrum of AuNPs generated in the presence of CRPTR.[141]

Taking advantage of the versatile properties of peptides, the group of Matsui investigated the ability of sequenced peptide nanotubes to serve as templates for the generation of AuNPs.[142-143] Peptidic nanotubes were self-assembled from bis(N-R-amido-glycylglycine)-1,7-heptane dicarboxylate molecules. The histidine rich peptide AHHAHHAAD, reported to be able to act as additive in the nanoparticle formation, was immobilized onto the nanotube.[99-100] After incubation with a gold salt and an external reducing agent, the reduction and formation of AuNPs took place, resulting in nanoparticle decorated nanotubes (Figure 38).

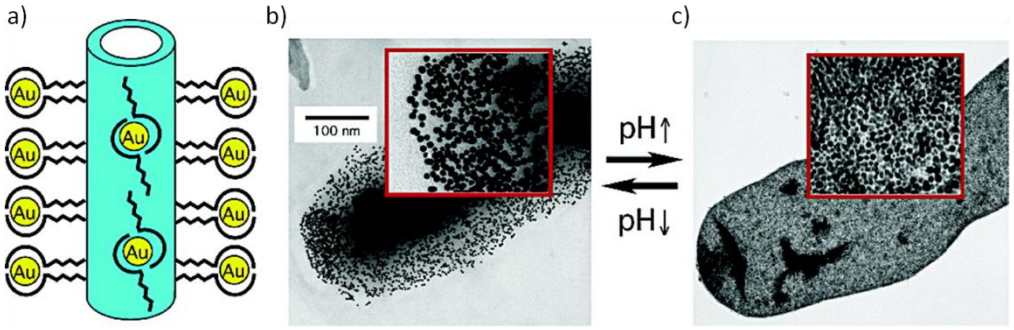

Figure 38: a) Peptidic nanotubes with AuNPs nucleated at the Au^{3+} binding sites, b) TEM image of peptidic nanotube with AuNPs generated at pH 8, c) TEM image of peptidic nanotube with AuNPs generated at pH 11.5.[143]

The size distribution AuNPs was narrow with an average diameter of 6 nm which is consistent with the spacing between the histidine-rich peptides on the nanotubes. A higher nanoparticle density was observed on the nanotubes at higher pH values (Figure 38).[143] This was explained by higher availability of the binding sites for ions at a higher pH which resulted in more nucleation sites during the reduction.

The work of Rosi *et al.* shows a new approach for the assembly of AuNPs into well-defined superstructures.[144] They used a peptide, identified within a phage-display library for the binding to gold surfaces and attached dodecanoic acid at the *N*-terminus. These molecules self-assembled into a left-handed twisted-ribbon structure. If chloroauric acid was present, self-assembly occured simultaneously with AuNP formation, resulting in a left-handed gold nanoparticle double helix (Figure 39). The nanoparticles had an average diameter of 8.2 nm and approximately 22 were found per pitch distance. The individual fibers had lengths in a micrometer range.

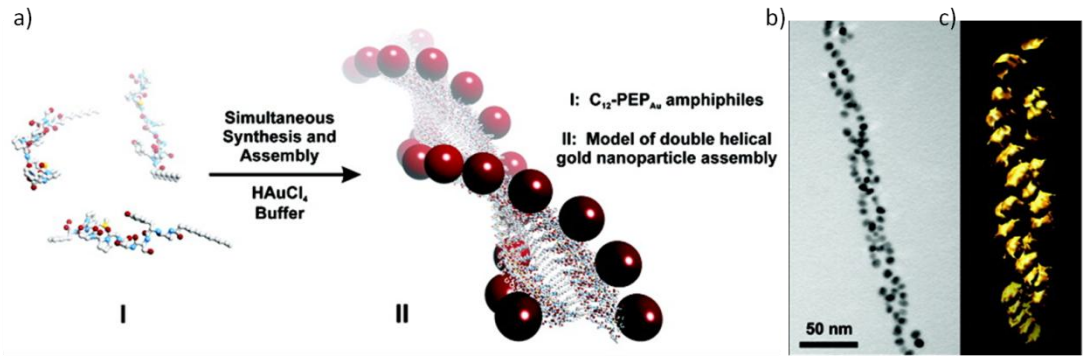

Figure 39: a) Schematic representation of the AuNP formation on the left-handed double helix, b) TEM image of AuNP double helix, c) 3D surface rendering of the tomographic volume from electron tomography data.[144]

The generation of AuNPs using peptides as additives is also not fully understood yet, just as it is with AgNPs. The particular role played by different functional groups needs to be further explored to be able to successfully and rationally design additives for the generation reaction.

1.4. Oligoprolines

1.4.1. Structure and Biological Function

Proline has several special properties compared to the other proteinogenic amino acids. It is the only cyclic amino acid and bears a secondary amine. When proline is incorporated into a peptide, the rotational freedom around the amide bond is conformationally constrained. This can result in the disruption of secondary structures like alpha helices or beta sheets within peptides or proteins. Additionally there is no proton available on the amide nitrogen for hydrogen bonding to support these structures.

Small oligoproline peptides, starting from six proline units already adopt a defined helical secondary structure. Depending on the solvent, two different structures can be formed.[145-147] In aqueous solution a polyproline II (PPII) helix is observed (Figure 40). In the left-handed PPII helix all amide bonds are in *trans* conformation with a dihedral angle of 180°. Every third residue is stacked on top of each other resulting in a C_3 symmetry when looking along the axis. The helical pitch is ~ 9.5 Å (Table 1).

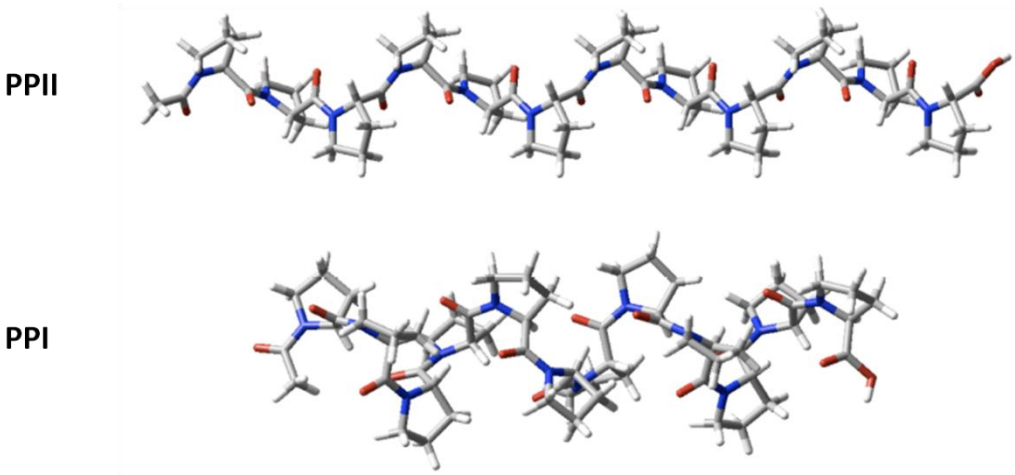

Figure 40: Model of PPII (top) and PPI (bottom) structure. Models constructed using MacroModel software.

In more hydrophobic solvents like *n*PrOH, the structure switches to the polyproline I (PPI) helix (Figure 40). This right-handed helix is more compact then the PPII helix which is reflected in the helical pitch of 5.6 Å. The amide bonds are in a *cis* conformation with a dihedral angle of 0° (Table 1).

Table 1: Characteristics of PPI and PPII helix secondary structure.[145-147]

PPI	**PPII**
Right-handed helix	Left-handed helix
All *cis* amide bonds	All *trans* amide bonds
ϕ = -75°, ψ = +160°, ω = 0°	ϕ = -75°, ψ = +145°, ω = 180°
~ 5.6 Å / turn	~ 9.5 Å / turn
3.3 amino acids per turn	3.0 amino acids per turn
Formed in organic solvents	Formed in aqueous solution

Circular dichroism (CD) spectroscopy is a very useful analytical tool to identify and investigate the two secondary structures as they show a significant difference in the resulting spectra. In CD spectroscopy, the difference in absorption of right and left circularly polarized light is measured, which can be observed for optically active, chiral molecules. Peptides with a PPI conformation show a minimum at ~232 nm and a maximum at ~215 nm in their CD spectra.[148-149] Peptides with the PPII structure have a distinct minimum at ~206 nm and a maximum at ~226 nm (Figure 41).

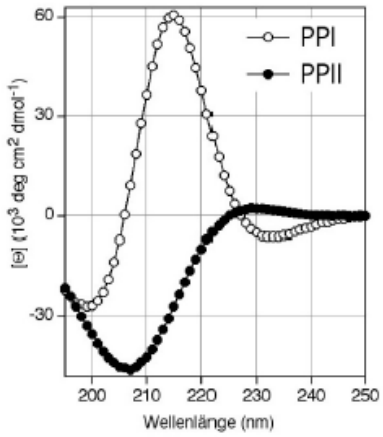

Figure 41: Representative CD spectra of PPI conformation and PPII conformation.[148, 150]

Proline-rich regions in proteins are found both in prokaryotes as well as eukaryotes often as multiple tandem repeats.[151] They are engaged in many cellular processes, for example in signaling pathways. Their binding specificity is supported by the unusual character of the amino acid proline. Different proline-rich motifs recognized inside cells in regulation processes are known. Six families of proline-rich binding domains that recognize proline rich sequences have been described: the SH3 domains,[152-153] the WW domain,[154-155] the EVH1 domains,[156-158] the GYF domains,[159-160] the UEV domains[161-162] and the single-domain[163-164] of profiling proteins. Another very prominent example

for proline rich peptides are the structural proteins collagen[165-166] and elastin[167] which are the main components of connective tissue in mammals and plants.[168] They are furthermore employed in cell-cell recognition[168] and cell motility.[169]

1.4.2. Functionalized Oligoproline as Molecular Scaffold

Oligoprolines have gained much attention for application as a molecular scaffold as they provide a well-defined secondary structure that forms already at short chain lengths of only six residues. They can be easily functionalized in the *γ*-position of the proline ring by modification of e.g. hydroxy proline or azidoproline (Figure 42).[170-171]

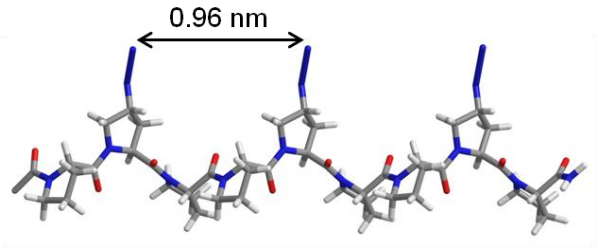

Figure 42: Model of an oligoproline 9mer in a PPII conformation with azidoproline in every third position.

The azido group allows for different synthetic strategies to be employed. One possibility for functionalization through the azide moiety is Cu (I) catalyzed Huisgen's 1,3 dipolar cycloaddition with alkynes, the so-called "click" reaction (Figure 43).[171-175] A second possibility is the reduction of the azide to an amine which can be easily derivatized further.[170]

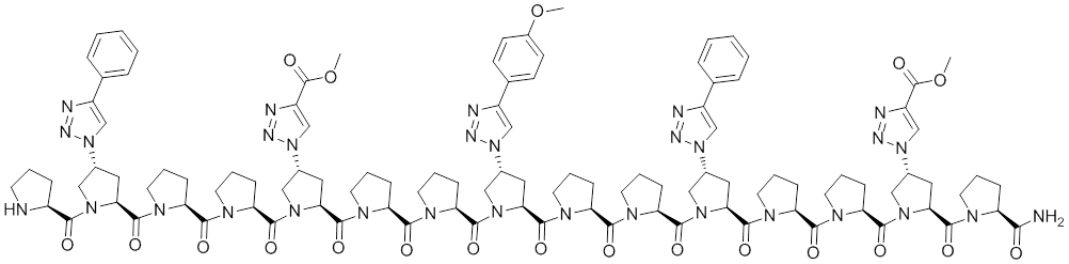

Figure 43: Functionalized oligoproline synthesized by sequential peptide coupling and "click" reaction steps on solid support.[171, 175]

One example of the application of a functionalized oligoproline is a molecular ruler for the calibration of distance measurements in Förster or fluorescence resonance energy transfer (FRET) systems.[176-178] This method is a tool to investigate protein-protein interactions and conformational changes in proteins.[179-180]

Oligoproline also turned out to be a suitable spacer for the investigation of electron transfer in peptides.[181-185] In the studies of Giese et al. they were able to identify an electron "hopping" mechanism in peptides and proteins over certain relay amino acids. By using oligoproline as spacer for their model peptides, it was possible to identify the optimal relative distance of the relay amino acids.[181-183]

Another example for the usage of oligoprolines as a molecular scaffold is the study of Overkleeft *et al.*.[186] They attached agonists of a G protein-coupled receptor (GPCR) to oligoprolines. They tested different functionalization patterns as well as different number of coupled ligands and found an increase in potency of the tumor targeting with peptides bearing more than one ligand compared to the monomeric counterparts.[186]

The Wennemers group is using oligoprolines as molecular scaffolds for many different applications. One example is tumor targeting. Peptidic agonists as well as antagonists for the specific binding to GPCR were attached to the oligoproline backbone, taking advantage of the enhanced binding through the two different binding modes that the agonist and the antagonist are using.[187]

Functionalized oligoprolines were also employed as cell-penetrating peptides (CPPs) where cationic groups were attached to their backbone which enhanced the cell permeability. Those peptides were also functionalized with a fluorescence dye which allowed for the observation of the penetration into an eukaryotic cell and the accumulation inside the nucleus.[150]

Another field of research currently being explored by the group, is the application of functionalized oligoproline peptides for the calibration of spin label systems. Furthermore this scaffold is investigated in its applicability in self-assembly of oligoproline semiconductor compounds that are envisioned to be used in electronics.

Last but not least, the functionalized oligoprolines were used as additives in the generation of AgNPs (chapter 1.2.2.2).[78] The oligoprolines functionalized with aldehyde moieties were employed as reducing agents, as well as stabilizing agents, displaying a unique linear correlation between the molecular dimensions of the peptide and the nanoscopic dimensions of the resulting AgNPs.[78]

The application of oligoproline-based additives for the nanoparticle formation will be further discussed in the following chapter, presenting the main part of this work.

2. Objective

The generation of metal nanoparticles has raised tremendous interest in recent years. They offer a huge variety of possible applications due to their unique properties which strongly depend on their morphology (chapter 1). However, the controlled formation of nanoparticles of desired, monodisperse sizes and shapes still remains a challenge which we intended to tackle with the research project described within the confines of this PhD thesis.

We envisioned that peptidic additives could be a useful tool to achieve control over the synthesis and therefore the properties of the obtained nanoparticles. As our group has previously demonstrated, aldehyde-functionalized oligoprolines are able to act as additives in the generation of monodisperse AgNPs, displaying an unprecedented linear correlation between the length of the peptides and the sizes of resulting nanoparticles.[78]

The aim of the work described in this thesis was the design and screening of different oligoproline based additives for the generation of metal nanoparticles. From the previous work, we knew that oligoprolines can serve as scaffold in the design of additives used in the formation of metal nanoparticles. Therefore, we wanted to use oligoprolines as scaffold, where different functional groups, beneficial for the generation reaction were attached (Figure 44). We intended to investigate the nanoparticle stabilizing ability of such functional groups, learn more about requirements for an efficient additive and determine the distinct influence of respective functional groups on the size and shape of resulting nanoparticles.

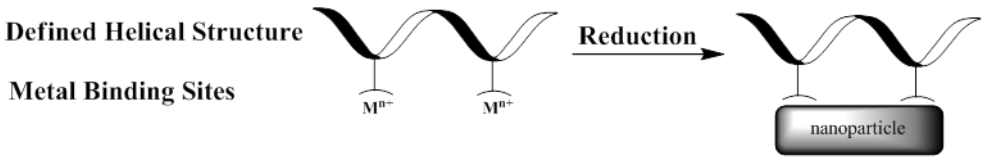

Figure 44: Schematic representation of the metal nanoparticle formation using the designed additive with a helical backbone and attached metal binding sites.

Guanidine, imidazole, primary amine, carboxylic acid, indole and pyrrolidinyl groups were chosen to be attached to the oligoproline backbone. The studied functional groups were selected depending on their ability to bind metal ions. Additional selection criteria were literature precedents of their presence in additives for nanoparticle formation.[12, 46, 57-58, 77-78, 96-101, 103-105, 137-144, 188]

Based on this, we chose to test the ability of such functionalized, helical peptides to act as additives in the metal nanoparticle synthesis. Furthermore we wanted to investigate, if the defined and rigid backbone is beneficial for the generation reaction. The defined structure is expected to help

generate defined nanoparticles as it was observed in the previously investigated system with aldehyde-functionalized oligoprolines.[78]

We decided to investigate both silver and gold nanoparticles, as they are both attractive targets for the synthesis due to the manifold possible applications. The synthesis is typically done by reduction of the respective metal salt, using a reducing agent in the presence of a stabilizing additive.

3. Results and Discussion

3.1. Identification of Novel Oligoproline Based Additives for the Generation of Metal Nanoparticles

In this thesis, the identification of peptidic additives is presented which were investigated in the generation of metal nanoparticles. First, the general design of the additives is discussed (Chapter 3.1.1.), where the backbone, as well as the choice of the attached functional groups is explained. Next, the syntheses of the building blocks and the peptides are presented (Chapter 3.1.2). Then, the analysis of the secondary structure of the peptides using circular dichroism (CD) spectroscopy is shown in chapter 3.1.3.. In the last two sections of this chapter, the use of the designed additives in the generation of metal nanoparticles is discussed. Chapter 3.1.4 focuses on the generation of AgNPs. The different peptides, used as additives are discussed separately. First the optimization of the reaction conditions is presented, followed by the screening of various peptides to address the questions about the roles, played by different parts of the additives, like the functional groups and the oligoproline backbone. The next part focuses on the use of the additives in the generation of AuNPs (Chapter 3.1.5). The last chapter presents some preliminary studies for the formation of PtNPs (Chapter 3.1.6).

3.1.1. Design

Based on the results obtained in our group by using aldehyde-functionalized oligoproline as additives in the formation of AgNPs, we envisioned to design peptidic additives that can influence the formation of metal nanoparticles. We intended to learn more about the relation between the molecular additive and the resulting nanoparticles. In contrast to the system investigated before, we chose functional groups that are able to bind to silver ions and require an external reducing agent for the formation of nanoparticles.

We used as a scaffold oligoprolines which provide for a defined secondary structure and for the possibility to attach functional groups in a defined spatial arrangement by introducing azidoproline in the sequence (chapter 1.4.). Furthermore they were already used in the design of additives for the generation of AgNPs by our group, where it was possible to generate nanoparticles in defined sizes and shapes (chapter 1.).[78] This peptide serves as a platform to install different functional groups. The binding of stabilizing moieties to the metal is supposed to be one of the crucial factors determining the final size and shape of the nanoparticles. The choice of potential stabilizing motifs was based on their ability to bind to Ag^+. We anticipated that this property made them promising candidates to stabilize the nanoparticles in a defined morphology. Another reason, we based our choice on, was that the functional groups were already found in successful additives used in the generation of metal nanoparticles. [12, 46, 57-58, 77-78, 96-101, 103-105, 137-144, 188]

The functional groups that were chosen were guanidine, imidazole, primary amine, carboxylic acid, indole and pyrrolidinyl groups (Figure 45).

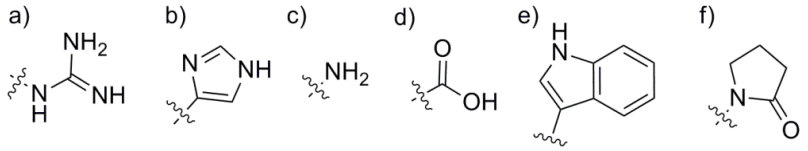

Figure 45: Functional groups that were attached to the oligoproline scaffold; **a)** guanidine; **b)** imidazole; **c)** primary amine; **d)** carboxylic acid; **e)** indole; **f)** (2-oxo-1-pyrrolidinyl) groups.

These functional groups all have distinctly different binding energies to Ag^+.[189-191] The relative binding energies of amino acid side chains to Ag^+ in gas phase were determined theoretically and experimentally in a study of Lee *et al*.[189] Taking inspiration from this, some of the functional groups, that were found in the side chains of the discussed amino acids, were chosen to be used in this work. Furthermore the pyrrolidinyl group was investigated, due to its application in the polymer polyvinylpyrrolidone (PVP), which is one of the most common additives, used for the metal

nanoparticle generation (chapter 1.2. and 1.3.). [66-67] Not only this group, but all of the chosen ones were found to be parts of investigated additives described in literature.[57-58, 66, 79, 102, 192-195] Typically these additives either not provided for a defined secondary structure or there was more than one type of functional group in the additive present. The individual role of the functional groups remained unclear. Therefore, we only attached one type of functional group in one peptide, to be able to assign the differences in morphology of the resulting nanoparticles to the used functional groups.

The functionalities were bound to the backbone through an amide bond, with an additional short, alkyl spacer separating them from the scaffold (Figure 46).

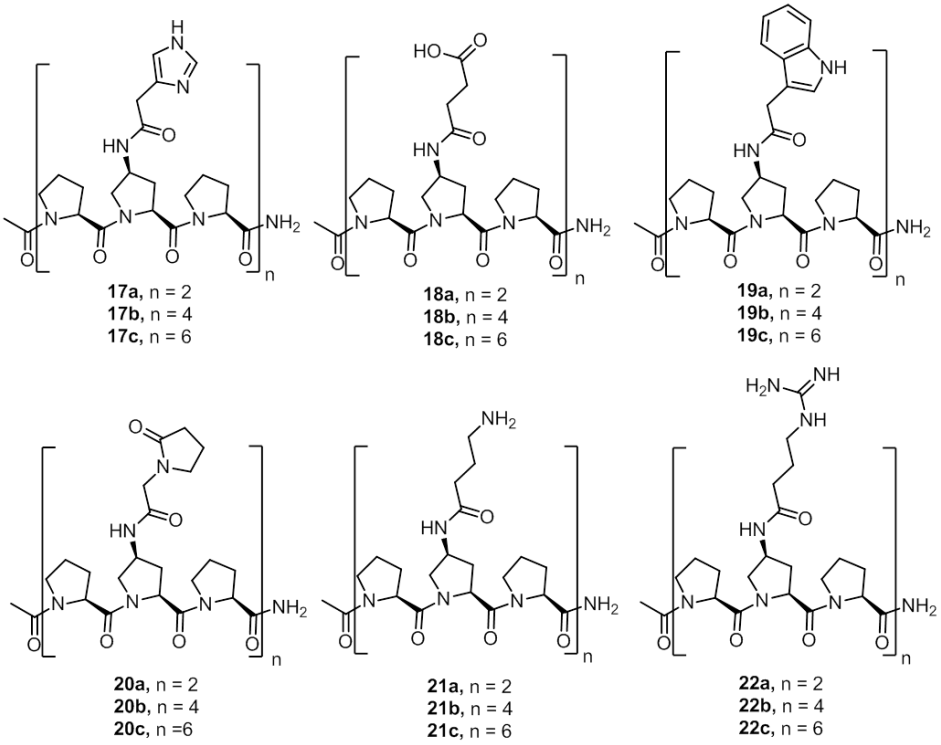

Figure 46: Designed peptides **17a** - **22c.**

The amide bond connection was chosen over the formation of a triazole in the Huisgens 1,3-dipolar cycloaddition to attach the functional group. Even though the reduction of the azide is an additional step in the synthesis, we assumed that the aromatic ring formed in this reaction would influence the formation process, due to its ability to bind to Ag^+.[196] To investigate the influence of the amide bond we synthesized a peptide bearing only an amide group on the backbone of the peptide (Figure 47, peptide **31**).

To address the question, whether a defined three dimensional structure is really needed for an additive to act in an efficient way, peptides with a flexible backbone, bearing imidazole and

guanidine groups were designed (Figure 47, peptides **29a** - **30c**). These functional groups were chosen because their rigid counterparts, when used in the generation of AgNPs, resulted in nanoparticles with defined sizes and shapes.

In addition, oligoprolines bearing primary amino and guanidine groups as derivatives without a linker between the functional group and the backbone were constructed. They served as models to study the influence of the flexibility of the linker, connecting the functional groups to the oligoproline scaffold, on the properties of the additives (Figure 47, peptides **23a** - **24c**).

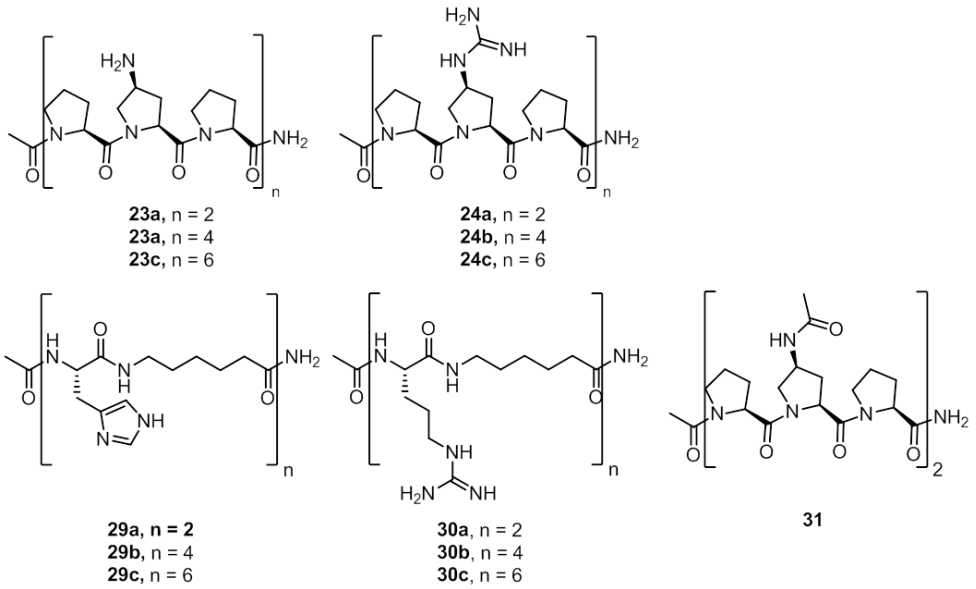

Figure 47: Designed peptides **23a** - **24c**, **29a** - **31.**

The *C*-terminal carboxamide group was preferred over a *C*-terminal carboxylic acid group as well as an amide group at the *N*-terminus instead of the free amine, to prevent charged termini, which could influence the performance of the obtained additives. Moreover capped termini stabilize the PPII structure in comparison to the free termini in water.[197]

To test the influence of the backbone in the generation reaction we also synthesize unfunctionalized oligoprolines (Figure 48).

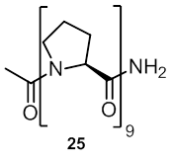

Figure 48: Designed peptides **25**

3.1.2. Syntheses of the Peptides

3.1.2.1. Syntheses of Azidoproline Containing Building Blocks

To incorporate azidoproline in the peptides, Fmoc-(4*S*)Azp-OH was synthesized (Scheme 1), as previously described in our group.[170, 198-199]

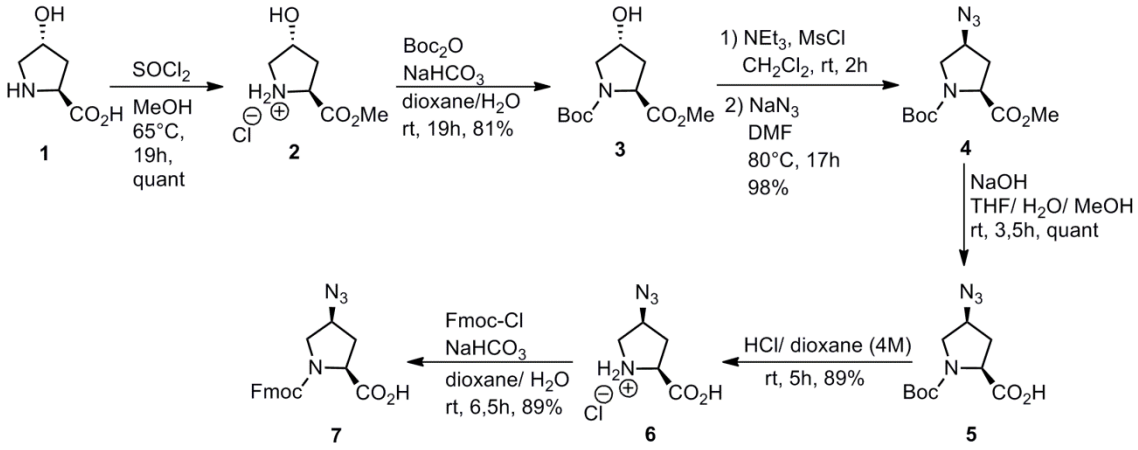

Scheme 1: Synthesis of Fmoc-(4S)Azp-OH **7**

The synthesis started with commercially available H-(4*R*)Hyp-OH **1**. The amino acid was transformed into H-(4*R*)Hyp-OMe **2** using thionyl chloride and MeOH for the esterification of the carboxylic acid. Then, the amine was protected with a *tert*-butyl oxycarbonyl (Boc) group. The hydroxy group of the resulting Boc-(4*R*)Hyp-OMe **3** was converted in the corresponding mesylate followed by a nucleophilic substitution at the activated C4 with sodium azide, to give Boc-(4*S*)Azp-OMe **4**. After hydrolysis of the methyl ester and cleavage of the Boc protecting group, the amine was re-protected with Fmoc-Cl to yield the desired product Fmoc-(4*S*)Azp-OH **7**. All of the reactions proceeded in good to quantitative yields to give an overall yield of 62% of **7** over seven steps.

It was shown in our group that the synthesis and purification of longer peptides with the monomeric building block **7** was difficult. Therefore the trimeric building block, Fmoc-Pro-(4*S*)Azp-Pro-OH **13** was synthesized. Fewer fragments were formed in peptide synthesis using the trimer **13**, due to the reduced amount of coupling steps which clearly simplified the purification. The synthesis of this trimeric building block was carried out as previously described (Scheme 2).[198]

For the synthesis of the trimer **13**, Boc-(4S)Azp-OH **4** was deprotected to obtain the free amine **8** followed by coupling of Boc-Pro-OH, leading to compound **9**. The methyl ester was saponificated and H-Pro-OMe was coupled to the dimer to give Boc-Pro-(4S)Azp-Pro-OMe **11**.

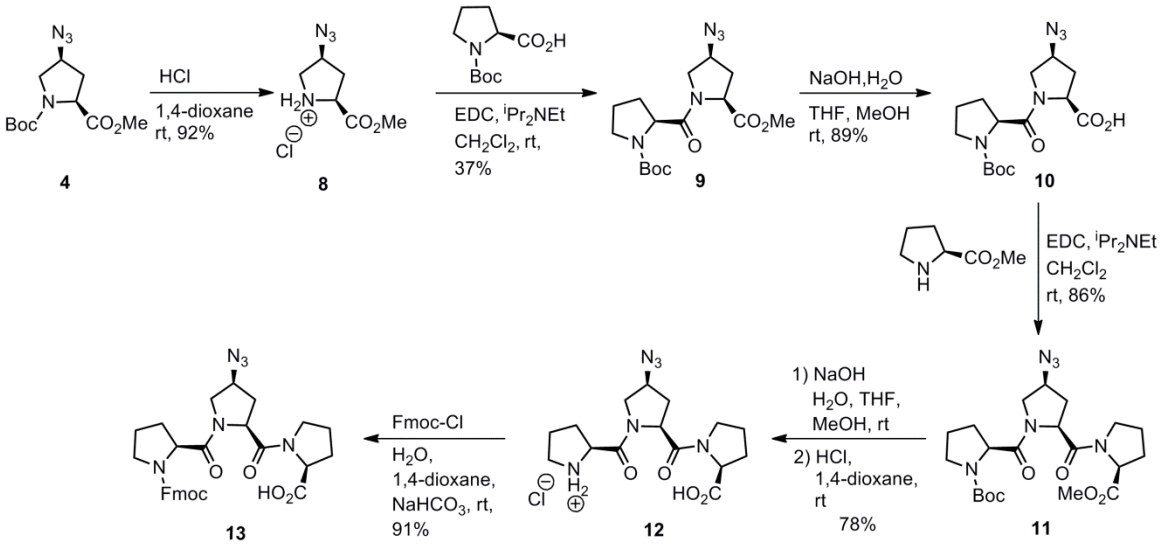

Scheme 2: Synthesis of Fmoc-Pro-(4S)Azp-Pro-OH **13**.

Subsequently the Boc group was removed and the ester hydrolysed. The last step was an Fmoc protection of the amine **12** with Fmoc-Cl to give Fmoc-Pro-(4S)Azp-Pro-OH **13**. The overall yield was 15% starting from H-Hyp-OH **1** over eleven steps.

3.1.2.2. Syntheses of the Peptides

The oligoproline peptides, containing azidoproline in every third position, were synthesized according to standard solid phase peptide synthesis (SPPS) protocols, using the Fmoc/*t*Bu strategy (Scheme 3; 5.3.).

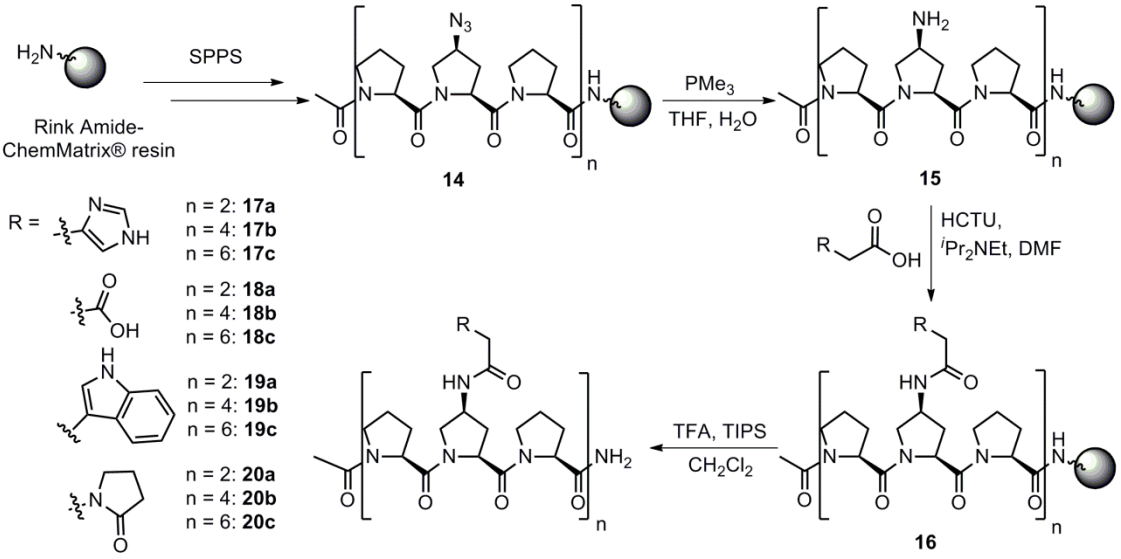

Scheme 3: Synthesis of peptides **17a** – **20c** on solid support (Rink amide-ChemMatrix®).

The synthesis was carried out on Rink amide-ChemMatrix® resin which results in a *C*-terminal carboxamide after cleavage from the resin. The peptides were synthesized by automated peptide synthesis using 4.0 equivalents of the respective Fmoc protected amino acid (Chapter 5.3.4). HCTU (4.0 equiv) was used as coupling reagent together with $^{i}Pr_2NEt$ (12 equiv) as base. Each coupling step was followed by Fmoc deprotection using piperidine (40% (v/v)) in DMF, followed by several washing steps. After the peptide synthesis, an acetylation of the *N*-terminus was carried out, using Ac_2O and NEt_3 to yield peptide **14**. The next step was the reduction of the azide group using Staudinger conditions to obtain the amine **15** (Chapter 5.3.7).[200] Then, the desired functional group was coupled as a carboxylic acid derivative to the amine **15**. Cleavage from the resin yielded the desired peptides **17a** – **20c** (Scheme 3).

For peptide **21a-c**, bearing primary amine groups and peptide **22a-c**, bearing guanidine groups the strategy had to be adapted (Scheme 4). After coupling of Fmoc-GABA to peptide **15** on solid support, Fmoc deprotection using piperidine (20% (v/v)) in DMF was carried out. This was followed by cleavage to yield peptides **21a-c**, bearing primary amines.

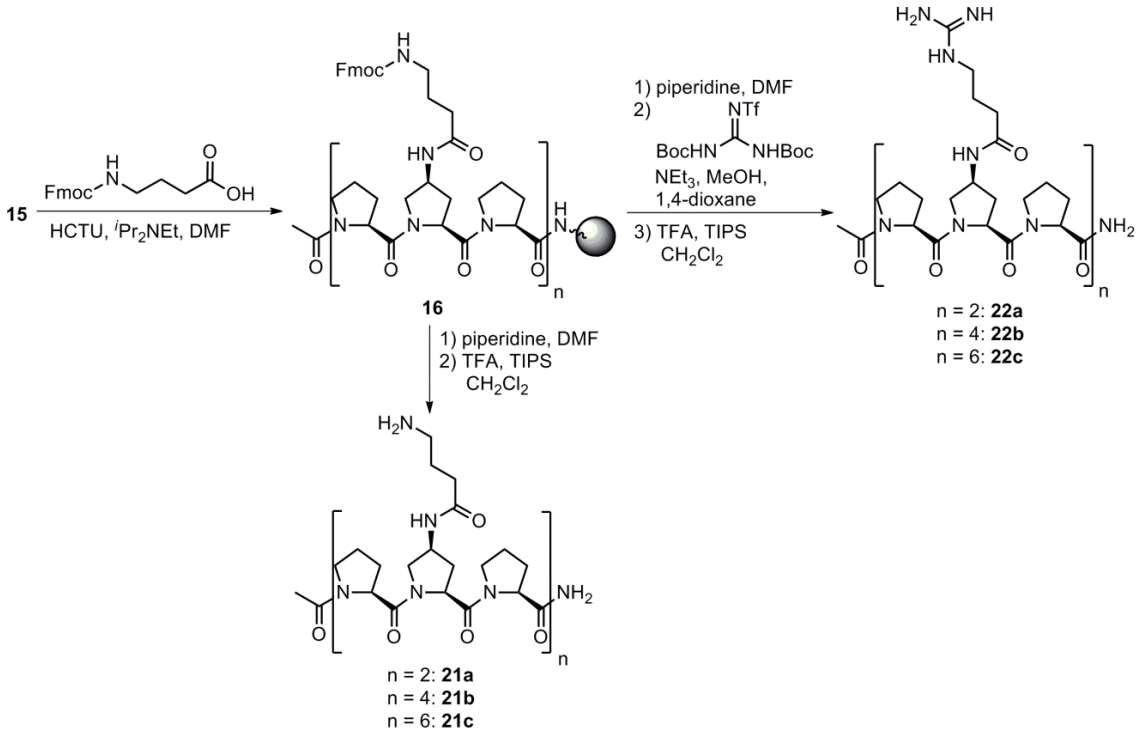

Scheme 4: Synthesis of peptides **21a-c** and **22a-c** on solid support (Rink amide-ChemMatrix®).

In the synthesis of the guanidine-functionalized peptides **22a-c**, an additional guanidylation was performed after the Fmoc-deprotection, using N,N'-di-Boc-N''-trifluoromethane sulfonylguanidine and NEt_3. Then peptide **22a-c** were cleaved from the resin.

Peptides **23a-c**, bearing primary amino groups and **24a-c**, bearing guanidine groups, both types without a linker, were synthesized in a similar manner. Peptides **23a-c**, bearing primary amino groups were obtained by cleaving peptide **15** from the resin. The guanidine-functionalized peptides **24a-c** were synthesized *via* guanidylation of peptide **15**, followed by cleavage from the resin (Scheme 5).

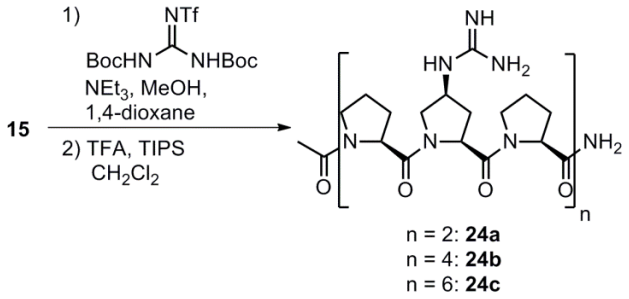

Scheme 5: Synthesis of peptides **24a-c**.

The unfunctionalized oligoprolines **25** was synthesized by standard SPPS, using the Fmoc/*t*Bu strategy on Rink amide-ChemMatrix® (Figure 49). The synthesis was followed by *N*-acetylation to obtain a capped *N*-terminus.

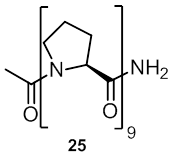

Figure 49: Oligoprolines **25**.

The flexible peptides **29a-c** and **30a-c** were synthesized using standard SPPS with the respective Fmoc amino acids followed by acetylation of the *N*-terminus (Figure 50).

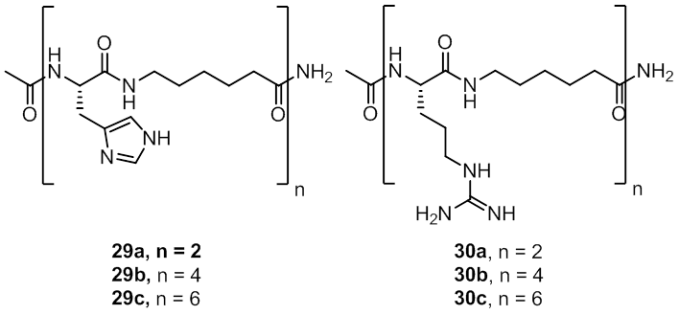

Figure 50: Flexible peptides **29a-c** and **30a-c**.

After cleavage of the peptides they were purified using RP-HPLC. TFA was used to remove the peptides from the acid labile Rink amide resin. Thus the peptides were obtained and isolated as TFA salts. Since the TFA might influence the nanoparticle formation, the peptides were “desalted” by an ion exchange column (5.3.10.). The removal of TFA was confirmed by ^{19}F-NMR. The usage of TFA was

preferred over the usage of another acid, like HCl because it was possible to easily control the removal using ^{19}F-NMR.

For peptides **18a-c**, bearing carboxylic acid groups, ion exchange chromatography could not be used. The acidic peptides cannot be eluted from the column. Even though, there is no counter ion present that binds to TFA in those peptides, there was an excess observed in ^{19}F-NMR that unfortunately could not be removed by repeated precipitation. To remove the TFA, a second RP-HPLC purification was carried out, using solvent mixtures without TFA. It was necessary to make two purification steps, as using solvent mixtures without TFA, resulted in a significant peak broadening.

3.1.3. Conformational Analysis

To investigate the secondary structures of the functionalized oligoprolines, CD spectroscopic studies were performed. The peptides were dissolved in ultrapure water and the measurements were carried out at 25°C. The ellipticity is given as the molar ellipticity, taking into account the concentration of the peptide solution, calculated for only one amino acid residue, to be able to compare different concentrations and lengths of peptides.

In Figure 51 is the CD spectrum of the unfunctionalized oligoproline presented. It has a minimum at 206 nm and a maximum at 226 nm which is indicative for a PPII helix (chapter 1.4.).[148, 201-202] This spectrum served as reference for a PPII structure for the functionalized oligoprolines.

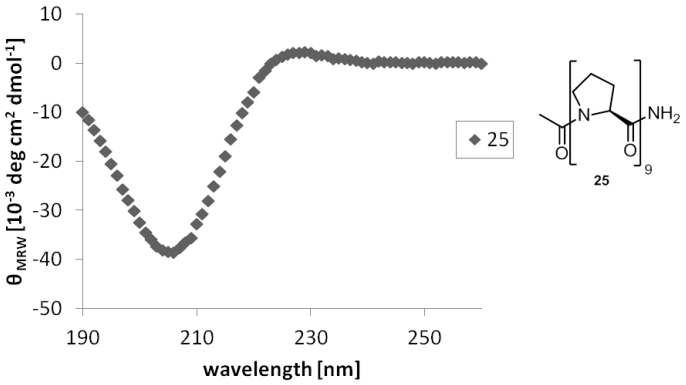

Figure 51: CD spectrum of peptide **25.**

In Figure 52 the CD spectra of peptides **17a-c**, bearing imidazole moieties, are shown. The longer the peptide, the more intense is the minimum at 206 nm. Beside this change in intensity, it was observed that the introduction of the functional groups had no influence on the shape of the CD spectra (compare to Figure 51). The same is true for the other functionalized peptides (Figure 52). In case of peptide **19a**, bearing an indole moiety a blue shift of the minimum is observed (Figure 52c). A possible reason for this is the presence of an aromatic group which is by itself a strong chromophore and therefore has a bigger influence on the ellipticity of the peptide. Due to the aromatic character of the indole in the side chains, peptides **19b** and **19c** showed a decreased solubility in water. This significantly obstructed the spectroscopic analysis. However the spectra recorded at very low concentrations clearly showed also a PPII structure.

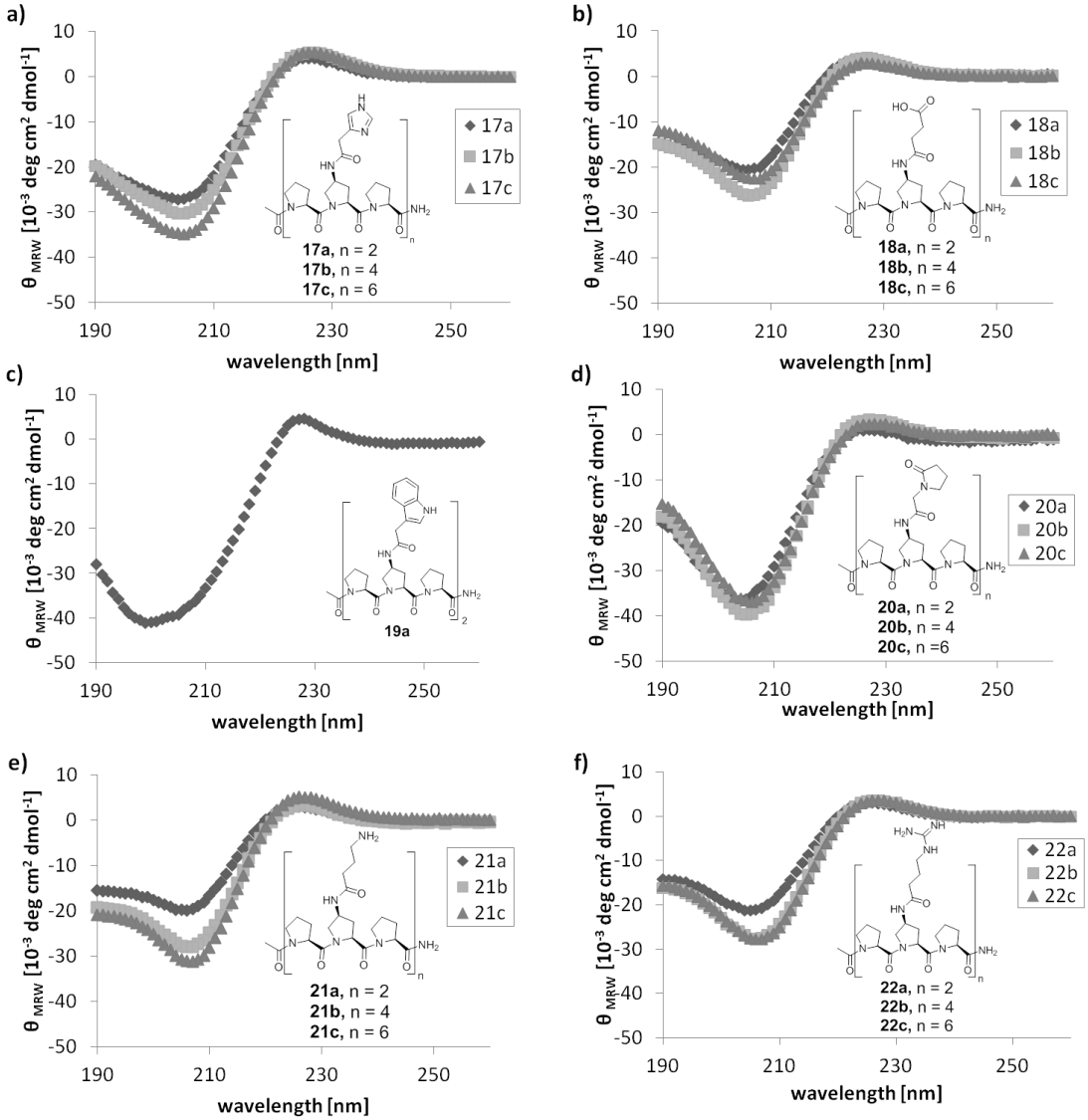

Figure 52: CD spectra of **a)** peptides **17a-c**, **b)** peptides **18a-c**, **c)** peptide **19a**, **d)** peptides **20a-c**, **e)** peptides **21a-c**, **f)** peptides **22a-c**.

In Figure 53 the spectra of the guanidine-functionalized peptides **22a**, **24a** and the unfunctionalized oligoproline **25** are shown. The unfunctionalized peptide **25** forms a PPII helix and therefore served as reference. The other two peptides have a guanidine group attached to the backbone. In peptide **24a**, the functional group is attached directly to the proline ring, whereas in peptide **22a**, an additional linker connects the functional group to the backbone. These differences in the side chain have an influence on the intensity of the minima in the CD spectra. The minimum of unfunctionalized oligoproline **25** is the most intense and the one of peptide **22a** the least intense. The observed changes probably result from the influence of the functional groups on the absorption. This effect is

more dominant in the case of peptide **22a**, probably due to the fact that the additional amide groups from the linker are contributing to the CD signal.

Clearly a PPII structure is formed in all of the investigated oligoproline based peptides, as they all had a maximum at 226 nm which is most indicative for a PPII helix. More profound information, also about the attached functional groups, would only be provided by an X-ray structure. It was tried to crystallize an oligoproline under various conditions. So far no crystals were obtained (Appendix).

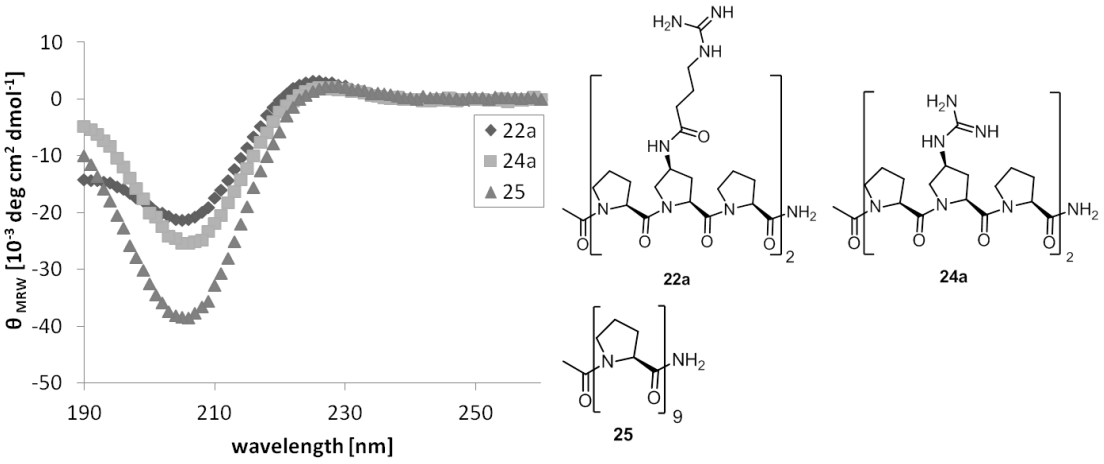

Figure 53: CD spectra of peptides **22a**, **24a** and **25**.

The peptides which were designed to adopt no defined secondary structure had CD spectra that indicate a random coil structure. The CD spectra of the flexible peptides **29a**, bearing an imidazole moiety and **30a**, bearing a guanidine moiety are shown in Figure 54. These spectra both display a minimum around 195 nm and a maximum around 216 nm which are indicative for a random coil structure.[203-204] In such a structure the amino acids are oriented randomly and are observed as a statistical distribution of shapes. These peptides were designed to have no defined secondary structure in order to investigate the influence of this property from the additives, on the generation of metal nanoparticles.

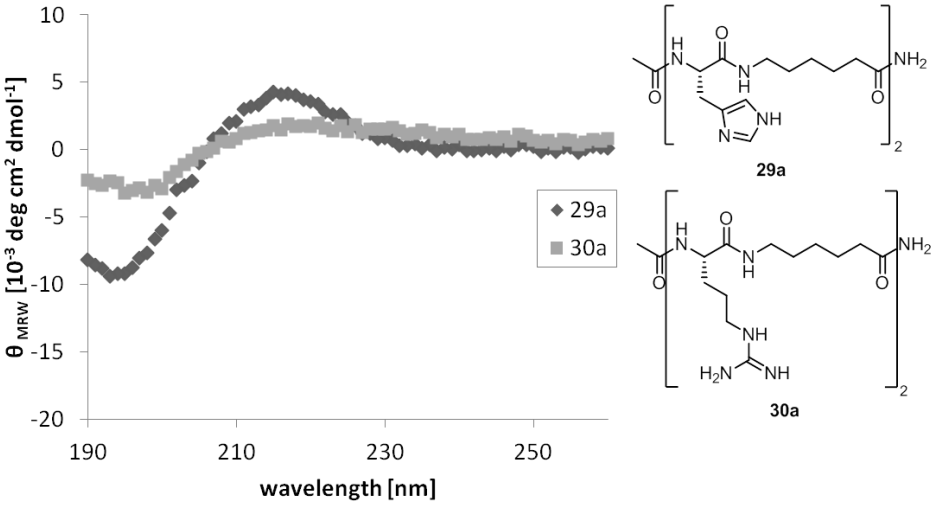

Figure 54: CD spectra of peptides **29a** and **30a**.

The CD spectra of the longer peptides **29b**, **29c** and **30b**, **30c** are shown in the appendix.

3.1.4. Silver Nanoparticle (AgNP) Formation

We tested the different peptides for their ability to act as additives in the formation of AgNPs. First the reaction conditions needed to be optimized, by testing different reducing agents, varying the pH and the ratio of Ag^+ to functional groups present in the reaction. The optimization studies were carried out in each case using the shortest peptide. Next we applied the optimized conditions in the formation reaction using also the longer derivatives.

We tested flexible derivatives of the designed additives to understand more about the role of the rigid backbone, we used in the stabilization of nanoparticles in defined size and shapes. We also evaluated the role of the linker between the functional group and the peptidic scaffold by testing peptides with and without a linker.

In our investigation, we also evaluated the possibility of using the additives as reducing agents by themselves and at the same time as stabilizing moieties. Therefore the formation reaction was carried out in the absence of an external reducing agent.

3.1.4.1. AgNP Formation in the Presence of Peptides Bearing Guanidine Moieties

3.1.4.1.1. Optimization of the Reaction Conditions: Peptide 22a

Investigation of guanidine-functionalized peptides **22a-c** and their ability to act as additives in the AgNP formation reaction required first the optimization of the reaction conditions. Ascorbic acid and sodium borohydride were chosen as external reducing agent, as they allowed us, to vary the strength of the reducing agent (chapter 1.2.2., 1.3.2.).[85, 87, 205] To find the optimal conditions for the formation reaction first, the reducing agents were tested and then the pH of the reaction and the ratio of Ag^+ to functional groups present in the reaction were varied.

Peptide **22a**, bearing two guanidine moieties, was used for the optimization of the reaction conditions. This peptide was the shortest peptide from the series, bearing two guanidine moieties, pointing in the same direction in space.

The evaluation of the external reducing agents showed, that well defined AgNPs were generated, using ascorbic acid, whereas aggregates formed, when the stronger reducing agent sodium borohydride was used. As a consequence, ascorbic acid was chosen as reducing agent, for the following experiments.

In the beginning a ratio of Ag^+ to guanidine groups of 1:5 was used with a silver concentration of 0.25 mM. Different studies reported in the literature described, an excess of additive to be

advantageous.[5, 43] Therefore this ratio seemed to be a reasonable starting point. Different pH values were tested, as they result in different protonation states of the entailed functional groups. We expected the pH, to have a significant influence on the binding strength of the additive to the silver and therefore on the ability for it to act as an additive.[102, 206] When the guanidine groups are not protonated, they can provide their electron lone pair, resulting in a stronger binding. If the functional group is protonated, it is positively charged and therefore repels the equally positively charged silver ions, which probably leads to a reduced control over the nanoparticle formation. By dissolving peptide **22a** in water, a solution with a pH around 9.6 was obtained. We also tested the reaction at pH 3, pH 11 and 12. Aqueous sodium hydroxide solution and nitric acid were used to adjust the pH. Then, $AgNO_3$ was dissolved and after 15 minutes of equilibration time, the reducing agent was added. The results are shown in Figure 55.

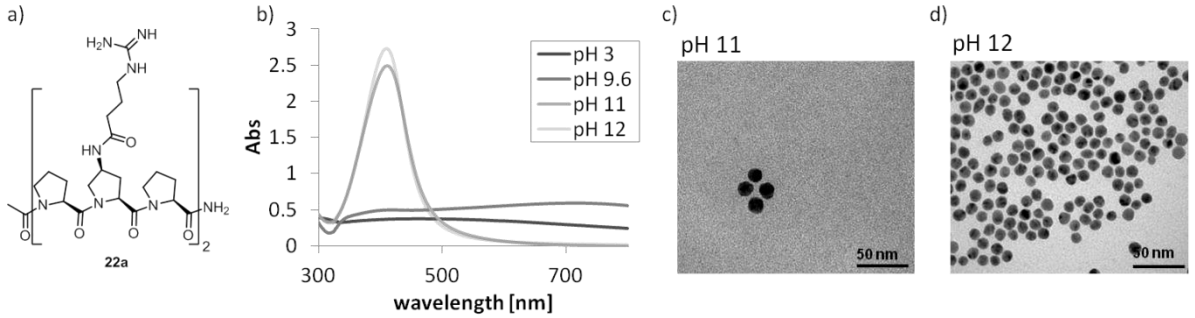

Figure 55: a) Peptide **22a**; formation of AgNPs in the presence of peptide **22a** at different pH values; **a)** UV-Vis spectra, **b)** TEM of AgNPs generated at pH 11, **c)** TEM of AgNPs generated at pH 12. Analysis was carried out after one day.

At pH 3 and pH 9.6, the formed AgNPs aggregated within one hour, which can be seen in the UV-Vis spectra. With increasing pH values, the stability of AgNPs increased. However a statistical evaluation showed that at pH 12, the distribution of the nanoparticle sizes was slightly narrower. To our delight, under these conditions and in the presence of peptide **22a**, monodisperse AgNPs were obtained. They were found to have a spherical shape with an average diameter of 12 nm and a narrow size distribution (12.0 nm ± 2.2), which was determined using transmission electron microscopy (TEM) (Figure 56).

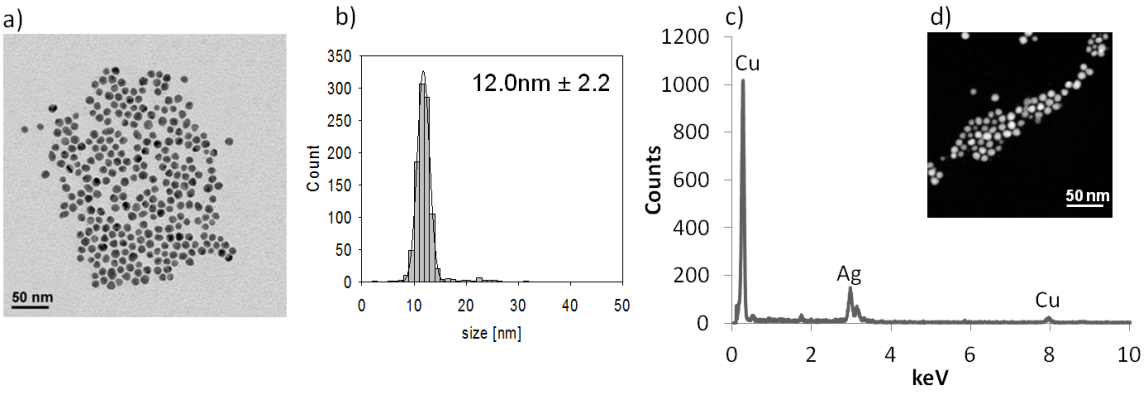

Figure 56: Formation of AgNPs generated in the presence of peptide **22a** with Ag^+ to functional group ratio of 1:5 at pH 12; **a)** TEM image, **b)** Histogram, **c)** EDX spectrum, **d)** STEM image. Analysis was carried out after one day.

In literature it is described that free Ag^+ is known to form Ag_2O at basic pH in aqueous solution.[207] As the formation takes place at basic pH, we tested if the resulting nanoparticles consisted of Ag (0) as it was intended, by energy dispersive X-ray (EDX) spectroscopy. It was shown that the nanoparticles consist of pure Ag (0) (Figure 56c). In the spectrum, silver peaks are observed and no oxygen peak. Copper peaks were originating from the copper grid on which the measurement was carried out. No Ag_2O was formed what suggests that Ag^+ was stabilized by binding with the peptide, preventing the oxide formation.

At the higher pH values tested, the guanidine group is protonated to a smaller extent. Using the Henderson-Hasselbalch equation (**1**) we calculated the degree of protonation.[208] If we assume that the pK_a value of the functional group is 12.48 like it is found in the corresponding amino acid arginine for the guanidine group, the functional group is to an extend of 69 % protonated at a pH of 12. At pH 11, the rate of protonation was increased to 97%.

$$pH = pK_a - log\frac{c[acid]}{c[base]} \qquad \textbf{(1)}$$

When the guanidine groups are not protonated, the free electron pairs can participate in the binding to the Ag (0), which might lead to a higher degree of control over the morphology of the nanoparticles. Additionally, the strength of the reducing agent, ascorbic acid, is increased at higher pH values, as the presence of the ascorbate anion is proposed to play a crucial role in the reduction process.[205, 209] This presumably facilitates the reduction of Ag^+ stabilized in aqueous solution by the guanidine moieties.

To test the influence of different peptide concentrations on the process, ratios of Ag^+ to guanidine groups of 1:1 and 1:10 were tested with a constant $AgNO_3$ concentration of 0.25 mM (Figure 57).

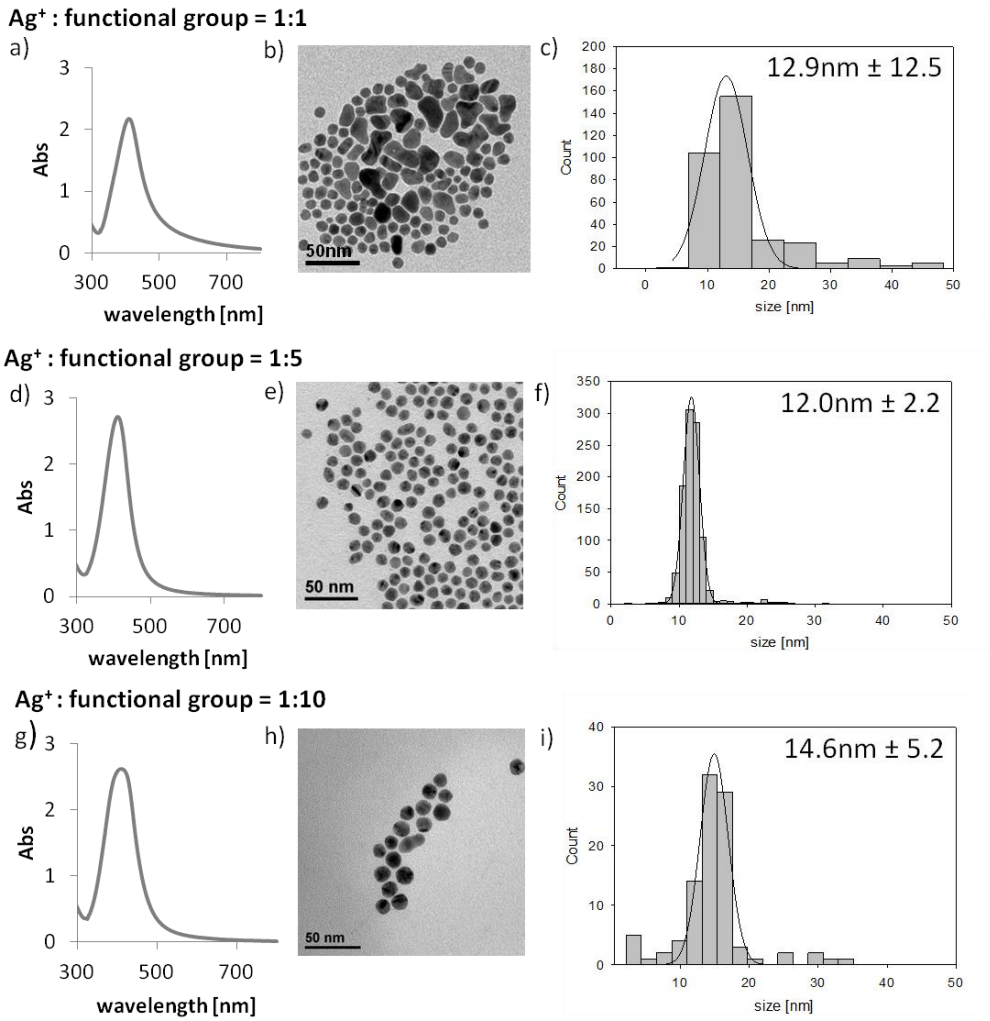

Figure 57: Formation of AgNPs generated in presence of peptide **22a** with ratio of Ag^+ to functional groups of 1:1 **a)** UV-Vis spectrum, **b)** TEM image, **c)** histogram; 1:5 **d)** UV-Vis spectrum, **e)** TEM image, **f)** histogram; and 1:10: **g)** UV-Vis spectrum, **h)** TEM image, **i)** histogram. Analysis was carried out after one day.

When a ratio of 1:1 was applied, the resulting AgNPs were polydisperse as shown in TEM (Figure 57b, c). Also when a ratio of 1:10 was used, the nanoparticles showed a broader size distribution compared to those generated in the presence of guanidine-functionalized peptide with a ratio of 1:5. These results prove that the ratio of Ag^+ to guanidine group of 1:5 is optimal for the AgNP generation. Below and above this, the resulting AgNPs were less stable or less monodisperse, respectively.

3.1.4.1.2. Testing Peptides of Different Lengths: 22a-c

With the optimized conditions for the generation of stable and monodisperse nanoparticles in the presence of guanidine-functionalized oligoprolines in hand, we next explored the influence of the peptide length on the resulting size and shape. Therefore we tested the formation reaction with an Ag^+ to guanidine group ratio of 1:5, at pH 12 using ascorbic acid as external reducing agent in the presence of peptides **22a-c**. The results are shown in Figure 58.

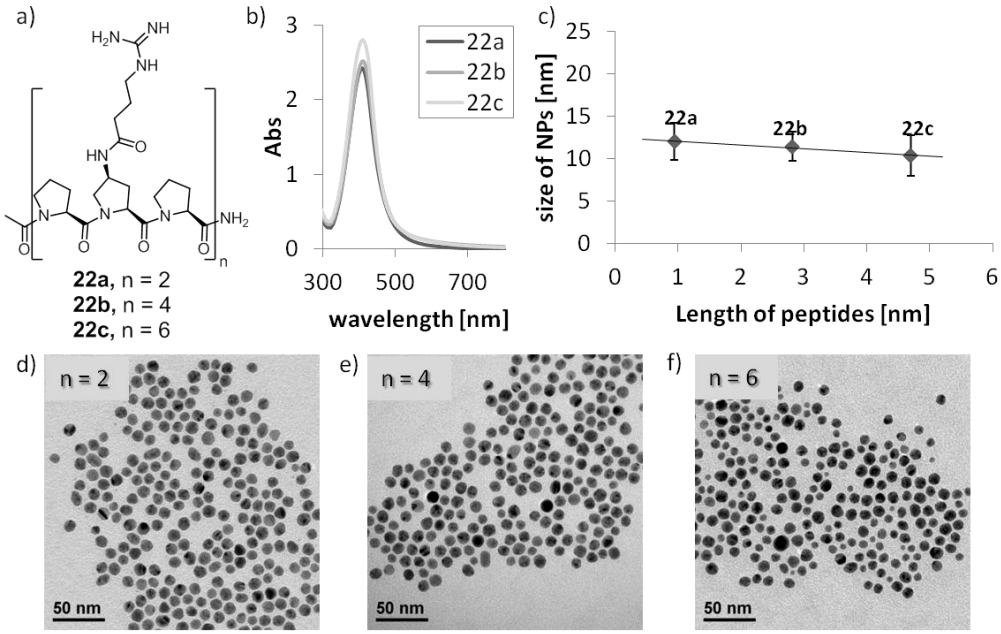

Figure 58: Formation of AgNPs in the presence of peptides **22a** (n = 2), **22b** (n = 4) and **22c** (n = 6): **a)** peptide **22a-c**, **b)** UV-Vis spectra, **c)** correlation between the length of peptides **22a-c** and the size of the resulting AgNPs, **d)** TEM image of AgNPs formed in presence of peptide **22a**, **e)** TEM image of AgNPs formed in presence of peptide **22b**, **f)** TEM image of AgNPs formed in presence of peptide **22c**. Analysis was carried out after one day.

Pleasingly, in the presence of all three different length of the guanidine-functionalized peptide (**22a-c**), monodisperse nanoparticles were formed (Figure 58). They all had an average diameter of 12 nm, demonstrating a minor influence of the length of the peptides to the morphology of the resulting AgNPs. It seems, as if there is a slight tendency for a decrease in size with increasing length of the peptide. But these variations are so small that the slope is negligible, taking the standard deviation into account. In case of guanidine-functionalized peptides **22a-c**, an increase in the amount of functional groups on the peptide had no significant influence on the size and shape of the resulting AgNPs. Two possible binding sites were sufficient to stabilize monodisperse AgNPs in defined size and shape.

The guanidine-functionalized oligoprolines proved to be able to act as additives in the AgNP formation reaction. The exact mechanism of stabilization is not yet understood, but the protonation state of the respective functional groups seems to be a very important factor. The nanoparticles were more stable if there was a higher degree of non protonated guanidine group present as observed in the pH dependent formation reactions. Therefore it seems likely that the binding ability is crucial for the controlled formation. Guanidine has a delocalized electron density which might be beneficial for the binding event. We also found that the ratio of the stabilizing moieties present during the reaction have a distinct influence on the size distribution of the resulting nanoparticles.

3.1.4.1.3. Testing the Importance of the Peptide Flexibility: Peptides 30a-c

An important feature of the design of the additives is the defined secondary structure provided by the oligoproline backbone. To test, whether the secondary structure was of any importance for the stabilization of AgNPs in a defined way, we tested flexible peptides **30a-c** as additives. They bear the same number of guanidine groups like the corresponding oligoproline counterparts **22a-c**, but lack a defined secondary structure (chapter 3.1.3) as evidenced by the CD spectroscopic studies. The flexible peptides were tested as additives in the formation reaction of AgNPs under the conditions optimized for the guanidine-functionalized oligoprolines **22a-c** (Figure 59). An Ag^+ to guanidine group ratio of 1:5 was used with a silver concentration of 0.25 mM at pH 12, with ascorbic acid as external reducing agent. The results are shown in Figure 59.

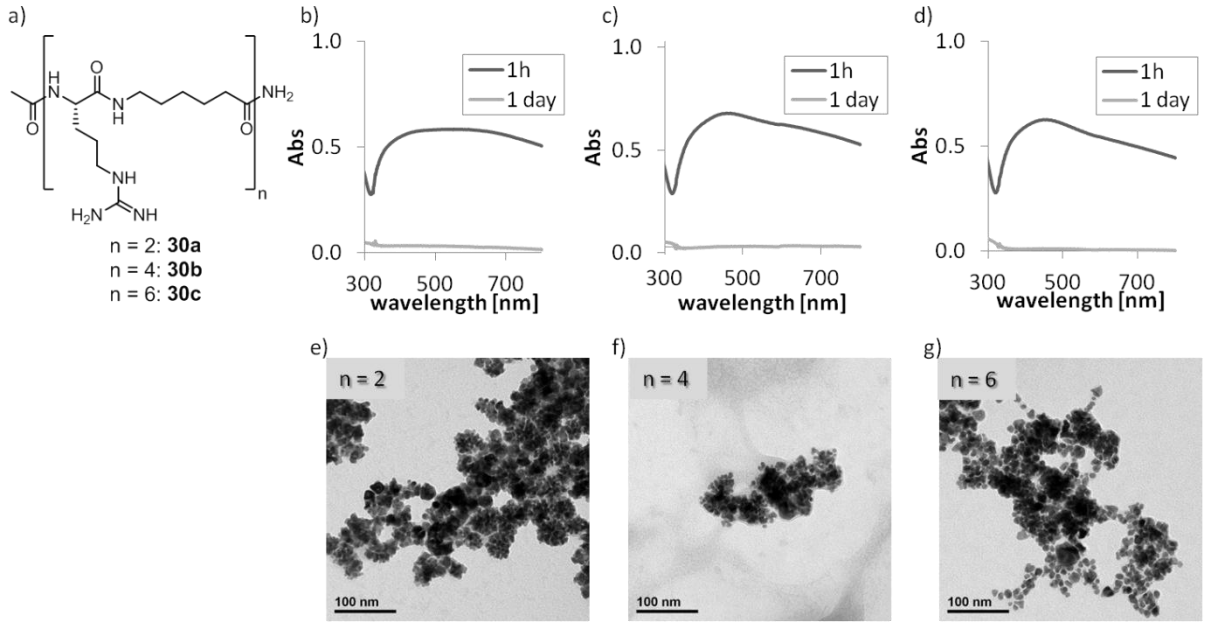

Figure 59: a) Peptides **30a-c**; formation of AgNPs in presence of peptides **30a**: **b)** UV-Vis spectra, **e)** TEM image; with peptide **30b c)** UV-Vis spectra, **f)** TEM image; with peptide **30c d)** UV-Vis spectra, **g)** TEM image. Analysis was carried out after one day.

The resulting nanoparticles were polydisperse and aggregated within one day as visualized by UV-Vis spectroscopy. Interestingly, these results clearly prove that the secondary structure is essential for the ability to act as additive.

3.1.4.1.4. Investigating the Importance of the Linker: Peptide 24a

The guanidine group is attached on the backbone by a linker in the peptides **22a-c**. To investigate the influence of the linker, peptides **24a-c** were evaluated. They bear guanidine groups like the peptides **22a-c**, but lack a linker between the oligoproline backbone and the functional group. To compare the results obtained with peptides **22a-c**, the same conditions found to be optimal for the generation process, were applied. An Ag^+ to guanidine group ratio of 1:5 at pH 12, with ascorbic acid as external reducing agent was used. The results are shown in Figure 60.

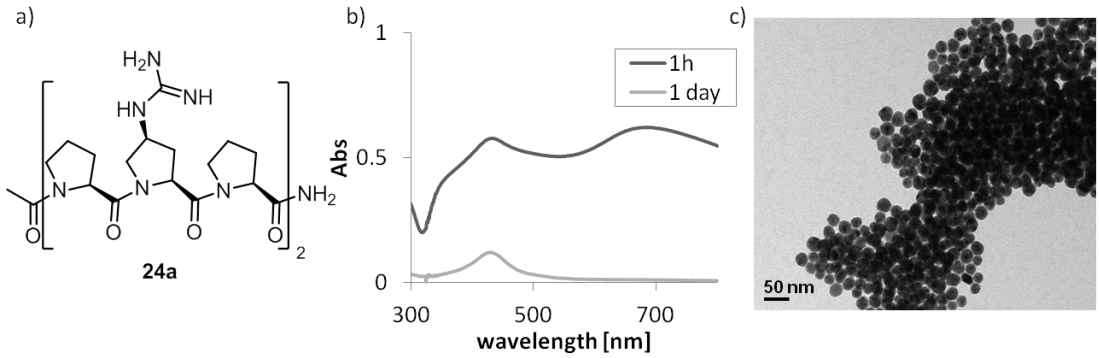

Figure 60: a) Peptide **24a;** formation of AgNPs in presence of peptide **24a**: **a)** UV-Vis spectra, **b)** TEM image. Analysis was carried out after one day.

The obtained AgNPs were bigger in size, than those obtained in the presence of peptide **22a-c** and aggregated within one day (Figure 60). Due to the fast aggregation, it was not possible to carry out a statistical evaluation of the average size. The formed AgNPs had a defined shape, judging from the TEM image, but the additive seems to provide insufficient stability to prevent aggregation. Concluding from these results, the additional flexibility of functional groups in peptides **22a-c** due to the linker is advantageous, when they act as an additive. Probably, this additional flexibility allows the functional group to be positioned in an optimal way for the binding and with this for the stabiliziation of the AgNPs in a defined size and shape.

3.1.4.1.5. Investigating the Role of the Additional Amide in the Linker: Peptide 31

To determine whether the amide bond connecting the functional groups to the backbone of the studied peptides had by itself an effect on the nanoparticle generation process, we tested peptide **31**. This oligoproline bears an acetylated aminoproline in every third position similar to the peptides bearing a functional group. The optimal conditions found for the guanidine-functionalized oligoproline **22a-c** were used in the nanoparticle formation reaction. An Ag^+ to amide group ratio of 1:5 with an $AgNO_3$ concentration of 0.25 mM, at pH 12 and ascorbic acid as external reducing agent were used.

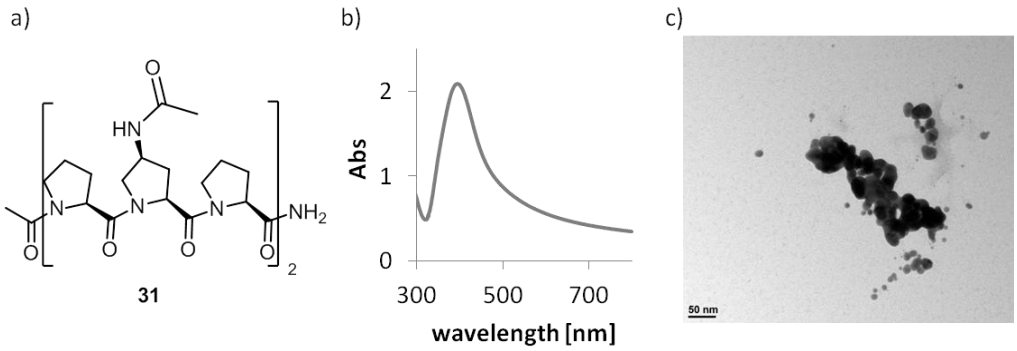

Figure 61: a) Peptide **31**; AgNPs formed in the presence of peptide **31**; **b)** UV-Vis spectra, **c)** TEM image of AgNPs formed in the presence of peptide **31**. Analysis was carried out after one hour.

Nanoparticles formation was observed (Figure 61). However, the nanoparticles were polydisperse in size and shape. Oligoproline **31** proved capable of stabilizing nanoparticles. However an additional functional group was crucial to form AgNPs in a defined size and shape.

3.1.4.1.6. Generation of AgNPs in the Presence of Peptide 22a-c without Additional Reducing Agent

The formation reaction without external reducing agent was carried out, to test if the guanidine-functionalized peptides **22a-c** were able to reduce silver ions by themselves and at the same time, still be able to stabilize the resulting nanoparticles. It was reported in previous studies, that nanoparticle generation was achieved, using amino acids and peptides without additional reducing agents (chapter 1.2.).[97, 101-102, 210-213] Especially the amino acids tyrosine and tryptophan, either on their own or incorporated into peptides, have been used for nanoparticles formation,[97, 102, 212] taking advantage of their redox potential. But also other amino acids, like arginine, aspartic acid, glutamic acid, and lysine were reported to be applicable in the reduction of metal salts, generating nanoparticles.[210-211, 213-214] Even though this approach was applied in several studies, the exact mechanism is not yet understood.

As before, we first tested different pH values, using a ratio of Ag^+ to functional group of 1:5, as it was found to be the best in the formation reaction with an external reducing agent. Dissolving peptide **22a** in H_2O resulted in a solution with a pH value of 9.6. We also tested solutions of pH 11 and pH 12 in the reaction. After addition of the $AgNO_3$ solution we monitored the reaction by UV-Vis spectroscopy, for up to three weeks.

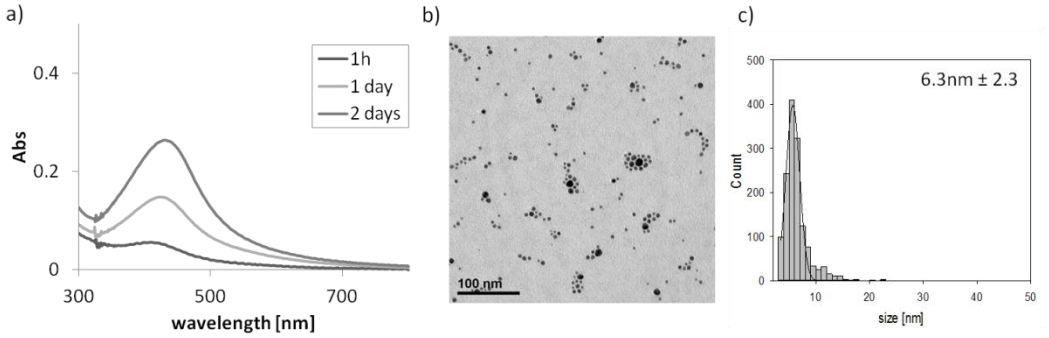

Figure 62: Formation of AgNPs generated in presence of peptide **22a** at pH 12 without reducing agent: **a)** UV-Vis spectra, **b)** TEM image, **c)** histogram. Analysis was carried out after one day.

At the two lower pH values, there was no AgNP formation observed. But at pH 12 nanoparticles were formed (Figure 62). They were smaller, than those generated with ascorbic acid as reducing agent, but also spherical in shape with an average diameter of 6.3 nm with a narrow dispersity. Interestingly, the resulting size in the case without an external reducing agent is about half the size, than those formed with ascorbic acid. Probably, the oxidized functional group had different stabilizing properties resulting in differently sized nanoparticles. The reduction only possible at higher pH values indicates that the hydroxyl ions took part in the reduction process by providing electrons for the reduction. Next, we tested the longer guanidine-functionalized peptides **22b** and **22c.**

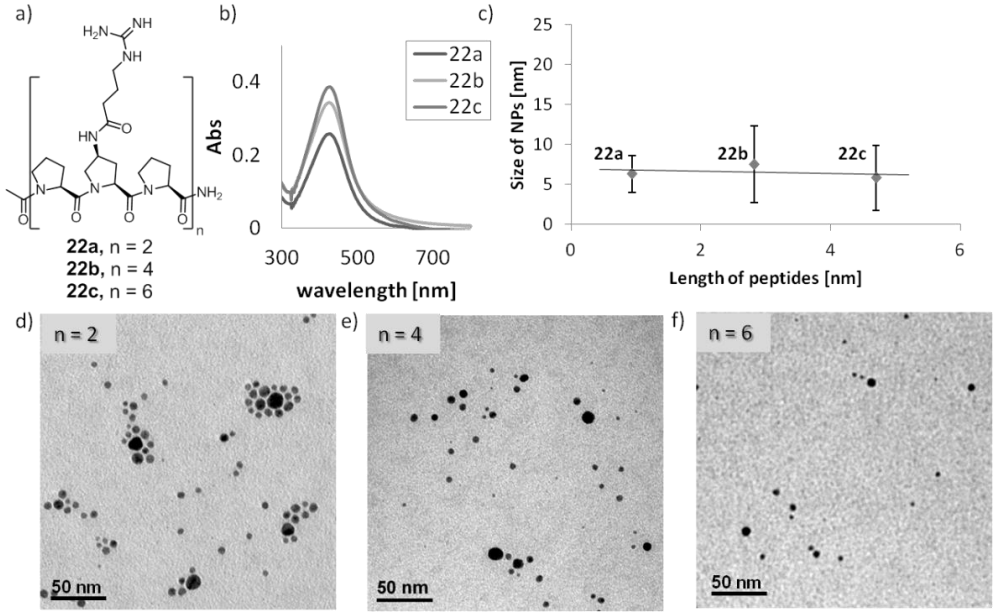

Figure 63: Formation of AgNPs in the presence of peptides **22a** (n = 2), **22b** (n = 4) and **22c** (n = 6) without additional reducing agent at pH 12: **a)** peptide **22a-c**, **b)** UV-Vis spectra, **c)** correlation between the length of peptides **22a-c** and the size of the resulting AgNPs, **d)** TEM image of AgNPs formed in presence of peptide **22a**, **e)** TEM image of AgNPs formed in presence of peptide **22b**, **f)** TEM image of AgNPs formed in presence of peptide **22c**. Analysis was carried out after one day.

These experiments resulted in about the same size of the AgNPs as obtained with peptide **22a**. However, the size distribution obtained is broader than found for the AgNPs formed in the reaction with additional reducing agent (Figure 58, Figure 63). The current state of our research does not provide yet a clear explanation for the mechanism of the reduction. Nevertheless, it is very interesting that it occurs only at higher pH values. It seems, that in the case of this peptide, the reductive capability is enhanced at higher pH values, as reduction occurred only at pH 12. This was also found for ascorbic acid, where the deprotonation is important for the reduction properties.[205, 209] The protonation state seems to be also very important for the ability to act as additive, for the guanidine-functionalized oligoprolines, when no external reducing agent was used. However, the resulting size distribution shows a higher dispersity which probably is due to a decreased binding ability of the oxidized functional group to the metal surface.

Recently, Lamani *et al* reported the application of different guanidine salts as catalysts for the reduction of olefins in presence of hydrazine.[215] Furthermore, Ishikawas study showed that a guanidine derivative was able to reduce DMSO to DMS.[216] These investigations further support our observation that this functional group displays a significant potential for the application as a reducing agent in a variety of systems.

3.1.4.2. AgNP Generation in the Presence of Peptides Bearing Imidazole Moieties

3.1.4.2.1. Optimization of the Reaction Conditions: Peptide 17a

After the investigation of guanidine-functionalized peptides **22a-c**, we also wanted to test the imidazole-functionalized peptides **17a-c** as additives in the AgNP formation reaction. Like before, this first required the optimization of reaction conditions to be performed. In preliminary experiments, we tested sodium borohydride and ascorbic acid as external reducing agents in the process. Using ascorbic acid as a reducing agent, no nanoparticles formation was observed, neither by UV-Vis nor by TEM. Therefore sodium borohydride was used in the following experiments, as AgNP generation was observed in presence of peptide **17a**. The need of a stronger reducing agent is probably due to the strong binding of Ag^+ to the imidazole group. Like reported in literature, the binding energy determined in the gas phase of the guanidine group to Ag^+ is stronger than the one of imidazole ($\Delta\Delta G°_{His}$ = 18 kcal/ mol, $\Delta\Delta G°_{Arg}$ >26.8 kcal/ mol).[189-191] However the values given are measured and calculated in the gas phase that do not consider the hydration of the functional group. This is expected to be considerable higher for guanidine than for imidazole.[217-218] This would explain the stronger binding and therefore the need of a stronger reducing agent. Since the experiments with guanidine-functionalized peptide **22a-c** had shown that an Ag^+ to functional group ratio of 1:5 is optimal (chapter 3.1.4.1), this ratio was used as a start for the optimization studies with the imidazole-functionalized oligoproline peptide **17a**. Also in this case, the 6mer oligoproline bearing two imidazole groups was used for the optimization of the formation conditions. First the influence of pH on the reaction was tested. When the peptide was dissolved in water, a solution with pH 9 was obtained. Analogous to guanidine-functionalized peptides **22a-c** the nanoparticle formation was furthermore tested at pH 3, pH 11 and pH 12 (Figure 64). After adjustment of the pH of the peptide solution, $AgNO_3$ was dissolved and the mixture was equilibrated for 15 minutes before the reducing agent was added.

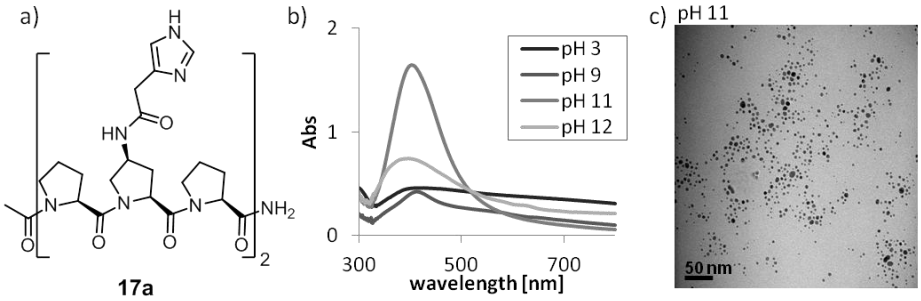

Figure 64: AgNPs generated in presence of peptide **17a** at different pH values; **a)** peptide **17a**; **b)** UV-Vis spectra, **c)** TEM image of AgNPs formed at pH 11. Analysis was carried out after one day.

At pH 3 the AgNPs aggregated within one hour as observed by UV-Vis. Only large aggregates were found in TEM. The nanoparticles obtained at pH 9 and pH 12 were polydisperse and in UV-Vis spectra a broad plasmon resonance was detected (Figure 64b). Pleasingly, nanoparticles generated at pH 11 were monodisperse with an average diameter of 4 nm and spherical in shape, as observed by TEM (Figure 64, Figure 65). These nanoparticles were much smaller than those formed in the presence of the guanidine-functionalized peptides **22a-c**.

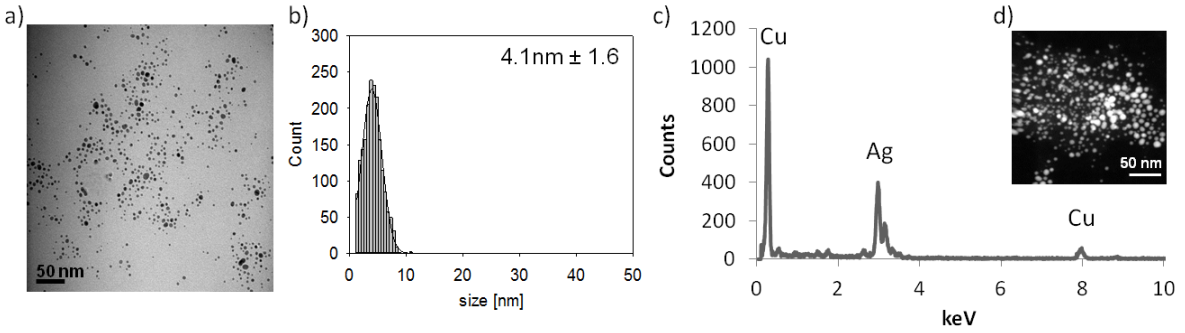

Figure 65: AgNPs generated with peptide **17a** with Ag^+ to functional group ratio of 1:5 at pH 11; **a)** TEM image, **b)** Histogram, **c)** EDX spectrum, **d)** STEM image. Analysis was carried out after one day.

To confirm the oxidation state of the nanoparticles, we performed EDX measurement. We found that also in this case the nanoparticles consisted of pure Ag (0) and no Ag_2O was formed like it was found before in (Figure 65c). The copper peaks were observed due to the measurement on a copper grid. The imidazole groups have a lower basicity compared to guanidine residues present in compounds **22a-c**. Therefore at pH 11 the imidazole group is predominantly non-protonated. If we assume that the pK_a value of the imidazole group is about the same like in histidine (pK_a = 6.04), at pH 11 the imidazole is not protonated, according to the Henderson-Hasselbalch equation **(1)** (chapter 3.1.4.1.1). The results of our experiments for the imidazole-functionalized as well as for the guanidine-functionalized peptides suggest that the free electron pair needs to be available for the stabilization of Ag^+ in order to obtain monodisperse AgNPs. However, the nanoparticles obtained at pH 12 were polydisperse in size and shape. A higher pH value was not advantageous and may even hamper the stabilization of the AgNPs in defined size and shape, probably due to the presence of an increased amount of hydroxy groups in solution.

To evaluate the influence of the different quantities of the additive in the generation process, we varied the Ag^+ to imidazol group ratio (from 1:5 to 1:1 and 1:10 (Figure 66)).

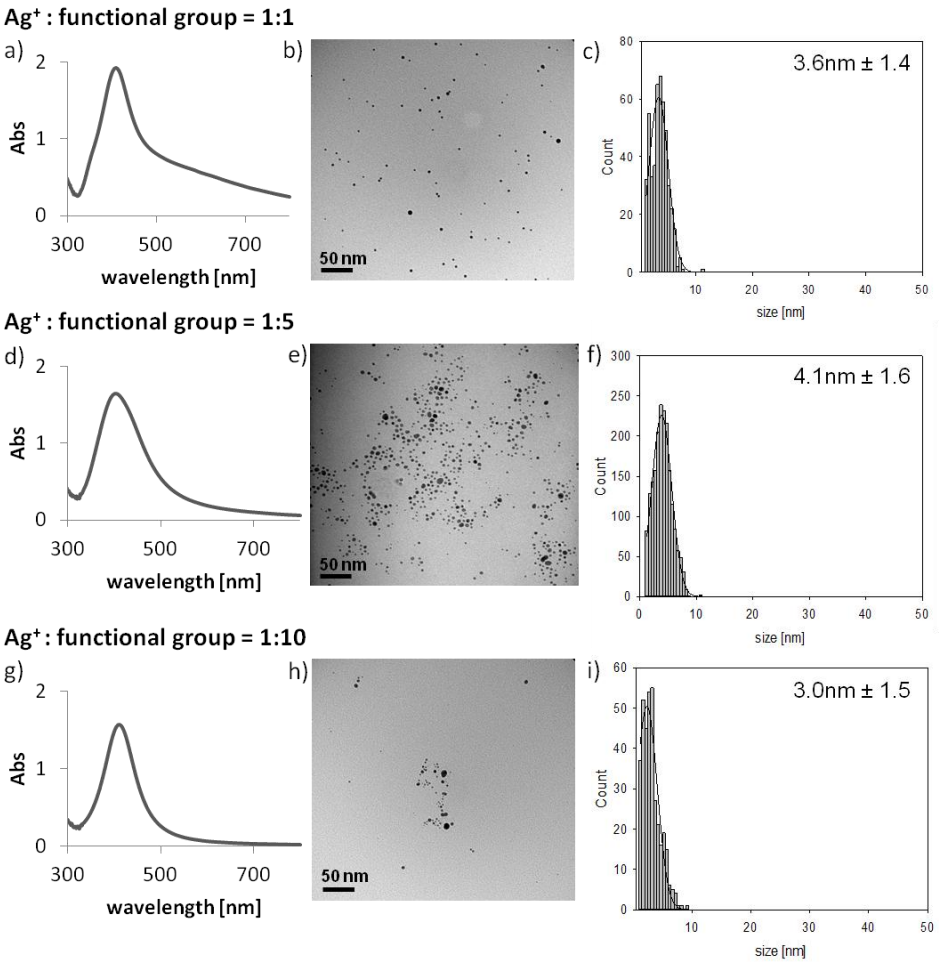

Figure 66: AgNPs formed in presence of peptide **17a** with ratios of Ag^+ to functional group ratio of 1:1 **a)** UV-Vis spectrum, **b)** TEM image, **c)** histogram; of 1:5 **d)** UV-Vis spectrum, **e)** TEM image, **f)** histogram; and of 1:10 **g)** UV-Vis spectrum, **h)** TEM image, **i)** histogram. Analysis was carried out after one day.

The increase as well as the decrease of the peptide concentration led to a slight decrease in nanoparticle stability. Furthermore the size distribution was also a bit broader than in the originally used ratio (Figure 66). Therefore in the further reaction a ratio of 1:5 of Ag^+ to imidazole groups, at pH 11 with sodium borohydride were used.

The formation reaction resulted in monodisperse, spherical nanoparticles. Like the guanidine group, the imidazole group is a basic moiety, which is probably advantageous for the stabilization of the AgNPs. The differences in sizes, comparing the AgNPs resulting from the generation with guanidine-functionalized peptides **22a-c** and with imidazole-functionalized peptide **17a** suggest a different stabilizing mechanism. However, also different reducing agents were used which probably had an influence on the growing of the particles.

3.1.4.2.2. Testing Peptides of Different Lengths: Peptides 17a-c

Having developed optimal conditions for nanoparticle formation with imidazole-functionalized peptide **17a**, also the longer peptides **17b** and **17c** were applied as additives in the formation of AgNPs (Figure 67). An Ag^+ to imidazole group ratio of 1:5, at pH 11 with sodium borohydride as external reducing agent was used.

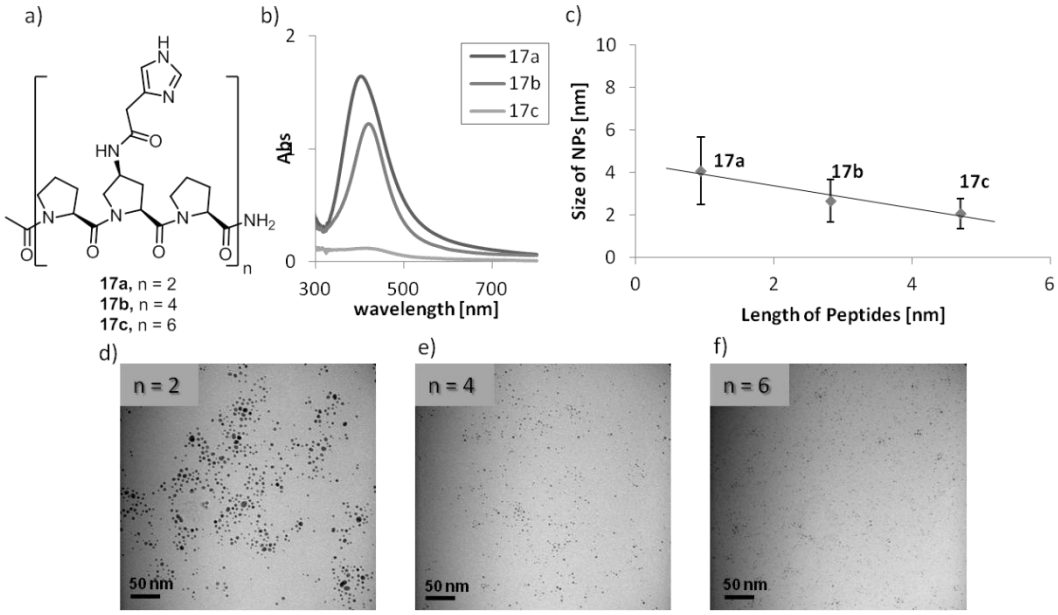

Figure 67: Formation of AgNPs with peptides **17a** (n = 2), **17b** (n = 4), **17c** (n = 6): **a)** peptides **17a-c**, **b)** UV-Vis spectra, **c)** correlation between the length of peptides **17a-c** and the size of the resulting AgNPs, **d)** TEM image of AgNPs formed in the presence of peptide **17a**, **e)** TEM image of AgNPs formed in the presence of peptide **17b**, **f)** TEM image of AgNPs formed in the presence of peptide **17c**. Analysis was carried out after one day.

With all three lengths of the imidazole-functionalized oligoprolines used as additives monodisperse, spherical AgNPs were formed with an average diameter of 4 nm (Figure 67). The UV-Vis absorption intensity decreases with increasing length of the peptides used as additive (Figure 67b). This reflects a smaller concentration of formed nanoparticles. It seems like the reduction efficiency is decreased with increased length of the peptide used as additive. However, the difference in length of the additive had no significant effect on the resulting size of nanoparticles. They were about the same as the ones obtained with peptide **17a** bearing two imidazole moieties. Two functional groups seemed to be sufficient for the stabilization of monodisperse nanoparticles under optimized conditions. These results are consistent with the results obtained for the previous investigated peptide where similar observations were made. It appears that there is a slight negative slope in the graph

correlating the size of the nanoparticles and the length of the peptide. However, these variations are in the range of the standard deviations and the slope can be neglected.

3.1.4.2.3. Testing the Importance of Peptide Flexibility: Peptides 29a-c

To evaluate the importance of the oligoproline backbone of the studied imidazole-functionalized additives, we prepared like before in the investigation for the guanidine-functionalized peptides **22a-c**, the flexible peptides **29a-c.** The imidazole groups were provided by histidines which were connected by aminohexanoic acids units. They bear the same number of imidazole moieties as in peptides **17a-c**, but adopt a random coil structure as shown by CD spectroscopy (Figure 54). Peptide **29a** was tested in the process of AgNP generation under the same conditions as found optimal for peptides **17a-c** which was an Ag^+ to imidazole ratio of 1:5 at pH 11 with sodium borohydride as external reducing agent (Figure 68).

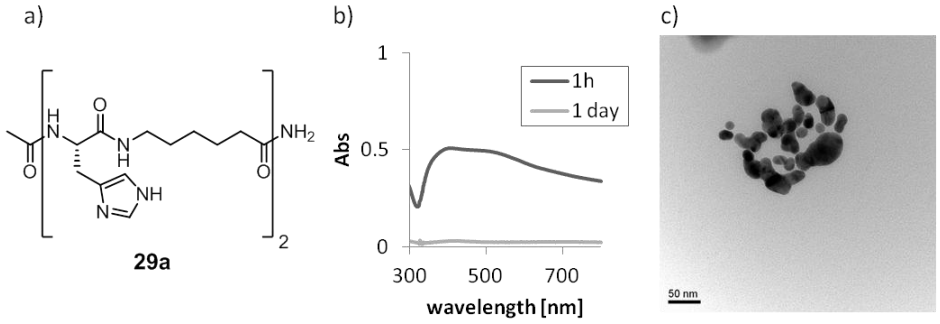

Figure 68: a) peptide **29a**; AgNPs generated in the presence of peptide **29a**: **b)** UV-Vis spectra, **c)** TEM image. Analysis was carried out after one day.

Only polydisperse nanoparticles were formed, which aggregated within one day (Figure 68). The flexible peptides bearing the investigated functional group were not able to stabilize the nanoparticles in a defined size and shape. Pleasingly, the study confirmed that the rigid structure of the backbone is a crucial factor that needs to be considered when designing a peptidic additive as it was found for guanidine-functionalized peptides **22a-c** and their flexible derivatives **30a-c**.

3.1.4.2.4. Investigating the Role of the Additional Amide in the Linker: Peptide 31

Using the imidazole-functionalized peptide **17a-c** required the application of the stronger reducing agent sodium borohydride. We therefore wanted to determine, whether the amide bond connecting the functional groups to the backbone of the studied peptides has by itself an effect on the nanoparticle generation process under the optimized conditions. To do this, we carried out the formation reaction using peptide **31** bearing an acetylated aminoproline in every third position, as

additive. We used an Ag^+ to functional group ratio of 1:5, at pH 11 with sodium borohydride as external reducing agent.

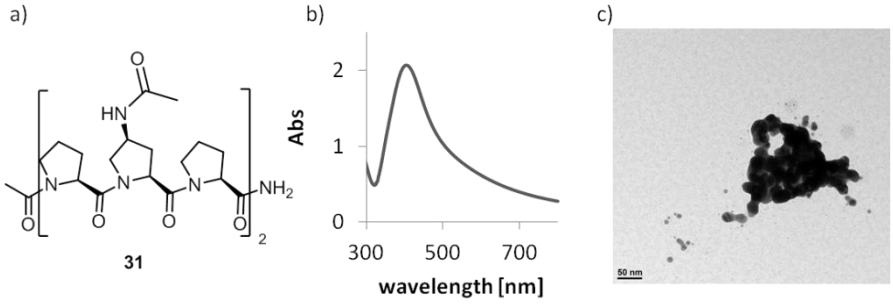

Figure 69: a) Peptide **31;** AgNPs formed in the presence of peptide **31** using sodium borohydride at pH 11; **b)** UV-Vis spectra, **c)** TEM image of. Analysis was carried out after one hour.

Nanoparticles formation was observed in presence of peptide **31** (Figure 69). However, they were polydisperse in size and shape. In agreement with the results obtained before, when ascorbic acid was used as external reducing agent (chapter 3.1.4.1.5), oligoproline **31** proved capable of stabilizing nanoparticles. However, these results underline the conclusion that a suitable functional group is crucial to form AgNPs in a defined size and shape.

3.1.4.2.5. Generation of AgNPs in the Presence of Peptide 17a-c without Additional Reducing Agent

In chapter 3.1.4.1.6 we described for the guanidine-functionalized peptides **22a-c**, the possibility of achieving nanoparticle formation without an additional reducing agent. Therefore, we tested the formation reaction also with the imidazole-functionalized peptides **17a-c** in absence of an external reducing agent. The reaction was performed at different pH values (pH 9, pH 11 and pH 12) and with different Ag^+ to imidazole ratios (1:1, 1:5, 1:10). Nevertheless, nanoparticle formation was not observed, neither by UV-Vis nor by TEM, even after two weeks time. One possible reason is the high binding affinity of imidazole to Ag^+, which also made it necessary to use a stronger reducing agent - sodium borohydride, in the previous investigation, and which here probably inhibits the reduction of Ag^+ by the peptide.

3.1.4.3. AgNP Generation in the Presence of Peptides Bearing Primary Amine Moieties

3.1.4.3.1. Optimization of the Reaction Conditions: Peptide 21a

The next peptides we tested for its ability to act as additive in the formation reaction were the amine-functionalized peptides **21a-c**. As it was found to be crucial to optimize the reaction conditions for the previous investigated peptides, we also started with the evaluation of the optimal reaction conditions.

Preliminary tests showed, that when sodium borohydride was used as external reducing agent, the resulting AgNPs aggregated within minutes. Applying ascorbic acid instead, resulted in stable nanoparticles, therefore this reducing agent was used. Initially a ratio of Ag^+ to amino groups of 1:5 was used, as it was found to give the best results for the previously studied peptides.

Again, different pH values were tested. Peptide **21a**, bearing two primary amino groups on the backbone was used for the optimization of the reaction conditions. When it was dissolved in water, it resulted in a solution with pH 9.5. In addition to that we also screened the reaction at pH 3, pH 11 and 12. The results are shown in Figure 70.

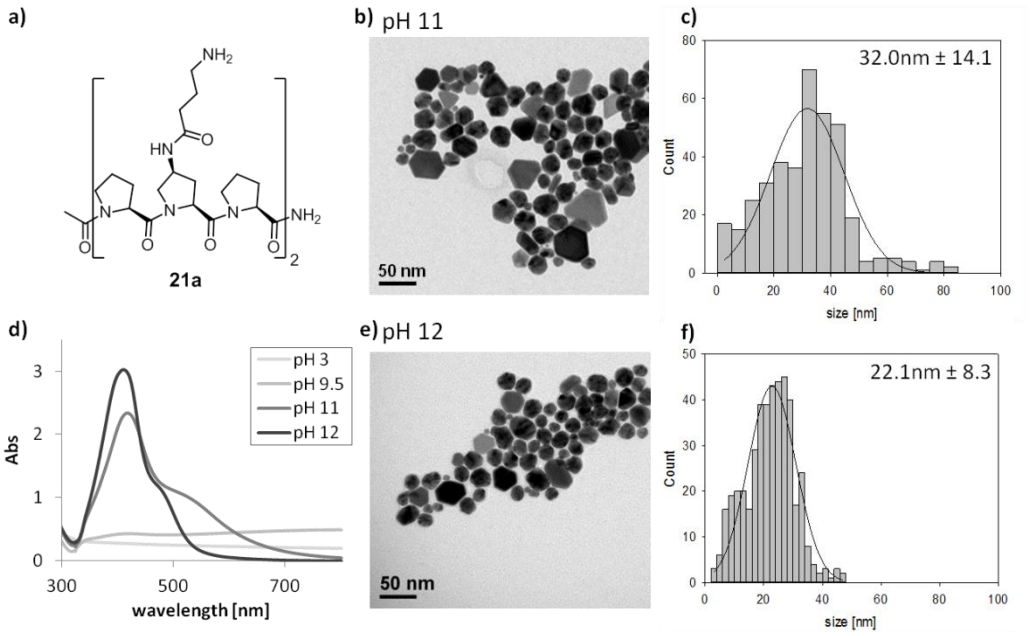

Figure 70: a) Peptide **21a**; AgNPs generated in presence of peptide **21a** at different pH values; AgNPs formed at pH 11: **b)** TEM image; **c)** histogram; **d)** UV-Vis spectra; AgNPs formed at pH 12: **e)** TEM image, **f)** histogram. Analysis was carried out after one day.

No nanoparticle formation occurred in the reaction performed at pH 3. A small plasmon absorbance was detected in UV-Vis at pH 9.5, which disappeared within one hour. AgNPs with an average diameter of about 32 nm formed at pH 11 and of about 22 nm at pH 12. Their morphology varied

from almost spherical to hexagons as well as truncated triangles. This results were very different to the shapes resulted with the previous investigated peptides used as additives where we found spherical shapes. The diversity in morphology caused a rather broad size distribution in both cases. A characteristic shoulder appeared in the UV-Vis spectrum which is indicative of a non-spherical shape formation. The size distribution of the resulting AgNPs was slightly narrower at pH 12, why the following experiments were carried out at this pH. Again we performed EDX measurement to confirm that only Ag (0) was formed and that no Ag_2O formation occurred (Figure 71). As observed for the AgNPs generated in the presence of guanidine-functionalized peptides **22a-c** and imidazole-functionalized peptides **17a-c** copper peaks are observed due to the copper grid on which the sample was applied for the measurements (Figure 71).

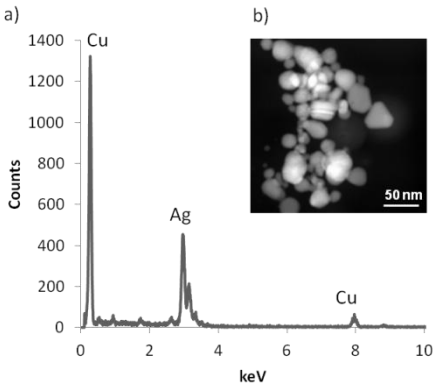

Figure 71: a) EDX spectrum for AgNPs formed at pH 12 in presence of peptide **21a**, **b)** STEM image. Analysis was carried out after one day.

To test, whether by variation of the peptide concentration, AgNPs with a more narrow size and shape distribution can be obtained, Ag^+ to amino group ratios of 1:1 and 1:10 were used (Figure 72).

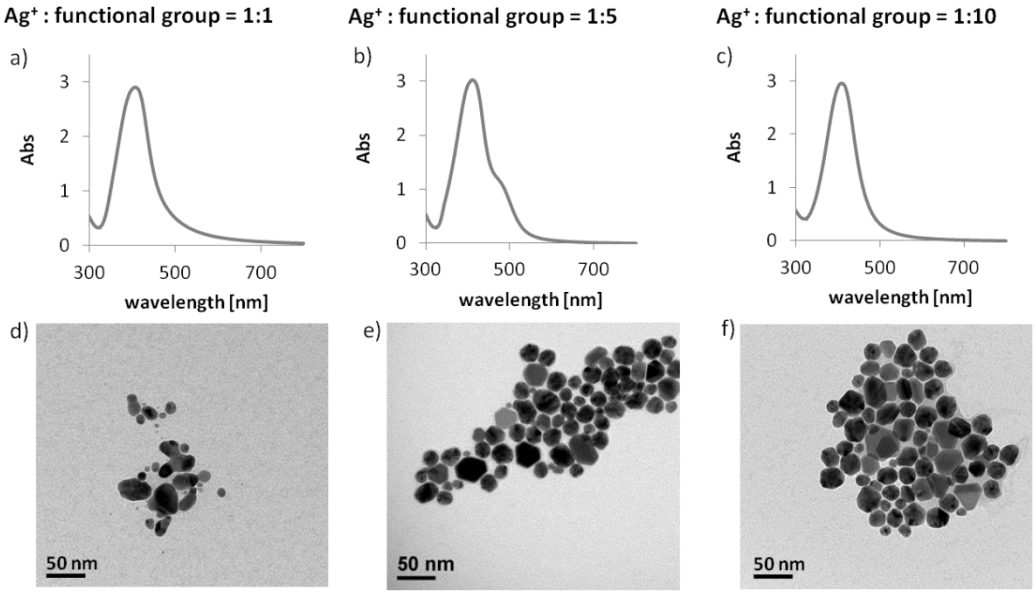

Figure 72: AgNPs generated in presence of peptide **21a** at different ratios of Ag^+ to functional groups; 1:1: **a)** UV-Vis spectrum, **d)** TEM image; 1:5: **b)** UV-Vis spectrum, **e)** TEM image; 1:10: **c)** UV-Vis spectrum, **f)** TEM image. Analysis was carried out after one day.

When a ratio of 1:1 was used, the nanoparticles were less stable and showed a high tendency to aggregate (Figure 72a, d). Ratios of 1:5 and 1:10 both led to AgNPs of very similar morphologies. But at a ratio of 1:10 there was not hexagonal shape observed. The obtained shapes showed a rather undefined morphology. The stability decreased with increasing peptide concentration and aggregation of the nanoparticles occurred like it was found before, for the other investigated peptides.

These results suggest that the primary amino functionalities on the peptide backbone provide insufficient stabilization to achieve a narrow size and shape distribution. Interestingly, the moiety seems to support anisotropic growth, resulting in the non-spherical shapes observed. This tendency is also not directed to one shape. Therefore this functional group probably is not optimal for the formation of defined sizes and shapes.

3.1.4.3.2. Testing Peptides of Different Lengths: Peptides 21a-c

Even though the formation reaction using amine-functionalized peptide **21a** did not resulted in nanoparticles with a narrow size distribution, the formation reaction was also tested in the presence of the longer amine-functionalized peptides **21b** and **21c**. The same conditions, found to be best for the formation of AgNPs in the presence of the amine-functionalized peptide **21a** were applied. The

nanoparticles were generated, using a ratio of Ag^+ to amino groups of 1:5, at pH 12 with ascorbic acid as reducing agent (Figure 73).

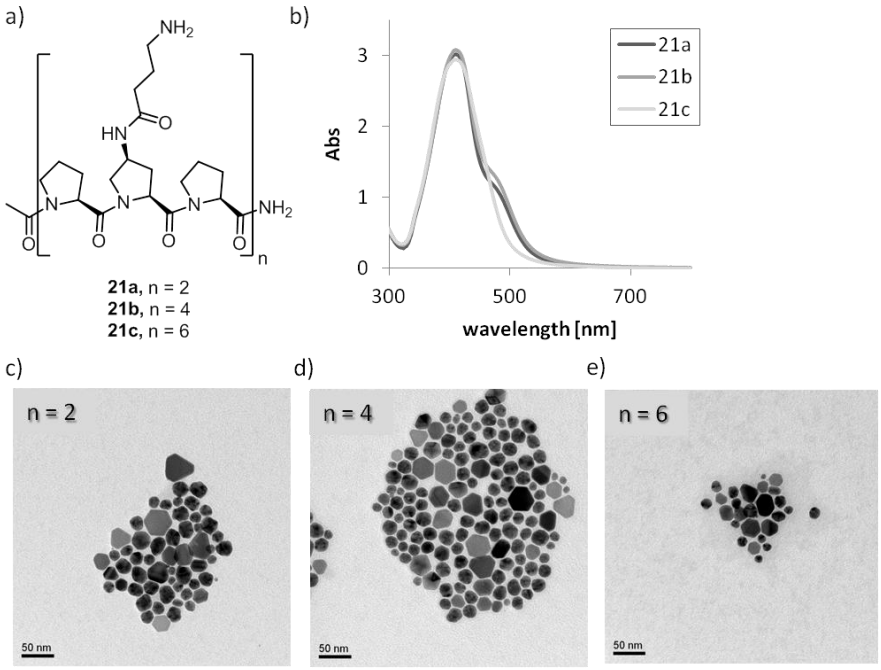

Figure 73: a) Peptides **21-c**; AgNPs generated in the presence of peptides **21a-c**: **b)** UV-Vis spectra, **c)** TEM image of AgNPs generated in the presence of peptide **21a**; **d** TEM image of AgNPs generated in the presence of peptide **21b**; **e)** TEM image of AgNPs generated in the presence of peptide **21c**. Analysis was carried out after one day.

The resulting AgNPs, formed in the presence of all three length of the amine-functionalized oligoprolines **21a-c** were non-spherical in shape and had an average diameter of 22 nm.

The screening of the length of the additives led to similar conclusions as in the case of guanidine-functionalized peptides **22a-c** and imidazole-functionalized peptides **17a-c** (chapter 3.1.4.1.2 and 3.1.4.2.2 respectively). The properties of resulting nanoparticles did not differ significantly from those obtained with the shortest peptide in the series (**21a)**. They displayed the same morphology as well as the same broad size distribution. These findings allowed us to draw the conclusion that in this system the nature of the functional groups in the additive is the size and shape determining factor.

3.1.4.3.3. Investigating the Importance of the Linker: Peptide 23a

Similar to the study presented in 3.1.4.1.4 for the guanidine-functionalized peptides, we synthesized peptides **23a-c** with the amino-groups directly attached to the backbone of the peptide, to investigate the influence of the linker in the formation reaction. In peptides **23a-c** aminoproline is incorporated in every third position in the peptide sequence. The same conditions, as used for

amino-functionalized peptides **21a-c** were applied in the generation reactions to be able to directly compare the obtained results. An Ag^+ to amino-group ratio of 1:5, at pH 12 with ascorbic acid as reducing agent was used.

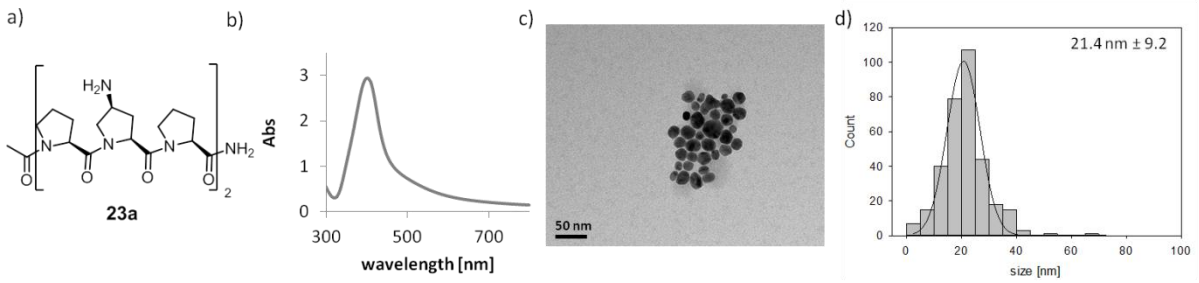

Figure 74: a) Peptide **23a**; AgNPs generated in presence of peptide **23a**: **b)** UV-Vis spectrum, **c)** TEM image, **d)** histogram. Analysis was carried out after one day.

As can be seen in Figure 74, the resulting AgNPs were about the same in size and shape compared to those, generated with amine-functionalized peptides **21a-c** which have a linker between the functional group and the backbone (Figure 70d-e) using the same reaction conditions. The resulting nanoparticles were about 21 nm in size and different shapes were observed. However the different shapes did not form in such pronounced way, as observed for the amine-functionalized peptide with the linker. Maybe the additional flexibility coming from the linker is helping the formation of the different shapes as observed in the presence of peptide **21a-c**.

These results are very different to those obtained in the comparative study of guanidine-functionalized peptides **22a-c** and peptides **24a-c** where the resulting nanoparticles were monodisperse in the presence of the peptide with linker and aggregated in the presence of the peptide without the linker (chapter 3.1.4.1.4). This may also be due to the fact, that the amino group in the additive is under the investigated conditions not able to stabilize monodisperse nanoparticles. Therefore a variation of the linker in these particular amine-functionalized peptides does not affect the size and shape of the resulting nanoparticles in such drastic way.

3.1.4.3.4. Generation of AgNPs in the Presence of Peptide 21a-c without Additional Reducing Agent

As in the case of previously studied compounds, we also tested the possibility of achieving nanoparticle formation using amine-functionalized peptides **21a-c** in the absence of an external reducing agent. We performed the reaction at different pH values (pH 9, pH 11 and pH 12) using an Ag^+ to amine group ratio of 1:5 and the test were carried out using the shortest amine-functionlized peptide **21a**.

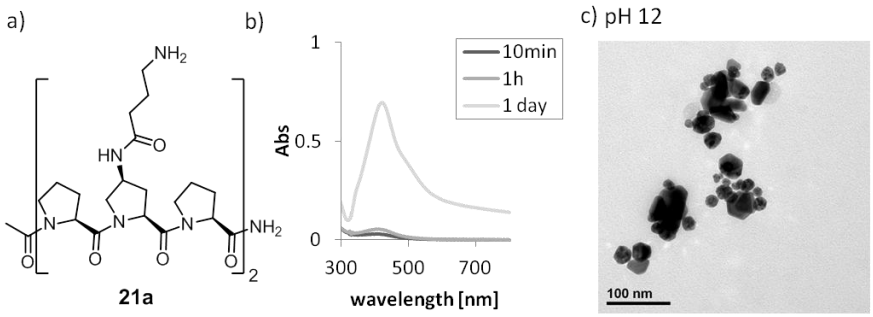

Figure 75: a) Peptide **21a**; AgNPs generation in presence of peptide **21a** without additional reducing agent: **b)** UV-Vis spectra, **b)** TEM image of AgNPs formed at pH 12. Analysis was carried out after one day.

Nanoparticle formation with peptide **21a** was observed only at pH 12 similarly to the findings for peptide **22** (Figure 75). The resulting nanoparticles were polydisperse and started to aggregate within one day. This showed that reduction of Ag^+ with the primary amino functionalities attached to the oligoproline backbone is possible. Similar observation has already been reported for lysine, the amino acid bearing a primary amino group, just like the designed peptides **21a-c**.[213] However, microwave radiation was necessary to activate the reaction, whereas in our case, room temperature was sufficient to achieve reduction of the Ag^+ ions. Even though the peptide was able to reduce Ag^+, it was unfortunately not able to additionally stabilize the resulting nanoparticles in a defined size and shape. Possibly the oxidation product of the peptide is disturbing the stabilization of the nanoparticles.

3.1.4.4. AgNP Generation in the Presence of Peptides Bearing Carboxylic Acid Moieties

3.1.4.4.1. Optimization of the Reaction Conditions: Peptide 18a

The next peptides we evaluated were oligoprolines **18a-c**, functionalized with carboxylic acid moieties to act as additives in the AgNP formation. After the evaluation of the peptides bearing basic nitrogen containing groups, these peptides were expected to have different properties. These peptides were the same, which developed during the formation reaction using the Tollens reaction and which stabilized the resulting AgNPs in defined sizes and shapes reported before in our group.[78] The formation reaction which was intended to be used here was different to the Tollens reaction. Therefore, we again first screened for the optimal conditions.

A ratio of Ag^+ to carboxylic acid moiety of 1:5 was used in the beginning, like in the investigations for the other peptides before. In initial experiments we tested ascorbic acid and sodium borohydride as external reducing agents. Using sodium borohydride resulted in fast aggregation of the formed nanoparticles. When ascorbic acid was utilized, more stable nanoparticles were formed. Therefore ascorbic acid was used in the following experiments as external reducing agent.

Different pH values in the reaction were tested (Figure 76). Dissolving the peptide in water resulted in a solution with a pH value of 4. Additionally the reaction was investigated at pH 10 and pH 12. After adjustment of the pH, $AgNO_3$ was dissolved. The mixture was equilibrated for 15 minutes before ascorbic acid was added.

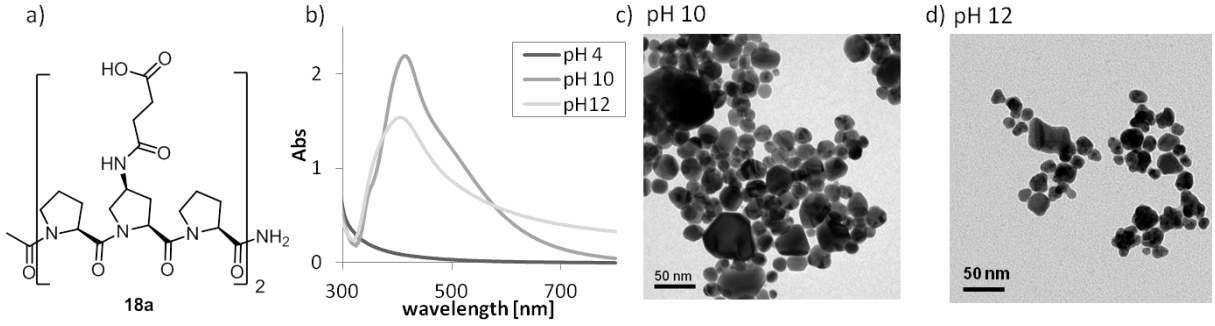

Figure 76: a) Peptide **18a**; AgNPs formed in presence of peptide **18a** at different pH values: **b)** UV-Vis spectra, **c)** TEM image (pH 10), **d)** TEM image (pH 12). Analysis was carried out after one day.

Formation of AgNPs was not achieved at pH 4. When the reaction was carried out at pH 10 and pH 12, nanoparticle generation was observed. However the nanoparticles were polydisperse in size and shape and aggregated within one day (Figure 76).

Peptides **18a-c**, bearing carboxylic acid moieties were successful in stabilizing nanoparticles in the previously reported system where nanoparticle formation was achieved *via* an *in situ* reduction of

aldehyde moieties attached on the backbone.[78] In the course of the reaction, the carboxylic acid moieties were formed which were able to stabilize the AgNPs at the same time when the silver ions were reduced resulting in nanoparticles in defined sizes and shapes. With the external reducing agent, we used in these experiments, the peptides were not able to stabilize the nanoparticles.

Therefore, we attempted to form AgNPs using the Tollens reaction in the studied system. Several aldehydes were tested as potential reducing agents: acetaldehyde, formic acid and formaldehyde. According to the reaction stoichiometry two Ag^+ ions are reduced when one aldehyde moiety is oxidized. Therefore a ratio of Ag^+ to reducing agent of 2:1 was used, as it was already found to be optimal in the previous reported system.[78] The same Ag^+ to peptide bound carboxylic acid ratio was applied. In the course of the reaction, initially a $[Ag(NH_3)_2]^+$ complex is formed by treating $AgNO_3$ with NH_4OH solution. The Ag^+ is then reduced to Ag (0), whereas the aldehyde or formic acid was oxidized to the corresponding carboxylic acid or CO_2 respectively. The results obtained with the different reducing agents are shown in Figure 77.

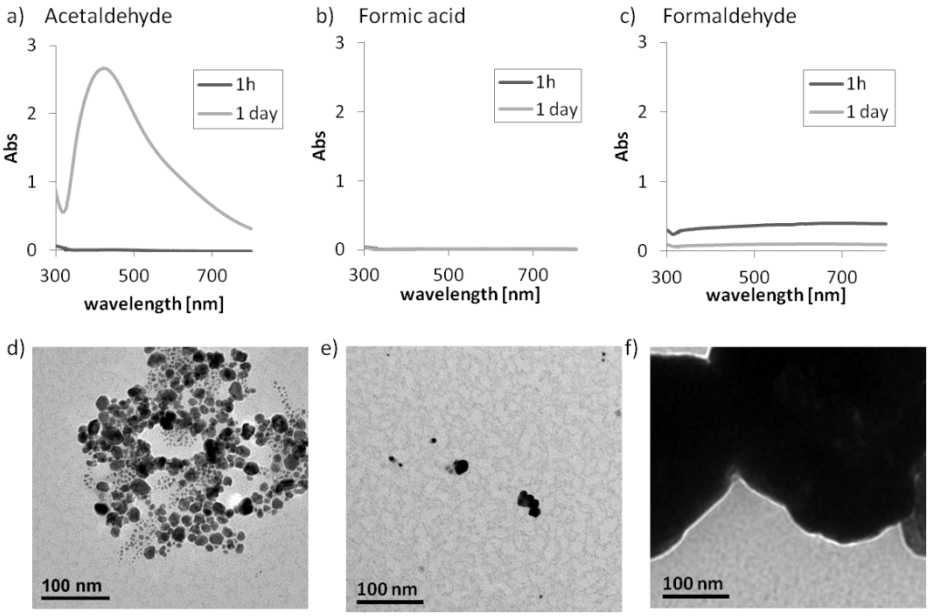

Figure 77: AgNPs generated in the presence of peptide **18a** under Tollens conditions with different reducing agents; Acetaldehyde: **a)** UV-Vis spectra, **d)** TEM image; Formic acid: **b)** UV-Vis spectra, **e)** TEM image; Formaldehyde: **c)** UV-Vis spectra, **f)** TEM image. Analysis was carried out after one day.

In all of the three cases, reduction of Ag^+ was observed. The slowest reduction took place when using acetaldehyde after one day nanoparticle formation was monitored by the UV-Vis (Figure 77a, d). However, TEM analysis showed that only polydisperse nanoparticles were formed. In this case, acetic acid is the oxidation product which may interfere with the stabilization of the AgNPs by peptide **18a**,

functionalized with carboxylic acid moieties. Formic acid and formaldehyde were chosen for the study because they form carbonic acid and CO_2 respectively, which were assumed not to affect the nanoparticle stabilization by the additive. In both cases however, almost no nanoparticle formation was observed by UV-Vis and only some aggregates were found in TEM (Figure 77b, c, e, f). Thus the Tollens reaction seems to produce monodisperse nanoparticles only when the aldehyde moieties are directly attached to the oligoproline backbone and are in the course of the reaction transformed into the stabilizing carboxylic acid residues like it was shown before.[78, 91]

To test if a different reducing agent may allow for the stabilization of formed nanoparticles by peptide **18a**, bearing carboxylic acid moieties, hydrazine was used (Figure 78). An Ag^+ to carboxylic acid ratio of 1:5 was used at pH 12.

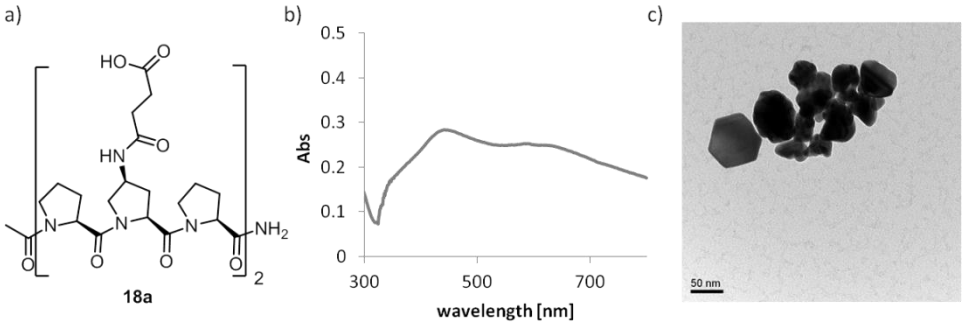

Figure 78: a) Peptide **18a**; AgNPs generated in the presence of peptide **18a** with hydrazine as reducing agent; **b)** UV-Vis spectrum, **c)** TEM image. Analysis was carried out after one day.

Nanoparticles were obtained using hydrazine as external reducing agent. Two plasmon bands were observed in the UV-Vis spectrum which is indicative of a non-spherical shape that can also be seen in Figure 78c. However, the majority of nanoparticles formed, were polydisperse and of an undefined shape.

In summary, we tested if these particular peptides, functionalized with carboxylic acid moieties were able to act as additives for AgNP formation. The carboxylic acid was found to be successfully applied for this purpose not only in the system described above, but also in others, reported in the literature.[101, 211, 219] However, obtaining monodisperse nanoparticles of defined sizes and shapes was not possible with peptides **18a-c**, bearing carboxylic acid moieties in the conditions studied in the course of this work. In the previous investigated system, the carboxylic acid was formed in the reducing process and the nucleation took place directly on the backbone, whereas in this system the nucleation took place in solution, which was probably responsible for the difference in ability of stabilization and the resulting nanoparticles.

3.1.4.4.2. Generation of AgNPs in the Presence of Peptide 18a-c without Additional Reducing Agent

The formation of AgNPs using peptide **18a**, bearing carboxylic acid, was tested in the absence of a reducing agent as some of the previous investigated peptides proved capable of reduce silver ions by themselves. Additionally literature precedents prove that glutamic acid and aspartic acid were both successfully applied as reducing agents for the formation of silver nanoparticles.[101, 211, 219] We screened different pH values in our experiments as this was found to be an important factor in the reported examples and in our experience. Dissolving the peptide in water resulted in a solution with pH 4. We furthermore also tested pH 10 and pH 12. After adjustment of the pH, $AgNO_3$ was added and the formation was monitored by UV-Vis and TEM.

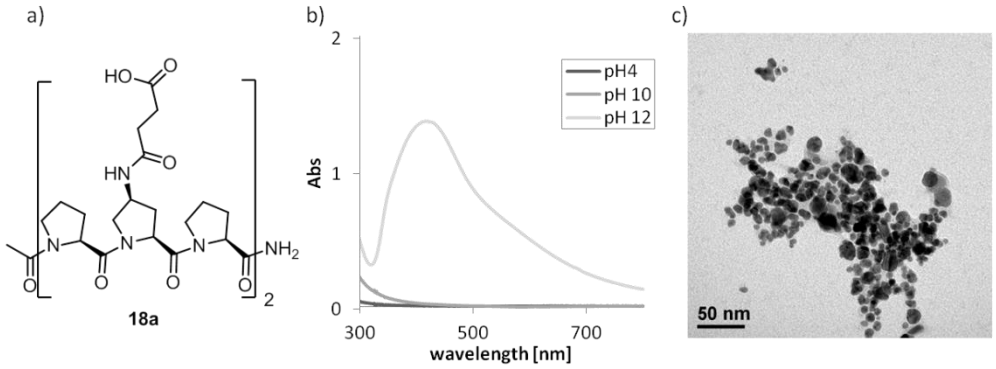

Figure 79: a) Peptide **18a**; AgNPs formed in the presence of peptide **18a** without additional reducing agent at different pH values; **b)** UV-Vis spectra, **c)** TEM image of AgNPs formed at pH 12. Analysis was carried out after one day.

The results are shown in Figure 79. At pH 4 and pH 10, no nanoparticle formation was observed. As for the previously tested peptides, also in this case, nanoparticle formation was only found to occur at pH 12. However, the resulting AgNPs were polydisperse and aggregated within one day. This showed that peptide **18a**, bearing carboxylic acids has a certain reducing power, just like the guanidine-functionalized peptides **22a-c** and amine-functionalized peptides **21a-c** described before. The stabilizing ability of these peptides after the reduction seemed to be insufficient to allow for monodisperse AgNPs to be obtained.

3.1.4.5. AgNP Generation in the Presence of Peptides Bearing Indole Moieties

3.1.4.5.1. Optimization of the Reaction Conditions: Peptide 19a

The next series of studied peptides **19a-c** had indole moieties attached to the oligoproline backbone. Their design was inspired by the amino acid tryptophan. This amino acid was successfully used in many different approaches for the generation of metal nanoparticles.[102, 192]

Again our investigation started with optimization of the reaction conditions. As before, a ratio of Ag^+ to indole moiety of 1:5 was initially used. Because the longer derivatives had a decreased solubility in water, additionally 27.5 % (v/v) of DMSO were added to the solution, which was found to be the smallest volume possible to be able to dissolve the longest peptide in water. DMSO was chosen as it was already reported in literature to a suitable co-solvent to dissolve tryptophan-rich peptides for the formation of AuNPs.[192] Even though we anticipated that the peptide itself would have a certain reducing capability, first external reducing agents, sodium borohydride and ascorbic acid, were evaluated, as it was the case with the previously tested peptides. Using sodium borohydride resulted in fast aggregation and precipitation of Ag (0). With ascorbic acid, nanoparticles were formed and fast aggregation did not occur.

The influence of the pH on the generation reaction was evaluated next, as it was found to be an important factor in the formation reaction for the previous investigated peptides. When indole-functionalized peptide **19a** was dissolved in water, a solution with pH 7 was obtained. Additionally, the reactions were tested at pH 11 and pH 12 (Figure 80). After the adjustment of the pH, $AgNO_3$ was dissolved and equilibrated for 15 minutes. Then ascorbic acid was added and the formation reaction was monitored by UV-Vis spectroscopy and analyzed by TEM.

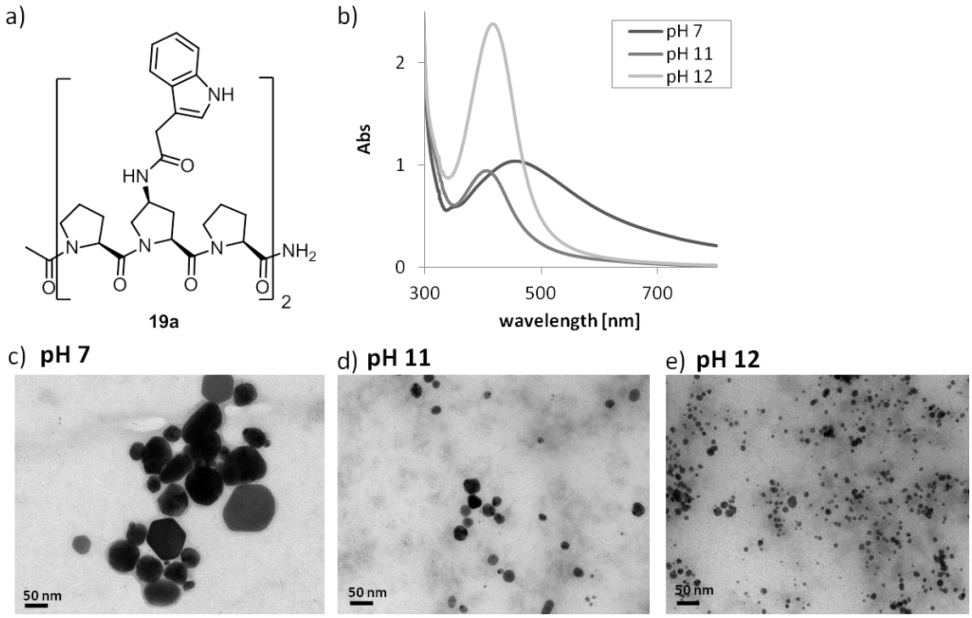

Figure 80: a) Peptide **19a**; AgNPs generated in presence of peptide **19a** at different pH values: **b)** UV-Vis spectrum, **c)** TEM image of AgNPs generated at pH 7: **d)** TEM image of AgNPs generated at pH 11, **e)** TEM image of AgNPs generated at pH 12. Analysis was carried out after one day.

The AgNPs formed at pH 7 were polydisperse in sizes ranging from 20 to 100 nm with non-spherical shapes (Figure 80c). With increasing pH the plasmon absorbance intensity increased, which could be due to increased reducing strength of ascorbic acid at higher pH values. [205, 209] At pH 11 and pH 12 the nanoparticles had diameters between 2 nm and 30 nm. It was chosen to continue the optimization at pH 11 as no significant difference between the two pH values was observed.

In a control experiment, the influence of DMSO was evaluated. The formation reaction was carried out with and without DMSO. The shortest indole-functionalized peptide **19a** was soluble in water and therefore used in these experiments. The resulting AgNPs were identical in size and shape. This showed that DMSO was not influencing the formation reaction in this system.

To further improve the formation reaction, the concentration of the peptide additive was altered. Ag^+ to indole moiety ratios of 1:1 and 1:10 were tested at pH 11 using ascorbic acid as external reducing agent (Figure 81).

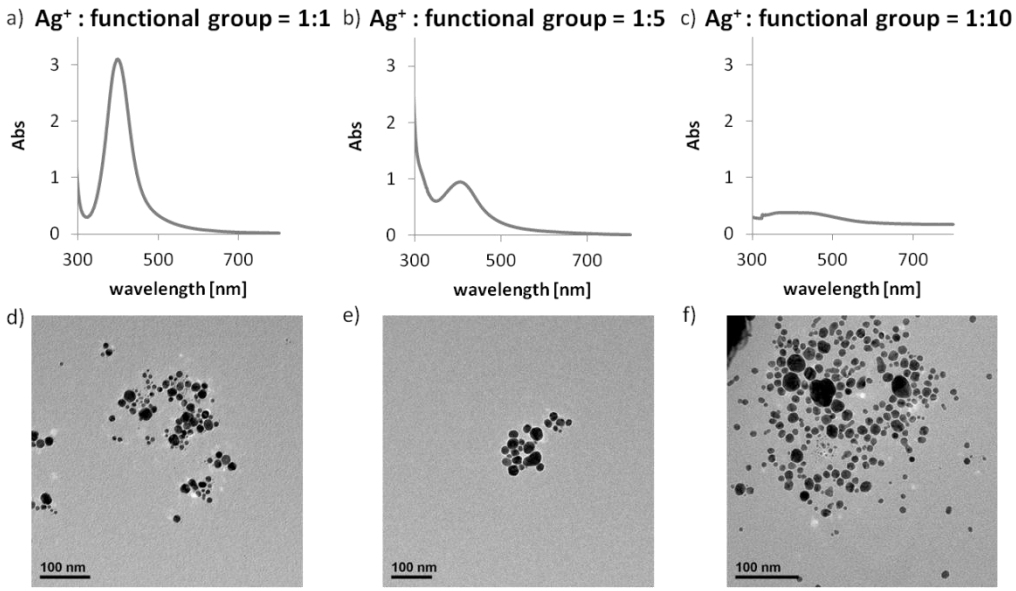

Figure 81: AgNPs generated in presence of peptide **19a** at pH 11 with different Ag^+ to functional groups ratios; 1:1 **a)** UV-Vis spectrum, **d)** TEM image; 1:5: **b)** UV-Vis spectrum, **e)** TEM image; 1:10: **c)** UV-Vis spectra, **f)** TEM image. Analysis was carried out after one day.

The changes in the Ag^+ to indole group ratio had no positive influence on the nanoparticles size distribution. On the contrary, broadening was observed. When less peptide was used in the generation reaction, polydisperse nanoparticles were formed. At a ratio of 1:10, the plasmon absorbance was low in intensity and bigger particles, up to 50 nm in diameter appeared. Thus this peptide seems unable to stabilize nanoparticles in a defined size and shape when an external reducing agent is used.

3.1.4.5.2. Generation of AgNPs in the Presence of Peptide 19a-c without Additional Reducing Agent

The ability of indole-functionalized peptide **19a** to reduce Ag^+ and stabilize the resulting AgNPs without additional reducing agent was investigated next. As we established earlier, the pH of the reaction environment plays a very important role in the case of the investigated systems, therefore we started our investigation with the evaluation of different pH values. A ratio of Ag^+ to indole moiety of 1:5 was used in the beginning. As mentioned before, dissolving the peptide in water resulted in a solution of pH 7. Furthermore the reduction was also tested at pH 10 and pH 12. After adjustment of the pH, $AgNO_3$ was added and the formation process was monitored by UV-Vis spectroscopy and analyzed by TEM (Figure 82). Also these experiments were carried out with 27.5% (v/v) DMSO in water.

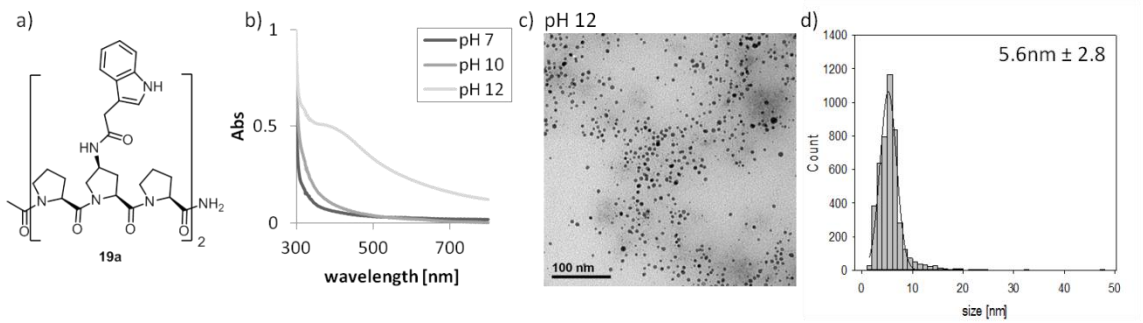

Figure 82: a) Peptide **19a**; Formation of AgNPs at different pH values in the presence of peptide **19a** without additional reducing agent: **b)** UV-Vis spectra, **c)** TEM image at pH 12; **d)** histogram of AgNPs formed at pH 12. Analysis was carried out after two days.

The experiments showed that formation of AgNPs was only achieved at pH 12 after two days. The generated nanoparticles had a narrower size distribution compared to the AgNPs formed with an external reducing agent. They were about 5.3 nm in diameter with a narrow dispersity and of a spherical shape (Figure 82b). The indole-functionalized peptide **19a** was able to reduce Ag^+ and also stabilize the resulting AgNPs. The reduction probably takes place like proposed by the group of Mandal presented in the introduction chapter (Chapter 1.2.2.; Figure 83), leading to dimerized indole moieties, kynureine and the reobtained indole moiety which are assumed to be the stabilizing moieties for the resulting AgNPs.[102]

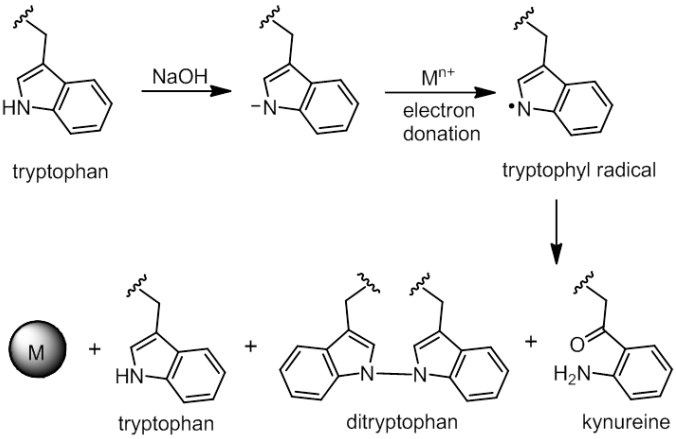

Figure 83: Reduction process proposed by the group of Mandal *et al.* using tryptophan containing peptides.

To further improve the nanoparticle formation, the amount of the used indole-functionalized peptide additive **19a** was varied (Figure 84). The reaction was performed at Ag^+ to indole moiety ratios of 1:1, 1:3, 1:5 and 1:10 at a pH of 12.

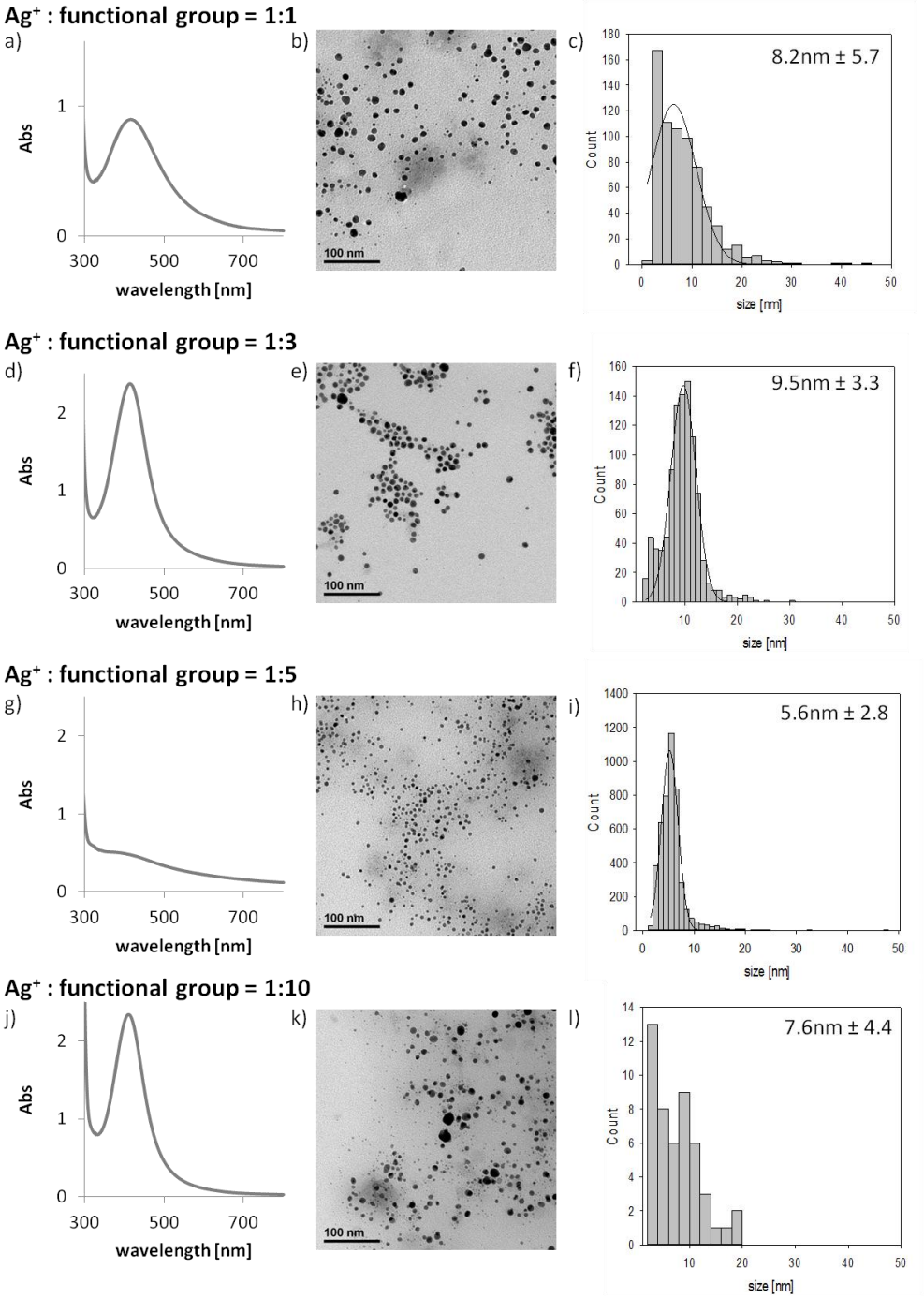

Figure 84: AgNPs generated in presence of peptide **19a** with different Ag+ to functional group ratios at pH 12; 1:1 **a)** UV-Vis spectrum, **b)** TEM image, **c)** histogram; 1:3 **d)** UV-Vis spectrum, **e)** TEM image, **f)** histogram; 1:5 **g)** UV-Vis spectrum, **h)** TEM image, **i)** histogram; 1:10 **j)** UV-Vis spectrum, **k)** TEM image, **l)** histogram. Analysis was carried out after one day.

At the lowest and highest peptide concentration, the resulting nanoparticles were the least monodisperse. At the ratios of 1:3 and 1:5 the nanoparticles developed a regular shape, with smaller nanoparticles formed at a ratio of 1:5. At a ratio of 1:3 the nanoparticles had an average diameter of

9.5 nm. Because the intensity was much higher in UV-Vis at this ratio and the size distribution was about the same than with a ratio of 1:5, the further tests were carried out with an Ag^+ to indole moiety ratio of 1:3.

To evaluate the influence of the length of the peptide chain on the nanoparticle formation, also the longer indole-functionalized peptides **19b** and **19c** were tested as additives in the reaction (Figure 85). The tests were performed in the optimised reaction conditions, without an additional reducing agent, with an Ag^+ to indole group ratio of 1:3 at pH 12 using 27.5% DMSO (v/v) in water.

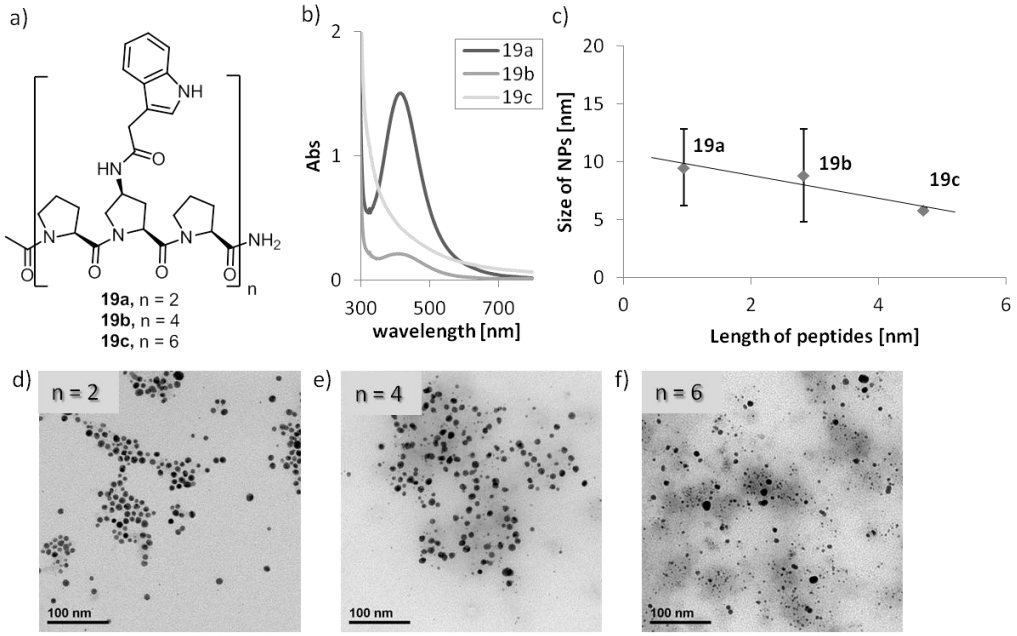

Figure 85: a) Peptide **19a-c**; Formation of AgNPs in the presence of peptides **19a** (n = 2), **19b** (n = 4) and **19c** (n = 6): **b)** UV-Vis spectra, **c)** correlation between the length of peptides **19a-c** and the size of the resulting AgNPs, **d)** TEM image of AgNPs formed in presence of peptide **19a**, **e)** TEM image of AgNPs formed in presence of peptide **19b**, **f)** TEM image of AgNPs formed in presence of peptide **19c**. Analysis was carried out after one day.

Nanoparticles obtained with **19a** and **19b** had about the same size and shape. Those generated with the longest indole-functionalized peptide **19c** were smaller (5.8 nm) and with a narrower size distribution. The plasmon absorbance showed a decrease in intensity with increasing length of the peptide. This could indicate that the peptides reducing strength decreases with increasing amount of the indole moieties on its backbone. Like the results obtained before for the guanidine-functionalized with peptides **22a-c** and the imidazole-functionalized peptides **17a-c** used with additional reducing agent, also in this case the AgNPs were about the same in size and shape in the presence of indole-functionalized peptides **19a-c** independent of the length of the used additive. These results underline the observations that were made before, that the length of the oligoprolines did not significantly

influence the resulting size and shapes. The functional groups attached on the backbone were the main influence to the morphology and as the experiments with the flexible peptides showed, also the spatial arrangement are important for them to be able to act as additives.

3.1.4.6. AgNP Generation in the Presence of Peptides Bearing Pyrrolidinyl Moieties

3.1.4.6.1. Optimization of the Reaction Conditions: Peptide 20a

Peptides **20a-c** bearing pyrrolidinyl groups were also tested as potential additives in the generation of AgNPs. This functional group is part of one of the most commonly used additives in the metal nanoparticle generation, the polymer polyvinylpyrrolidone (PVP).[66-67] Even though the polymer contains an excess of pyrrolidinyl groups, we estimated that a limited number of these functionalities should be sufficient to stabilize the AgNPs.

As in all previous cases, the reaction conditions were to be optimized first. Sodium borohydride and ascorbic acid were again tested as reducing agents. The nanoparticles generated with sodium borohydride did not aggregate within the first hours, but showed polydisperse and undefined shapes. Therefore sodium ascorbate was used in the following experiments, where more regular shapes were observed. A ratio of Ag^+ to pyrrolidinyl group of 1:4 was used for the evaluation of the optimal pH value. This ratio was slightly different to the previous studies. Dissolving the peptide in water resulted in a solution of pH 7. Tests at pH 10 and pH 12 were carried out as well (Figure 86).

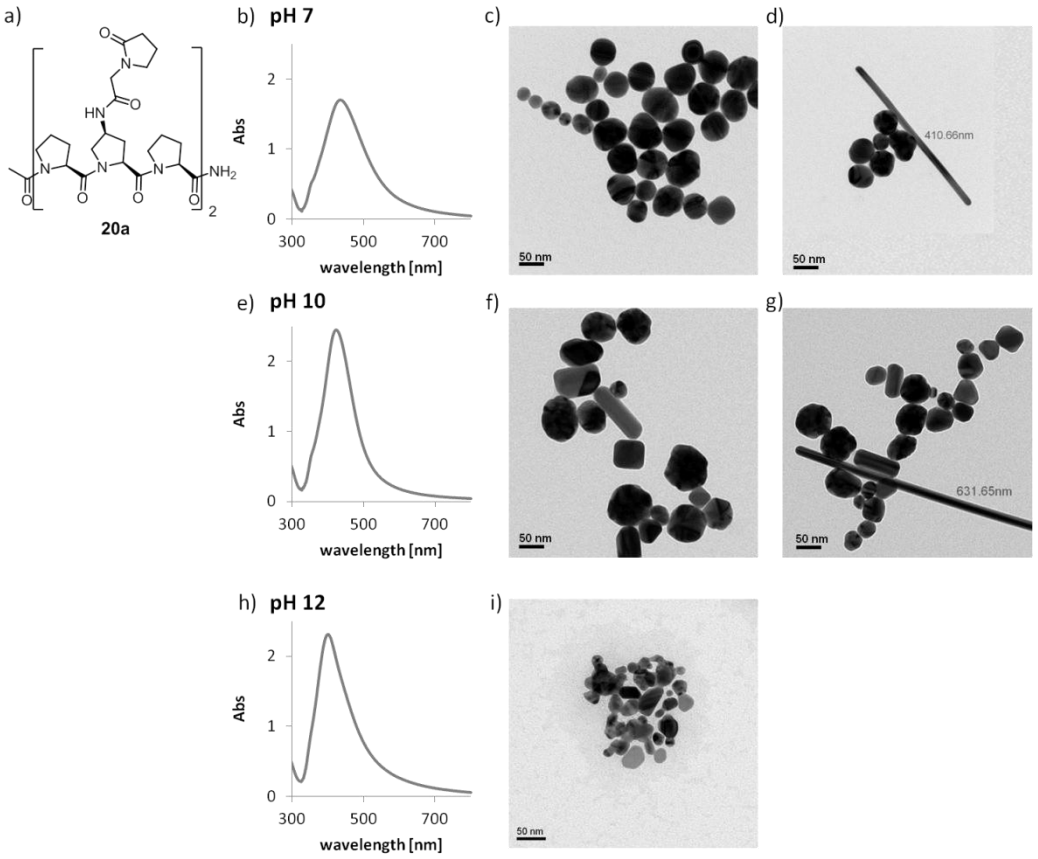

Figure 86: a) Peptide **20a**; AgNPs generated in presence of peptide **20a** at different pH values. pH 7: **b)** UV-Vis spectrum, **c), d)** TEM image; pH 10: **e)** UV-Vis spectrum, **f), g)** TEM image; pH 12: **h)** UV-Vis spectrum, **i)** TEM image: Analysis was carried out after one day.

The nanoparticles formed at pH 12 were polydisperse in size and shape. At lower pH values, the nanoparticles showed more defined shapes, but the sizes were also polydisperse. Additionally, another shape evolved. At pH 7 and pH 10 nanorods were found (Figure 86c, f). Surprisingly, there was only one peak observed in UV-Vis. A typical sign of rod formation is the appearance of a longitudinal plasmon peak. It is not visible in this case, probably due to the small amount of rods compared to the spherical nanoparticles. The pyrrolidinyl group attached to the oligoproline backbone was able to successfully stabilize AgNPs. The stabilization probably occurred over the nitrogen atom in the pyrrolidinyl group as it was found for the PVP polymer, described in literature.[67] To see, if the formation of the rods can be enhanced or if it is possible to form monodisperse nanoparticles using this peptide, further screening of conditions was performed.

At pH 7, the ratio of Ag^+ to pyrrolidinyl groups was varied from the initial 1:4 to 1:5, 1:10 but also 4:1. The results are shown in Figure 87.

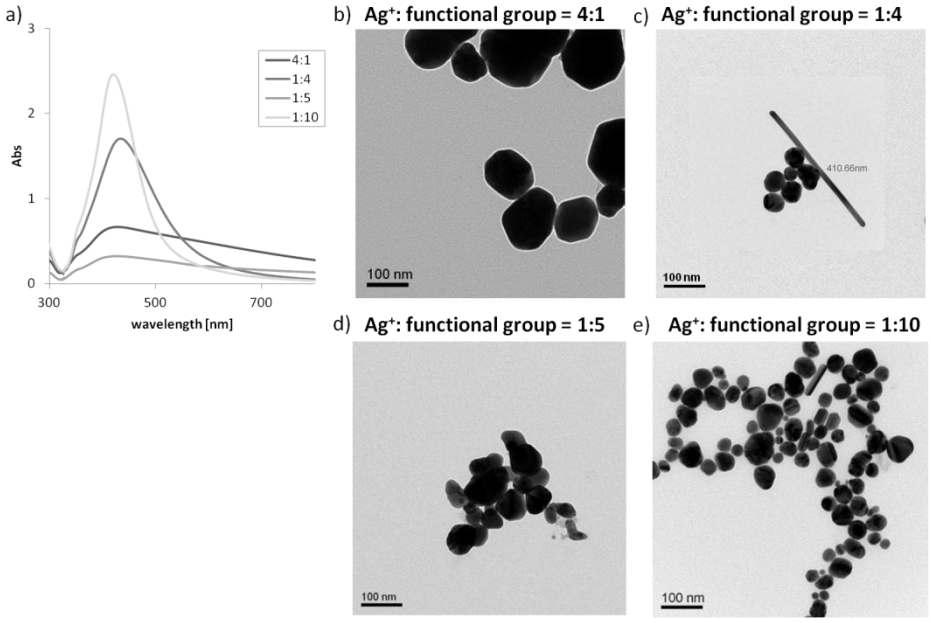

Figure 87: AgNPs generated in presence of peptide **20a** using different Ag^+ to functional group ratios: **a)** UV-Vis spectra; **b)** 4:1 TEM image, **c)** 1:4 TEM image, **d)** 1:5 TEM image, **e)** 1:10 TEM image. Analysis was carried out after one day.

Using the different ratios of pyrrolidinyl groups resulted in AgNPs in all cases. It seems that 1:4 is the optimal ratio in the case of the pyrrolidinyl-functionalized peptide **20a**. The rods formed in these conditions were ranging from 50 nm up to 400 nm in length. At a ratio of 1:10 there were also some rods appearing but they were shorter with length from about 50 nm to 200 nm.

Next, we wanted to investigate whether longer pyrrolidinyl group functionalized peptides **20b** and **20c** might lead to formation of an increased amount of nanorods or monodisperse nanoparticles. The experiments were carried out under the established conditions with an Ag^+ to pyrrolidinyl group ratio of 1:4, at pH 7 using ascorbic acid as external reducing agent.

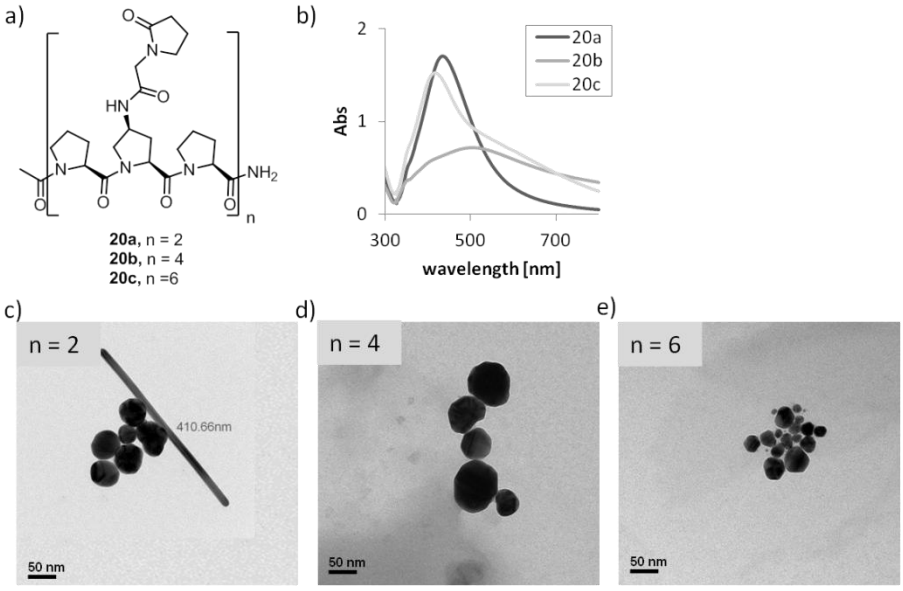

Figure 88: a) Peptide **20a-c**; Formation of AgNPs in the presence of peptides **20a** (n = 2), **20b** (n = 4) and **20c** (n = 6): **b)** UV-Vis spectra, **c)** TEM image of AgNPs formed in presence of peptide **20a**, **d)** TEM image of AgNPs formed in presence of peptide **20b**, **e)** TEM image of AgNPs formed in presence of peptide **20c**. Analysis was carried out after one day.

In the presence of all peptides, AgNPs were formed (Figure 88). However with the longer peptides, no rod formation was observed and the formation reaction did not led to more uniform sizes and shapes.

3.1.4.6.2. Generation of AgNPs in the Presence of Peptide 20a-c without Additional Reducing Agent

The AgNPs generation reaction was also evaluated without an external reducing agent, to test the reducing capability of pyrrolidinyl-functionalized peptide **20a** towards Ag^+ and the ability to act as a stabilizing agent at the same time. To evaluate these properties, suitable reaction conditions had to be found. First of all the optimal pH value was determined. As mentioned before, dissolving the peptide **20a** in water resulted in a solution of pH 7. Additionally pH 12 and pH 13 were tested. Higher pH values than in the previous study were chosen, as the experiments with other peptides showed that the reduction of Ag^+ occurs only at pH 12. Like before, a ratio of Ag^+ to pyrrolidinyl group of 1:5 was initially used.

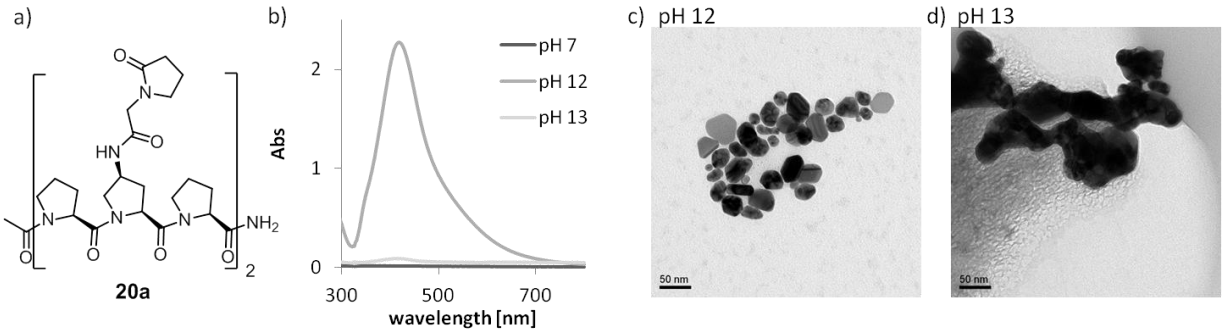

Figure 89: a) Peptide **20a**; AgNPs generated in the presence of peptide **20a** without additional reducing agents at different pH values: **b)** UV-Vis spectra, **c)** TEM image of AgNPs formed at pH 12, **d)** TEM image of AgNPs formed at pH 13. Analysis was carried out after one day.

The results are shown in Figure 89. Nanoparticle formation was observed at pH 12 and pH 13. In the latter conditions, the plasmon absorbance was very low and the nanoparticles aggregated very fast after the formation (Figure 89c). The nanoparticles formed at pH 12 were polydisperse but did not aggregate as fast as at pH 13.

To improve the size and shape distribution of the AgNPs, the ratio of Ag^+ to pyrrolidinyl group was varied. Ratios of 1:4, 1:5, 1:10 and 1:50 were tested at pH 12 (Figure 90).

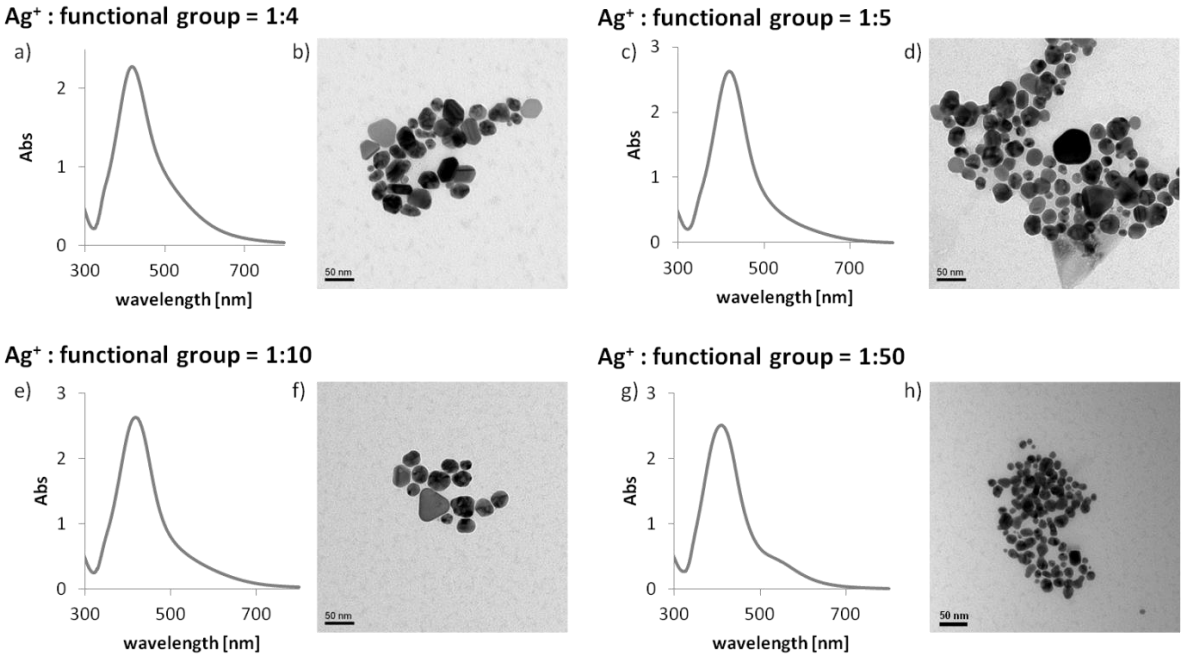

Figure 90: AgNPs generated in the presence of peptide **20a** without additional reducing agent with different Ag^+ to functional group ratios; 1:4: **a)** UV-Vis spectrum, **b)** TEM image; 1:5: **c)** UV-Vis spectrum, **d)** TEM image; 1:10: **e)** UV-Vis spectrum, **f)** TEM image; 1:50: **g)** UV-Vis spectrum, **h)** TEM image. Analysis was carried out after one day.

None of the conducted experiments led to an improvement of the size and shape distribution. The nanoparticles obtained at ratios of 1:4 and 1:10 were very similar to the ones formed at the ratio of 1:5. When a ratio of 1:50 was used, the nanoparticles had even less defined shapes. Furthermore, the increased peptide concentration resulted in a decrease in AgNPs stability. Rod formation was not observed in any of the cases, in contrast to the experiments conducted with an external reducing agent. This implies that the oxidized functional groups, on the peptide backbone have very different stabilization capabilities towards Ag (0) nanostructures. In summary, reduction of Ag^{+} and stabilization of formed AgNPs is possible with pyrrolidinyl-functionalized peptide **20a**, but the resulting AgNPs did not develop a defined size and shape under the conditions investigated in the course of this work.

3.1.4.7. AgNP Generation in the Presence of Unfunctionalized Peptide 25

To investigate the influence of the scaffold to the formation reaction and whether unfunctionalized oligoprolines can also act as additives, we tested unfunctionalized oligoproline **25** as additive. This peptide can probably bind through the amide bond to the Ag (0) which may be enough to act as additives in the formation reaction. The properties of peptide **25** were studied using sodium borohydride and ascorbic acid as external reducing agents as they were used in the course of this study. A tenfold excess of the peptide was applied in the test reaction. It carried out at a pH 12 which was adjusted using aqueous sodium hydroxide solution. This amount was used, because in this peptide, no functional groups can serve as reference and an excess was intended to be used.

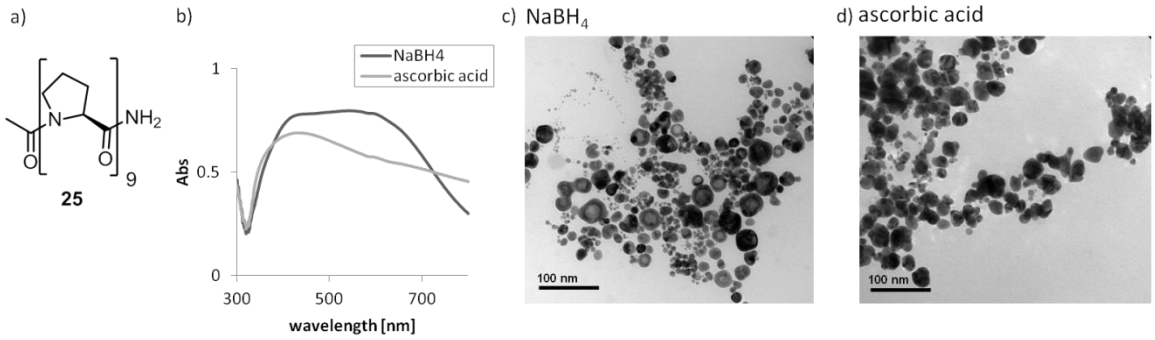

Figure 91: a) Peptide **25**; AgNPs formed in the presence of peptide **25** with sodium borohydride and ascorbic acid; **b)** UV-Vis spectra, **c)** TEM image of AgNPs formed with sodium borohydride, **d)** TEM image of AgNPs formed with ascorbic acid. Analysis was carried out after one hour.

The results are shown in Figure 91. In both cases polydisperse AgNPs were formed. Interestingly, a new nanoparticle shape, hollow spheres, was detected in the experiment using sodium borohydride. To further investigate this finding and to see if it is possible to enhance the amount of the hollow spheres formed, we varied the Ag^+ to peptide ratios in the following experiments. Ratios of 1:1, 1:5, 1:10 and 1:50 were tested (Figure 92).

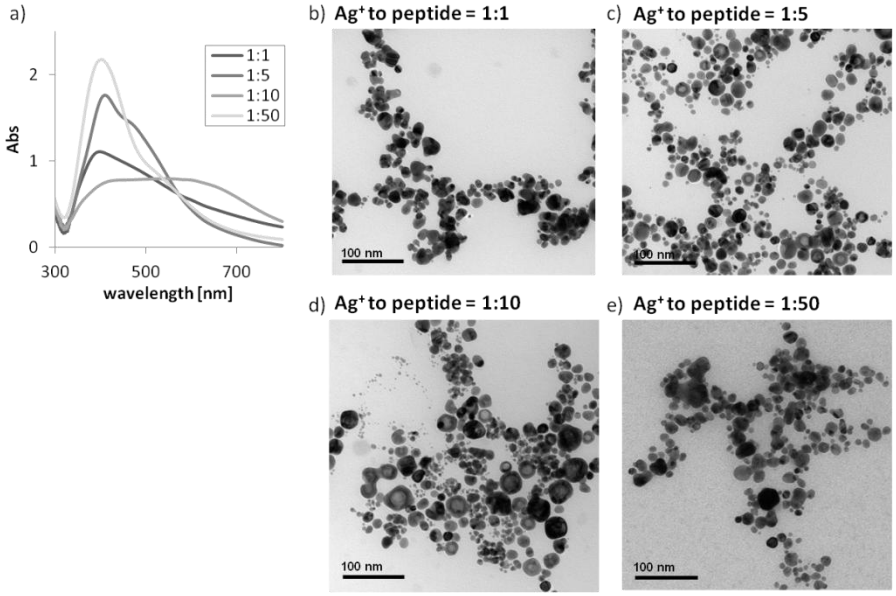

Figure 92: AgNPs generated in presence of peptide **25** with sodium borohydride under different Ag^+ to peptide ratios: **a)** UV-Vis spectra, **b)** TEM image of nanoparticles generated at a ratio of 1:1; **c)** TEM image of nanoparticles generated with a ratio of 1:5; **d)** TEM image of nanoparticles generated at a ratio of 1:10, **e)** TEM image of nanoparticles generated at a ratio of 1:50. Analysis was carried out after one hour.

The amount of hollow spheres did not increase in any of the reactions compared to the initial test, although such shapes were also observed at the ratio of 1:5.

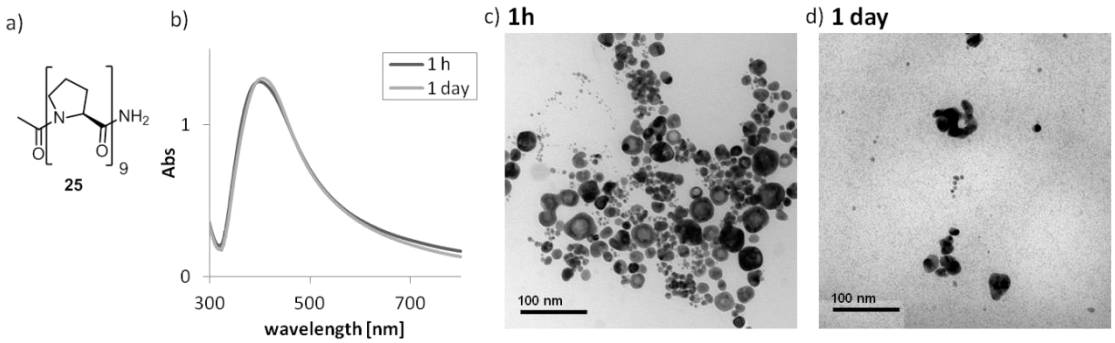

Figure 93: a) Peptide **25**; b) UV-Vis spectra; c) TEM image of AgNPs generated in the presence of peptide **25** after 1 hour; d) TEM image of AgNPs generated in the presence of peptide **25** after 1 day.

It was found, that this shape disappeared within one day (Figure 93). We therefore assumed that the hollow spheres are probably intermediates in the nanoparticle formation process which are not sufficiently stabilized and therefore dissapear in the course of the reaction. The binding of the amide groups to the Ag^+ could possibly lead to an enhanced local concentration of the oligoprolines which does not occur with the larger peptide derivatives bearing charged functional groups. This is probably

why this shape was never found in the previous studies, where functionalized oligoprolines were used as additives.

3.1.5. Gold Nanoparticle (AuNP) Generation

Next, we also tested the designed peptides for their ability to act as additives in the formation of AuNPs. Peptidic additives were reported to be able to act as additives for the formation of AuNPs.[12, 57-58, 99-100, 137-144] Even though the design was aiming for the formation of AgNPs, we envisioned the designed peptides, to have also considerable ability in the stabilization of AuNPs. Like before, first we were optimizing the reaction conditions using the shortest of each peptide by variation of the pH and the Au^{3+} to functional group ratio. The optimal conditions were applied using also the longer derivatives as additives in the generation reaction.

As described in the previous chapter, some of the peptides proved to be able to reduce silver ions and stabilize AgNPs. Therefore, we also evaluated the reducing and stabilizing properties of these peptides without additional reducing agent in the formation of AuNPs.

3.1.5.1. AuNP Generation in the Presence of Peptides Bearing Guanidine Moieties

3.1.5.1.1. Optimization of the Reaction Conditions: Peptide 22a

We started the evaluation of the ability to act as an additive with the guanidine-functionalized peptides **22a-c**. Like in all previous cases, optimal conditions, required to generate AuNPs needed to be evaluated. Peptide **22a**, bearing two guanidine moieties, was used as a model compound for this purpose. Ascorbic acid was applied as external reducing agent as it was found to perform best, in the formation of AgNPs (3.1.4.1). With a ratio of Au^{3+} to guanidine groups of 1:5, different pH values were tested. As reported before, a solution with a pH of 9.5 was obtained when peptide **22a** was dissolved in water. We tested the reaction furthermore at pH 11 and pH 12. Aqueous sodium hydroxide solution was used to adjust the pH. Then $HAuCl_4$ was dissolved, equilibrated for 15 minutes and ascorbic acid was added.

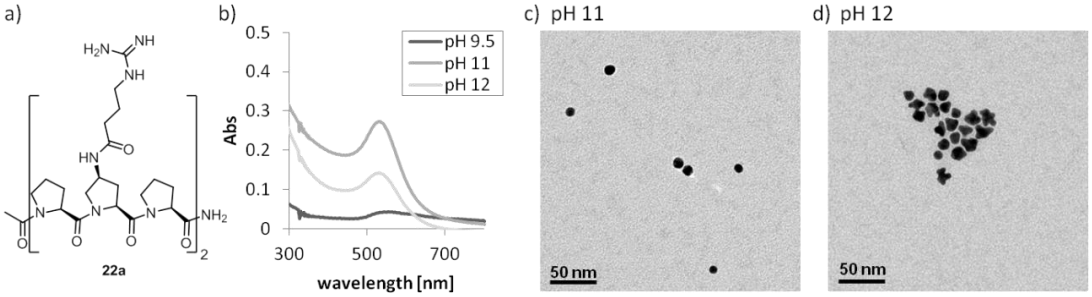

Figure 94: a) Peptide **22a**; AuNPs formed in the presence of peptide **22a** at different pH values; **b)** UV-Vis spectra, **c)** TEM image of AuNPs generated at pH 11, **d)** TEM image of AuNPs generated at pH 12. Analysis was carried out after one day.

The results are shown in Figure 94. No nanoparticle formation was observed at pH 9.5. At pH 11 and pH 12 a plasmon absorbance band at 520 nm was found by UV-Vis spectroscopy (Figure 94a), indicating AuNP formation. TEM microscopy revealed that at pH 11 monodisperse spherical particles were formed with an average diameter of 12 nm (11.6 nm ± 1.6). The nanoparticles obtained at pH 12 had a different shape with no clear geometrical form and with an average diameter of about 14 nm (13.5 nm ± 6.3). Both pH values resulted in different sizes and shapes. This is a convenient method to adjust the morphology by just changing the pH value. These results are in contrast to the investigation with AgNPs where only at one pH value defined nanoparticles were formed. The guanidine group acts very different in the formation of AuNPs and it seems to be able to tune size and shape with the different pH values.

As we calculated with the Henderson-Hasselbalch equation the grade of protonation of the guanidine-functionalized peptide is very different at pH 11 and at pH 12 (chapter 3.1.4.1). This is probably the reason for the difference in the resulting nanoparticles.

3.1.5.1.2. Testing Peptides of Different Length: Peptides 22a-c

To investigate the influence of the length of the peptide on the nanoparticle generation process, the experiments with longer guanidine-functionalized derivatives **22b** and **22c** were carried out. The reactions were performed at pH 11 and at pH 12, using a ratio of Au^{3+} to functional group of 1:5 and ascorbic acid as external reducing agent. First of all we tested the reaction at pH 11 which resulted in nanoparticles with an average size of 12 nm in the experiments using the shortest guanidine functionalized peptide **22a**. First we adjusted the pH of the solution before the $HAuCl_4$ was added and equilibrated for 15 minutes followed by the addition of ascorbic acid (Figure 95).

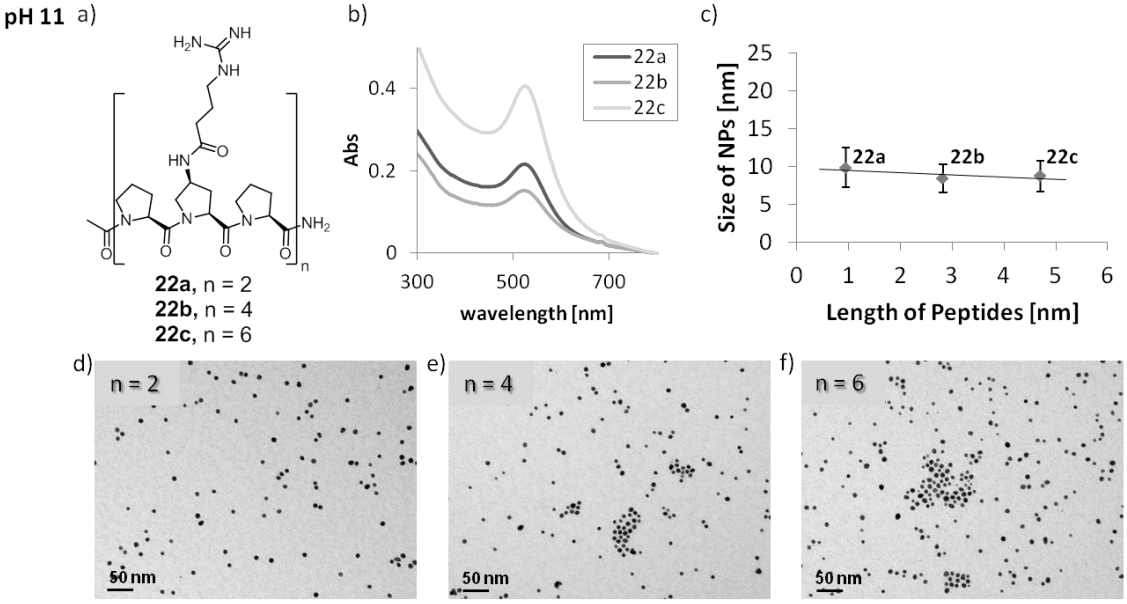

Figure 95: a) Peptide **22a-c**; AuNPs formed in the presence of peptides **22a** (n = 2), **22b** (n = 4) and **22c** (n = 6) at pH 11: **b)** UV-Vis spectra, **c)** correlation between the length of peptides **22a-c** and the size of the resulting AgNPs, **d)** TEM image of AgNPs formed in presence of peptide **22a**, **e)** TEM image of AgNPs formed in presence of peptide **22b**, **f)** TEM image of AgNPs formed in presence of peptide **22c**. Analysis was carried out after one day.

With all three lengths of the guanidine-functionalized oligoprolines, monodisperse spherical AuNPs were formed with an average diameter of about 9 nm. The reaction conditions resulted in monodisperse nanoparticles with defined size and shape. The size of the nanoparticles was smaller than the size of the AgNP formed in the presence of this peptide. Similar to the formation of AgNPs, the different length did not have a significant influence on the resulting size. These results underline the findings from the investigation so far, that the functional groups are the main factor that influences the size and shape.

Next we were evaluating the formation reaction with all three lengths of the peptide at pH 12 (Figure 96).

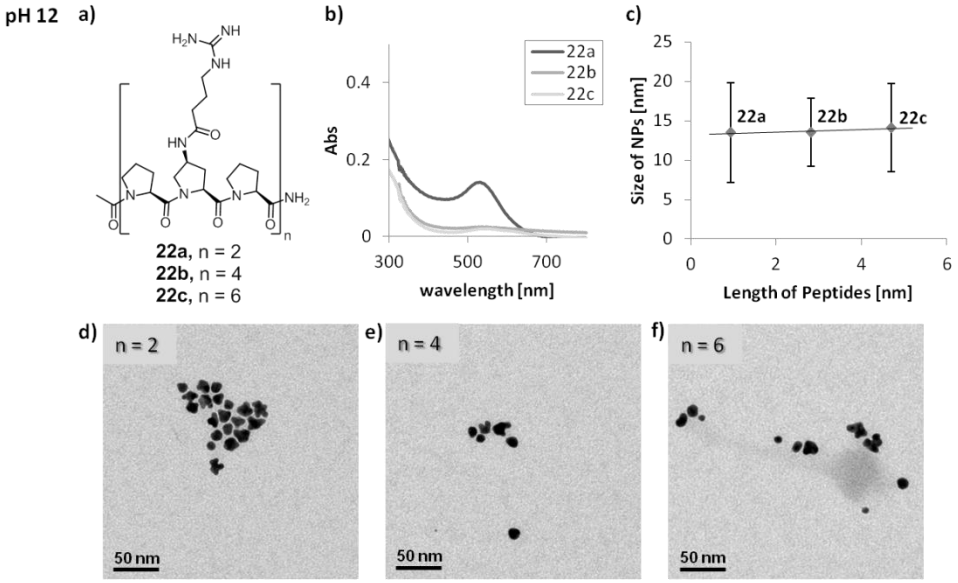

Figure 96: a) Peptide **22a-c**; AuNPs formed in the presence of peptides **22a** (n = 2), **22b** (n = 4) and **22c** (n = 6) at pH 12: **b)** UV-Vis spectra, **c)** correlation between the length of peptides **22a-c** and the size of the resulting AgNPs, **d)** TEM image of AgNPs formed in presence of peptide **22a**, **e)** TEM image of AgNPs formed in presence of peptide **22b**, **f)** TEM image of AgNPs formed in presence of peptide **22c**. Analysis was carried out after one day.

The results are shown in Figure 96. At pH 12, AuNPs were formed with all three guanidine-functionalized oligoprolines **22a-c** with about the same size and shape. They showed the same undefined non-spherical shape, different to those formed at pH 11. The intensity of the plasmon absorbance of the nanoparticles generated in the presence of peptides **22b** and **22c** was very small. However, the AuNPs were all of about the same size and shape (Figure 96c-f). Just as observed previously for pH 11, also in the case of pH 12, the length of the peptidic additive had little influence on the size and shape of resulting nanoparticles.

Although the size of AuNPs obtained with peptides **22a-c** is actually comparable to the size of the obtained AgNPs, they show an interesting dependence on the pH to the resulting size and shape. This clearly proves, that the results obtained for one metal cannot be directly transferred to another one as they were found to behave quite differently and thus individual optimization is required for each group of peptides. This difference was already reported in literature, for example in the studies of Wright *et al* where they investigated the HRE peptide for its ability to act as additive in the formation of different metal nanoparticles[99-100] or in the studies from Naik *et al.* where they tested the AG4 peptide, identified within a library screening, also as additive for different metal nanoparticles[97, 140] (Introduction).

3.1.5.1.3. Investigating the Importance of the Linker: Peptide 24a

In line with the investigation for the AgNP formation, we also tested peptides **24a-c**, bearing guanidine groups, attached directly to the oligoproline backbone, as additive in the AuNP formation. By removing the linker we wanted to determine whether the flexibility of the functional groups has any impact on the formation reaction or properties of AuNPs. We performed the generation reaction at different pH values (9.5, 11, 12), using an Au^{3+} to functional group ratio of 1:5 (Figure 97) using ascorbic acid as reducing agent. The pH values were adjusted and the gold salt was dissolved. After 15 minutes of equilibration the reducing agent was added.

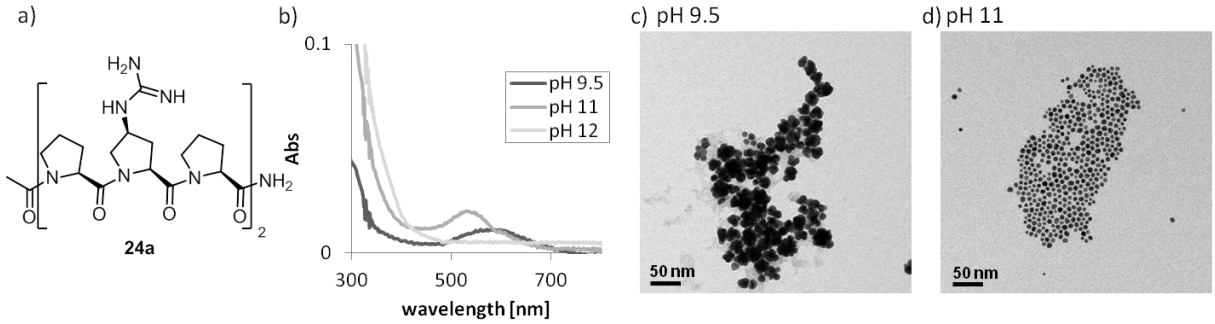

Figure 97: a) Peptide **24a**; AuNPs generated in the presence of peptide 24a; **b)** UV-Vis spectra, **c)** TEM image of AuNPs generated at pH 9.5, **d)** TEM image of AuNPs generated at pH 11. Analysis was carried out after one day.

The plasmon absorbance had a very low intensity as observed in UV-Vis spectroscopy (Figure 97a). At pH 9.5 the absorption band was very broad and the maximum was around 580 nm. The nanoparticles formed at this pH were polydisperse and aggregated within one day (Figure 97b). No nanoparticle formation was observed at pH 12. The formation process carried out at pH 11, resulted in monodisperse spherical AuNPs with an average size of 9 nm (9.0 nm ± 1.7). These huge differences were quite surprising. This means that in the case of this peptide the pH value played a crucial role in the formation of AuNPs and needs to be adjusted carefully. In contrary to the experiments with the guanidine-functionalized oligoprolines with the linker **21a-c**, only the formation reaction at pH 11 resulted in AuNPs with defined size and shape. Also in this case, the linker seems to play a distinct role in the ability to act as additive like it was already found for AgNPs. However in contrary to the formation of AgNPs, here it was possible in both cases to form monodisperse nanoparticles under the same conditions. To further investigate this system, the formation was carried out using all three different length of the guanidine-functionalized oligoprolines **24a-c**. In the formation reaction an Au^{3+} to guanidine ratio of 1:5, at pH 11 using ascorbic acid as external reducing agent were used (Figure 98).

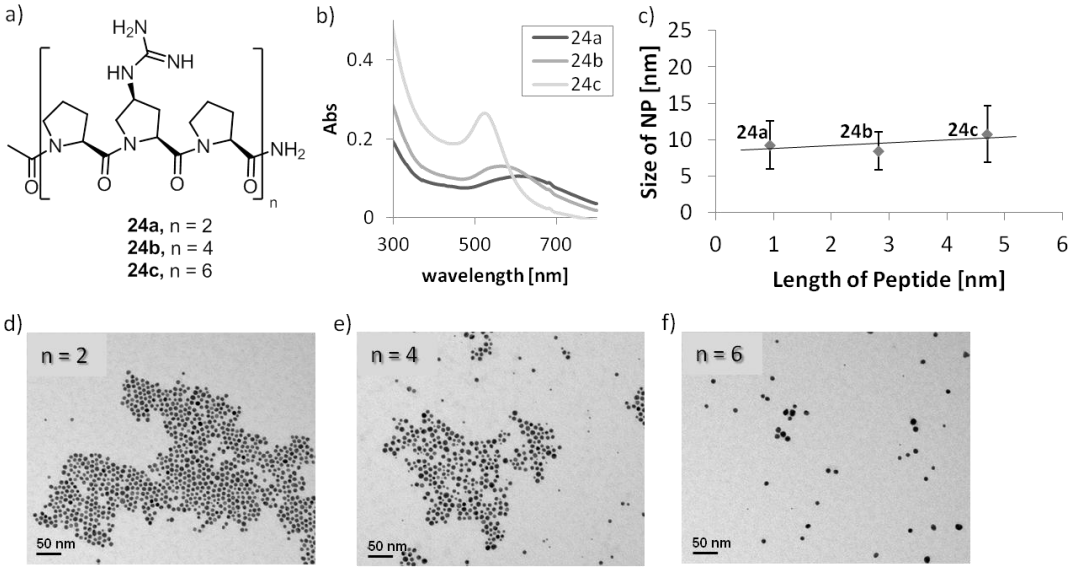

Figure 98: a) Peptide **24a-c**; AuNPs formed in the presence of peptides **24a** (n = 2), **24b** (n = 4) and **24c** (n = 6) at pH 11: **b)** UV-Vis spectra, **c)** correlation between the length of peptides **24a-c** and the size of the resulting AgNPs, **d)** TEM image of AgNPs formed in presence of peptide **24a**, **e)** TEM image of AgNPs formed in presence of peptide **24b**, **f)** TEM image of AgNPs formed in presence of peptide **24c**. Analysis was carried out after one day.

The results are shown in Figure 98. With all three different lengths monodisperse spherical nanoparticles were formed. They all had in average the same diameter (Figure 98c-f). This behaviour when comparing the different length of the peptides in their ability to act as an additive was already found in the previous experiments with the other investigated peptides. Also in this case, it was found that the conditions and the functional groups have the most dominant influence on the final size and shape. The length of the peptide seems to play only a minor role.

3.1.5.1.4. Generation of AuNPs in the Presence of Peptide 22a-c without Additional Reducing Agent

After the successful reduction and stabilization, that was achieved using solely guanidine-functionalized oligoproline **22a-c** to form AgNPs, we also evaluated the ability of these peptides to generate AuNPs without an additional reducing agent present. Different pH values were tested (pH 9.5, pH 11, pH 12) but no nanoparticle formation was observed, neither by UV-Vis spectroscopy, nor by TEM. This might be explained by the difference in the reduction potential of silver (E° = 0.799 V) and gold (E°= 1.691 V). For the reduction of Au^{3+} three electrons were needed which peptide **22a-c** seems not able to provide.

3.1.5.2. AuNP Generation in the Presence of Peptides Bearing Imidazole Moieties

The utility of imidazole-functionalized oligoprolines **17a-c** as additive in the AuNP formation was evaluated next. These peptides were found to be efficient additives in the AgNPs generation reaction yielding monodisperse nanoparticles (chapter 3.1.4.2). First the optimal conditions found for the formation of AgNPs were applied. We performed the generation reaction at pH 11 with an Au^{3+} to imidazole group ratio of 1:5, using sodium borohydride as a reducing agent. We were delighted to see that under these conditions, originally optimized for AgNPs, also AuNPs were formed in a monodisperse fashion (Figure 99).

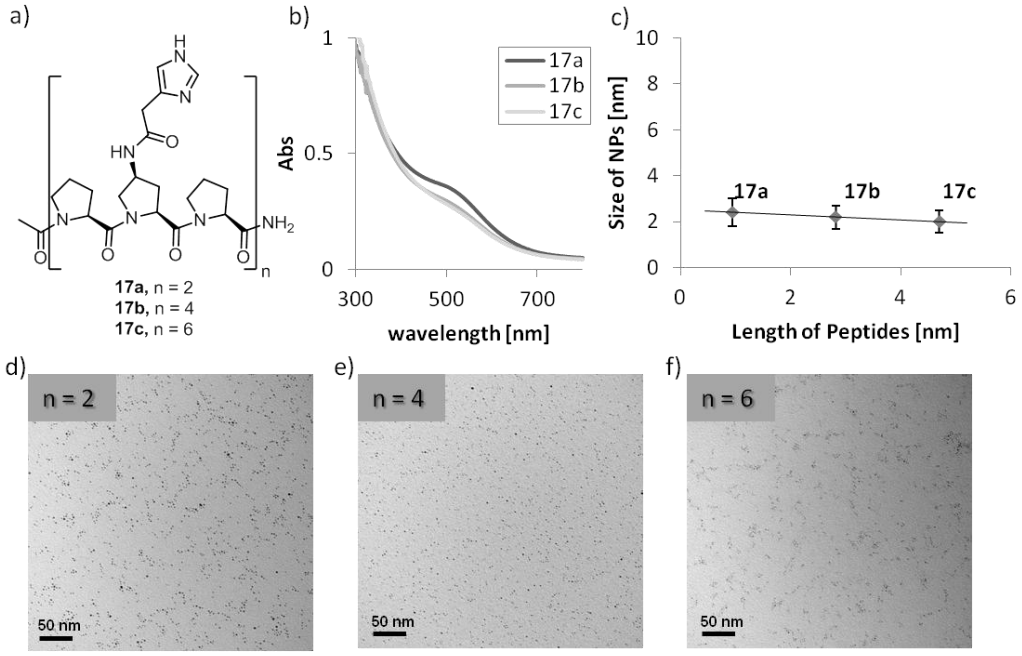

Figure 99: a) Peptides **17a-c**; AuNPs formed in the presence of peptide **17a** (n = 2), **17b** (n = 4) and **17c** (n = 6): **b)** UV-Vis spectra, **c)** correlation between the length of peptides **17a-c** and the size of the resulting AuNPs, **d)** TEM image of AuNPs formed in the presence of peptide **17a**, **e)** TEM image of AuNPs formed in the presence of peptide **17b**, **f)** TEM image of AuNPs formed in the presence of peptide **17c**. Analysis was carried out after one day.

As show in Figure 99, there was no big difference in the size and shape of the AuNPs, when imidazole-functionalized peptides **17a-c** of different lengths were used as additives. They were all around 2 nm (2.4 nm ± 0.6) in diameter with a spherical shape and a narrow size distribution.

These findings suggest that these conditions are optimal for the application of peptides **17a-c** as additives in the nanoparticle formation, regardless if silver or gold is the investigated metal and therefore no further screening was required. However, the resulting sizes were different in each case. These results were in direct contrast to the results from the investigation made with guanidine-

functionalized oligoprolines **21a-c** and **24a-c** where differences in the ability to act as additive and the resulting nanoparticles were found between AgNPs and AuNPs. At the current state of our research the conditions needs to be individually tested for each additive.

3.1.5.3. AuNP Generation in the Presence of Peptides Bearing Primary Amine Moieties

3.1.5.3.1. Optimization of the Reaction Conditions: Peptide 21a

To evaluate the AuNP formation using peptide **21a**, bearing primary amino groups, reaction conditions that proved successful in the AgNP generation were used as a starting point for the study. A ratio of Au^{3+} to functional group of 1:5 and ascorbic acid as reducing agent were used and different pH values were tested. By dissolving the peptide in water, a solution of pH 9.5 was obtained. Additionally pH values of 11 and 12 were tested in the formation reaction.

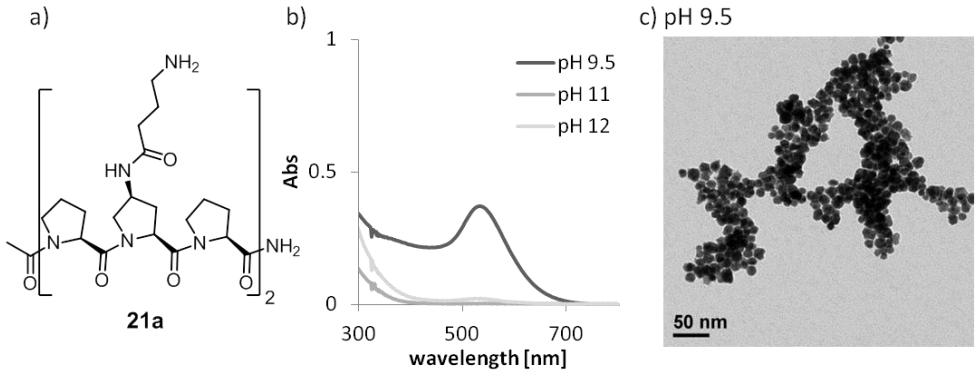

Figure 100: a) Peptide **21a**; AuNPs formed in the presence of peptide **21a** at different pH values; **b)** UV-Vis spectra, **c)** TEM image of AuNPs generated at pH 9.5. Analysis was carried out after one day.

The results are shown in Figure 100. Nanoparticle formation was observed only at pH 9.5. However they were polydisperse, as seen in TEM (Figure 100c). The amine-functionalized peptide **21a** seems not able to stabilize AuNPs in defined size and shape.

When this peptide was used as an additive in the AgNP generation, non-spherical nanoparticles were formed. In the case of AuNPs, no defined nanoparticle formation was achieved. Similar to the case of guanidine-functionalized peptides **22a-c**, application of amino-functionalized peptide **21a** gave very different results in the AuNP formation, compared to its results in the AgNP generation. The conditions and functional groups of the additive that can be applied in the process are an individual matter for each metal in case of the investigated peptides.

3.1.5.3.2. Investigating the Importance of the Linker: Peptide 23a

As the experiment in the presence of amine-functionalized peptide **21a**, bearing a flexible linker, did not form AuNPs of a defined size and shape, we decided to investigate whether attachment of a

primary amino group directly to the oligoproline backbone, without an additional linker, might change the outcome of the nanoparticle formation reaction.

We carried out the generation of AuNPs in the presence of peptide **23a** using an Au^{3+} to amine group ratio of 1:5 screening different pH values. A solution with a pH of 8.5 was obtained by dissolving the peptide in water. We also performed the reaction at pH 11 and pH 12 with ascorbic acid as the reducing agent (Figure 101).

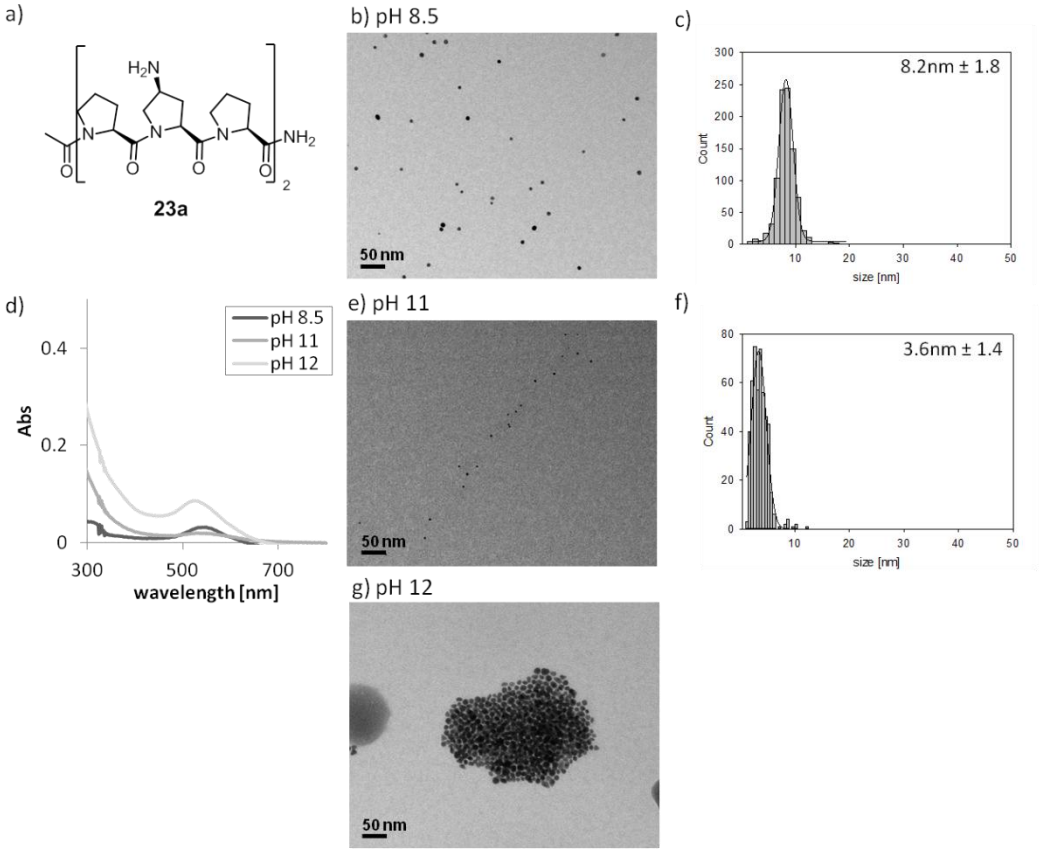

Figure 101: a) Peptide **23a**; AuNPs generated in the presence of peptide **23a** at different pH values; **b)** TEM image at pH 8.5, **c)** histogram of AuNPs generated at pH 8.5; **d)** UV-Vis spectra, **e)** TEM image at pH 11, **f)** histogram of AuNPs generated at pH 11; **g)** TEM image at pH 12. Analysis was carried out after one day.

The results are shown in Figure 101. In contrary to the results obtained with the amine-functionalized oligoprolines with linker **21a**, with peptide **23a** lacking a linker between amine group and the backbone, monodisperse, spherical nanoparticles were formed at pH 8.5 and 11. The ones formed at pH 8.5 were about 8 nm in diameter and those obtained at pH 11 were more or less half that size (3.6 nm). The nanoparticles formed at pH 12 were polydisperse and aggregated within a day. As already found before, also in this case, the pH of the reaction mixture had a very strong impact on the size and shape of the resulting nanoparticles. The size difference was about 4 nm with

the pH difference of about 2.5 pH values. These results were further investigated by testing the other lengths of the amine-functionalized oligoproline **23a-c** as additives in the AuNP formation reaction at the two different pH values. First, we carried out the reaction at pH 8.5 using again ascorbic acid as external reducing agent.

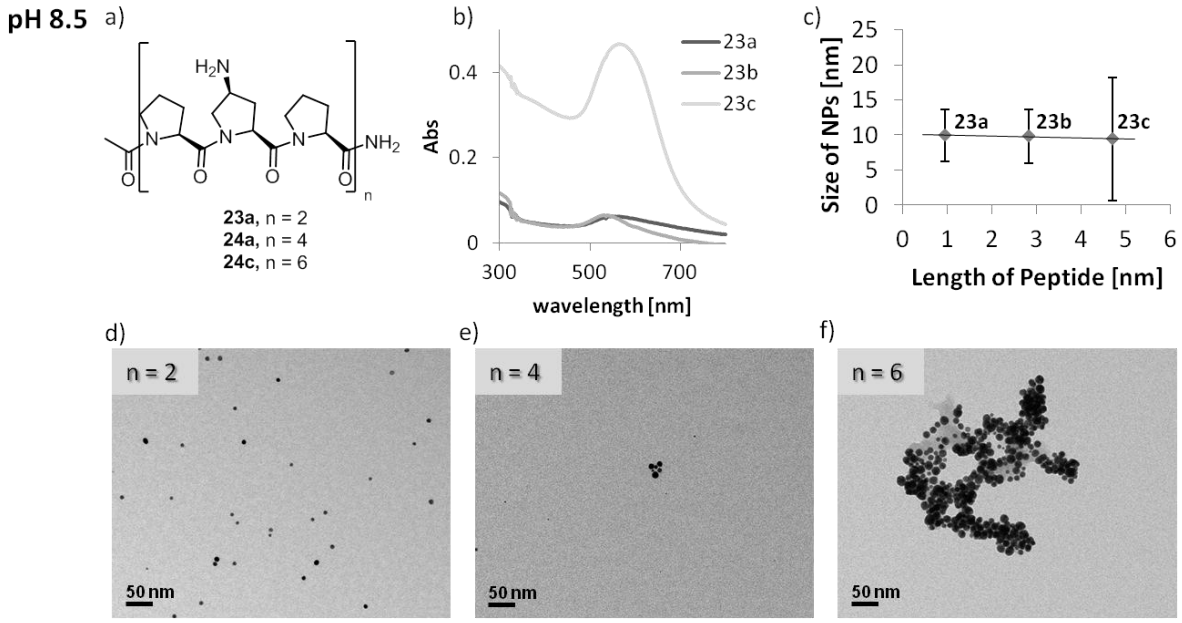

Figure 102: a) Peptides **23a-c**; AuNPs formed in the presence of peptide **23a** (n = 2), **23b** (n = 4) and **23c** (n = 6) at pH 8.5: **b)** UV-Vis spectra, **c)** correlation between the length of peptides **23a-c** and the size of the resulting AuNPs, **d)** TEM image of AuNPs formed in the presence of peptide **23a**, **e)** TEM image of AuNPs formed in the presence of peptide **23b**, **f)** TEM image of AuNPs formed in the presence of peptide **23c**. Analysis was carried out after one day.

The results are shown in Figure 102. The nanoparticles formed at pH 8.5 using the amine-functionalized peptides **23a-c** had about the same size and shape like it was found in the investigations of the different peptides before. However the AuNPs formed with the longest derivative **23c** had a much broader size distribution and aggregated within one day. These observations are in contrary to the observations made before when the length of the peptide did not affect the resulting size and shape. This is probably due to the missing linker which might hinder the stabilization when the peptide becomes longer.

To further investigate this system, the formation reaction was also carried out in the presence of peptides **23a-c** at pH 11 (Figure 103)

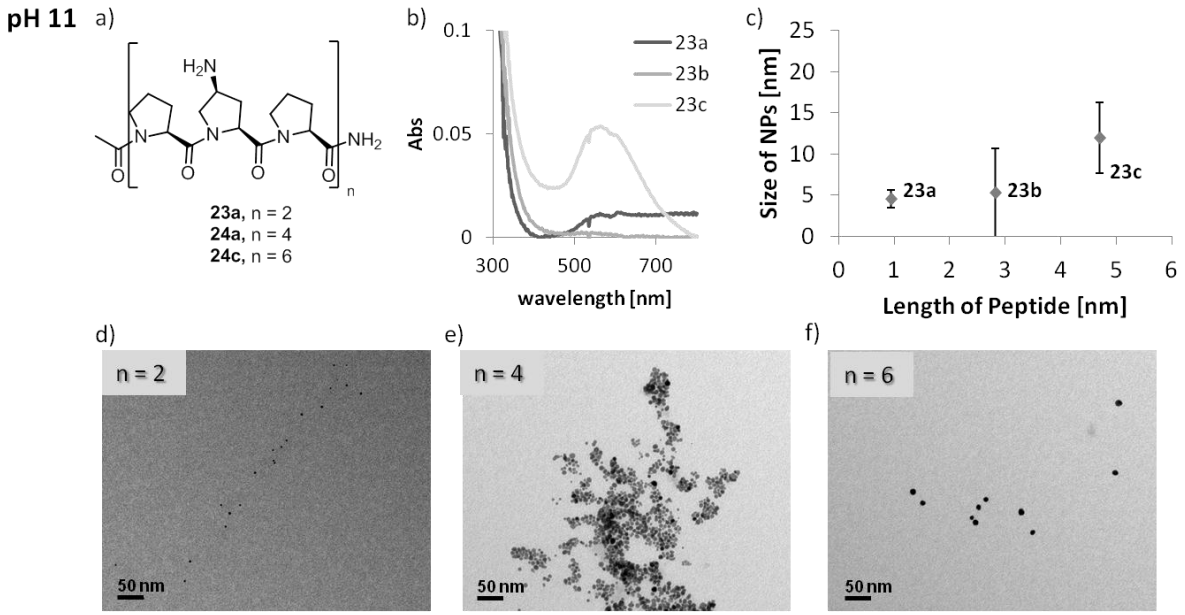

Figure 103: a) Peptides **23a-c**; AuNPs formed in the presence of peptide **23a** (n = 2), **23b** (n = 4) and **23c** (n = 6) at pH 11: **b)** UV-Vis spectra, **c)** correlation between the length of peptides **23a-c** and the size of the resulting AuNPs, **d)** TEM image of AuNPs formed in the presence of peptide **23a**, **e)** TEM image of AuNPs formed in the presence of peptide **23b**, **f)** TEM image of AuNPs formed in the presence of peptide **23c**. Analysis was carried out after one day.

The results are shown in Figure 103. In all three cases, spherical AuNPs were formed. However, using peptide **23b** as additive resulted in AuNPs with a high dispersity and which were aggregating within one day. In the presence of the longest amine-functionalized peptide **23c**, the AuNPs formed were bigger in diameter as the nanoparticles formed in the presence of the shorter derivatives **23a-b** (Figure 103c). These peptides clearly behave differently than found before, where no differences in resulting nanoparticles were found when using different lengths of the same kind of peptides. The longest derivative **23c** did not to stabilize the nanoparticles in the same size as it was found for the shortest oligoproline **23a**. This is probably due to the missing linker which allows the functional group to adopt to the different conditions and which is hindered by the increased rigidity present in the peptide without linker, used in these experiments.

3.1.5.3.3. Generation of AuNPs in the Presence of Peptide 21a without Additional Reducing Agent

Next, we evaluated the ability of peptide **21a** to reduce Au^{3+} in solution. In the case of silver, reduction was achieved using this peptide, but no defined nanoparticles were formed. To test this for gold, the AuNP formation reaction was performed in the absence of an external reducing agent at a

ratio of Au^{3+} to functional group of 1:5. Different pH values (9.5, 11, 12) were tested. However, nanoparticle formation was not observed in any of the three experiments.

3.1.5.4. AuNP Generation in the Presence of Peptides Bearing Carboxylic Acid Moieties

3.1.5.4.1. Optimization of the Reaction Conditions: Peptide 18a

Next peptide **18a**, bearing carboxylic acid moieties was studied for the ability to act as additive in the AuNP generation. Previously, we have shown that using this peptide, it was not possible to stabilize AgNPs in a defined size and shape (chapter 3.1.4.4).

To evaluate the ability of carboxylic acid-functionalized peptides **18a-c** to act as additive in the AuNP formation reaction, as shown in the investigation of the other peptides, first the reaction conditions needed to be optimized. We screened different pH values, applying an Au^{3+} to functional group ratio of 1:5 and ascorbic acid as external reducing agent in each experiment. A solution with a pH of 4 was obtained by dissolving the peptide **18a** in water. Additionally the reaction was performed at pH 10 and pH 12. After pH adjustment and equilibration with the metal salt, the external reducing agent was added and the formation reaction was monitored by UV-Vis and analyzed by TEM.

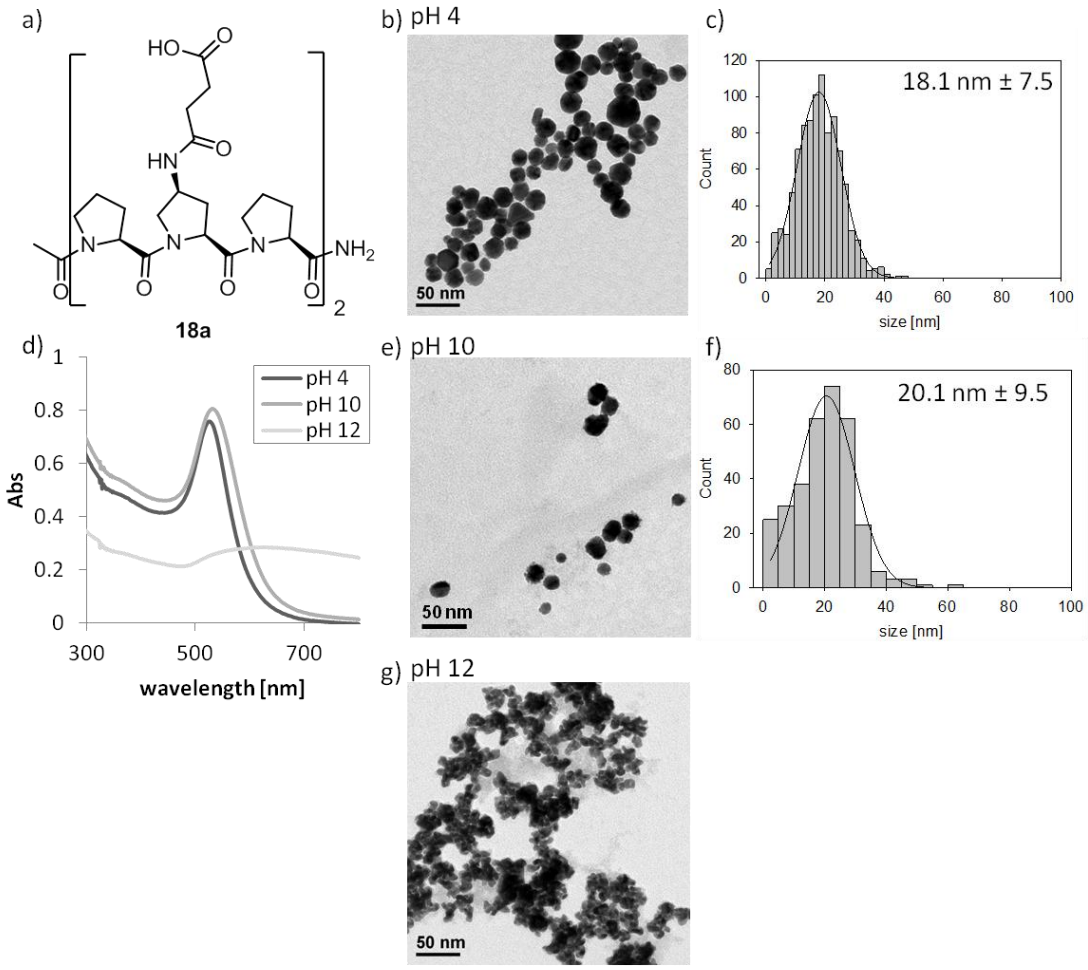

Figure 104: a) Peptide **18a**; AuNPs generated in the presence of peptide **18a** at different pH values; **b)** TEM image at pH 4, **c)** histogram of AuNPs generated at pH 4; **d)** UV-Vis spectra, **e)** TEM image at pH 10, **f)** histogram of AuNPs generated at pH 10; **g)** TEM image at pH 12. Analysis was carried out after one day.

Nanoparticle formation was observed at all investigated pH values (Figure 104). At pH 4 they were polydisperse with an average diameter of 18 nm. Many different shapes were found, including spheres, truncated triangles and hexagons with diameters between 1 nm and 50 nm (Figure 104b-c). The AuNPs formed at pH 10 had an average diameter of 20 nm, but were also polydisperse. On the contrary to those obtained at pH 4 they were all more or less spherical but also varied in diameter between 1 nm and 50 nm. At pH 12, only polydisperse nanoparticles, without a defined shape were found. The AuNPs were aggregating within two days as can be seen in Figure 104f. Application of peptide **18a**, bearing carboxylic acid groups as an additive resulted exclusively in formation of polydisperse nanoparticles not only in the case of silver, but also as shown in this chapter, in the case of gold.

3.1.5.4.2. Generation of AuNPs in Presence of Peptide 18a without Additional Reducing Agent

The capability of peptide **18a**, to reduce Au^{3+} was also evaluated. The reactions were carried out at an Au^{3+} to functional group ratio of 1:5 without external reducing agent at different pH values as we did already for the other peptides before, to screen for optimal reaction conditions. The tests with peptide **18a** were performed at pH 4, 8 and 12.

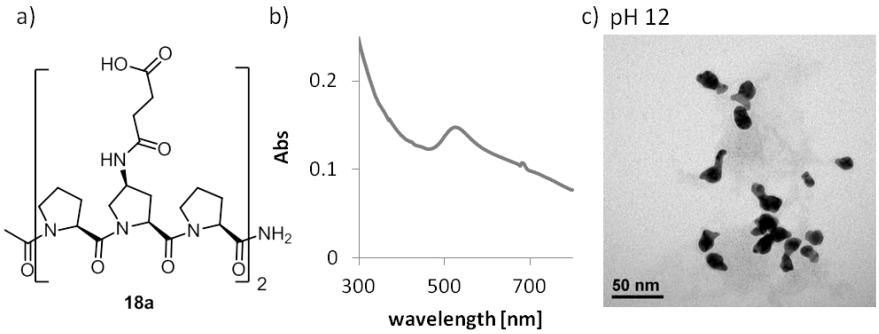

Figure 105: a) Peptide **18a**; AuNPs generated in the presence of peptide **18a** without additional reducing agent at pH 12, **b)** UV-Vis spectrum at pH 12, **c)** TEM image. Analysis was carried out after two days.

Nanoparticle formation was observed only at pH 12 (Figure 105). The reduction was relatively slow. After two days a plasmon absorbance appeared in the UV-Vis spectrum. The resulting AuNPs were polydisperse and of a non-defined shape.

This peptide is able to reduce Au^{3+} ions just as it was for the case with Ag^{+}. However, it is, also in this case, not able to stabilize the formed nanoparticles after reduction of the metal ions.

3.1.5.5. AuNP Generation in the Presence of Peptides Bearing Indole Moieties

3.1.5.5.1. Optimization of the Reaction Conditions Using Peptide 19a without Additional Reducing Agent

The last compounds studied as a potential additive in the AuNP formation were peptides **19a-c**, bearing indole moieties on the backbone. The AuNP generation was performed without additional reducing agent, as the indole motif already has a considerable reducing capability like already demonstrated in the AgNP formation (chapter 3.1.4.5). First we used the shortest peptide **19a** for the screening for the optimal conditions. A ratio of Au^{3+} to functional group of 1:3 was used, as it was found to be optimal for the generation of AgNPs with this peptide. We tested pH values of 7, obtained by dissolving peptide **19a** in water, 10 and 12 (Figure 106).

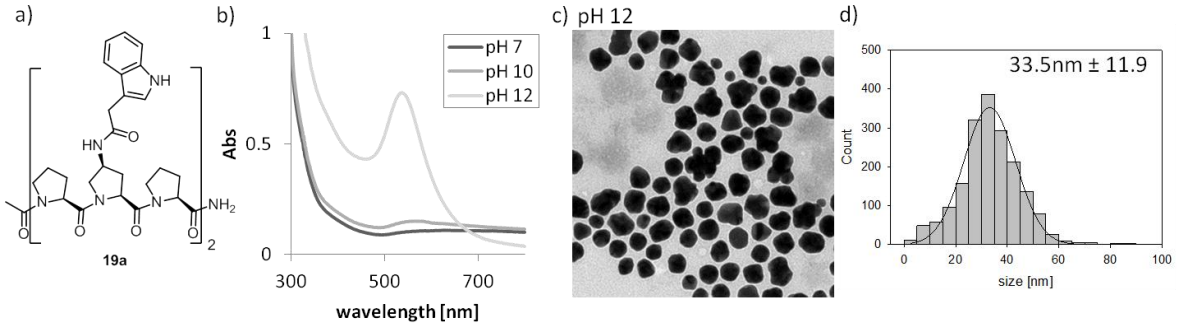

Figure 106: a) Peptide **19a**; AuNPs formed in the presence of peptide **19a** at different pH values, **b)** UV-Vis spectra, **c)** TEM image at pH 12; **d)** histogram of AuNPs at pH 12. Analysis was carried out after one day.

Nanoparticle formation was only observed at pH 12. The resulting AuNPs were polydisperse in size and shape. It seems that the oxidized form of the peptide is not able to stabilize the particles in a monodisperse fashion. In case of AgNP formation this peptide was able to act as additive and reducing agent resulting in monodisperse nanoparticles. With the indole-functionalized peptide **19a**, used as additive in the formation of AuNP, non-spherical polydisperse nanoparticles with an average diameter of 33.5 nm were formed (Figure 106).

3.1.5.5.2. Testing Peptides with Different Lengths: Peptides 19a-c

The longer derivatives of indole-functionalized peptide **19a**, **19b** and **19c** were also tested in the nanoparticle generation at pH 12 with a ratio of Au^{3+} to functional group of 1:3 in the absence of an external reducing agent, as this pH value was found to be the only one, nanoparticle formation was observed for peptide **19a**.

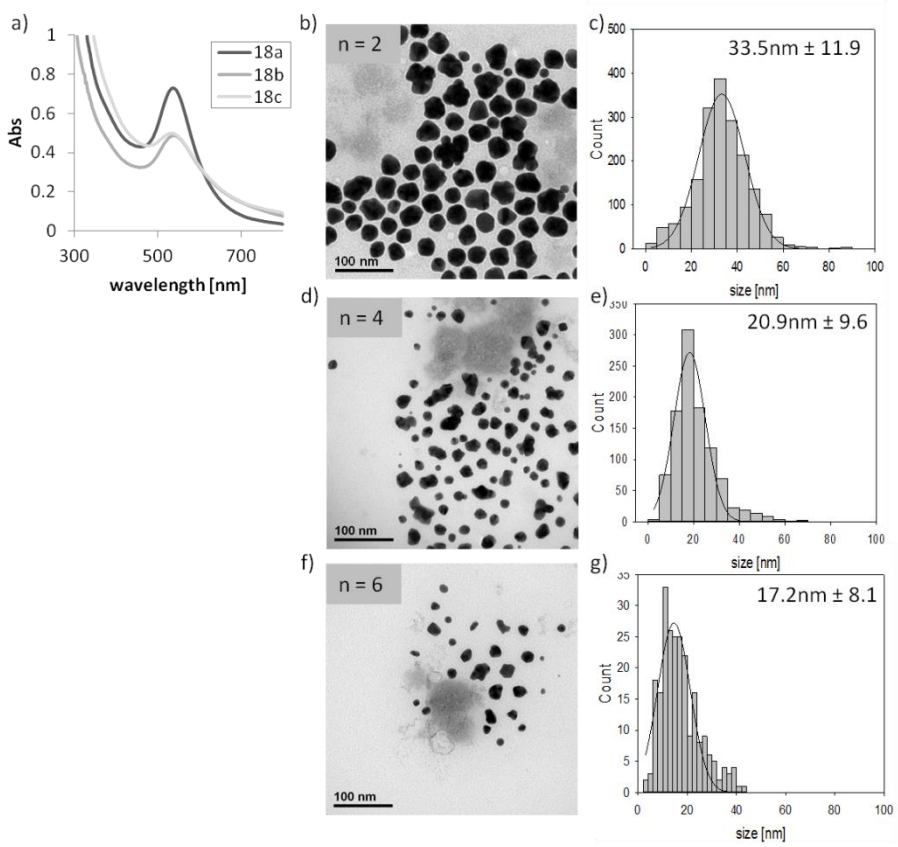

Figure 107: AuNPs generated in the presence of peptides **19a** (n = 2), **19b** (n = 4) and **19c** (n = 6): **a)** UV-Vis spectra, **b)** TEM image of AuNPs formed in presence of peptide **18a**, **c)** histogram of AuNPs formed in presence of peptide **19a**, **d)** TEM image of AgNPs formed in presence of peptide **19b**, **e)** histogram of AuNPs formed in presence of peptide **19b**, **f)** TEM image of AgNPs formed in presence of peptide **19c**, **g)** histogram of AuNPs formed in presence of peptide **19c**. Analysis was carried out after one day.

The results are shown in Figure 107. Unfortunately, application of longer peptides also yielded polydisperse nanoparticles. Interestingly, their average size decreased with increasing length of the peptides. The size distribution also did narrow slightly. Nonetheless, they were still polydisperse.

The indole moieties are also able to act as reducing agents for Au^{3+} ions, just as it was observed for Ag^{+} (chapter 3.1.4.5.2). However, they are not able to stabilize the nanoparticles in defined sizes and shapes.

3.1.6. Platinum Nanoparticle (PtNP) Generation

After the studies on the generation of AgNPs and AuNPs we decided to carry out some preliminary tests with imidazole-functionalized peptide **17a-c**, as a potential additive in the formation of PtNPs. These nanoparticles are highly attractive targets, due to their potential applications in catalysis and medicinal chemistry.[12, 220] These peptides were chosen, due to their ability to act as additive for the defined formation of AgNPs as well as AuNPs.

Like in all previous cases, we first evaluated the pH for the generation reaction. A Pt^{2+} to imidazole group ratio of 1:5 was used, as this was found to be the optimal conditions for this peptide as an additive (chapter 3.1.4.2.1.). Two equivalents of sodium borohydride as reducing agent were used as preliminary experiments showed that the reduction using only one equivalent of reducing agent was not complete. We tested the generation reaction at pH 9, obtained by dissolving peptide **17a** in water, and pH 12. The formation was analyzed using TEM (Figure 108).

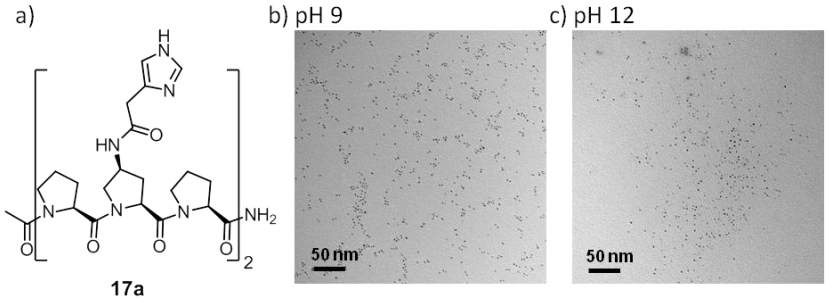

Figure 108: a) Peptide **17a**; PtNPs generated in the presence of peptide **17a**, **b)** TEM image of PtNPs at pH 9, **c)** TEM image of PtNPs at pH 12. Analysis was carried out after one day.

Monodisperse nanoparticles were formed in both experiments. They were spherical in shape and about 3 nm in diameter. As pH doesn't seem to play a significant role in this case, we decided to use pH 9 for the following experiments, to omit the adjustment step for each reaction. These findings are different to those obtained in the formation of AgNPs and AuNPs.

Under these conditions, the generation of nanoparticles in the presence of the longer imidazole-functionalized peptides **17b** and **17c** was also performed (Figure 109).

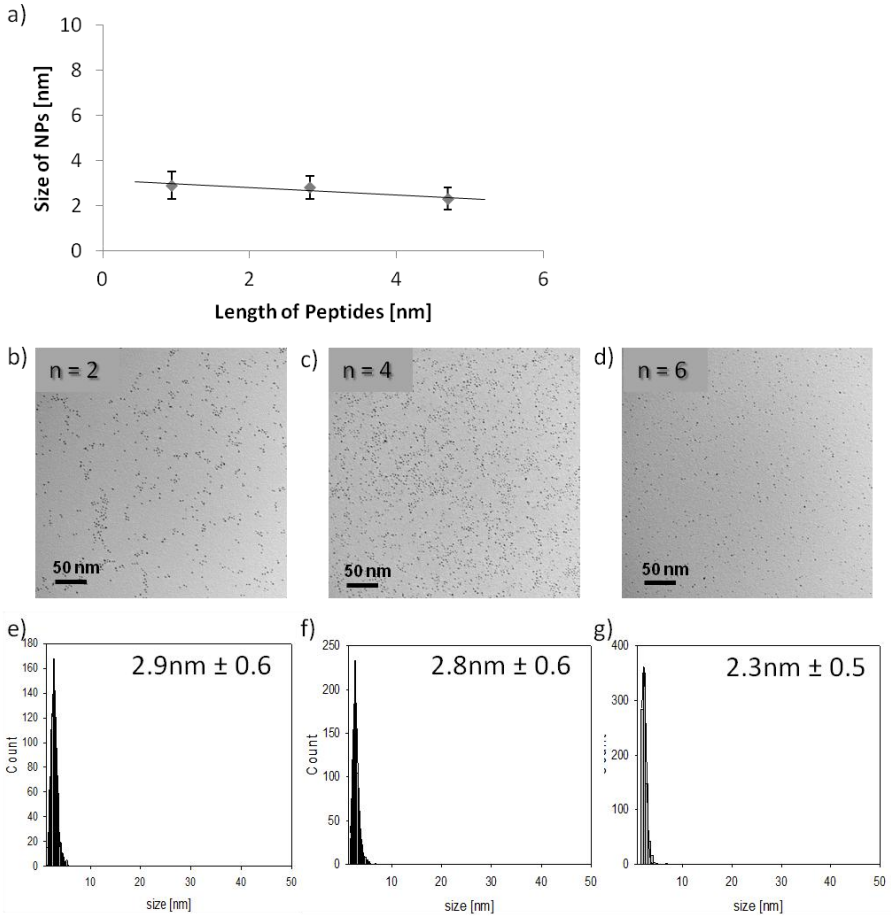

Figure 109: PtNPs generated in the presence of peptide **17a** (n = 2), **17b** (n = 4) and **17c** (n = 6): **a)** correlation between the length of peptides **17a-c** and the size of the resulting PtNPs, **b)** TEM image of PtNPs formed in the presence of peptide **17a**, **c)** TEM image of PtNPs formed in the presence of peptide **17b**, **d)** TEM image of PtNPs formed in the presence of peptide **17c**. **e)** histogram of PtNPs generated in the presence of **17a**, **f)** histogram of PtNPs generated in the presence of **17b**, **g)** histogram of PtNPs generated in the presence of **17c**. Analysis was carried out after one day.

The resulting nanoparticles were monodisperse with a diameter of around 3 nm for each of the investigated peptides. The difference in backbone length had no influence on the size and shape of nanoparticles, as already observed for other metals with this and the other investigated peptides.

Generation of PtNPs was successfully achieved using imidazole-functionalized peptides **17a-c** as additives. This is a very promising result as it renders the possibility for a more in-depth investigation of platinum and in the future maybe, even studies on other metals.

3.2. Additive for the AgNP Generation Based on a Simple Tripeptide

Following up, on the investigations carried out in our group, where tripeptides, suitable to act as additives for nanoparticle formation were identified within a split-and-mix library,[77, 206] we chose one peptide and attempted to improve its performance. To achieve this, structural changes were made by introducing additional amino acids in the sequence. Peptide Ac-His-Ahx-Asp-NH_2 **32** was selected (Figure 110a) for our study.[77, 206] When it was applied as an additive using ascorbic acid as external reducing agent, AgNPs with an average diameter of 29 nm were formed. Unfortunately in the beginning of this study there were problems with the stabilization of these nanoparticles by the peptide. For this reason we attempted to tune the additive's performance by structural modifications. The problems with the stability of the nanoparticles formed in the presence of the tripeptides **32** were solved during this study in the PhD thesis of Conelious Pfumbidzai.[206]

3.2.1. Design

Two crucial changes were made in the structure of peptide **32**. First the amount of functional groups, imidazole and carboxylic acid, per one molecule was increased by a factor of two. We envisioned that this will increase the additive's binding affinity which will be beneficial for the stabilization of resulting AgNPs. Furthermore, we incorporated proline units in the sequence. The structure of the modified peptide **33** is shown in Figure 110b, whereas the structure of the tripeptide **32** being the inspiration for the new design is displayed in Figure 110a.

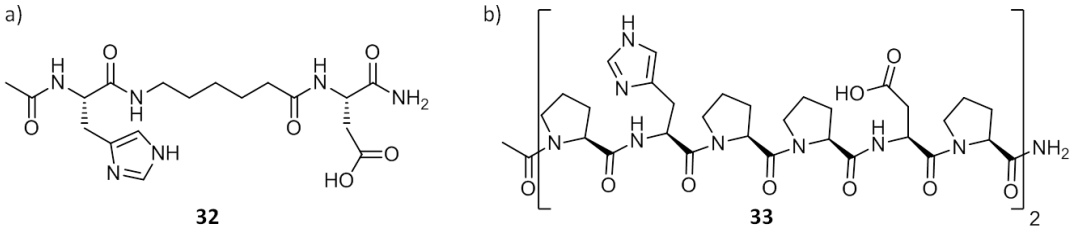

Figure 110: a) Structure of peptide **32**, **b)** structure of peptide **33**.

3.2.2. Synthesis and Conformational Analysis

The synthesis was carried out using standard SPPS protocols (5.3.) on Rink amide – ChemMatrix resin, followed by acetylation of the *N*-terminus and cleavage with TFA. To investigate the secondary structure CD spectroscopy was carried out (Figure 111). It was expected that the peptide has a

decreased flexibility due to the many prolines in the sequence and therefore not adopt a random coil structure.

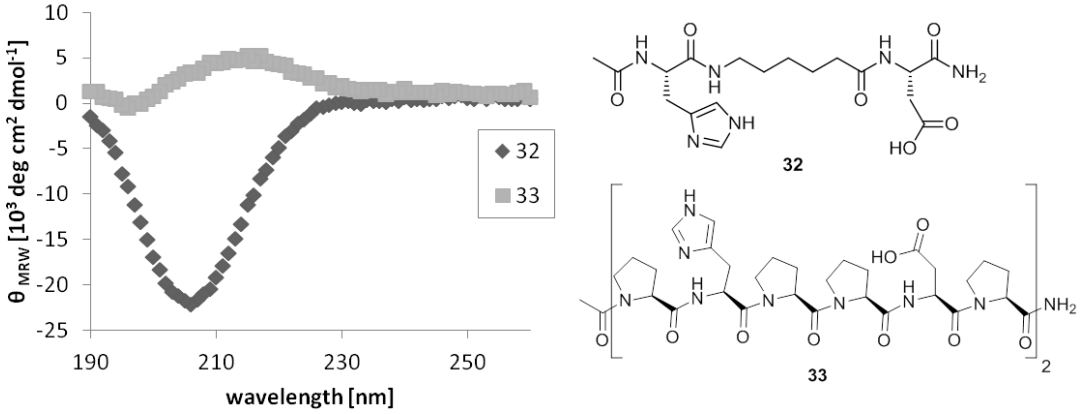

Figure 111: CD spectra of peptides **32** and **33**.

The CD spectra of peptide **32** and **33** are presented in Figure 111. Peptide **32** adopts a random coil structure with a minimum at 195 nm and a maximum at 216 nm. The spectrum of peptide **33** shows a shift of the minimum to a wavelength of 206 nm which is characteristic of a PPII structure. However, no maximum is observed which suggests that the secondary structure of **33** is considerably different to the previously studied oligoproline-based peptides, but also not form a random coil.

3.2.3. Silver Nanoparticle (AgNP) Generation

First, the ability of peptide **33** to act as an additive in the nanoparticle generation was tested. Ascorbic acid was used in the beginning. This reducing agent was also successfully used in combination with peptide **32** in our previous studies.[77, 206] Then we expanded the investigation by using the stronger reducing agent sodium borohydride. To screen the versatility of the new peptide to act as additive, we also tested the usage of light for the reduction of Ag^+.

3.2.3.1. AgNP Generation Using Ascorbic Acid as Reducing Agent

The performance of peptide **33** was evaluated. Optimized conditions, found in the previous study of an Ag^+ to functional group ratio of 1:10 at pH 10 with 1.2 equivalents of ascorbic acid were used. The formation reaction was performed in the presence of peptides **32** and **33** to be able to compare the performance and resulting size and shape of the formed AgNPs.

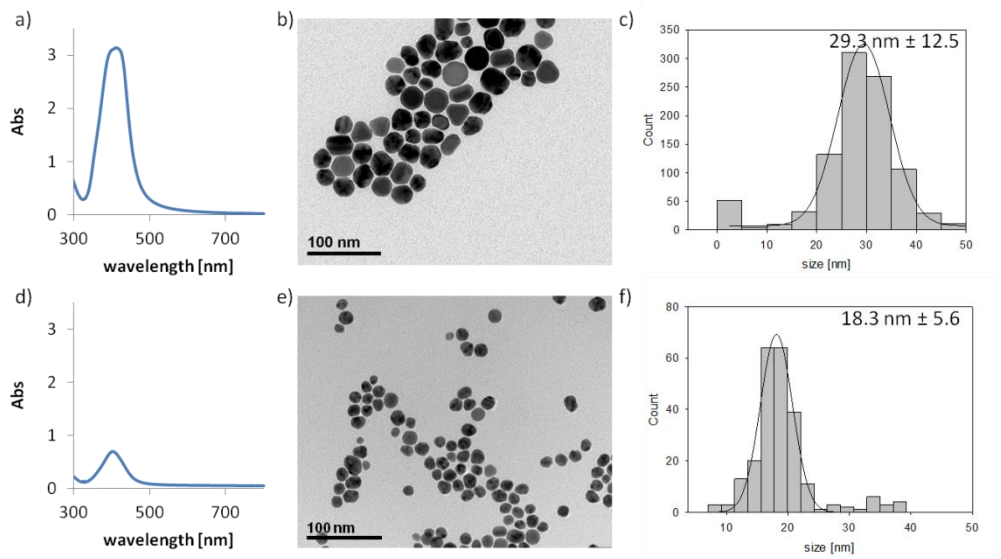

Figure 112: AgNPs generated using ascorbic acid as reducing agent in the presence of peptide **32**: **a)** UV-Vis spectrum, **b)** TEM image, **c)** histogram; AgNPs generated using ascorbic acid as reducing agent in the presence of peptide **33**: **d)** UV-Vis spectrum, **e)** TEM image, **f)** histogram. Analysis was carried out after one day.

The results are shown in Figure 112. Nanoparticles formed in both cases. The ones formed in the presence of tripeptide **32** had a truncated hexagon like shape with an average diameter of 29 nm, as already reported before.[77, 206] Nanoparticles generated in the presence of the new peptide **33** had an average diameter of 18 nm and were of about the same shape. The modifications in the additive are the reason for the 11 nm difference in diameter. Presumably the increased amount of functional groups supports a faster surface passivation, therefore yielding smaller nanoparticles. This assumption is also supported by a more narrow size distribution of the nanoparticles generated in presence of peptide **33** compared to those generated in presence of peptide **32** (Figure 112c, f). Furthermore there was a big difference in intensity of UV-Vis absorbance (Figure 112a, d), which can be explained by a lower concentration of nanoparticles formed in presence of peptide **33**.

3.2.3.2. AgNP Generation Using Sodium Borohydride as a Reducing Agent

To explore the scope of peptide **33**'s applicability as additive for the nanoparticle generation, we also performed the reaction using a stronger reducing agent - sodium borohydride.

In this case, first optimal conditions needed to be evaluated. An Ag^+ to functional group ratio of 1:5 and 1.2 equivalents of sodium borohydride were initially applied and different pH values were screened. A solution with pH 8 was obtained by dissolving the peptide in water. Furthermore the generation reaction was also tested at pH 11 and at pH 12.

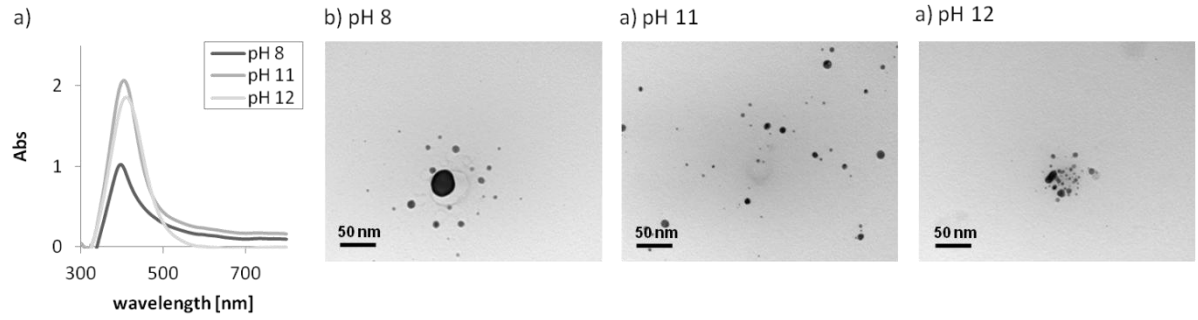

Figure 113: AgNPs generated in the presence of peptide **33** at different pH values using sodium borohydride as reducing agent; **a)** UV-Vis spectra, **b)** TEM image at pH 8, **c)** TEM image at pH 11; **d)** TEM image at pH 12. Analysis was carried out after one day.

The results are shown in Figure 113. The formation of AgNPs was observed at all pH values having a spherical shape. At pH 11 there was a regular size distribution observed. The average diameter of the AgNPs generated in this experiment was 3 nm. At pH 8 and pH 12 a broader size distribution was obtained. Therefore, the further investigations were carried out at pH 11. To further improve the outcome of the generation reaction different Ag^+ to functional group ratios were tested. To cover a broad range, ratios of 10:1, 5:1, 1:5 and 1:10 were applied.

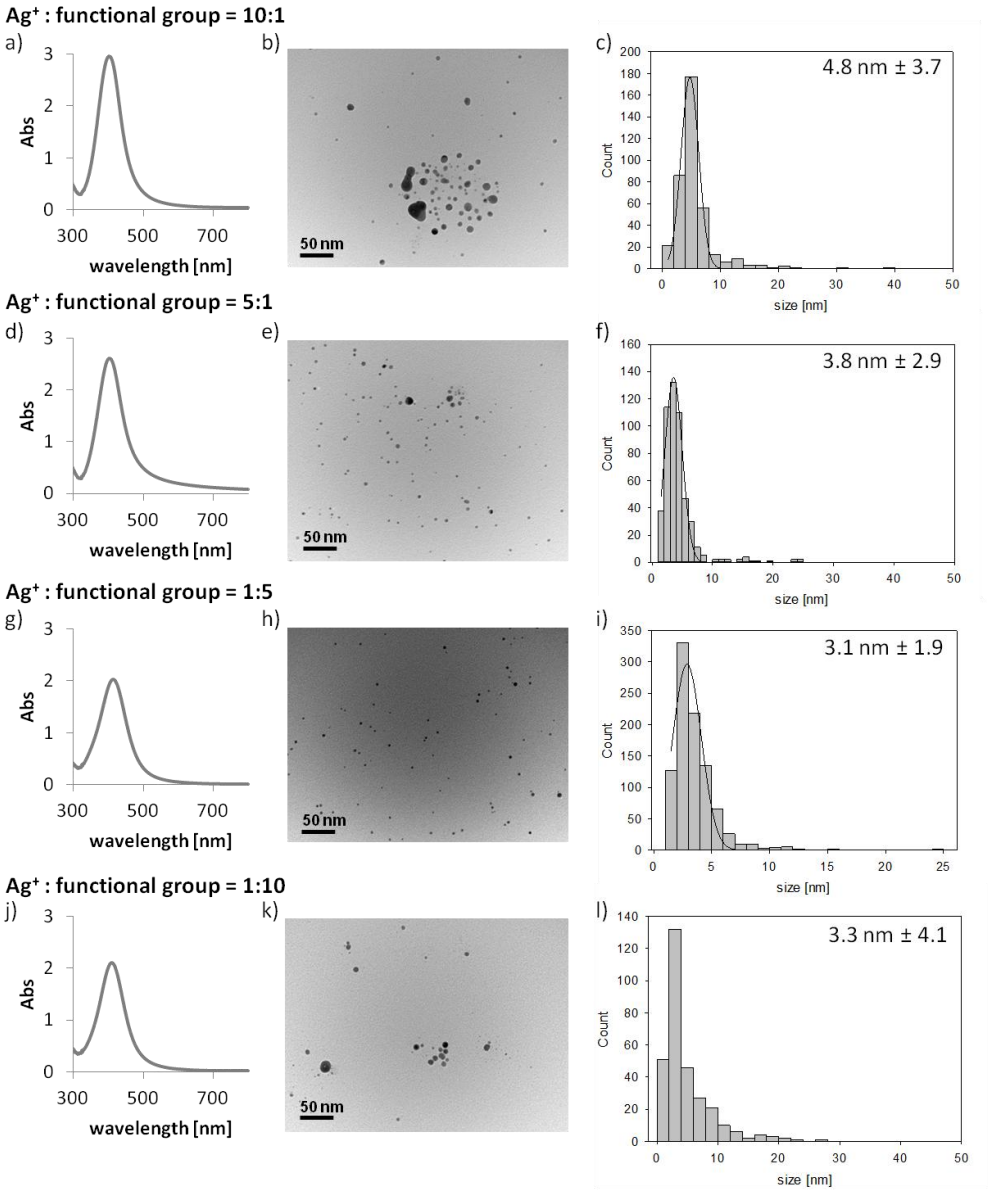

Figure 114: AgNPs generated in the presence of peptide **33** using different Ag^+ to functional group ratios and sodium borohydride as reducing agent: 10:1 **a)** UV-Vis spectrum, **b)** TEM image, **c)** histogram, 5:1 **d)** UV-Vis spectrum, **e)** TEM image, **f)** histogram, 1:5 **g)** UV-Vis spectrum, **h)** TEM image, **i)** histogram, 1:10 **j)** UV-Vis spectrum, **k)** TEM image, **l)** histogram. Analysis was carried out after one day.

The results are shown in Figure 114. The formed AgNPs were all between 3 and 5 nm in diameter. However the optimal ratio, resulting in the most narrow size distribution was the original used ratio of 1:5 as already found in the investigations for the oligoproline based peptides as additives. Spherical nanoparticles with an average diameter of 3 nm were obtained (Figure 114g-i).

Having optimized the reaction conditions, we next wanted to investigate the differences in resulting nanoparticles depending on which peptide (**32** or **33**) was used as an additive. We therefore

performed the generation reaction, in the presence of both peptides in the established conditions (a ratio of Ag^+ to functional group of 1:5, pH 11, sodium borohydride) in order to be able to compare the results.

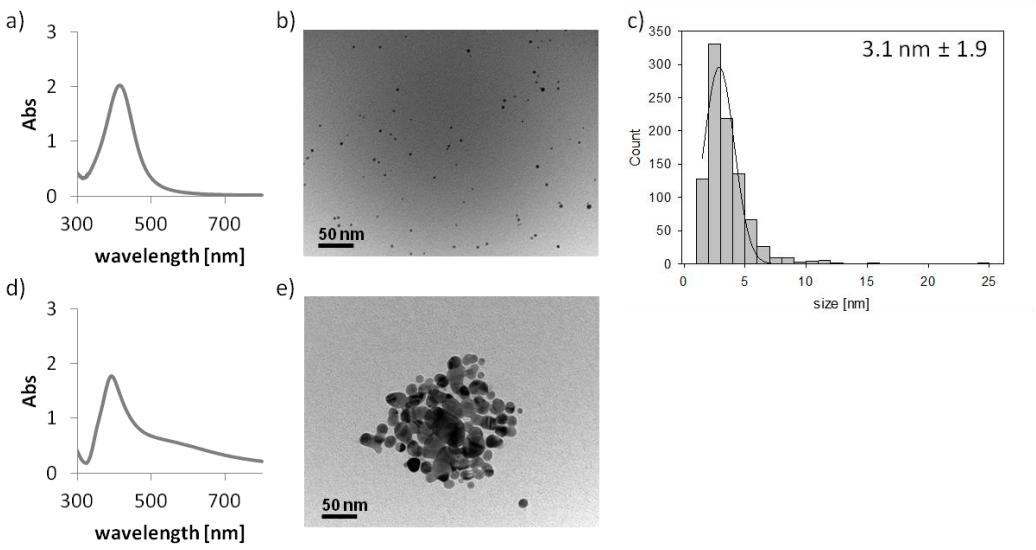

Figure 115: AgNPs generated in the presence of peptide **33**: **a)** UV-Vis spectrum, **b)** TEM image, **c)** histogram; AgNPs generated in the presence of peptide **32**: **d)** UV-Vis spectrum, **e)** TEM image. Analysis was carried out after one day.

Tripeptide **33** was not able to stabilize AgNPs in defined size and shape (Figure 115d-e). The resulting nanoparticles were polydisperse with an undefined shape and aggregated within two days. On the other hand, applying the new peptide **33** yielded spherical nanoparticles with an average diameter of 3 nm, as described before (Figure 115a-c).

With the new peptide, used as additive in the formation reaction of AgNPs, we are able to improve the quality of generated nanoparticles. Furthermore, it allowed us to use different reducing agents in the reaction, yielding differently sized monodisperse nanoparticles. With ascorbic acid, the nanoparticles were about 18 nm in diameter, whereas with sodium borohydride they were much smaller, with an average diameter of 3 nm. Formation of larger particles with ascorbic acid compared to smaller particles obtained with sodium borohydride was already observed in other systems described in the literature.[86, 89] However, it is remarkable, that we can use the same additive with both reducing agents and that under both conditions, monodisperse AgNPs were formed.

3.2.3.3. AgNP Generation Using Visible Light

Reduction of Ag^+ can also be achieved with visible light (Introduction).[80, 188, 221] This approach was for example successfully applied in the library screening conducted in our group.[77, 206] However, the investigated tripeptide **32** was not identified within the screening using light as reducing agent, but in the screening using chemical reduction. We tested the AgNP formation *via* light reduction using the newly designed peptide **33** as additive.

In a preliminary test, an Ag^+ to functional group ratio of 1:1 was used. Silver salt was added and this mixture was exposed to ambient light. Then it was observed if any nanoparticle formation took place. After a few minutes the solution became yellow and showed plasmon absorbance in UV-Vis, which is indicative for AgNP formation. The analysis by TEM confirmed this assumption.

We then started the screening to determine the optimal conditions for the generation process. First, we tested different pH values. As mentioned before, when peptide **33** was dissolved in water, a solution with a pH of 8 was obtained. We therefore tested pH 8 but also pH 10 and pH 12. The solution was exposed for one hour to ambient light and then kept in the dark.

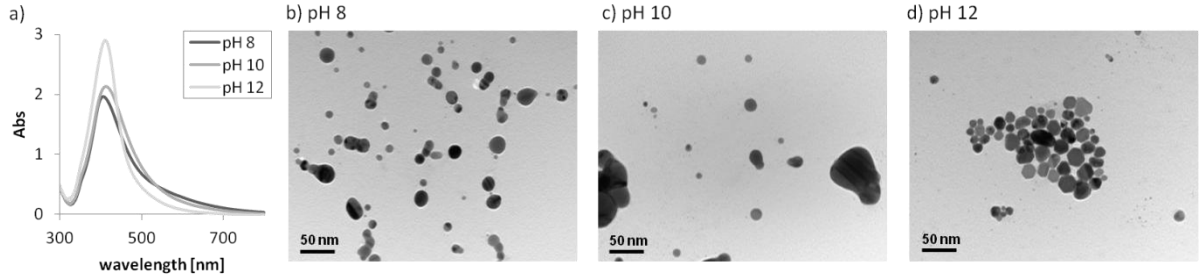

Figure 116: AgNPs generated in the presence of peptide **33** at different pH values using ambient light: **a)** UV-Vis spectra, **b)** TEM image at pH 8, **c)** TEM image at pH 10, **d)** TEM image at pH 12. Analysis was carried out after one day.

As presented in Figure 116, nanoparticle formation was observed at all tested pH values. However, they were all polydisperse. The ones generated at pH 12 were the most defined regarding their shape and therefore, this pH was used in the following experiments.

To improve the formation reaction, irradiation with defined wavelengths was attempted. The wavelengths of 254 nm and 366 nm were used. We used the same Ag^+ to functional group ratio of 1:1 like in the experiments before as well as the same pH (pH 12). The reaction was carried out, exposing the mixtures of silver salt and peptide at the desired pH, for one hour to the irradiation source. After this time, it was kept in the dark and the formation process was monitored by UV-Vis spectroscopy and analyzed by TEM.

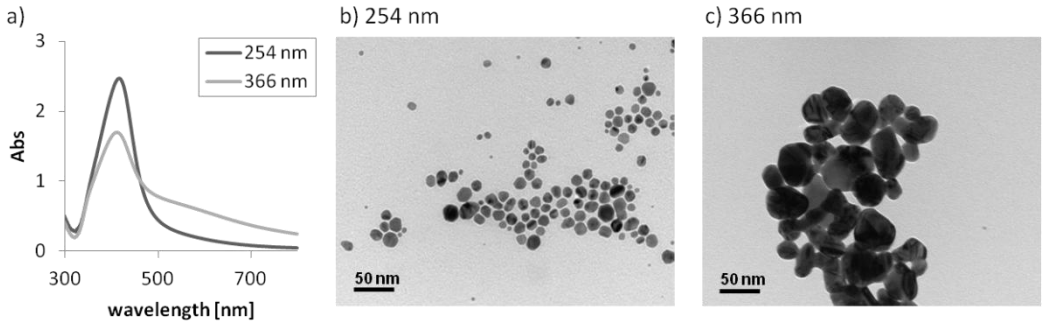

Figure 117: AgNPs generated in the presence of peptide **33** using irradiation with light of different wavelengths: **a)** UV-Vis spectra, **b)** TEM image (254 nm), **c)** TEM image (366 nm). Analysis was carried out after one day.

Nanoparticle formation was achieved under both conditions as shown in Figure 117. The nanoparticles formed upon irradiation with a wavelength of 254 nm were spherical with a diameter of about 8 nm (7.8 nm ± 4.8). The AgNPs generated upon irradiation with a wavelength of 366 nm were polydisperse and aggregated within two days. Therefore we decided to use irradiation with a wavelength of 254 nm for the following experiments. To further improve the conditions we then tested Ag^+ to functional group ratios of 10:1, 5:1, 1:1, 1:5 and 1:10 (Figure 118).

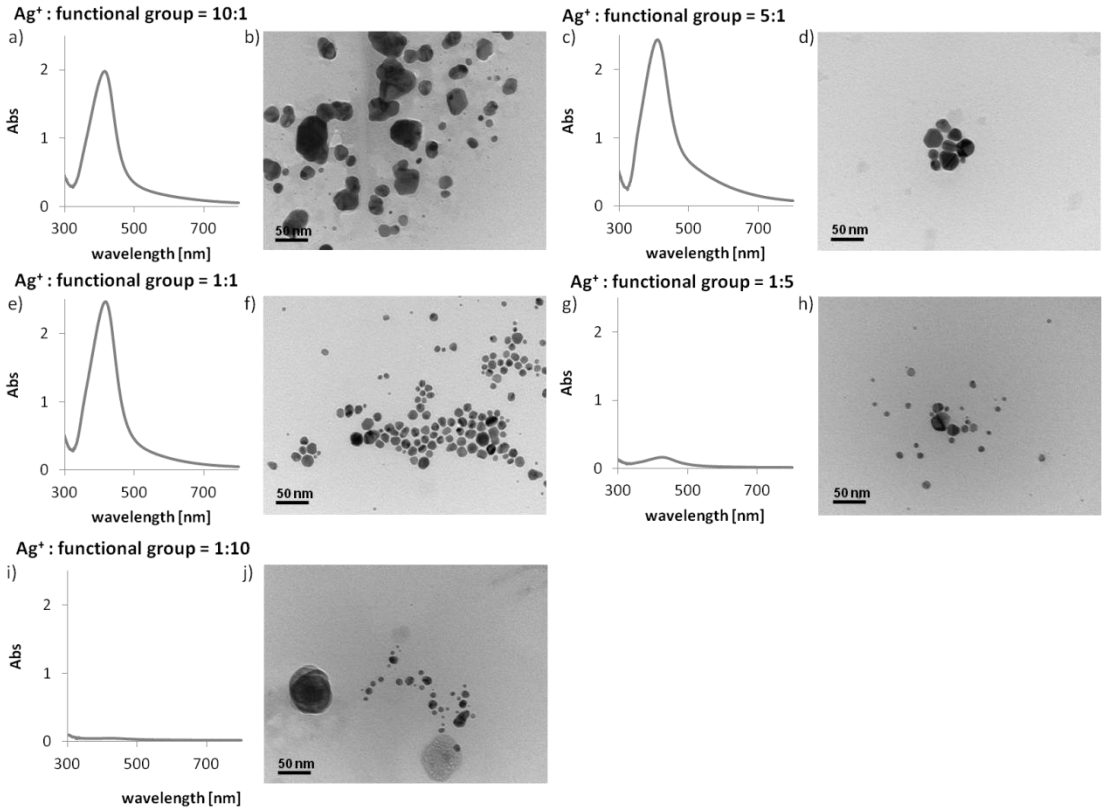

Figure 118: AgNPs generated in the presence of peptide **33** using different Ag^+ to functional group ratios and irradiation with a wavelength of 254 nm; 10:1 **a)** UV-Vis spectrum, **b)** TEM image, 5:1 **c)** UV-Vis spectrum, **d)** TEM image, 1:1 **e)** UV-Vis spectrum, **f)** TEM image,, 1:5 **g)** UV-Vis spectrum, **h)** TEM image, 1:10 **i)** UV-Vis spectrum, **j)** TEM image. Analysis was carried out after one day.

As shown in Figure 118, neither lower, nor higher peptide concentration was beneficial for the generation reaction. The experiments were less peptide was used, led to a broader size distribution and aggregation of the nanoparticles (Figure 118a-d). When a higher peptide concentration was applied, less AgNPs were formed as can be seen in the respective UV-Vis spectra, represented by a lower intense plasmon absorbance band (Figure 118g, i). Additionally, no improvement in the size distribution was achieved. In contrary, it resulted in a broader size distribution. For the ratio of 1:5 an average diameter of 7.8 nm ± 7.4 was found and with a ratio of 1:10 a diameter of 6.8 nm ± 10.6.

Finally the reaction was also carried out, under the optimized conditions using tripeptide **32** as additive to compare its ability to act as an additive for the generation of AgNPs by irradiation. An Ag^+ to functional group ratio of 1:1 at pH 12 using irradiation with a wavelength of 254 nm were applied.

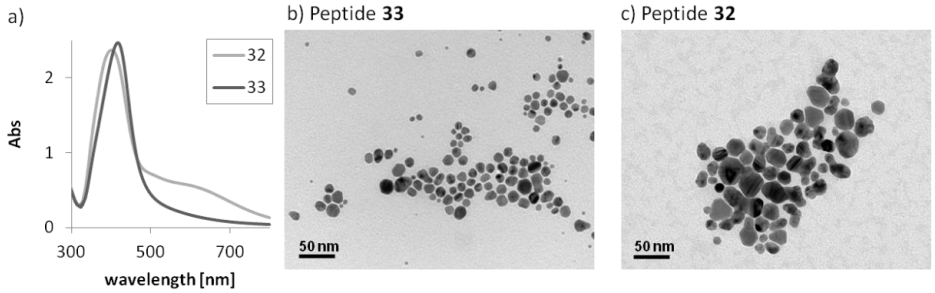

Figure 119: AgNPs generated by irradiation (254 nm) in the presence of peptide **32** and peptide **33**; **a)** UV-Vis spectra, **b)** TEM image of AgNPs generated in the presence **33**, **c)** TEM image of AgNPs generated in the presence **32**. Analysis was carried out after one day.

As shown in Figure 119, nanoparticle formation was also observed, when tripeptide **32** was used as additive. However the resulting AgNPs were polydisperse under these conditions.

This results show, that also in the case of AgNP formation using visible light to reduce the Ag^{+}, the newly designed peptide **33** was more versatile in comparison to tripeptidic additive **32** in stabilizing the AgNPs in defined size and shape.

4. Summary and Outlook

In the course of this work, we investigated different peptidic additives for their ability to act in the formation reaction of metal nanoparticles. The peptides had an oligoproline backbone, functionalized in every third position. This resulted in the functional groups pointing in the same direction in space. The groups attached were chosen based on their ability to bind to silver ions in the gas phase, which we expected to be a crucial factor to be able to act as stabilizing moiety in the nanoparticle formation. Therefore guanidine, imidazole, primary amine, carboxylic acid, indole and pyrrolidinyl groups were attached to an oligoproline backbone with different lengths.

We investigated the secondary structure of the new peptides with CD spectroscopy. A defined PPII helical structure was found for all the peptides which showed that the functionalization on the backbone did not influence the defined secondary structure of the oligoproline backbone.
First of all the reaction conditions for the formation needed to be optimized. The formation reaction was carried out in an aqueous solution of the respective metal salt in the presence of a peptides used as additive. Ascorbic acid and sodium borohydride were evaluated as external reducing agent. The formation was also carried out without an external reducing agent, to test the ability of the peptides as reducing agent and stabilizer at the same time. Different pH values were screened for the formation reaction which turned out to be crucial to obtain defined nanoparticles. In the course of the optimization, furthermore the ratio of metal to peptide was altered. The formation reaction was first evaluated for silver nanoparticles (AgNPs) using the different peptidic additives and then for the formation of gold nanoparticles (AuNPs).

In the investigation of AgNPs, using ascorbic acid as external reducing agent, monodisperse spherical AgNPs were formed with an average diameter of 12 nm with the peptides **22a-c**, functionalized with guanidine groups. With sodium borohydride as external reducing agent, monodisperse nanoparticles only formed in the presence of imidazole-functionalized peptides **17a-c**. Ascorbic acid was not strong enough to reduce the metal ions in the presence of this peptide, but using sodium borohydride resulted in monodisperse AgNPs (4 nm). In the generation reaction using ascorbic acid in the presence of amine-functionalized oligoprolines **21a-c** interestingly, non-spherical shapes were found. Also in the case of pyrrolidinyl-functionalized peptides **20a-c** using ascorbic acid a new shape, rods were found. In the presence of the other investigated peptides in the formation reaction of AgNPs using ascorbic acid, only polydisperse nanoparticles were obtained. When we tested the ability of the

peptidic additives to act as reducing agents as well as stabilizing moiety, we found monodisperse AgNPs formed in the presence of guanidine-functionalized peptides **22a-c** (6 nm) as well as with the indole-functionalized peptides **19a-c** (10 nm).
We observed that the length of the peptide had only a minor influence on the resulting morphology. To test the importance of the oligoproline backbone, to be able to act as an additive, we used flexible derivatives of the guanidine-functionalized and imidazole-functionalized peptides. These functional groups were chosen because the corresponding oligoprolines resulted in monodisperse nanoparticles. In the presence of these peptides only polydisperse AgNPs were formed which aggregated within a day. We therefore concluded, that the spatial orientation is essential for the additives to act in the formation of metal nanoparticles.

Next we evaluated the peptidic additives in the formation reaction of AuNPs. With ascorbic acid as external reducing agent, two of the investigated peptides were able to stabilize monodisperse nanoparticles: In the presence of peptides with guanidine functional groups (**24a-c**, 9 nm) and amine-functional groups (**23a-c**, 8 nm at pH 8.5, 4 nm at pH 11) attached on the backbone. Interestingly, using the latter peptides **23a-c** showed different stabilizing abilities depending on the pH of the reaction resulting in differently sized nanoparticles. With sodium borohydride as external reducing agent, it was possible to obtain monodisperse AuNPs in the presence of imidazole-functionalized peptides **17a-c** (2 nm).
In the case of AuNP with none of the investigated peptides monodisperse nanoparticles were formed without an additional reducing agent, they were all polydisperse. Reduction took place, but the peptides were not able to successfully stabilize the AuNPs in defined size and shape.

We also tested the influence of the linker for the guanidine and the amine-functionalized peptides by screening peptides with and without linker between the functional group and the oligoproline backbone. The results were very different depending on the metal and the functional group. In the case of the guanidine group in the formation of the AgNPs it proved to be important to have a certain flexibility which is provided by the linker. The formation reaction in the presence of the peptide without the linker resulted in bigger aggregates whereas with the linker monodisperse nanoparticles were formed. In the AuNP formation, the resulting nanoparticles formed in the presence of the two kind of peptides, were very similar in size and shape.
When the peptide with an amine group attached was tested in the formation of AgNPs, the nanoparticles formed in the presence of the peptides with and without linker, had about the same

size and shape. In both cases polydisperse nanoparticles with non-spherical shapes were formed. When they were used in the formation of AuNPs, the nanoparticles were polydisperse when the additive with linker was used and monodisperse with the additive without linker. In this case the increased rigidity was beneficial for the stabilization in defined size and shape. These very diverse results showed clearly that first, the results obtained for silver and for gold cannot be directly compared and second that the degree of flexibility needed is very dependent on the functional group and metal.

In order to expand the variability of the peptidic additives towards other metals, we evaluated the usage of imidazole-functionalized peptides **17a-c** as additives in the platinum nanoparticle (PtNP) formation. It was possible to use this peptidic additive in the formation reaction which resulted in monodisperse nanoparticles for all three lengths of the peptide (3 nm). These results showed that it is possible to extend the research using these peptidic additives for the formation of other metals.

We furthermore attempted the design of new additives based on tripeptides indentified within split-and-mix libraries. We found the new designed peptide **33,** bearing imidazole and carboxylic acid groups was able to act as additive in the AgNP formation using mild and strong chemical reducing agents, resulting in both cases in monodisperse AgNPs with different sizes (18 nm using ascorbic acid, 3 nm using sodium borohydride). It was furthermore possible to use irradiation for the reduction in the presence of the same new designed peptide (8 nm).

Future investigations will be driven by two main interests. First, there is the question, how the stabilization takes place to result in nanoparticles with defined size and shape. With this work we already gained some insight into the needs of the design of a peptidic additive that is able to stabilize metal nanoparticles in defined size and shapes. The oligoproline backbone proved to be essential as well as the choice of the attached functional group. Different functional groups could be investigated in future studies to expand the scope for application, like for example phenols. The distance of the functional groups to the backbone, depending on the group and the metal, turned out to be important. However no clear tendency was so far observed. This would be another open question which needs to be investigated further. Also not yet understood is the binding mode responsible for the final size and shape and how we can tune the morphology further to obtain desired sizes and shapes. For example X-ray studies could be carried out to determine the crystal plane that the functional groups are binding to, to learn more about the direct correlation between the binding and the morphology. As we found the oligoproline to be a good scaffold we can functionalize it with for

example different types of functional groups on one peptide and use them in the formation reaction to test the influence of two different binders on the resulting morphology. Here we could take advantage from the library studies, carried out before and chose functional groups that proved to be able to act as additives there.[206]

A second interest is, to use the metal nanoparticles in applications. The AgNPs could be used in antimicrobial applications, as it was already successfully demonstrated by our group with nanoparticles formed in the presence of tripeptides indentified within a split-and-mix library.[206] A second possibility which would be interesting for all of the investigated nanoparticles, is the application in catalysis. As it was presented in the introduction, there are already some examples for catalysis using metal nanoparticles. However this field still needs to be developed further. Here it would be also very interesting to extend the investigations to other metals, like it was already successfully demonstrated for platinum.

5. Experimental Procedures

5.1. Materials and Instruments

Solvents and reagents were of the highest commercially available grade and used without further purification. They were purchased from Aldrich, Fischer, Fluka and Acros Organics. Solvents used for HPLC were used in HPLC-grade quality. Water used in HPLC and reaction was filtered in a Mili-Q system (Milipore) and when used for nanoparticle generation it was purchased from Aldrich in ultrapure quality. Solvents that were used for column chromatography and extractions were distilled from a technical grade before using.

Chromatography

Reactions were monitored using thin layer chromatography using Merck silica gel 60 F_{254} aluminum plates. The plates were analyzed by UV (254 nm) radiation by staining with ninhydrin or $KMnO_4$ solution. For purification via flash chromatography, Fluka high purity grade silica gel 60, 230-400 mesh was used.

At the University of Basel, analytical RP-HPLC was performed on a Shimadzu HPLC (Prominence) and at the ETH Zurich on a Dionex UHPLC, Ultimate 3000. The analytical columns used were a Reprosil gold 120 C18 (150 x 4 mm, 5 µm) and a Phenomenex Acris Peptide 1 7u XB-C18 (100 x 2.1 mm) with a flow of 1mL/min for the HPLC system. On the UHPLC system at the ETH Zurich analytical columns Reprosil gold 120 C18 (3 µm) and Phenomenex Acris Peptide 1 7u XB-C18 (3 µm) with a flow of 0.7 mL/min or 0.5 mL/min were used respectively. The preparative RP-HPLC was carried out at the University of Basel on a LC-10 system from Shimadzu and at the ETH Zurich on a Dionex UHPLC, Ultimate 3000 using in both cases a Reprosil gold 100 C18 (150 x 10 mm, 5 µm) with a flow of 6 mL/min. Two different solvents were used. Solvent A was assigned to be pure acetonitrile and solvent B was a mixture of 1 % acetonitrile and 0.1 % TFA in Mili-Q pure water.

NMR spectra (^{1}H -, ^{13}C - and ^{19}F - NMR) were recorded on a Bruker DPX 400 (University of Basel), a Varian Mercury-vx 300 and a Bruker AVIII400 (both ETH Zurich). Deuterated solvents were purchased from Cambridge Isotope Laboratories. Chemical shifts (δ) are given in ppm referring to tetramethylsilane (TMS) or the residual solvent peak. The signals are listed as s = singlet, d = doublet, t = triplet, q = quartet and m = multiplet. All measured spectra were recorded at room temperature. Coupling constants are given in Hz.

Mass Analysis

MALDI-TOF (Matrix-assisted laser desorption/ionization – time of flight mass) spectrometry was carried out using an applied Biosystems Voyager-DE PRO apparatus (University of Basel) and a Bruker solariX 94 (ETH Zurich). The matrices used were 2,5 - Dihydroxbenzoic acid (5 mg/mL in CH_3CN/ H_2O/ EtOH 1:1:1) and 4 – nitroanilin (10 mg/mL in CH_2Cl_2/ MeOH 9:1). The values are given in the ratio of atom mass per charge (m/z).

ESI – MS (electrospray ionization mass spectrometry) was performed on a Bruker Amazon speed. LC-MS (liquid chromatography mass spectrometry) was done with a Dionex UHPLC, Ultimate 3000 using a Reprosil gold C18 (125 x 3 mm, 3 µm) and a Phenomenex (3 µm) with a flow of 0.7 mL/min or 0.5 mL/min respectively. The values are given in the ratio of atom mass per charge (m/z).

UV-Vis Spectroscopy

For UV-Vis spectroscopy, Micro Fisherbrand Disposable Cuvettes (Methacrylate) (path length 1 cm) were used in a Varian Carry 300 Bio.

Electron Microscopy

TEM (transmission electron microscopy) measurements were carried out on a Philips EM 400 microscope (80 kV) at the *Zentrum für Mikroskopie* in the *Pharmazentrum* in the University of Basel, on a Philips CM 12 (100 kV) at the electron microscopy center (EMEZ) of the ETH Zurich and on a Philips CM 100 (80 kV) at the *Zentrum für Mikroskopie* in the University of Zurich. EDX measurements were done on a FEI Tecnai F30 FEG at the EMEZ. Samples were prepared by depositing a drop on a carbon-coated copper grid with 200 or 400 mesh size. After drying on air the grids were analyzed. The grids were provided by the Zentrum für Mikroskopie (University of Basel) or purchased from Quantifoil (Germany).

Solid Phase Peptide Synthesis

Solid phase peptide synthesis (SPPS) was performed using the Fmoc-Strategy[222]. The used resins were ChemMatrix from pcas BioMatrix and Biotage or 2-chlorotrityl chloride resin from Rapp Polymere. Amino acids and coupling reagents are from Bachem, IRIS Biotech and Protein Technologies.

For automated peptide synthesis a Syro I Peptide Synthesizer (Biotage, Upsala, Sweden) was used.

Lyophylization

For drying of the peptides an Eppendorf Concentrator plus or an Alpha 2-4 LD plus lyophilizator (Christ) was used

CD Spectroscopy

Circular Dichroism (CD) spectroscopy was done using a Chirascan (University of Basel) and a Chirascan Plus (ETH Zurich) both from Applied Photophysics Ltd (UK). The measurements were carried out in quartz SUPRASIL cuvettes (Hellma, Typ 114-QS, d = 1 mm).

Evaluation of Nanoparticle Size

The analysis of the nanoparticle size was carried out using the software Image J (from the National Institutes of Health, USA Government). The resulting data was then converted into histograms using Sigma plot™ (Systat software). The errors given are the standard deviations.

5.2. Builiding Block Synthesis for SPPS

5.2.1. Synthesis of Fmoc-(4S)Azp-OH

Synthesis of H-(R)Hyp-OMe*HCl

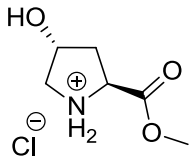

Chemical Formula: $C_6H_{12}ClNO_3$
Molecular Weight: 181.6 g/mol

100 g of H-Hyp-OH (0.763 mol, 1.0 equiv) were dissolved in 1200 mL MeOH. While cooling with an ice bath, 1.5 equiv (83 mL, 1.144 mol) thionyl chloride were added dropwise within 1 h. Then the solution was stirred under reflux for 18 h. After cooling to room temperature, the solvent was removed under reduced pressure. The product was obtained as 138.6 g of a white powder (0.763 mol, quant).

TLC (SiO_2, CH_2Cl_2/ MeOH 9:1, ninhydrin): R_f = 0.53

^{1}H-NMR (400 MHz, DMSO-d_6): δ = 10.50 (s, 1H, NH_2), 9.41 (s, 1H, NH), 5.36 (s, 1H, OH), 4.43 (dd, *J* = 10.8, 7.6, 1H, H_α), 4.38 (m, 1H, $H_{\gamma'}$), 3.72 (s, 3H, OMe), 3.36 (dd, *J* = 12.0, 4.3, 1H, H_δ), 3.04 (d, *J* = 12.0, 1H, H_δ), 2.17 (dd, *J* = 13.3, 7.3, 1H, H_β), 2.06 (m, 1H, $H_{\beta'}$).

^{13}C-NMR (100 MHz, DMSO-d_6): δ = 169.0 (C_q, CO_2), 68.4 (CH, C_γ), 57.3 (CH, C_α), 52.9 (CH_3, CH_3), 52.8 (CH_2, C_δ), 36.8 (CH_2, C_β).

MS (ESI, pos) m/z = 145.8 $[M]^+$, 146.6 $[M + H]^+$, (145.07 g/mol calculated for $C_6H_{11}NO_3$)

Synthesis of Boc-(4R)Hyp-Ome

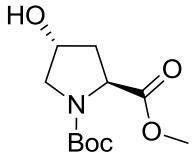

Chemical Formula: $C_{11}H_{19}NO_5$
Molecular Weight: 245.3 g/mol

139 g H-Hyp-OMe*HCl (0.763 mol, 1 equiv) were dissolved in an aqueous solution of $NaHCO_3$ (1M, 1760 mL, 2.3 equiv) and then a solution of 200 g Boc_2O (0.916 mol, 1.2 equiv) in dioxane (333 mL) was slowly added under inert atmosphere. The reaction mixture was stirred at room temperature for 18 h. Then it was extracted with EtOAc and the combined organic layers were washed with 1 M HCl and dried over $MgSO_4$. The solvent was removed under reduced pressure yielding 151.5 g of the product as colorless crystals (0.618 mol, 81%).

TLC (SiO_2, CH_2Cl_2/ MeOH 9:1, ninhydrin): R_f = 0.54

^{1}H- and ^{13}C-NMR show a double set of peaks due to the *cis* and *trans* conformers around the tertiary carbamate in a ratio of 1:1.8.

^{1}H-NMR (400 MHz, DMSO-d_6, *major conformer*): δ = 5.09 (d, *J* = 3.6, 1H, OH), 4.25 (m, 1H, $H_{\gamma'}$), 4.20 (m, 1H, H_α), 3.65 (s, 3H, CH_3), 3.37 (dd, *J* = 11.2, 4.1, 1H, H_δ), 3.26 (m, 1H, $H_{\delta'}$), 2.11 (m, 1H, H_β), 1.88 (m, 1H, H_β), 1.32 (s, 9H, *t*Bu).

^{1}H-NMR (400 MHz, DMSO-d_6, *minor conformer*): δ = 3.65 (s, 3H, CH_3), 3.40 (dd, *J* = 11.1, .4, 1H, H_δ), 1.39 (s, 9H, *t*Bu).

^{13}C-NMR (100 MHz, DMSO-d_6, *major conformer*): δ = 174.2 (C_q, CO_2), 153.8 (C_q, *t*Bu), 79.8 (C_q, *t*Bu), 68.7 (CH, C_γ), 58.5 (CH, C_α), 55.3 (CH2, C_δ), 52.6 (CH_3, CH_3), 40.5 (CH_2, C_β), 28.7 (CH_3, *t*Bu).

^{13}C-NMR (100 MHz, DMSO-d_6, *minor conformer*): δ = 173.7 (C_q, CO2), 154.6 (C_q, *t*Bu), 69.4 (CH, C_γ), 58.5 (CH, C_α), 55.3 (CH_2, C_δ), 52.7 (CH_3, CH_3).

MS (ESI, pos.) m/z = 146.1 $[M + 2Na]^{2+}$, 268.0 $[M + Na]^+$, 513.1 $[2M + Na]^+$, (245.13 g/mol calculated for $C_{11}H_{19}NO_5$).

Synthesis of Boc-(4S)Azp-OMe

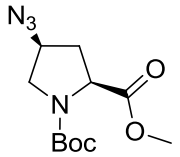

Chemical Formula: $C_{11}H_{18}N_4O_4$
Molecular Weight: 270.3 g/mol

40 g Boc-(4R)Hyp-OMe (0.163 mol, 1 equiv) were dissolved in CH_2Cl_2 (310 mL). 28 mL NEt_3 (0.196 mol, 1.2 equiv) was added and stirred for 15 min. Then the solution was cooled to 0 °C and 15 mL methanesulfonyl chloride (0.196 mol, 1.2 equiv) were added dropwise. The reaction mixture was stirred at room temperature for 2 h. Then it was washed with saturated aqueous $NaHCO_3$, dried over $MgSO_4$ and the solvent was removed under reduced pressure. The product was redissolved in DMF (160 mL) and 53.0 g NaN_3 (0.815 mol, 5 equiv) were added. The reaction mixture was stirred at 80 °C for 18 h. The solvent was removed under reduced pressure to yield 43.2 g of the desired product as a yellow oil (0.160 mol, 98%).

TLC (SiO_2, pentane/ EtOAc 1:1, ninhydrin): R_f = 0.6

^{1}H and ^{13}C NMR show a double set of peaks due to *cis* and *trans* conformers around the tertiary carbamate in a ratio of 1:1.3.

^{1}H NMR (400 MHz, $CDCl_3$, *major conformer*): δ = 4.26 (dd, *J* = 8.8, 4.2, 1H, H_α), 4.11 (m, 1H, H_γ), 3.69 (s, 3H, CH_3), 3.63 (m, 1H, H_δ), 3.41 (m, 1H, $H_{\delta'}$), 2.41 (m, 1H, H_β), 2.10 (m, 1H, $H_{\beta'}$), 1.35 (s, 9H, *t*Bu).

^{1}H NMR (400 MHz, $CDCl_3$, *minor conformer, separated signals*): δ = 4.36 (dd, *J* = 8.9, 3.6, 1H, Hα), 1.40 (s, 9H, *t*Bu).

^{13}C NMR (100 MHz, $CDCl_3$, *major conformer*): δ = 172.6, 154.3, 80.8, 59.6, 58.0, 52.6, 51.2, 36.3, 28.5.

^{13}C NMR (100 MHz, $CDCl_3$, *minor conformer, separated signals*): δ = 172.3, 153.8, 58.6, 57.7, 52.7, 51.6, 35.4, 28.7.

MS (ESI, pos.) m/z (%) = 293.0 $[M + Na]^+$, (270.13 g/mol calculated for $C_{11}H_{18}N_4O_4$).

Synthesis of Boc-(4S)Azp-OH

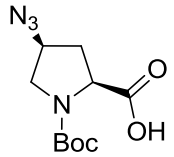

Chemical Formula: $C_{10}H_{16}N_4O_4$
Molecular Weight: 256.3 g/mol

25 g Boc-(4S)Azp-OMe (0.092 mol, 1.0 equiv) were dissolved in THF (48 mL) and MeOH (48 mL). An aqueous NaOH solution (7.4 g, 0.185 mol, 2.0 equiv in 8 mL H_2O) was added to the reaction mixture and then stirred at room temperature for 3.5 h. Then the pH was adjusted to 3 by adding 1 M HCl solution. The mixture was extracted with EtOAc and the combined organic layers were dried over $MgSO_4$. Then the solvent was removed under reduced pressure to give 23.8 g of the product as a white powder (0.092 mol, quant).

TLC (SiO_2, CH_2Cl_2/ MeOH 9:1, 254 nm): R_f = 0.51

^{1}H and ^{13}C NMR show a double set of peaks due to *cis* and *trans* conformers around the tertiary carbamate in a ratio of 1:1.

^{1}H NMR (400 MHz, $CDCl_3$, *major conformer*): δ = 10.66 (s, 1H, COOH), 4.40 (m, 1H, H_α), 4.13 (m, 1H, H_γ), 3.69 (m, 1H, H_δ), 3.45 (m, 1H, H_δ), 2.46 (m, 1H, H_β), 2.36 (m, 1H, H_β), 1.42 (s, 9H, *t*Bu).

^{1}H NMR (400 MHz, $CDCl_3$, *minor conformer*): δ = 10.66 (s, 1H, COOH), 4.30 (m, 1H, H_α), 4.13 (m, 1H, H_γ), 3.59 (m, 1H, H_δ), 3.38 (m, 1H, H_δ), 2.36 (m, 1H, H_β), 2.18 (m, 1H, H_β), 1.36 (s, 9H, *t*Bu).

^{13}C NMR (100 MHz, $CDCl_3$, *major conformer*): δ = 177.5, 155.8, 82.2, 59.6, 57.9, 52.1, 36.3, 28.7.

^{13}C NMR (100 MHz, $CDCl_3$, *minor conformer*): δ = 175.3, 154.1, 81.5, 59.6, 58.7, 51.3, 34.6, 28.6.

MS (ESI, pos.) m/z (%) = 255.7 $[M]^+$, 511.2 $[2M]^+$, (256.12 g/mol calculated for $C_{10}H_{16}N_4O_4$).

Synthesis of H-(4S)Azp-OH*HCl

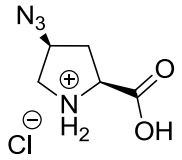

Chemical Formula: $C_5H_9ClN_4O_2$
Molecular Weight: 192.6 g/mol

24 g Boc-(4S)Azp-OH (0.092 mol, 1 equiv) were dissolved in 4 M HCl in dioxone (300 mL). The reaction mixture was stirred at room temperature for 5 h. Then the solvent was removed under reduced pressure. The remaining solid was dissolved in a minimum of a 1:1 (v/v) mixture of CH_2Cl_2 and MeOH and then precipitated in Et_2O. The precipitate was filtered and dried under reduced pressure to yield 15.7 g of the desired product as a white powder (0.082 mol, 89%).

TLC (SiO_2, CH_3CN/H_2O 4:1, ninhydrin): R_f = 0.24

^{1}H NMR (400 MHz, D_2O): δ = 4.57 (m, 2H; H_α, H_γ), 3.49 (m, 2H; H_δ, H_δ), 2.60 (ddd, *J* = 15.3, 10.1, 5.3 Hz, 1H, H_β), 2.45 (m, 1H, H_β).

^{13}C NMR (100 MHz, $CDCl_3$): δ = 170.8, 60.7, 59.5, 52.0, 35.3.

MS (ESI, pos.) m/z (%) = 156.9 $[M]^+$, (156,06 g/mol calculated for $C_5H_8N_4O_2$).

Synthesis of Fmoc-(4S)Azp-OH

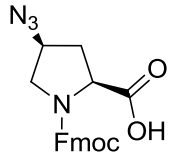

Chemical Formula: $C_{20}H_{18}N_4O_4$
Molecular Weight: 378.4 g/mol

16 g H-(4S)Azp-OH*HCl (0.082 mol, 1 equiv) were dissolved in dioxane (40 mL) and in an aqueous $NaHCO_3$ solution (17 g, 0.205 mol, 2.5 equiv in 160 mL H_2O). Then a solution of 25 g Fmoc chloride (0.098 mol, 1.2 equiv) in dioxane (40 mL) was added. The reaction mixture was stirred at room temperature for 3 h. The organic solvent was removed and saturated $NaHCO_3$ solution (250 mL) was added to change the pH to be around 8. The aqueous solution was washed with Et_2O and then acidified with 1 M HCl to reach a pH of around 2, when a white solid precipitated. The mixture was extracted with EtOAc and the combined organic phases were dried over $MgSO_4$. The solvent was removed under reduced pressure to yield 27.5 gof the desired product as a white powder (0.073 mol, 89%).

TLC (SiO_2, CH_2Cl_2/ MeOH 9:1, ninhydrin): R_f = 0.42

Analytical HPLC: R_t = 12.8 min, 70% to 10% B in 27 min, Reprosil gold, 1 mL/min, 254 nm.

^{1}H and ^{13}C NMR show a double set of peaks due to *cis* and *trans* conformers around the tertiary carbamate in a ratio of 1:1.

^{1}H NMR (400 MHz, $CDCl_3$/CD_3OD, *conformer a*): δ = 7.55 (d, *J* = 7.8 Hz, 2H, Fmoc), 7.38 (m, 2H, Fmoc), 7.18 (m, 2H, Fmoc), 7.10 (m, 2H, Fmoc), 3.97 – 4.28 (m, 5H, Fmoc, H_α, H_γ), 3.57 (dd, *J* = 11.8, 5.9 Hz, 1H, H_δ), 3.35 (dd, *J* = 12.7, 3.0 Hz, 1H, H_δ), 2.29 (m, 1H, H_β), 2.09 (m, 1H, H_β).

^{1}H NMR (400 MHz, $CDCl_3$/CD_3OD, *conformer b*): δ = 7.53 (d, *J* = 7.8 Hz, 2H, Fmoc), 7.38 (m, 2H, Fmoc), 7.18 (m, 2H, Fmoc), (m, 2H, Fmoc), 3.97 – 4.28 (m, 5H, Fmoc, H_α, H_γ), 3.49 (dd, *J* = 11.8, 5.9 Hz, 1H, H_δ), 3.32 (dd, *J* = 12.7, 3.0 Hz, 1H, H_δ), 2.29 (m, 1H, H_β), 2.09 (m, 1H, H_β).

^{13}C NMR (100 MHz, DMSO:d_6, both conformers): δ = 172.6, 172.0, 153.6, 153.6, 143.8, 143.6, 140.6, 140.6, 127.4, 127.1, 125.0, 120.0, 66.8, 66.5, 58.8, 58.1, 57.4, 57.2, 51.4, 50.8, 46.7, 46.5, 35.5, 35.4.

MS (ESI, pos.) m/z (%) = 379.3 $[M + H]^+$, 401.2 $[M + Na]^+$, (378.13 g/mol calculated for $C_{20}H_{18}N_4O_4$).

5.2.2. Synthesis of Fmoc-Pro-(4*S*)Azp-Pro-OH

Synthesis of H-(4S)Azp-OMe*HCl

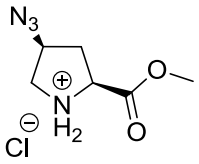

Chemical Formula: $C_6H_{11}ClN_4O_2$
Molecular Weight: 206.6 g/mol

31.1 g Boc-(4S)Azp-OMe (0.115 mol, 1 equiv) were dissolved in a 4 M HCl solution in dioxane (372 mL). The reaction mixture was stirred at room temperature for 1 h. Then the solvent was removed under reduced pressure. The remaining solid was dissolved in a minimum of a mixture of CH_2Cl_2 and MeOH in a ratio of 1:1 (v/v). Et_2O was added to precipitate a white solid. The supernatant solution was removed and the precipitation was repeated to yield 21.91 g of the desired product (0.106 mol, 92%).

TLC (CH_3CN/ H_2O 4:1, ninhydrin): R_f = 0.5

^{1}H NMR (400 MHz, CD_3OD): δ = 4.64 - 4.57 (m, 2H, H_α, H_γ), 3.89 (s, 3H, OCH_3), 3.51 (dd, *J* = 12.5 Hz, 5.0 Hz, 1H, H_δ), 3.45 (dm, *J* = 12.5 Hz, 1H, H_δ), 2.56 (ddd, *J* = 14.4 Hz, 9.8 Hz, 5.6 Hz, 1.7 Hz, 1H, H_β), 2.43 (dm, *J* = 14.4 Hz, 1H, H_β).

^{13}C NMR (100 MHz, CD_3OD): δ = 170.0, 60.6, 59.7, 54.3, 52.2, 35.3.

MS (ESI, pos.) m/z (%) = 229.7 $[M + Na]^+$, (206.06 g/mol calculated for $C_6H_{11}ClN_4O_2$).

Synthesis of Boc-Pro-(4S)Azp-OMe

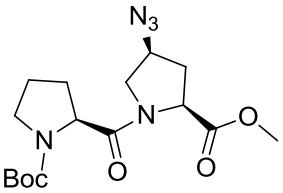

Chemical Formula: $C_{16}H_{25}N_5O_5$
Molecular Weight: 367.4 g/mol

21.9 g H-(4S)Azp-OMe*HCl (0.106 mol, 1 equiv) and 29.7 g Boc-Pro-OH (0.138 mol, 1.3 equiv) were dissolved in CH_2Cl_2 (933 mL). 24 mL $^{i}Pr_2NEt$ (0.138 mol, 1.3 equiv) and 30.5 g EDC (0.159 mol, 1.5 equiv) were added and the solution was stirred at room temperature for 18 h. The solution was washed with 1 M HCl solution and dried over Na_2SO_4. Removal of the solvent under reduced pressure yielded 14.5 g of the desired product as a white solid (0.040 mol, 37%).

TLC (CH_2Cl_2/ MeOH 95:5, ninhydrin): R_f = 0.4

^{1}H NMR shows a double set of peaks due to *cis* and *trans* conformers around the tertiary carbamate in a ratio of 2:5.

^{1}H NMR (500 MHz, $CDCl_3$, *major conformer*): δ = 4.71 (dd, *J* = 8.9 Hz, 4.3 Hz, 1H, Azp-H_α), 4.43 (dd, *J* = 8.3 Hz, 3.5 Hz, 1H, Pro-H_α), 4.27 (m, 1H, Azp-H_γ), 4.10 (dd, *J* = 10.6 Hz, 6.1 Hz, 1H, Azp-H_δ), 3.73 (s, 3H, OCH_3), 3.62 – 3.50 (m, 2H, Pro-H_δ, Azp-H_δ), 3.42 – 3.36 (m, 1H, Pro-H_δ), 2.46 (ddd, *J* = 13.6 Hz, 9.0 Hz, 6.0 Hz, 1H, Azp-H_β), 2.24-2.01 (m, 4H, Pro-H_β, Azp-H_β, Pro-H_γ, Pro-H_β); 1.86 (m, 1H, Pro-H_γ), 1.43 (s, 9H, *t*Bu)

^{1}H NMR (500 MHz, $CDCl_3$, *minor conformer*): δ = 4.68 (dd, *J* = 8.9 Hz, 4.3 Hz, 1H, Azp-H_α), 4.33 (dd, *J* = 8.5 Hz, 3.8 Hz, 1H, Pro-H_α), 4.27 (m, 1H, Azp-H_γ), 3.91 (dd, *J* = 10.6 Hz, 6.1 Hz, 1H, Azp-H_δ), 3.74 (s, 3H, OCH_3), 3.62 - 3.50 (m, 2H, Pro-H_δ, Azp-H_δ), 3.46 (m, 1H, Pro-H_δ), 2.43 (m, 1H, Azp-H_β), 2.24 – 2.01 (m, 4H, Pro-H_β, Azp-H_β, Pro-Hγ, Pro-H_β), 1.86 (m, 1H, Pro-H_γ), 1.38 (s, 9H, *t*Bu).

^{13}C NMR (126 MHz, $CDCl_3$, *major conformer*): δ = 171.5, 154.8, 79.8, 59.8, 57.7, 57.4, 52.5, 51.4, 47.0, 34.1, 29.4, 28.6, 24.3.

^{13}C NMR (126 MHz, $CDCl_3$, *minor conformer*): δ = 171.8, 171.2, 153.7, 79.8, 59.7, 58.0, 57.7, 57.4, 52.7, 51.3, 46.8, 34.2, 30.3, 28.5, 23.6.

MS (ESI, pos.) m/z (%) = 390.1 $[M + Na]^+$, (367.19 g/mol calculated for $C_{16}H_{25}N_5O_5$).

Synthesis of Boc-Pro-(4S)Azp-OH

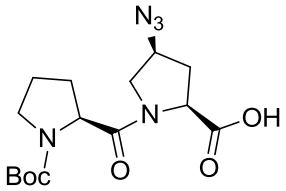

Chemical Formula: $C_{15}H_{23}N_5O_5$
Molecular Weight: 353.4 g/mol

14.5 g Boc-Pro-(4S)Azp-OMe (0.041 mol, 1 equiv) were dissolved in THF (21 mL) and MeOH (21 mL). An aqueous NaOH solution (3.3 g, 0.082 mol, 2 equiv in 2.8 mL H_2O) was added. A white precipitate formed, therefore another 20 mL MeOH were added. The reaction mixture was stirred at room temperature for 2.5 h. Then the solution was washed with 1 M HCl and dried over Na_2SO_4. The solvent was removed under reduced pressure to yield 12.9 g of the desired product as a white solid (0.037 mol, 89%).

TLC (CH_3CN/ H_2O 4:1, ninhydrin): R_f = 0.5

^{1}H NMR shows a double set of peaks due to *cis* and *trans* conformers around the tertiary carbamate in a ratio of 2:7.

^{1}H NMR (250 MHz, $CDCl_3$/CD_3OD, *major conformer*): δ = 4.73 (dd, *J* = 9.1 Hz, 3.3 Hz, 1H, Azp-H_α), 4.44 (dd, *J* = 7.8 Hz, 3.6 Hz, 1H, Pro-H_α), 4.39 – 4.27 (m, 1H, Azp-H_γ), 4.06 (dd, *J* = 10.6 Hz, 5.8 Hz, Azp-H_δ), 3.64 – 3.36 (m, 3H, Pro-H_δ, Azp—H_δ), 2.53 – 1.78 (m, 6H, H_β, Pro-H_γ), 1.45 (s, 9H, *t*Bu).

^{1}H NMR (250 MHz, $CDCl_3$/CD_3OD, *minor conformer*): δ = 3.85 (dd, *J* = 10.5 HZ, 5.8 Hz, 1H, Azp-H_δ), 1.39 (s, 9H, *t*Bu).

^{13}C NMR (100MHz, $CDCl_3$): δ = 174.5, 172.0, 154.7, 80.2, 59.5, 58.7, 57.6, 52.4, 46.9, 32.3, 29.5, 28.4, 24.3.

Synthesis of Boc-Pro-(4S)Azp-Pro-OMe

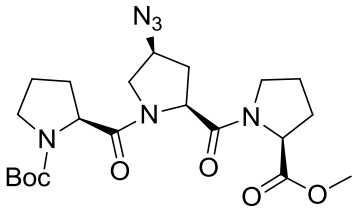

Chemical Formula: $C_{21}H_{32}N_6O_6$
Molecular Weight: 464.5 g/mol

12.9 g Boc-Pro-(4S)Azp-OH (0.037 mol, 1 equiv) and 7.4 g H-Pro-OMe*HCl (0.044 mol, 1.2 equiv) were dissolved in CH_2Cl_2 (112 mL) and 7.7 mL $^{i}Pr_2NEt$ (0.044 mol, 1.2 equiv) were added. Then 10.6 g EDC (0.056 mol, 1.5 equiv) were put into the reaction mixture. The reaction was stirred at room temperature for 18 h. The solution was washed with 1 M HCl solution and dried over Na_2SO_4. Then the solvent was removed under reduced pressure to yield 14.9 g of the desired product as a white solid (0.032 mol, 86%).

TLC (CH_2Cl_2/ MeOH 9:1, ninhydrin): R_f = 0.5

^{1}H NMR shows a double set of peaks due to *cis* and *trans* conformers around the tertiary carbamate in a ratio of 1:3.

^{1}H NMR (500 MHz, $CDCl_3$, *major conformer*): δ = 4.74 (t, *J* = 7.9 Hz, 1H, Azp-H_α), 4.55 (dd, *J* = 8.7 Hz, 3.9 Hz, 1H, Pro^C-H_α), 4.45 (dd, *J* = 8.2 Hz, 3.2 Hz, 1H, Pro^N-H_α), 4.22 – 4.14 (m, 2H, Azp-H_γ, Azp-H_δ), 3.79 (m, 1H, Pro^C-H_δ), 3.71 (s, 3H, OCH_3), 3.61 – 3.33 (m, 4H, Pro^C-H_δ, Pro^N-H_δ, Azp-H_δ, Pro-H_δ), 2.66 – 2.57 (m, 1H, Azp-H_β), 2.25 – 1.93 (m, 8H, Pro^C-H_β, Pro^N-H_β, Pro^C-H_γ, Pro^N-H_γ, Azp-H_β, Pro^N-H_γ, Pro^C-H_β), 1.86 – 1.78 (m, 1H, Pro^N-H_γ), 1.43 (s, 9H, *t*Bu)

^{1}H NMR (500 MHz, $CDCl_3$, *minor conformer*): δ = 4.67 (t, *J* = 7.9 Hz, 1H, Azp-H_α), 4.56 (dd, *J* = 8.7 Hz, 4.1 Hz, 1H, Pro^C-H_α), 4.36 (dd, *J* = 8.1 Hz, 3.5 Hz, 1H, Pro^N-H_α), 4.14 – 4.00 (m, 2H, Azp-H_γ, Azp-H_δ), 3.84 – 3.75 (m, 1H, Pro^C-H_δ), 3.71 (s, 3H, OCH_3), 3.61 – 3.33 (m, 4H, Pro^C-H_δ, Pro^N-H_δ, Azp-H_δ, Pro-H_δ), 2.66 – 2.57 (m, 1H, Azp-H_β), 2.25 – 1.93 (m, 8H, Pro^C-H_β, Pro^N-H_β, Pro^C-H_γ, Pro^N-H_γ, Azp-H_β, Pro^N-H_γ, Pro^C-H_β), 1.86 – 1.78 (m, 1H, Pro^N-H_γ), 1.43 (s, 9H, *t*Bu)

^{13}C NMR (126 MHz, $CDCl_3$, *major conformer*): δ = 172.5, 170.9, 169.5, 154.6, 79.5, 58.9, 58.7, 57.7, 56.5, 52.2, 51.0, 46.9, 33.0, 28.9, 28.8, 28.6, 24.8, 24.2.

^{13}C NMR (126 MHz, $CDCl_3$, *minor conformer*): δ = 172.5, 171.4, 169.2, 153.6, 79.4, 58.9, 58.7, 57.7, 56.4, 52.2, 51.0, 46.7, 33.1, 29.9, 28.4, 24.8, 23.5.

MS (ESI, pos.) m/z (%) = 487.1 $[M + Na]^+$, (464.24 g/mol calculated for $C_{21}H_{32}N_6O_6$).

Synthesis of Boc-Pro-(4S)Azp-Pro-OH

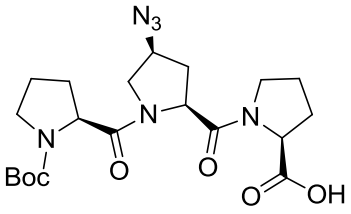

Chemical Formula: $C_{20}H_{30}N_6O_6$
Molecular Weight: 450.5 g/mol

14.9 g (0.032 mol, 1 equiv) Boc-Pro-(4S)Azp-Pro-OMe were dissolved in 330 mL THF and 165 mL MeOH. An aqueous NaOH solution (3.1 g, 2.4 equiv in 6 mL H_2O) was added and the reaction mixture was stirred at room temperature for 2.5 h. Then the solution was extracted with CH_2Cl_2 and 1 M HCl solution. The combined organic phases were dried over Na_2SO_4 and the solvent was removed under reduced pressure. The product was obtained as a white powder (11.3 g, 0.025 mol, 78%).

TLC (CH_3CN/ H_2O 4:1, ninhydrin): R_f = 0.5

^{1}H NMR shows a double set of peaks due to *cis* and *trans* conformers around the tertiary carbamate in a ratio of 1:3.

^{1}H NMR (250 MHz, $CDCl_3$, *major conformer*): δ = 4.73 (t, *J* = 7.9 Hz, 1H), 4.64 (m, 1H), 4.49 – 4.32 (m, 1H), 4.25 – 4.02 (m, 2H), 3.82 -3.31 (m, 5H), 2.66 – 2.52 (m, 1H), 2.39 – 2.23 (m, 1H), 2.19 – 1.76 (m, 8H), 1.44 (s, 9H, *t*Bu)

^{1}H NMR (500 MHz, $CDCl_3$, *minor conformer, separated signals*): δ = 1.40 (s, 9H, *t*Bu)

^{13}C NMR (100 MHz, $CDCl_3$): δ = 173.0, 171.8, 171.2, 79.8, 59.7, 58.9, 57.7, 56.6, 51.0, 47.3, 46.9, 33.3, 29.0, 28.5, 27.5, 25.0, 24.3.

MS (ESI, pos.) m/z (%) = 473.1 $[M + Na]^+$, (450.22 g/mol calculated for $C_{20}H_{30}N_6O_6$).

Synthesis of H-Pro-(4S)Azp-Pro-OH*HCl

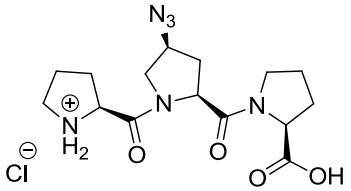

Chemical Formula: $C_{15}H_{23}ClN_6O_4$
Molecular Weight: 386.8 g/mol

11.3 g Boc-Pro-(4S)Azp-Pro-OH (0.025 mol, 1 equiv) were dissolved in a 4 M solution of HCl in dioxane (65 mL) and stirred at room temperature for 2 h. The solvent was removed and the remaining solid was dissolved in a minimum of CH_2Cl_2 and MeOH. By addition of Et_2O, the product precipitated as a white solid. It was filtrated and dried under reduced pressure to yield 9.0 g of H-Pro-(4S)Azp-Pro-OH*HCl (0.023 mol, 93%).

TLC (CH_3CN/ H_2O 4:1, ninhydrin): R_f = 0.1.

^{1}H NMR (250 MHz, CD_3OD): δ = 4.80 (dd, *J* = 8.1 Hz, 8.1 Hz, 1H), 4.65 – 4.55 (m, 1H), 4.46 – 4.20 (m, 2H), 4.09 (dd, *J* = 10.1Hz, 6.9 Hz, 1H), 3.90 – 3.56 (m, 2H), 3.42 – 3.3 (m, 3H), 2.88 – 2.75 (m, 1H), 2.55 – 1.81 (m, 9H).

^{13}C NMR (100 MHz, $CDCl_3$): δ = 175.0, 170.9, 168.2, 60.6, 60.5, 60.0, 58.7, 52.4, 48.1, 47.6, 34.1, 30.1, 29.3, 25.9, 25.1.

MS (ESI, pos.) m/z (%) = 350.3 $[M + H]^+$, (386.15g/mol calculated for $C_{15}H_{22}N_6O_4$).

Synthesis of Fmoc-Pro-(4S)Azp-Pro-OH

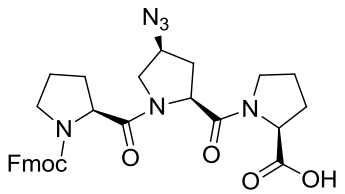

Chemical Formula: $C_{30}H_{32}N_6O_6$
Molecular Weight: 572.6 g/mol

9.0 g H-Pro-(4S)Azp-Pro-OH*HCl (0.023 mol, 1 equiv) were dissolved in dioxane (41 mL). An aqueous $NaHCO_3$ solution (4.9 g, 0.058 mol, 2.5 equiv in 81 mL H_2O) was added. Then 7.2 g Fmoc-Cl (0.028 mol, 1.2 equiv)in dioxane (48 mL) were added and the reaction mixture was stirred at room temperature for 18 h. The pH was brought to around pH 10 with a saturated aqueous $NaHCO_3$ solution. The solution was extracted with Et_2O and the aqueous layer was brought to acidic pH with 2 M HCl solution. The aqueous layer was extracted with ethyl acetate. The solution was dried over Na_2SO_4. The solvent was removed under reduced pressure to yield 12.2 g of the desired product as a white solid (0.021 mol, 91%).

TLC (CH_3CN/ H_2O 4:1, ninhydrin): R_f = 0.3.

^{1}H NMR shows a double set of peaks due to *cis* and *trans* conformers around the tertiary carbamate in a ratio of 1:2.3.

^{1}H-NMR (500 MHz, $CDCl_3$, major conformer): δ= 7.76 (m, 2H, Fmoc), 7.63 - 7.53 (m, 2H, Fmoc), 7.43 - 7.37 (m, 2H, Fmoc), 7.34 - 7.28 (m, 2H, Fmoc), 4.74 (t, *J* = 7.9 Hz, 1H, Azp-H_α), 4.62 (dd, *J* = 8.6 Hz, 3.2 Hz, 1H, Pro^C-H_α), 4.52 (dd, *J* = 8.2 Hz, *J* = 3.6 Hz,1H, Pro^N-H_α), 4.35 - 4.30 (m, 2H, Fmoc), 4.26 - 4.20 (m, 3H, Fmoc, Azp-H_γ, Azp-H_δ), 3.76 (dd, 1H, Pro^C-H_δ), 3.69 (m, 1H, Pro^N-H_δ), 3.58 - 3.45 (m, 3H, Pro^N-H_δ, Pro^C-H_δ, Azp-H_δ), 2.59 (m, 1H, Azp-H_β), 2.30 - 1.70 (m, 9H, Pro^C-H_β, Pro^N-H_β, Pro^N-H_β, Pro^N-H_γ, Pro^C-H_β, Pro^C-H_γ, Azp-H_β, Pro^C-H_γ, Pro^N-H_γ).

^{1}H-NMR (500 MHz, $CDCl_3$, minor conformer): δ= 7.76 (m, 2H, Fmoc), 7.63 - 7.53 (m, 2H, Fmoc), 7.43 - 7.37 (m, 2H, Fmoc), 7.34 - 7.28 (m, 2H, Fmoc), 4.59 – 5.54 (m, 2H, Fmoc, Pro^C-H_α), 4.35 (m, 1H, Azp-H_α), 4.15 (t, *J* = 5.0 Hz, 1H, Fmoc), 4.00 (dd, *J* = 8.5 Hz, *J* = 3.2 Hz, 1H, Pro^N-H_α), 3.92 (q, 1H, Azp-H_γ), 3.70 (m, 1H, Pro^C-H_δ), 3.58 – 3.45 (m, 2H, Pro^N-H_δ, Pro^C-H_δ), 3.45 – 3.36 (m, 2H, Pro^N-H_δ, Azp-H_δ), 3.21 (dd, *J* = 9.8 Hz, 8.0 Hz, 1H, Azp-H_δ), 2.45 (m, 1H, Azp-H_β), 2.30 - 1.70 (m, 9H, Pro^C-H_β, Pro^N-H_β, Pro^N-H_β, Pro^N-H_γ, Pro^C-H_β, Pro^C-H_γ, Azp-H_β, Pro^C-Hγ, Pro^N-H_γ).

^{13}C NMR (126 MHz, $CDCl_3$, *major conformer*): δ = 173.5, 171.2, 171.0, 155.1, 144.1, 143.9, 141.3, 127.7, 127.1, 125.2, 125.1, 120.0, 67.6, 59.5, 58.8, 58.1, 56.7, 51.2, 47.7, 47.2, 27.1, 46.8, 34.1, 29.0, 27.8,25.0, 24.7.

^{13}C NMR (126 MHz, $CDCl_3$, *minor conformer*): δ = 173.5, 171.2, 171.0, 155.1, 144.6, 143.7, 141.4, 141.1, 127.8, 127.5, 127.2, 126.8, 124.9, 124.8, 119.7, 65.6, 59.4, 58.7, 57.5, 56.4, 50.4, 47.7, 47.2, 47.1, 46.8, 33.2, 29.6, 27.8, 25.0, 23.3.

MS (ESI, pos.) m/z (%) = 595.0 $[M + Na]^+$, (572.24 g/mol calculated for $C_{30}H_{32}N_6O_6$).

5.3. Solid Phase Peptide Synthesis (SPPS)

5.3.1. General Procedure for Manual Amino Acid Coupling

The manual coupling of amino acids on solid support followed the next steps. First the resin needed to be swollen in CH_2Cl_2 (8 mL/g resin) for 30 min. Then a pre-reaction was carried out using $^{i}Pr_2NEt$ (9 equiv), HCTU (0.5 M, 3 equiv) and amino acid (0.5 M, 3 equiv) in DMF (5 mL / g resin) by shaking at room temperature for 3 min. The mixture was then added to the resin and agitated at room temperature for 1 h. After the reaction the solution was removed and the resin was washed with DMF (3 x 2 mL/ g resin) and CH_2Cl_2 (3 x 2 mL/ g resin). To test the completeness of the coupling a color test on bead was carried out. To prepare the next coupling step, the *N*-terminal Fmoc group needed to be removed by addition of 20% (v/v) piperidine solution in DMF (2 mL/ g resin) and agitation for 10 min. This procedure was repeated for 20 min. Then the resin was washed with DMF (3 x 2 mL/ g resin) and CH_2Cl_2 (3 x 2 mL/ g resin). The reactions were repeated until the peptide was complete.

5.3.2. General Procedure for the Quantitative Fmoc-test

With the quantitative Fmoc-test, the loading of the resin is determined. 500 µL of a 30% (v/v) piperidine solution in DMF were added to 3 mg of dry resin. The mixture was agitated for 30 min. The solution was diluted 1:10 and then the UV absorption was measured at a wavelength of 301 nm. The respective loading can be calculated according to formula (**2)**.

$$Loading\ \left[\frac{mmol}{g}\right] = \frac{A_{301\,nm} * V_{dilution}[mL]}{\varepsilon_{301\,nm} * m_{resin}[mg]} \qquad \textbf{(2)}$$

$\varepsilon_{301\,nm}$ = 7.8 mL·mmol^{-1}·cm^{-1}.

5.3.3. General Procedure for Automated Peptide Synthesis

For automated peptide synthesis, a Syro I Peptide Synthesizer (Biotage, Upsala, Sweden) was used. The resin was swollen in DMF and then $^{i}Pr_2NEt$ (9 equiv as a 3 M solution in N-methylpyrrolidone), HCTU (3 equiv, 0.5 M in DMF) and Fmoc-amino acid (3 equiv, 0.5 M) in DMF (5 mL / g resin) was added to the resin. The reaction mixture was allowed to react in intervals of 1 min agitation and 5 min break in between for 1 h, followed by a washing step with DMF (5 x). The coupling step was followed by Fmoc deprotection. This was carried out by addition of 40% (v/v) piperidine in DMF and

reaction for 5 min. This step was repeated with 20% (v/v) piperidine in DMF for 10 min. Then the resin was washed with DMF (5 x). The reactions were repeated until the peptide was finished.

5.3.4. General Procedure for Color Tests on Resin

For the monitoring of coupling and deprotection of the amino acids on resin, different color tests were applied.

5.3.4.1. Kaiser Test for Primary Amines[223]

A few beads were put into a vial and three drops of solution 1 (5 g ninhydrin in 100 mL ethanol), solution 2 (80 g phenol in 20 mL ethanol) and solution 3 (2 mL 0.001 M aqueous KCN in 98 mL pyridine) were added. The reaction mixture was heated to 100 °C for 5 min. If the test was negative, meaning no primary amine was present the beads showed no coloration or a slight yellow color. In case of a positive test, meaning a free amino function was present, the beads showed a blue color. If secondary amines were present, the beads were colored brownish or red but the test is less reliable for secondary amines. If the heating was carried out for longer time, there was the danger that side chains were deprotected (Boc group) or that the Fmoc group was removed by the pyridine.

5.3.4.2. Acetaldehyde / Chloranil test for Secondary Amines[224]

A few beads were put into a vial and three drops of solution 1 (2% acetaldehyde in DMF) and solution 2 (2% chloranil in DMF) were added. The mixture was allowed to react at room temperature for 5 min. The beads were analyzed under a microscope. In case of a positive test, when secondary amine groups were present, the beads showed a blue coloration. In case of a negative test the beads have no coloration or a slightly yellow color. The solution 1 and 2 should be stored at -20 °C. Instead of 2% acetaldehyde solution in DMF also pure acetone can be used instead.

5.3.4.3. TNBS Test for Secondary Amines[225]

A few beads were placed into a vial and three drops of solution 1 (10% DIPEA in DMF) and solution 2 (1 M aqueous TNBS) were added. The mixture was allowed to react for 5 min. The beads were analyzed under a microscope. In case of a positive test, when secondary amine groups were present, the beads showed an orange to red coloration. In case of a negative test the beads were colorless.

5.3.5. General Procedure for N-terminal Acetylation

The resin was swollen for 30 min in CH_2Cl_2 at room temperature. Then Ac_2O (20 equiv) and NEt_3 (20 equiv) in CH_2Cl_2 were added. The reaction mixture was shaken at room temperature for 1 h and then washed with CH_2Cl_2 (3 x 2 mL/ g resin). To test whether the acetylation was complete a color test was applied.

5.3.6. Staudinger Reduction on Solid Support

The resin with the peptide, containing an azido functionality was swollen for 30 min in THF. Water (65 equiv *per* N_3 group) and PMe_3 (1 M in THF, 5 equiv *per* N_3 group) were added to the resin. The reaction mixture was shaken at room temperature for 2 h. The resin was washed with THF (3 x 2 mL/ g resin), DMF (3 x 2 mL/ g resin) and CH_2Cl_2 (3 x 2 mL/ g resin).

5.3.7. Guanidinylation on Solid Support

The resin was swollen in CH_2Cl_2 for 30 min. *N*,*N'*-di-Boc-*N''*-trifluormethane sulfonylguanidine (2.2 eqiuv *per* NH_2 group) was dissolved in MeOH : CH_2Cl_2 (*v/v*, 1:1) and added to the resin. The mixture was shaken for 10 min and then NEt_3 (2.8 equiv per NH_2 group) was added. The reaction was agitated at room temperature for 2 d. After the reaction the resin was washed with DMF (3 x 2 mL/ g resin) and CH_2Cl_2 (3 x 2 mL/ g resin).

5.3.8. General Procedure for Cleavage of the Peptides from the Resin and Simultaneous Side-Chain Deprotection

The resin was swollen for 30 min in CH_2Cl_2. A solution of 87.5% TFA, 5% CH_2Cl_2, 5% H_2O and 2.5% TIS was added to the resin and the mixture was agitated for 1 h. The cleavage mixture was removed and a solution of TFA : CH_2Cl_2 (v/v, 1:1) was added to the resin and shaken for 10 min. The combined filtrates were concentrated under reduced pressure and the remaining peptide was precipitated with Et_2O. The solid was washed three times with Et_2O and then dried.

5.3.9. General Procedure for Ion Exchange of Peptides

Ion exchange was done using VariPure™ IPE tubes from Varian. The prepacked column was first washed with MeOH and then with the respective elution solvent, typically nanopure H_2O : ACN (v/v, 1:1). The peptide as a TFA salt was dissolved in the elution solution and applied on the column. The fractions were analyzed by TLC and visualized with ninhydrin. Peptide containing fractions were

combined and lyophilized. The new counterion HCO_3^- was herewith removed as CO_2 to give the desalted peptide as a white solid. The absence of TFA was shown by ^{19}F – NMR spectroscopy.

5.3.10. General Procedure for Peptide synthesis

The peptides were synthesized as described above on ChemMatrix® Rink amide resin with a loading of 0.64 or 0.52 mmol/ g or on 2-chlrorotrityl chloride resin with a loading of 1.1 mmol/g. Fmoc-(4S)Azp-OH, Fmoc-Pro-(4S)Azp-Pro-OH and the respective Fmoc- amino acids were used on the Syro I Peptide Synthesizer or in manual performed coupling steps. This was followed by acetylation of the N-terminus as described under 5.3.4.. The Staudinger reduction of the azido groups was carried out using the previously described procedures. The next step was the coupling of acids bearing the desired functional groups. In case of the peptides bearing guanidinium functionalities the coupling of an amine was followed by a guanidinylation on solid support. The peptides were cleaved from the solid support and the peptides were purified by preparative RP-HPLC on a Reprosil Gold 100 C18, 150 x 10 mm, 5 µm column with a flow of 6 mL/min at 50°C. The pure peptide was desalted according to the procedure given above.

5.4. Peptides Prepared by Solid Phase Synthesis

5.4.1. Synthesis of Peptide Bearing Imidazole Moieties

5.4.1.1. Synthesis of Peptide 17a

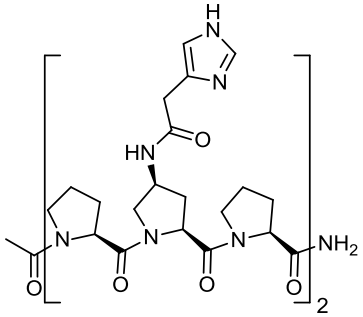

Chemical Formula: $C_{42}H_{57}N_{13}O_9$
Molecular Weight: 888.0 g/mol

Ac-[Pro-Azp-Pro]$_2$-NH$_2$ was synthesized according to the general procedures in a 100 µmol scale on Rink amide - ChemMatrix resin. The coupling steps were followed by an acetylation of the N-terminus. The azido groups were reduced under Staudinger conditions according to the procedure given above. Then, 4-Imidazoleacetic acid hydrochloride was coupled to the amine on the oligoproline backbone. The peptide was cleaved from the resin, purified *via* HPLC and desalted over an ion-exchange column.

HPLC: t_R = 1.7 min; Reprosil gold 120 C18 (3 µm); gradient 98% to 40% B over 5 min at 50°C (PDA @214 nm), flow 0.7 mL/min

HR-MS (MALDI-FT-ICR): *m/z*: = 910.4293 (M + Na^+), calculated for $C_{42}H_{57}N_{13}NaO_9$: *m/z* = 910.4294
m/z = 888.4473(M + H^+), calculated for $C_{42}H_{58}N_{13}O_9$: *m/z* = 888.4475

5.4.1.2. Synthesis of Peptide 17b

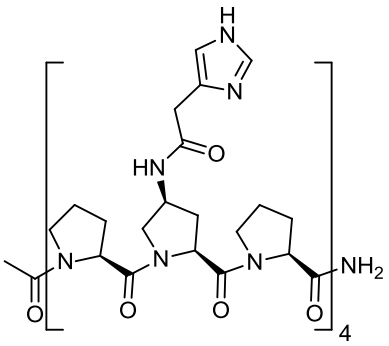

Chemical Formula: $C_{82}H_{109}N_{25}O_{17}$
Molecular Weight: 1716.9 g/mol

Peptide **17b** was synthesized, as described for peptide **17a**.

HPLC: t_R = 2.0 min; Reprosil gold 120 C18 (3 µm); gradient 98% to 40% B over 5 min at 50°C (PDA @214 nm), flow 0.7 mL/min

HR-MS (MALDI-FT-ICR): *m/z* = 1738.8314 ($M + Na^+$), calculated for $C_{82}H_{109}N_{25}NaO_{17}$: *m/z* = 1738.8325
m/z = 1716.8495 ($M + H^+$), calculated for $C_{82}H_{110}N_{25}O_{17}$: *m/z* = 1716.8506

5.4.1.3. Synthesis of Peptide 17c

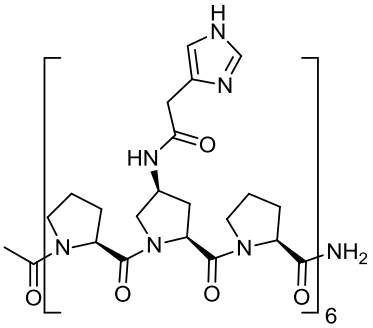

Chemical Formula: $C_{122}H_{161}N_{37}O_{25}$
Molecular Weight: 2545.8 g/mol

Peptide **17c** was synthesized, as described for peptide **17a**.

HPLC: t_R = 7.0 min; Reprosil gold 120 C18 (5 µm); gradient 98% to 40% B over 20 min at 50°C (PDA @214 nm), flow 1.0 mL/min

HR-MS (MALDI-FT-ICR): *m/z* = 2567.2357 ($M + Na^+$), calculated for $C_{122}H_{161}N_{37}NaO_{25}$: *m/z* = 2567.2357

5.4.2. Synthesis of Peptides Bearing Guanidine Moieties

5.4.2.1. Synthesis of Peptide 22a

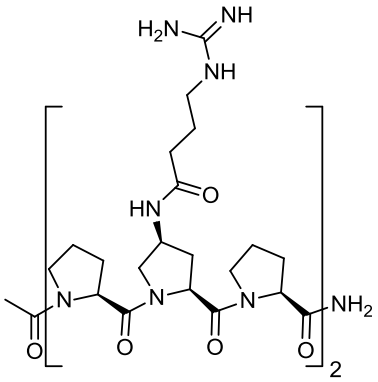

Chemical Formula: $C_{42}H_{67}N_{15}O_9$
Molecular Weight: 926.1 g/mol

Ac-[Pro-Azp-Pro]$_2$-NH$_2$ was synthesized according to the general procedures in a 100 µmol scale on Rink amide - ChemMatrix resin. The coupling steps were followed by an acetylation of the *N*-terminus. The azido groups were reduced under Staudinger conditions according to the procedure given above. Then, Fmoc-GABA was coupled to the amine on the oligoproline backbone. After Fmoc-deprotection a guanidinylation was performed as described. The peptide was cleaved from the resin, purified *via* HPLC and desalted over an ion-exchange column.

HPLC: t_R = 1.8 min; Reprosil gold 120 C18 (3 µm); gradient 98% to 40% B over 5 min at 50°C (PDA @214 nm), flow 0.7 mL/min

HR-MS (MALDI-FT-ICR): *m/z* = 948.5133 (M + Na^+), calculated for $C_{42}H_{67}N_{15}NaO_9$: *m/z* = 948.5138
m/z = 926.5312 (M + H^+), calculated for $C_{42}H_{68}N_{15}O_9$: *m/z* = 926.5319

5.4.2.2. Synthesis of Peptide 22b

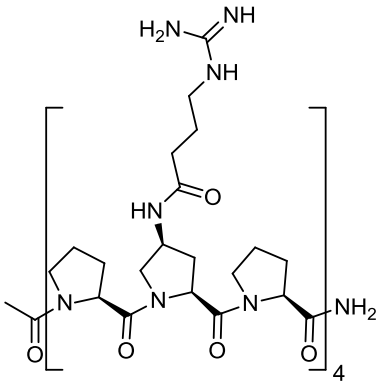

Chemical Formula: $C_{82}H_{129}N_{29}O_{17}$
Molecular Weight: 1793.1 g/mol

Peptide **22b** was synthesized, as described for peptide **22a**.

HPLC: t_R = 2.1 min; Reprosil gold 120 C18 (3 µm); gradient 98% to 40% B over 5 min at 50°C (PDA @214 nm), flow 0.7 mL/min

HR-MS (MALDI-FT-ICR): *m/z* = 1815.0005 ($M + Na^+$), calculated for $C_{82}H_{129}N_{29}NaO_{17}$: *m/z* = 1815.0013
m/z = 1793.0187 ($M + H^+$), calculated for $C_{82}H_{130}N_{29}O_{17}$: *m/z* = 1793.0194

5.4.2.3. Synthesis of Peptide 22c

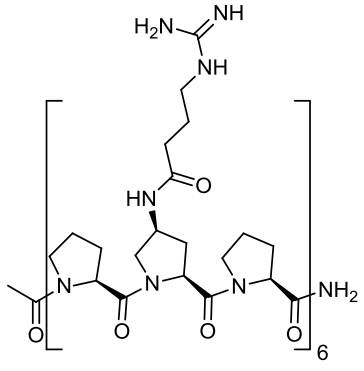

Chemical Formula: $C_{122}H_{191}N_{43}O_{25}$
Molecular Weight: 2660.1 g/mol

Peptide **22c** was synthesized, as described for peptide 2**2a**.

HPLC: t_R = 2.2 min; Reprosil gold 120 C18 (3 µm); gradient 98% to 40% B over 5 min at 50°C (PDA @214 nm), flow 0.7 mL/min

HR-MS (MALDI-FT-ICR): *m/z* = 2659.5104 ($M + H^+$), calculated for $C_{122}H_{192}N_{43}O_{25}$: *m/z* = 2659.5069

5.4.2.4. Synthesis of Peptide 24a

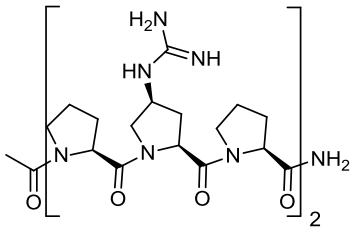

Chemical Formula: $C_{34}H_{53}N_{13}O_7$
Molecular Weight: 755.9 g/mol

Ac-[Pro-Azp-Pro]$_2$-NH_2 was synthesized according to the general procedures in a 100 µmol scale on Rink amide - ChemMatrix resin. The coupling steps were followed by an acetylation of the *N*-terminus. The azido groups were reduced under Staudinger conditions according to the procedure given above. Then a guanidinylation was performed as described. The peptide was cleaved from the resin, purified *via* HPLC and desalted over an ion-exchange column.

HPLC: t_R = 3.1 min; Reprosil gold 120 C18 (3 µm); gradient 98% to 20% B over 5 min at 50°C (PDA @214 nm), flow 0.5 mL/min

HR-MS (MALDI-FT-ICR): *m/z* = 778.4048 ($M + Na^+$), calculated for $C_{34}H_{53}N_{13}NaO_7$: *m/z* = 778.4083
m/z = 756.4262 ($M + H^+$), calculated for $C_{34}H_{54}N_{13}O_7$: *m/z* = 756.4264

5.4.2.5. Synthesis of Peptide 24b

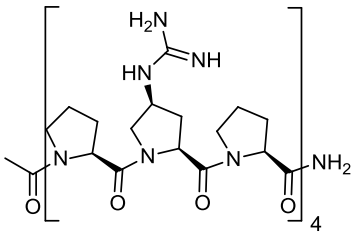

Chemical Formula: $C_{66}H_{101}N_{25}O_{13}$
Molecular Weight: 1452.7 g/mol

Peptide **24b** was synthesized, as described for peptide **24a**.

HPLC: t_R = 3.2 min; Reprosil gold 120 C18 (3 µm); gradient 98% to 20% B over 5 min at 50°C (PDA @214 nm), flow 0.5 mL/min

HR-MS (MALDI-FT-ICR): *m/z* = 1474.7905 ($M + Na^+$), calculated for $C_{66}H_{101}N_{25}NaO_{13}$: *m/z* = 1474.7903
m/z = 1452.8081 ($M + H^+$), calculated for $C_{66}H_{102}N_{25}O_{13}$: *m/z* = 1452.8083

5.4.2.6. Synthesis of Peptide 24c

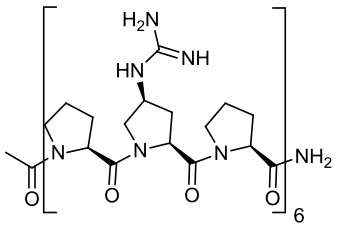

Chemical Formula: $C_{98}H_{149}N_{37}O_{19}$
Molecular Weight: 2149.5 g/mol

Peptide **24c** was synthesized, as described for peptide **24a**.

HPLC: t_R = 3.2 min; Reprosil gold 120 C18 (3 µm); gradient 98% to 20% B over 5 min at 50°C (PDA @214 nm), flow 0.5 mL/min

HR-MS (MALDI-FT-ICR): *m/z* = 2171.1718 ($M + Na^+$), calculated for $C_{98}H_{149}N_{37}NaO_{19}$: *m/z* = 2171.1723
m/z = 2149.1894 ($M + H^+$), calculated for $C_{98}H_{150}N_{37}O_{19}$: *m/z* = 2149.1903

5.4.3. Synthesis of Peptide Bearing Amino Moieties

5.4.3.1. Synthesis of Peptide 21a

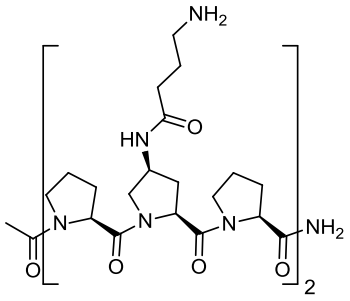

Chemical Formula: $C_{40}H_{63}N_{11}O_9$
Molecular Weight: 842.0 g/mol

Ac-[Pro-Azp-Pro]$_2$-NH_2 was synthesized according to the general procedures in a 100 µmol scale on Rink amide - ChemMatrix resin. The coupling steps were followed by an acetylation of the *N*-terminus. The azido groups were reduced under Staudinger conditions according to the procedure given above. Then, Fmoc-GABA was coupled to the amine on the oligoproline backbone. After Fmoc-deprotection, the peptide was cleaved from the resin, purified *via* HPLC and desalted over an ion-exchange column.

HPLC: t_R = 1.6 min; Reprosil gold 120 C18 (3 µm); gradient 98% to 40% B over 5 min at 50°C (PDA @214 nm), flow 0.7 mL/min

HR-MS (MALDI-FT-ICR): *m/z* = 864.4702 ($M + Na^+$), calculated for $C_{40}H_{63}N_{11}NaO_9$: *m/z* = 864.4702
m/z = 842.4881 ($M + H^+$), calculated for $C_{40}H_{64}N_{11}O_9$: *m/z* = 842.4883

5.4.3.2. Synthesis of Peptide 21b

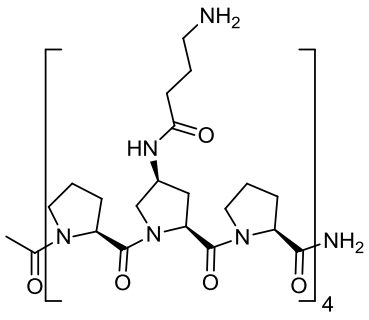

Chemical Formula: $C_{78}H_{121}N_{21}O_{17}$
Molecular Weight: 1624.9 g/mol

Peptide **21b** was synthesized, as described for peptide **21a**.

HPLC: t_R = 1.9 min; Reprosil gold 120 C18 (3 µm); gradient 98% to 40% B over 5 min at 50°C (PDA @214 nm), flow 0.7 mL/min

HR-MS (MALDI-FT-ICR): *m/z* = 1624.9317 ($M + H^+$), calculated for $C_{78}H_{122}N_{21}O_{17}$: *m/z* = 1624.9322

5.4.3.3. Synthesis of Peptide 21c

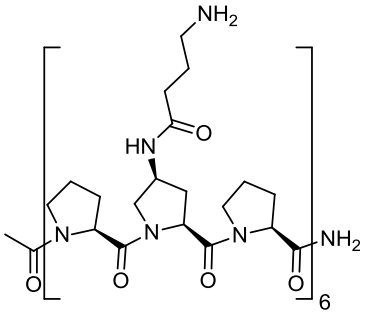

Chemical Formula: $C_{116}H_{179}N_{31}O_{25}$
Molecular Weight: 2407.9 g/mol

Peptide **21c** was synthesized, as described for peptide **21a**.

HPLC: t_R = 2.1 min; Reprosil gold 120 C18 (3 µm); gradient 98% to 40% B over 5 min at 50°C (PDA @214 nm), flow 0.7 mL/min

HR-MS (MALDI-FT-ICR): *m/z* = 2429.3548 ($M + Na^+$), calculated for $C_{116}H_{179}N_{31}NaO_{25}$: *m/z* = 2429.3581

5.4.3.4. Synthesis of Peptide 23a

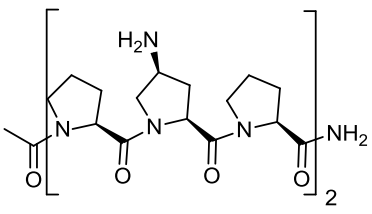

Chemical Formula: $C_{32}H_{49}N_9O_7$
Molecular Weight: 671.8 g/mol

Ac-[Pro-Azp-Pro]$_2$-NH_2 was synthesized according to the general procedures in a 100 µmol scale on Rink amide - ChemMatrix resin. The coupling steps were followed by an acetylation of the *N*-

terminus. The azido groups were reduced under Staudinger conditions according to the procedure given above. Then, the peptide was cleaved from the resin, purified *via* HPLC and desalted over an ion-exchange column.

HPLC: t_R = 3.0 min; Reprosil gold 120 C18 (3 µm); gradient 98% to 20% B over 5 min at 50°C (PDA @214 nm), flow 0.5 mL/min

HR-MS (MALDI-FT-ICR): *m/z* = 694.3829 ($M + Na^+$), calculated for $C_{32}H_{49}N_9NaO_7$: *m/z* = 694.3647

m/z = 672.3829 ($M + H^+$), calculated for $C_{32}H_{50}N_9O_7$: *m/z* = 672.3828

5.4.3.5. Synthesis of Peptide 23b

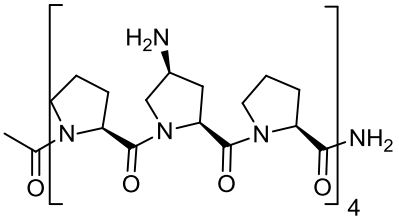

Chemical Formula: $C_{62}H_{93}N_{17}O_{13}$
Molecular Weight: 1284.5 g/mol

Peptide **23b** was synthesized, as described for peptide **23a**.

HPLC: t_R = 3.2 min; Reprosil gold 120 C18 (3 µm); gradient 98% to 20% B over 5 min at 50°C (PDA @214 nm), flow 0.5 mL/min

HR-MS (MALDI-FT-ICR): *m/z* = 1306.7032 ($M + Na^+$), calculated for $C_{62}H_{93}N_{17}NaO_{13}$: *m/z* = 1306.7031

m/z = 1284.7210 ($M + H^+$), calculated for $C_{62}H_{94}N_{17}O_{13}$: *m/z* = 1284.7212

5.4.3.6. Synthesis of Peptide 23c

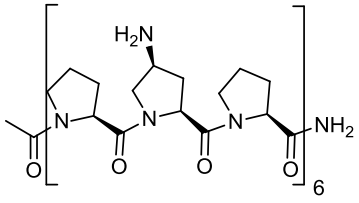

Chemical Formula: $C_{92}H_{137}N_{25}O_{19}$
Molecular Weight: 1897.2 g/mol

Peptide **23c** was synthesized, as described for peptide **23a**.

HPLC: t_R = 3.3 min; Reprosil gold 120 C18 (3 µm); gradient 98% to 20% B over 5 min at 50°C (PDA @214 nm), flow 0.5 mL/min

HR-MS (MALDI-FT-ICR): *m/z* = 1919.0414 ($M + Na^+$), calculated for $C_{92}H_{137}N_{25}NaO_{19}$: *m/z* = 1919.0415

m/z = 1897.0595 ($M + H^+$), calculated for $C_{92}H_{138}N_{25}O_{19}$: *m/z* = 1897.0595

5.4.3.7. Synthesis of peptide 31

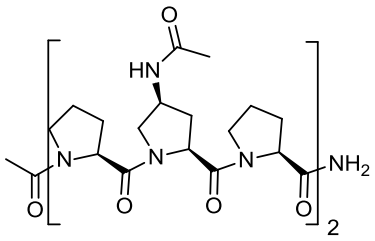

Chemical Formula: $C_{36}H_{53}N_9O_9$
Molecular Weight: 755.9 g/mol

Peptide **23a** was acetylated by addition of 20 equiv acetic anhydride and agitation for 10 h, followed by repeated precipitation with cold Et_2O and drying under high vacuum.

HPLC: t_R = 3.3 min; Reprosil gold 120 C18 (3 µm); gradient 98% to 20% B over 5 min at 50°C (PDA @214 nm), flow 0.5 mL/min

HR-MS (MALDI-FT-ICR): *m/z* = 778.3861 ($M + Na^+$), calculated for $C_{36}H_{53}N_9NaO_9$: *m/z* = 778.3858

m/z = 756.4040 ($M + H^+$), calculated for $C_{36}H_{54}N_9O_9$: *m/z* = 756.4039

5.4.4. Synthesis of Peptides Bearing Carboxylic Acid Moieties

5.4.4.1. Synthesis of Peptide 18a

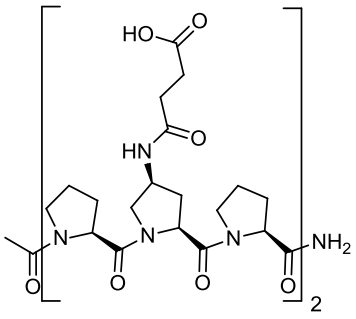

Chemical Formula: $C_{40}H_{57}N_9O_{13}$
Molecular Weight: 871.9 g/mol

Ac-[Pro-Azp-Pro]$_2$-NH_2 was synthesized according to the general procedures in a 100 µmol scale on Rink amide - ChemMatrix resin. The coupling steps were followed by an acetylation of the *N*-terminus. The azido groups were reduced under Staudinger conditions according to the procedure given above. Then, mono-*tert*-Butyl succinate was coupled to the amine on the oligoproline backbone. The peptide was cleaved from the resin and purified *via* HPLC.

HPLC: t_R = 1.9 min; Phenomenex Acris Peptide 1 7u XB-C18 (3 µm); gradient 98% to 40% B over 5 min at 50°C (PDA @214 nm), flow 0.7 mL/min

HR-MS (MALDI-FT-ICR): *m/z* = 894.3965 ($M + Na^+$), calculated for $C_{40}H_{57}N_9NaO_{13}$: *m/z* = 894.3974
m/z = 872.4147 ($M + H^+$), calculated for $C_{40}H_{58}N_9O_{13}$: *m/z* = 872.4154

5.4.4.2. Synthesis of Peptide 18b

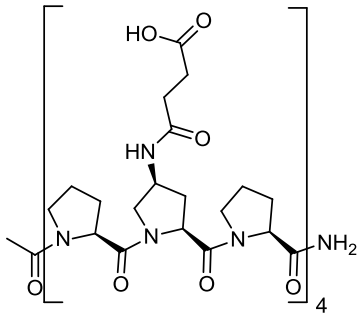

Chemical Formula: $C_{78}H_{109}N_{17}O_{25}$
Molecular Weight: 1684.8 g/mol

Peptide **18b** was synthesized, as described for peptide **18a**.

HPLC: t_R = 2.3 min; Phenomenex Acris Peptide 1 7u XB-C18 (3 µm); gradient 98% to 40% B over 5 min at 50°C (PDA @214 nm), flow 0.7 mL/min

HR-MS (MALDI-FT-ICR): *m/z* = 1706.7655 ($M + Na^+$), calculated for $C_{78}H_{109}N_{17}NaO_{25}$: *m/z* = 1706.7678
m/z = 1684.7835 ($M + H^+$), calculated for $C_{78}H_{110}N_{17}O_{25}$: *m/z* = 1684.7859

5.4.4.3. Synthesis of Peptide 18c

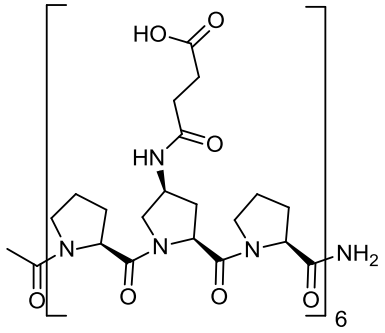

Chemical Formula: $C_{116}H_{161}N_{25}O_{37}$
Molecular Weight: 2497.7 g/mol

Peptide **18b** was synthesized, as described for peptide **18a**.

HPLC: t_R = 2.5 min; Phenomenex Acris Peptide 1 7u XB-C18 (3 µm); gradient 98% to 40% B over 5 min at 50°C (PDA @214 nm), flow 0.7 mL/min

HR-MS (MALDI-FT-ICR): *m/z* = 2519.1403 ($M + Na^+$), calculated for $C_{116}H_{161}N_{25}NaO_{37}$: *m/z* = 2519.1377

5.4.5. Synthesis of Peptides Bearing Indole Moieties

5.4.5.1. Synthesis of Peptide 19a

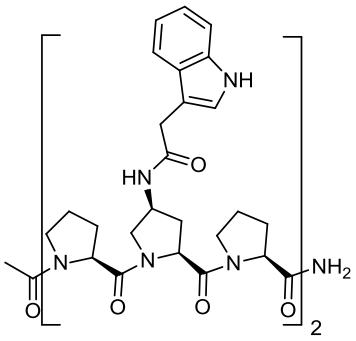

Chemical Formula: $C_{52}H_{63}N_{11}O_9$
Molecular Weight: 986.1 g/mol

Ac-[Pro-Azp-Pro]$_2$-NH_2 was synthesized according to the general procedures in a 100 µmol scale on Rink amide - ChemMatrix resin. The coupling steps were followed by an acetylation of the *N*-terminus. The azido groups were reduced under Staudinger conditions according to the procedure given above. Then, 3-Indoleacetic acid was coupled to the amine on the oligoproline backbone. The peptide was cleaved from the resin, purified *via* HPLC and desalted over an ion-exchange column.

HPLC: t_R = 3.4 min; Phenomenex Acris Peptide 1 7u XB-C18 (3 µm); gradient 98% to 40% B over 5 min at 50°C (PDA @214 nm), flow 0.7 mL/min

HR-MS (MALDI-FT-ICR): *m/z* = 986.4874 ($M + H^+$), calculated for $C_{52}H_{63}N_{11}O_9$: *m/z* = 986.4883

5.4.5.2. Synthesis of Peptide 19b

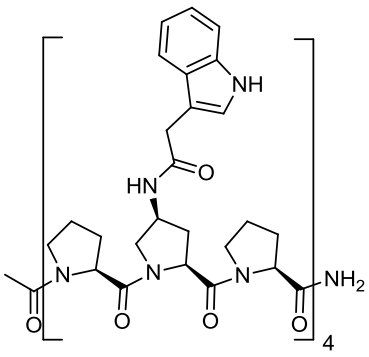

Chemical Formula: $C_{102}H_{121}N_{21}O_{17}$
Molecular Weight: 1913.2 g/mol

Peptide **19b** was synthesized, as described for peptide **19a**.

HPLC: t_R = 4.0 min; Phenomenex Acris Peptide 1 7u XB-C18 (3 µm); gradient 98% to 40% B over 5 min at 50°C (PDA @214 nm), flow 0.7 mL/min

HR-MS (MALDI-FT-ICR): *m/z* = 1934.9131 ($M + Na^+$), calculated for $C_{102}H_{121}N_{21}NaO_{17}$: *m/z* = 1934.9142
m/z = 1912.9309 ($M + H^+$), calculated for $C_{102}H_{122}N_{21}O_{17}$: *m/z* = 1912.9322

5.4.5.3. Synthesis of Peptide 19c

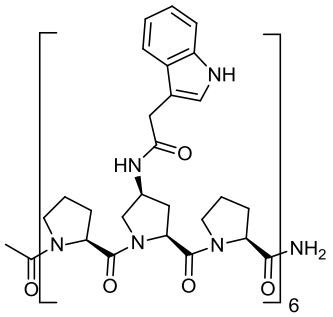

Chemical Formula: $C_{152}H_{179}N_{31}O_{25}$
Molecular Weight: 2840.2 g/mol

Peptide **19c** was synthesized, as described for peptide **19a**.

HPLC: t_R = 4.4 min; Phenomenex Acris Peptide 1 7u XB-C18 (3 µm); gradient 98% to 40% B over 5 min at 50°C (PDA @214 nm), flow 0.7 mL/min

HR-MS (MALDI-FT-ICR): *m/z* = 2861.3595 ($M + Na^+$), calculated for $C_{152}H_{179}N_{31}NaO_{25}$: *m/z* = 2861.3581

5.4.6. Synthesis of Peptides Bearing Pyrrolidinyl Moieties

5.4.6.1. Synthesis of Peptide 20a

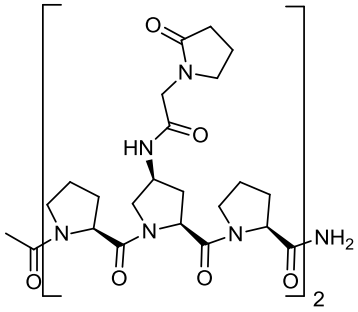

Chemical Formula: $C_{44}H_{63}N_{11}O_{11}$
Molecular Weight: 922.0 g/mol

Ac-[Pro-Azp-Pro]$_2$-NH$_2$ was synthesized according to the general procedures in a 100 µmol scale on Rink amide - ChemMatrix resin. The coupling steps were followed by an acetylation of the *N*-terminus. The azido groups were reduced under Staudinger conditions according to the procedure given above. Then, (2-oxo-1-pyrrolidinyl) acetic acid was coupled to the amine on the oligoproline backbone. The peptide was cleaved from the resin, purified *via* HPLC and desalted over an ion-exchange column.

HPLC: t_R = 2.2 min Reprosil gold 120 C18 (3 µm); gradient 98% to 40% B over 5 min at 50°C (PDA @214 nm), flow 0.7 mL/min

HR-MS (MALDI-FT-ICR): *m/z* = 944.4602 (M + Na^+), calculated for $C_{44}H_{63}N_{11}NaO_{11}$: *m/z* = 944.4601
m/z = 922.4779 (M + H^+), calculated for $C_{44}H_{64}N_{11}O_{11}$: *m/z* = 922.4781

5.4.6.2. Synthesis of Peptide 20b

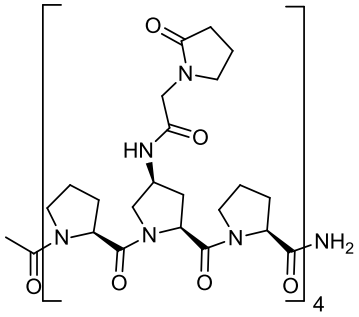

Chemical Formula: $C_{86}H_{121}N_{21}O_{21}$
Molecular Weight: 1785.0 g/mol

Peptide **20b** was synthesized, as described for peptide **20a**.

HPLC: t_R = 2.6 min; Reprosil gold 120 C18 (3 µm); gradient 98% to 40% B over 5 min at 50°C (PDA @214 nm), flow 0.7 mL/min

HR-MS (MALDI-FT-ICR): *m/z* = 1806.8947 ($M + Na^+$), calculated for $C_{86}H_{121}N_{21}NaO_{21}$: *m/z* = 1806.8938
m/z = 1784.9119 ($M + H^+$), calculated for $C_{86}H_{122}N_{21}O_{21}$: *m/z* = 1784.9119

5.4.6.3. Synthesis of Peptide 20c

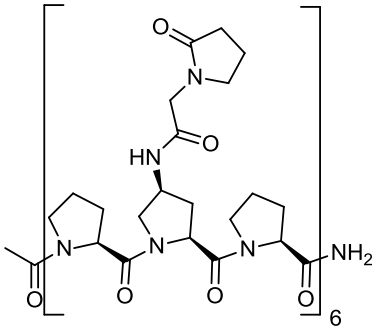

Chemical Formula: $C_{128}H_{179}N_{31}O_{31}$
Molecular Weight: 2648.0 g/mol

Peptide **20c** was synthesized, as described for peptide **20a**.

HPLC: t_R = 4.6 min; Reprosil gold 120 C18 (3 µm); gradient 98% to 20% B over 5 min at 50°C (PDA @214 nm), flow 0.5 mL/min

HR-MS (MALDI-FT-ICR): *m/z* = 2669.3285 ($M + Na^+$), calculated for $C_{128}H_{179}N_{31}NaO_{31}$: *m/z* = 2669.3275

m/z = 2647.3423 ($M + H^+$), calculated for $C_{128}H_{180}N_{31}O_{31}$: *m/z* = 2647.3456

5.4.7. Synthesis of Flexible Peptides

5.4.7.1. Synthesis of Peptide 29a

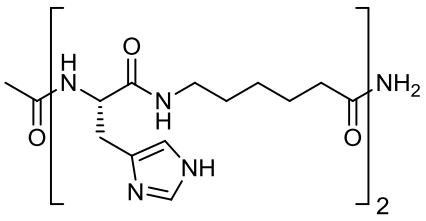

Chemical Formula: $C_{26}H_{41}N_9O_5$
Molecular Weight: 559.7 g/mol

The peptide was synthesized according to the general procedures in a 100 µmol scale on Rink amide - ChemMatrix resin, using Fmoc-His-OH and Fmoc-Ahx-OH as building blocks. The coupling steps were followed by an acetylation of the *N*-terminus. The peptide was cleaved from the resin, purified *via* HPLC and desalted over an ion-exchange column.

HPLC: t_R = 2.8 min Reprosil gold 120 C18 (3 µm); gradient 98% to 40% B over 5 min at 50°C (PDA @214 nm), flow 0.7 mL/min

HR-MS (MALDI-FT-ICR): *m/z* = 560.3302 ($M + H^+$), calculated for $C_{26}H_{42}N_9O_5$: *m/z* = 560.3303

5.4.7.2. Synthesis of Peptide 29b

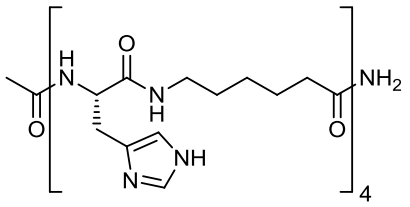

Chemical Formula: $C_{50}H_{77}N_{17}O_9$
Molecular Weight: 1060.3 g/mol

Peptide **29b** was synthesized, as described for peptide 2**9a**.

HPLC: t_R = 2.7 min; Reprosil gold 120 C18 (3 µm); gradient 98% to 40% B over 5 min at 50°C (PDA @214 nm), flow 0.7 mL/min

HR-MS (MALDI-FT-ICR): *m/z* = 1060.6160 ($M + H^+$), calculated for $C_{50}H_{78}N_{17}O_9$: *m/z* = 1060.6163

5.4.7.3. Synthesis of Peptide 29c

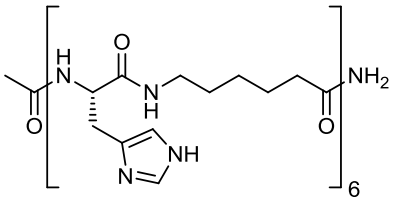

Chemical Formula: $C_{74}H_{113}N_{25}O_{13}$
Molecular Weight: 1560.8 g/mol

Peptide **29c** was synthesized, as described for peptide 2**9a**.

HPLC: t_R = 2.7 min; Reprosil gold 120 C18 (3 µm); gradient 98% to 40% B over 5 min at 50°C (PDA @214 nm), flow 0.7 mL/min

HR-MS (MALDI-FT-ICR): *m/z* = 1560.9023 ($M + H^+$), calculated for $C_{74}H_{113}N_{25}O_{13}$: *m/z* = 1560.9022

5.4.7.4. Synthesis of Peptide 30a

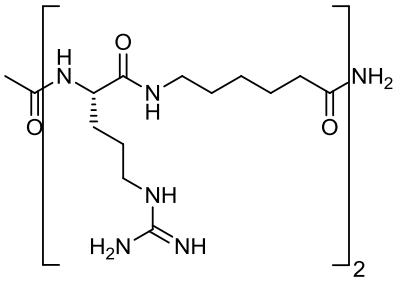

Chemical Formula: $C_{26}H_{51}N_{11}O_5$
Molecular Weight: 597.8 g/mol

The peptide was synthesized according to the general procedures in a 100 µmol scale on Rink amide - ChemMatrix resin, using Fmoc-Arg-OH and Fmoc-Ahx-OH as building blocks. The coupling steps were followed by an acetylation of the *N*-terminus. The peptide was cleaved from the resin, purified *via* HPLC and desalted over an ion-exchange column.

HPLC: t_R = 2.5 min Reprosil gold 120 C18 (3 µm); gradient 98% to 40% B over 5 min at 50°C (PDA @214 nm), flow 0.7 mL/min

HR-MS (MALDI-FT-ICR): *m/z* = 620.3968 ($M + Na^+$), calculated for $C_{26}H_{51}N_{11}NaO_5$: *m/z* = 620.3967

m/z = 598.4148 ($M + H^+$), calculated for $C_{26}H_{51}N_{11}O_5$: *m/z* = 598.4147

5.4.7.5. Synthesis of Peptide 30b

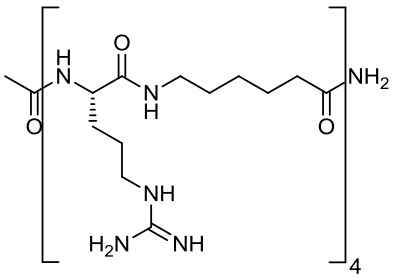

Chemical Formula: $C_{50}H_{97}N_{21}O_9$
Molecular Weight: 1136.4 g/mol

Peptide **30b** was synthesized, as described for peptide **30a**.

HPLC: t_R = 2.7 min; Reprosil gold 120 C18 (3 µm); gradient 98% to 40% B over 5 min at 50°C (PDA @214 nm), flow 0.7 mL/min

HR-MS (MALDI-FT-ICR): *m/z* = 1158.7670 ($M + Na^+$), calculated for $C_{50}H_{97}N_{21}NaO_9$: *m/z* = 1158.7670

m/z = 1136.7851 ($M + H^+$), calculated for $C_{50}H_{98}N_{21}O_9$: *m/z* = 1136.7851

5.4.7.6. Synthesis of Peptide 30c

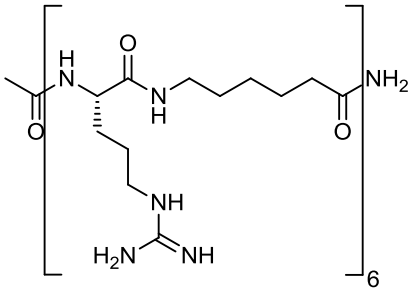

Chemical Formula: $C_{74}H_{143}N_{31}O_{13}$
Molecular Weight: 1675.1 g/mol

Peptide **30c** was synthesized, as described for peptide **30a**.

HPLC: t_R = 2.8 min; Reprosil gold 120 C18 (3 µm); gradient 98% to 40% B over 5 min at 50°C (PDA @214 nm), flow 0.7 mL/min

HR-MS (MALDI-FT-ICR): *m/z* = 1697.1377 ($M + Na^+$), calculated for $C_{74}H_{143}N_{31}NaO_{13}$: *m/z* = 1697.1374

m/z = 1675.1557 ($M + H^+$), calculated for $C_{74}H_{144}N_{31}O_{13}$: *m/z* = 1675.1554

5.4.7.7. Synthesis of Peptide 32

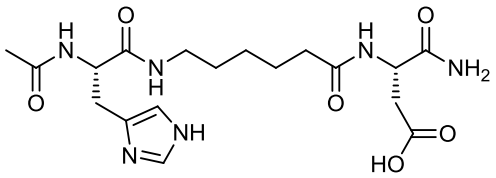

Chemical Formula: $C_{18}H_{28}N_6O_6$
Molecular Weight: 424.5 g/mol

The peptide was synthesized according to the general procedures in a 100 µmol scale on Rink amide - ChemMatrix resin, using Fmoc-His-OH, Fmoc-Ahx-OH and Fmoc-Asp-OH as building blocks. The coupling steps were followed by an acetylation of the *N*-terminus. The peptide was cleaved from the resin, purified *via* HPLC and desalted over an ion-exchange column.

HPLC: t_R = 2.2 min Reprosil gold 120 C18 (3 µm); gradient 98% to 40% B over 5 min at 50°C (PDA @214 nm), flow 0.7 mL/min

HR-MS (MALDI-FT-ICR): *m/z* = 425.2147 ($M + H^+$), calculated for $C_{18}H_{29}N_6O_6$: *m/z* = 425.2143

5.4.7.8. Synthesis of Peptide 33

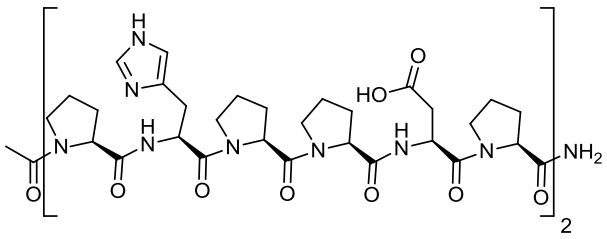

Chemical Formula: $C_{62}H_{85}N_{17}O_{17}$
Molecular Weight: 1340.4 g/mol

The peptide was synthesized according to the general procedures in a 100 µmol scale on Rink amide - ChemMatrix resin, using Fmoc-Pro-OH, Fmoc-His-OH and Fmoc-Asp-OH as building blocks. The coupling steps were followed by an acetylation of the *N*-terminus. The peptide was cleaved from the resin, purified *via* HPLC and desalted over an ion-exchange column.

HPLC: t_R = 3.2 min Reprosil gold 120 C18 (3 µm); gradient 98% to 40% B over 5 min at 50°C (PDA @214 nm), flow 0.7 mL/min

HR-MS (MALDI-FT-ICR): *m/z* = 1340.6375 ($M + H^+$), calculated for $C_{62}H_{86}N_{17}O_{17}$: *m/z* = 1340.6382

5.4.8. Synthesis of Unfunctionalized Oligoprolines

5.4.8.1. Synthesis of Peptide 25

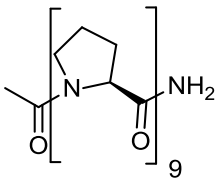

Chemical Formula: $C_{47}H_{68}N_{10}O_{10}$
Molecular Weight: 933.1 g/mol

The peptide was synthesized according to the general procedures in a 100 µmol scale on Rink amide - ChemMatrix resin, using Fmoc-Pro-OH as building block. The coupling steps were followed by an acetylation of the *N*-terminus. The peptide was cleaved from the resin, purified *via* HPLC and desalted over an ion-exchange column.

HPLC: t_R = 7.8 min Reprosil gold 120 C18 (5 µm); gradient 98% to 40% B over 20 min at 50°C (PDA @214 nm), flow 1.0 mL/min

HR-MS (MALDI-FT-ICR): *m/z* = 956.4853 ($M + Na^+$), calculated for $C_{47}H_{68}N_{10}NaO_{10}$: *m/z* = 956.4852

m/z = 934.5036 ($M + H^+$), calculated for $C_{47}H_{69}N_{10}O_{10}$: *m/z* = 934.5033

5.5. CD spectroscopy

For CD spectroscopy the peptides were dissolved in ultrapure H_2O. Depending on the length, different concentrations were adjusted to have about 6 x 10^{-4} M per amino acid residue. For the measurement a quartz cell with a path length of 1 mm was used. The temperature was set to 25°C, with a step resolution of 1 nm and for the Chirascan a time constant of 5 s and with the Chirascan Plus a time constant of 0.5 s. A background measurement with ultrapure H_2O was performed and subtracted from the measured spectra. The values given are in molar elipticities (θ_{MRW} [10^3 deg cm^2 $dmol^{-1}$]). The values are calculated according to formula (**3**).

$$\boldsymbol{\theta_{MRW}} = \frac{\boldsymbol{\theta}}{\boldsymbol{n*c*w}} \qquad \textbf{(3)}$$

θ = total ellipticity

n = number of amino acids

c = concentration

w = width of cuvette

5.6. AgNP generation

5.6.1. AgNP Generation via Chemical Reduction

The respective peptide was dissolved in ultrapure H_2O and the pH was adjusted using 2 M NaOH solution and 2 M HNO_3. Aqueous 2 M $AgNO_3$ solution was added to reach a final concentration of 0.25 M. The mixture was equilibrated for 15 minutes and then the reducing agent was added. The generation process was monitored by UV-Vis spectroscopy and the resulting AgNPs were analyzed by TEM microscopy.

5.6.2. AgNP Generation via Radiation with Visible Light

The respective peptide was dissolved in ultrapure H_2O and the pH was adjusted using 2 M NaOH solution and 2 M HNO_3. Aqueous 2 M $AgNO_3$ solution was added to reach a final concentration of 0.25 M. The mixture was equilibrated for 15 minutes and then exposed for one hour to the radiation source. After this it was kept in the dark. The generation process was monitored by UV-Vis spectroscopy and the resulting AgNPs were analyzed by TEM microscopy.

5.7. AuNP generation

The respective peptide was dissolved in ultrapure H_2O and the pH was adjusted using 2 M NaOH solution. Aqueous 2 M $HAuCl_4$ solution was added to reach a final concentration of 0.25 M. The mixture was equilibrated for 15 min and then the respective reducing agent was added. The generation process was monitored by UV-Vis spectroscopy and the resulting AuNPs were analyzed by TEM microscopy.

5.8. PtNP generation

The respective peptide was dissolved in ultrapure H_2O and the pH was adjusted using 2 M NaOH solution. Aqueous 2 M K_2PtCl_4 solution was added to reach a final concentration of 0.25 M. The mixture was equilibrated for 15 min and then the respective reducing agent was added. The resulting PtNPs were analyzed by TEM microscopy.

6. Appendix

6.1. Abbreviations

Å	Angström
Ac	Acetyl
ACN	Acetonitrile
Ac_2O	Acetic anhydride
AgNP	Silver nanoparticle
Ahx	Aminohexanoic acid
Amp	(4*S*)-amino-L-proline
AuNP	Gold nanoparticle
Azp	Azidoproline
Boc	*tert*-Butyyloxycarbonyl
Boc_2O	Di-*tert*-butyl dicarbonate
°C	Celsius degree
c	Concentration
CD	Circular dichroism
$CDCl_3$	Deuterated chloroform
CH_2Cl_2	Dichloromethane
d	day(s)
d	Doublet
δ	Chemical shift [ppm]
DIPEA	N,N´-diisopropylethylamine
D_2O	Deuterium oxide
DMF	Dimethylformamide
DMSO	N,N-Dimethylsulfoxide
EDC	1-Ethyl-3-(3-dimethylaminopropyl)carbodiimid
EDX spectroscopy	Energy dispersive X-ray spectroscopy
Equiv	Equivalents
Et	Ethyl
EtOAc	Ethylacetate

EtOH	Ethanol
Fmoc	9-Fluorenylmethosycarbonyl
g	Gram
GABA	4-Aminobutanoic acid
Gup	(4*S*)-guanidinylated L-proline
h	Hour
H_2O	Water
HCl	Hydrochloric acid
HCTU	2-(6-Chloro-1-H-benzotriazole1—y)-1,1,3,3-Tetramethyluroniumhexafluorophosphate
H-Hyp-OH	Hydroxyproline
J	Scalar coupling constant [Hz]
λ	Wavelength [nm]
m	Multiplet
M	Molar
MALDI	Matrix assisted laser desorption or ionization
MALDI-FT-ICR	Matrix assisted laser desorption or ionization Fourier transform ion cyclotron resonance
Me	Methyl
MeOH	Methanol
MHz	Megahertz
min	Minute(s)
m/z	Mass to charge ratio
NEt_3	Triethylamine
NMR	Nuclear magnetic resonance
^tBu	*tert*-Butyl
PDA	Photodiode array
PMe_3	Trimethylphosphine
ppm	Parts per million
PPI	Polyproline type I helix
PPII	Polyproline type II helix
PtNP	Platinum nanoparticle

q	Quartet
quint	Quintet
R_t	Retention time
RT	Room temperature
s	Singlet
SERS	surface enhanced Raman spectroscopy
SPPS	Solid phase peptide synthesis
SPR	Surface plasmon resonance
TEM	Transmission electron microscopy
Θ_{MRW}	Mean residues weight ellipticity
TFA	2,2,2-Trifluoroacetic acid
THF	Tetrhydrofurane
TLC	Thin layer chromatography
TMS	tetramethylsilane
TIS	Triisopropylsilane
TNBS	2,4,6-Trinitrobenzenesulfonic acid
TOF	Time of flight
Trt	Trityl (Triphenylmethyl-)
UPLC	Ultra Performance Liquid Chromatography
UV-Vis spectroscopy	Ultraviolet- visible spectroscopy

6.2. CD spectra

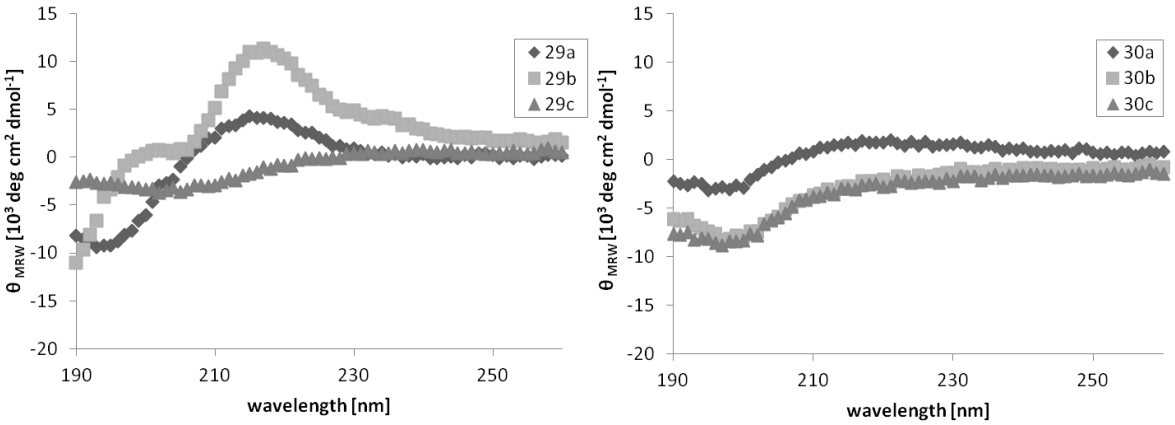

Figure 120: CD spectra of flexible peptides Ac-[His-Ahx]$_n$-NH_2 (**29a** n = 2, **29b** n = 4, **29c** n = 6) and Ac-[Arg-Ahx]$_n$-NH_2 (**30a** n = 2, **30b** n = 4, **30c** n = 6).

6.3 Conditions for Crystallization

The attempts for crystallization were carried out using peptide **17b**, a 12mer bearing four imidazole moieties. The setup was done according to the hanging drop method.[226-227] A solution with a concentration of 1 mg/ 50 µL was made of which 1 µL was mixed with 1 µL of the respective crystallization mixture listed below. The drop was applied on a cover slip that was laid on the top of a vial, containing the same crystallization mixture. The seam of the vial was covered with grease to provide for an airtight sealing. The set up was checked regularly for crystal growth.

Table 2: Crystallization mixtures, used for the attempt to crystallize peptide **17b**.

No	Mixture	Solvent
1	2 M NaCl, 0.1 M sodium acetate	H_2O
2	2 M $(NH_4)_2SO_4$, 0.2 M tartaric acid, 0.1 M sodium acetate	H_2O
3	40% EtOH, 0.1 sodium acetate	H_2O
4	25% tBuOH, 0.1 M Tris	H_2O
5	0.001 M $AgNO_3$, 0.1 M Tris	H_2O
6	0.001 M $HAuCl_4$, 0.1 M Tris	H_2O
7	0.001 M $AgNO_3$, 0.1 M sodium acetate	H_2O
8	0.2 M tartaric acid, 2 M NaCl	H_2O
9	0.001 M $AgNO_3$, 1 M NaCl	H_2O
10	0.2 M tartaric acid	H_2O
11	0.1 M sodium acetate	H_2O
12	25% tBuOH, 40% EtOH	-
13	1 M $(NH_4)_2SO_4$, 0.1 M Tris	H_2O

6.4 References

[1] D. J. Barber, I. C. Freestone, *Archaeometry* **1990**, *32*, 33-45.

[2] A. Caiger-Smith, *Lustre pottery : technique, tradition, and innovation in Islam and the Western world*, Faber and Faber, London ; Boston, **1985**.

[3] J. Perez-Arantegui, A. Larrea, *Trac-Trend Anal Chem* **2003**, *22*, 327-329.

[4] P. S. Rawson, *Ceramics*, 1st pbk. ed., University of Pennsylvania Press, Philadelphia, **1984**.

[5] J. Garcia-Barrasa, J. M. Lopez-de-Luzuriaga, M. Monge, *Cent Eur J Chem* **2011**, *9*, 7-19.

[6] M. Ratner, D. Ratner, *Nanotechnology a gentle introduction to the next big idea*, Prentice Hall, Upper Saddle River, NJ, **2003**.

[7] M. Reibold, A. A. Levin, D. C. Meyer, P. Paufler, W. Kochmann, *Int J Mater Res* **2006**, *97*, 1172-1182.

[8] M. Reibold, P. Paufler, A. A. Levin, W. Kochmann, N. Patzke, D. C. Meyer, *Nature* **2006**, *444*, 286-286.

[9] M. Faraday, *Experimental Relations of Gold <and other Metals> to Light*, London, **1857**.

[10] R. Feynman, P., *Engineering and Science* **1960**, *23*, 22-36.

[11] M. Vert, Y. Doi, K. H. Hellwich, M. Hess, P. Hodge, P. Kubisa, M. Rinaudo, F. Schue, *Pure Appl. Chem.* **2012**, *84*, 377-408.

[12] Y. N. Xia, Y. J. Xiong, B. Lim, S. E. Skrabalak, *Angew Chem Int Edit* **2009**, *48*, 60-103.

[13] A. H. Alshehri, M. Jakubowska, A. Mlozniak, M. Horaczek, D. Rudka, C. Free, J. D. Carey, *Acs Appl Mater Inter* **2012**, *4*, 7006-7009.

[14] H. A. Cong, C. F. Becker, S. J. Elliott, M. W. Grinstaff, J. A. Porco, *J Am Chem Soc* **2010**, *132*, 7514-7518.

[15] S. Sarina, E. R. Waclawik, H. Y. Zhu, *Green Chem* **2013**, *15*, 1814-1833.

[16] C. J. Murphy, T. K. San, A. M. Gole, C. J. Orendorff, J. X. Gao, L. Gou, S. E. Hunyadi, T. Li, *J. Phys. Chem. B* **2005**, *109*, 13857-13870.

[17] S. Eustis, M. A. El-Sayed, *Chem. Soc. Rev.* **2006**, *35*, 209-217.

[18] M. Rycenga, C. M. Cobley, J. Zeng, W. Y. Li, C. H. Moran, Q. Zhang, D. Qin, Y. N. Xia, *Chem. Rev.* **2011**, *111*, 3669-3712.

[19] N. L. Rosi, C. A. Mirkin, *Chem. Rev.* **2005**, *105*, 1547-1562.

[20] R. R. Arvizo, S. Bhattacharyya, R. A. Kudgus, K. Giri, R. Bhattacharya, P. Mukherjee, *Chem. Soc. Rev.* **2012**, *41*, 2943-2970.

[21] Z. M. Xiu, Q. B. Zhang, H. L. Puppala, V. L. Colvin, P. J. J. Alvarez, *Nano Lett.* **2012**, *12*, 4271-4275.

[22] C. C. Caro, P. M.; Klippstein, R.; Pozo, D.; Zaderenko, A. P., in *Silver Nanoparticles*, InTech, **2010**.

[23] K. A. Willets, R. P. Van Duyne, *Annu. Rev. Phys. Chem.* **2007**, *58*, 267-297.

[24] K. G. Stamplecoskie, J. C. Scaiano, *Photochem. Photobiol.* **2012**, *88*, 762-768.

[25] Y. J. Zhang, R. Huang, X. F. Zhu, L. Z. Wang, C. X. Wu, *Chin. Sci. Bull.* **2012**, *57*, 238-246.

[26] A. J. Haes, L. Chang, W. L. Klein, R. P. Van Duyne, *J Am Chem Soc* **2005**, *127*, 2264-2271.

[27] H. Wei, C. G. Chen, B. Y. Han, E. K. Wang, *Anal. Chem.* **2008**, *80*, 7051-7055.

[28] H. Cong, J. A. Porco, *Acs Catal* **2012**, *2*, 65-70.

[29] K. Shimizu, R. Sato, A. Satsuma, *Angew Chem Int Edit* **2009**, *48*, 3982-3986.

[30] A. Murugadoss, P. Goswami, A. Paul, A. Chattopadhyay, *J Mol Catal a-Chem* **2009**, *304*, 153-158.

[31] K. S. Shin, J. Y. Choi, C. S. Park, H. J. Jang, K. Kim, *Catal. Lett.* **2009**, *133*, 1-7.

[32] K. D. Santos, W. C. Elias, A. M. Signori, F. C. Giacomelli, H. Yang, J. B. Domingos, *J Phys Chem C* **2012**, *116*, 4594-4604.

[33] H. Cong, J. A. Porco, *Org. Lett.* **2012**, *14*, 2516-2519.

[34] E. M. O'Brien, B. J. Morgan, M. C. Kozlowski, *Angew Chem Int Edit* **2008**, *47*, 6877-6880.
[35] S. Takizawa, T. Katayama, H. Sasai, *Chem. Commun.* **2008**, 4113-4122.
[36] B. J. Morgan, S. Dey, S. W. Johnson, M. C. Kozlowski, *J Am Chem Soc* **2009**, *131*, 9413-9425.
[37] J. W. Alexander, *Surg Infect* **2009**, *10*, 289-292.
[38] S. Chernousova, M. Epple, *Angew Chem Int Edit* **2013**, *52*, 1636-1653.
[39] H. J. Klasen, *Burns* **2000**, *26*, 131-138.
[40] B. S. Atiyeh, M. Costagliola, S. N. Hayek, S. A. Dibo, *Burns* **2007**, *33*, 139-148.
[41] B. Hamad, *Nat Rev Drug Discov* **2010**, *9*, 675-675.
[42] L. S. Nair, C. T. Laurencin, *J Biomed Nanotechnol* **2007**, *3*, 301-316.
[43] V. K. Sharma, R. A. Yngard, Y. Lin, *Adv. Colloid Interface Sci.* **2009**, *145*, 83-96.
[44] M. Rai, A. Yadav, A. Gade, *Biotechnol. Adv.* **2009**, *27*, 76-83.
[45] A. Panacek, L. Kvitek, R. Prucek, M. Kolar, R. Vecerova, N. Pizurova, V. K. Sharma, T. Nevecna, R. Zboril, *J. Phys. Chem. B* **2006**, *110*, 16248-16253.
[46] S. Eckhardt, P. S. Brunetto, J. Gagnon, M. Priebe, B. Giese, K. M. Fromm, *Chem. Rev.* **2013**, *113*, 4708-4754.
[47] I. Sondi, B. Salopek-Sondi, *J. Colloid Interface Sci.* **2004**, *275*, 177-182.
[48] L. Kvitek, A. Panacek, J. Soukupova, M. Kolar, R. Vecerova, R. Prucek, M. Holecova, R. Zboril, *J Phys Chem C* **2008**, *112*, 5825-5834.
[49] J. R. Morones, J. L. Elechiguerra, A. Camacho, K. Holt, J. B. Kouri, J. T. Ramirez, M. J. Yacaman, *Nanotechnology* **2005**, *16*, 2346-2353.
[50] B. Y. Ahn, E. B. Duoss, M. J. Motala, X. Y. Guo, S. I. Park, Y. J. Xiong, J. Yoon, R. G. Nuzzo, J. A. Rogers, J. A. Lewis, *Science* **2009**, *323*, 1590-1593.
[51] S. M. Wang, C. W. Leung, P. K. L. Chan, *Appl. Phys. Lett.* **2010**, *97*.
[52] Y. N. Li, Y. L. Wu, B. S. Ong, *J Am Chem Soc* **2005**, *127*, 3266-3267.
[53] P. Buffat, J. P. Borel, *Phys Rev A* **1976**, *13*, 2287-2298.
[54] T. Castro, R. Reifenberger, E. Choi, R. P. Andres, *Phys Rev B* **1990**, *42*, 8548-8556.
[55] S. L. C. Hsu, R. T. Wu, *Mater. Lett.* **2007**, *61*, 3719-3722.
[56] Y. A. Krutyakov, A. A. Kudrinskiy, A. Y. Olenin, G. V. Lisichkin, *Usp. Khim.* **2008**, *77*, 242-269.
[57] M. B. Dickerson, K. H. Sandhage, R. R. Naik, *Chem. Rev.* **2008**, *108*, 4935-4978.
[58] C. L. Chen, N. L. Rosi, *Angew Chem Int Edit* **2010**, *49*, 1924-1942.
[59] E. Gaffet, M. Tachikart, O. ElKedim, R. Rahouadj, *Mater. Charact.* **1996**, *36*, 185-190.
[60] G. Cao, *Nanostructures & nanomaterials synthesis, properties & applications*, Imperial College Press, London, **2004**.
[61] A. H. Fojtik, A., *Ber. Bunsen-Ges. Phys. Chem* **1993**, *97*, 252-254.
[62] P. Smejkal, K. Siskova, B. Vlckova, J. Pfleger, I. Sloufova, M. Slouf, P. Mojzes, *Spectrochim Acta A* **2003**, *59*, 2321-2329.
[63] T. Tsuji, D. H. Thang, Y. Okazaki, M. Nakanishi, Y. Tsuboi, M. Tsuji, *Appl. Surf. Sci.* **2008**, *254*, 5224-5230.
[64] F. Mafune, J. Kohno, Y. Takeda, T. Kondow, H. Sawabe, *J. Phys. Chem. B* **2000**, *104*, 8333-8337.
[65] R. Paul, R. N. Gayen, S. Hussain, V. Khanna, R. Bhar, A. K. Pal, *Eur Phys J-Appl Phys* **2009**, *47*.
[66] Y. G. Sun, Y. N. Xia, *Science* **2002**, *298*, 2176-2179.
[67] H. S. Wang, X. L. Qiao, J. G. Chen, X. J. Wang, S. Y. Ding, *Mater. Chem. Phys.* **2005**, *94*, 449-453.
[68] J. Zeng, Y. Q. Zheng, M. Rycenga, J. Tao, Z. Y. Li, Q. A. Zhang, Y. M. Zhu, Y. N. Xia, *J Am Chem Soc* **2010**, *132*, 8552-+.
[69] X. L. Ding, C. X. Kan, B. Mo, S. L. Ke, B. Cong, L. H. Xu, J. J. Zhu, *J. Nanopart. Res.* **2012**, *14*.

[70] K. S. Kumar, A. Divya, S. P. Kumar, B. Ajitha, V. S. Chaithanya, K. J. Prasad, P. S. Reddy, *Micro Nano Lett* **2011**, *6*, 975-977.
[71] G. A. Bhaduri, R. Little, R. B. Khomane, S. U. Lokhande, B. D. Kulkarni, B. G. Mendis, L. Siller, *J Photoch Photobio A* **2013**, *258*, 1-9.
[72] A. Y. Obaid, S. A. AL-Thabaiti, E. H. El-Mossalamy, J. I. Hussain, Z. Khan, *Mater. Res. Bull.* **2013**, *48*, 1137-1142.
[73] N. R. Jana, L. Gearheart, C. J. Murphy, *Chem. Commun.* **2001**, 617-618.
[74] L. M. Bronstein, Z. B. Shifrina, *Chem. Rev.* **2011**, *111*, 5301-5344.
[75] A. Latorre, A. Somoza, *Chembiochem* **2012**, *13*, 951-958.
[76] S. Ashraf, A. Z. Abbasi, C. Pfeiffer, S. Z. Hussain, Z. M. Khalid, P. R. Gil, W. J. Parak, I. Hussain, *Colloid Surface B* **2013**, *102*, 511-518.
[77] K. Belser, T. V. Slenters, C. Pfumbidzai, G. Upert, L. Mirolo, K. M. Fromm, H. Wennemers, *Angew Chem Int Edit* **2009**, *48*, 3661-3664.
[78] G. Upert, F. Bouillere, H. Wennemers, *Angew Chem Int Edit* **2012**, *51*, 4231-4234.
[79] A. Rafey, K. B. L. Shrivastavaa, S. A. Iqbal, Z. Khan, *J. Colloid Interface Sci.* **2011**, *354*, 190-195.
[80] K. G. Stamplecoskie, J. C. Scaiano, *J Am Chem Soc* **2010**, *132*, 1825-1827.
[81] M. Sakamoto, M. Fujistuka, T. Majima, *J Photoch Photobio C* **2009**, *10*, 33-56.
[82] A. Pal, T. Pal, *J Raman Spectrosc* **1999**, *30*, 199-204.
[83] R. C. Jin, Y. W. Cao, C. A. Mirkin, K. L. Kelly, G. C. Schatz, J. G. Zheng, *Science* **2001**, *294*, 1901-1903.
[84] R. C. Jin, Y. C. Cao, E. C. Hao, G. S. Metraux, G. C. Schatz, C. A. Mirkin, *Nature* **2003**, *425*, 487-490.
[85] T. M. Tolaymat, A. M. El Badawy, A. Genaidy, K. G. Scheckel, T. P. Luxton, M. Suidan, *Sci. Total Environ.* **2010**, *408*, 999-1006.
[86] J. A. Creighton, C. G. Blatchford, M. G. Albrecht, *J Chem Soc Farad T 2* **1979**, *75*, 790-798.
[87] P. C. Lee, D. Meisel, *J. Phys. Chem.* **1982**, *86*, 3391-3395.
[88] S. I, D. V. Goia, E. Matijevic, *J. Colloid Interface Sci.* **2003**, *260*, 75-81.
[89] K. P. Velikov, G. E. Zegers, A. van Blaaderen, *Langmuir* **2003**, *19*, 1384-1389.
[90] Y. D. Yin, Z. Y. Li, Z. Y. Zhong, B. Gates, Y. N. Xia, S. Venkateswaran, *J. Mater. Chem.* **2002**, *12*, 522-527.
[91] C. T. Wirges, J. Timper, M. Fischler, A. S. Sologubenko, J. Mayer, U. Simon, T. Carell, *Angew Chem Int Edit* **2009**, *48*, 219-223.
[92] M. Sarikaya, C. Tamerler, A. K. Y. Jen, K. Schulten, F. Baneyx, *Nat Mater* **2003**, *2*, 577-585.
[93] K. B. Narayanan, N. Sakthivel, *Adv. Colloid Interface Sci.* **2011**, *169*, 59-79.
[94] C. Haefeli, C. Franklin, K. Hardy, *J. Bacteriol.* **1984**, *158*, 389-392.
[95] T. Klaus, R. Joerger, E. Olsson, C. G. Granqvist, *P Natl Acad Sci USA* **1999**, *96*, 13611-13614.
[96] A. Gupta, K. Matsui, J. F. Lo, S. Silver, *Nat Med* **1999**, *5*, 183-188.
[97] R. R. Naik, S. J. Stringer, G. Agarwal, S. E. Jones, M. O. Stone, *Nat Mater* **2002**, *1*, 169-172.
[98] E. Lee, D. H. Kim, Y. Woo, H. G. Hur, Y. Lim, *Biochem. Biophys. Res. Commun.* **2008**, *376*, 595-598.
[99] J. M. Slocik, J. T. Moore, D. W. Wright, *Nano Lett.* **2002**, *2*, 169-173.
[100] J. M. Slocik, D. W. Wright, *Biomacromolecules* **2003**, *4*, 1135-1141.
[101] J. P. Xie, J. Y. Lee, D. I. C. Wang, Y. P. Ting, *Acs Nano* **2007**, *1*, 429-439.
[102] S. Si, T. K. Mandal, *Chem-Eur J* **2007**, *13*, 3160-3168.
[103] S. K. Li, Y. H. Shen, A. J. Xie, X. R. Yu, L. G. Qiu, L. Zhang, Q. F. Zhang, *Green Chem* **2007**, *9*, 852-858.
[104] H. Bar, D. K. Bhui, G. P. Sahoo, P. Sarkar, S. Pyne, A. Misra, *Colloid Surface A* **2009**, *348*, 212-216.

[105] H. Bar, D. K. Bhui, G. R. Sahoo, P. Sarkar, S. R. De, A. Misra, *Colloid Surface A* **2009**, *339*, 134-139.
[106] M. Reches, E. Gazit, *Science* **2003**, *300*, 625-627.
[107] R. Wilson, *Chem. Soc. Rev.* **2008**, *37*, 2028-2045.
[108] C. A. Mirkin, R. L. Letsinger, R. C. Mucic, J. J. Storhoff, *Nature* **1996**, *382*, 607-609.
[109] R. Elghanian, J. J. Storhoff, R. C. Mucic, R. L. Letsinger, C. A. Mirkin, *Science* **1997**, *277*, 1078-1081.
[110] J. H. W. Leuvering, P. J. H. M. Thal, M. V. D. Waart, A. H. W. M. Schuurs, *Fresen Z Anal Chem* **1980**, *301*, 132-132.
[111] J. H. W. Leuvering, P. J. H. M. Thal, M. Vanderwaart, A. H. W. M. Schuurs, *J Immunol Methods* **1981**, *45*, 183-194.
[112] J. H. W. Leuvering, B. C. Goverde, P. J. H. M. Thal, A. H. W. M. Schuurs, *J Immunol Methods* **1983**, *60*, 9-23.
[113] M. D. Porter, R. J. Lipert, L. M. Siperko, G. Wang, R. Narayanana, *Chem. Soc. Rev.* **2008**, *37*, 1001-1011.
[114] S. W. Bishnoi, C. J. Rozell, C. S. Levin, M. K. Gheith, B. R. Johnson, D. H. Johnson, N. J. Halas, *Nano Lett.* **2006**, *6*, 1687-1692.
[115] A. Corma, H. Garcia, *Chem. Soc. Rev.* **2008**, *37*, 2096-2126.
[116] Y. Mikami, A. Dhakshinamoorthy, M. Alvaro, H. Garcia, *Catal Sci Technol* **2013**, *3*, 58-69.
[117] H. Tsunoyama, H. Sakurai, Y. Negishi, T. Tsukuda, *J Am Chem Soc* **2005**, *127*, 9374-9375.
[118] H. Tsunoyama, T. Tsukuda, H. Sakurai, *Chem. Lett.* **2007**, *36*, 212-213.
[119] H. Tsunoyama, N. Ichikuni, H. Sakurai, T. Tsukuda, *J Am Chem Soc* **2009**, *131*, 7086-7093.
[120] B. Kang, M. A. Mackey, M. A. El-Sayed, *J Am Chem Soc* **2010**, *132*, 1517-+.
[121] R. Hong, G. Han, J. M. Fernandez, B. J. Kim, N. S. Forbes, V. M. Rotello, *J Am Chem Soc* **2006**, *128*, 1078-1079.
[122] T. Dadosh, Y. Gordin, R. Krahne, I. Khivrich, D. Mahalu, V. Frydman, J. Sperling, A. Yacoby, I. Bar-Joseph, *Nature* **2005**, *436*, 1200-1200.
[123] T. Panda, K. Deepa, *J Nanosci Nanotechno* **2011**, *11*, 10279-10294.
[124] P. X. Zhao, N. Li, D. Astruc, *Coord. Chem. Rev.* **2013**, *257*, 638-665.
[125] M. Hu, F. S. Ou, W. Wu, I. Naumov, X. M. Li, A. M. Bratkovsky, R. S. Williams, Z. Y. Li, *J Am Chem Soc* **2010**, *132*, 12820-12822.
[126] W. Huang, W. Qian, M. A. El-Sayed, *J Am Chem Soc* **2006**, *128*, 13330-13331.
[127] S. Besner, A. V. Kabashin, F. M. Winnik, M. Meunier, *J Phys Chem C* **2009**, *113*, 9526-9531.
[128] K. Torigoe, K. Esumi, *Langmuir* **1992**, *8*, 59-63.
[129] J. Turkevich, P. C. Stevenson, J. Hillier, *Discuss Faraday Soc* **1951**, 55-&.
[130] G. Frens, *Nature-Phys Sci* **1973**, *241*, 20-22.
[131] Y. Li, O. Zaluzhna, B. L. Xu, Y. A. Gao, J. M. Modest, Y. J. Tong, *J Am Chem Soc* **2011**, *133*, 2092-2095.
[132] L. M. Liz-Marzan, *Chem. Commun.* **2013**, *49*, 16-18.
[133] T. K. Sau, C. J. Murphy, *J Am Chem Soc* **2004**, *126*, 8648-8649.
[134] K. B. Narayanan, N. Sakthivel, *Adv. Colloid Interface Sci.* **2010**, *156*, 1-13.
[135] T. J. Beveridge, R. G. E. Murray, *J. Bacteriol.* **1980**, *141*, 876-887.
[136] L. W. Du, H. Jiang, X. H. Liu, E. K. Wang, *Electrochem. Commun.* **2007**, *9*, 1165-1170.
[137] S. Brown, *Nat. Biotechnol.* **1997**, *15*, 269-272.
[138] S. Brown, M. Sarikaya, E. Johnson, *J. Mol. Biol.* **2000**, *299*, 725-735.
[139] Z. Wang, J. C. Chen, P. Yang, W. T. Yang, *Appl. Organomet. Chem.* **2007**, *21*, 645-651.
[140] J. M. Slocik, M. O. Stone, R. R. Naik, *Small* **2005**, *1*, 1048-1052.
[141] T. Serizawa, Y. Hirai, M. Aizawa, *Langmuir* **2009**, *25*, 12229-12234.

[142] R. Djalali, Y. Chen, H. Matsui, *J Am Chem Soc* **2002**, *124*, 13660-13661.
[143] R. Djalali, Chen, Y., Matsui, H., *J Am Chem Soc* **2003**, *125*, 5873-5879.
[144] C. L. Chen, P. J. Zhang, N. L. Rosi, *J Am Chem Soc* **2008**, *130*, 13555.
[145] P. M. Cowan, S. Mcgavin, *Nature* **1955**, *176*, 501-503.
[146] I. Z. Steinberg, W. F. Harrington, A. Berger, M. Sela, E. Katchalski, *J Am Chem Soc* **1960**, *82*, 5263-5279.
[147] W. Traub, U. Shueli, *Nature* **1963**, *198*, 1165-&.
[148] F. Rabanal, M. D. Ludevid, M. Pons, E. Giralt, *Biopolymers* **1993**, *33*, 1019-1028.
[149] J. C. Horng, R. T. Raines, *Protein Sci.* **2006**, *15*, 74-83.
[150] Y. A. Nagel, PdD thesis, University of Basel (Basel), **2012**.
[151] M. P. Williamson, *Biochem. J* **1994**, *297*, 249-260.
[152] H. T. Yu, J. K. Chen, S. B. Feng, D. C. Dalgarno, A. W. Brauer, S. L. Schreiber, *Cell* **1994**, *76*, 933-945.
[153] A. B. Sparks, J. E. Rider, N. G. Hoffman, D. M. Fowlkes, L. A. Quilliam, B. K. Kay, *P Natl Acad Sci USA* **1996**, *93*, 1540-1544.
[154] H. I. Chen, M. Sudol, *P Natl Acad Sci USA* **1995**, *92*, 7819-7823.
[155] M. J. Macias, M. Hyvonen, E. Baraldi, J. Schultz, M. Sudol, M. Saraste, H. Oschkinat, *Nature* **1996**, *382*, 646-649.
[156] M. Reinhard, K. Jouvenal, D. Tripier, U. Walter, *P Natl Acad Sci USA* **1995**, *92*, 7956-7960.
[157] M. Reinhard, K. Giehl, K. Abel, C. Haffner, T. Jarchau, V. Hoppe, B. M. Jockusch, U. Walter, *EMBO J.* **1995**, *14*, 1583-1589.
[158] M. Reinhard, M. Rudiger, B. M. Jockusch, U. Walter, *FEBS Lett.* **1996**, *399*, 103-107.
[159] K. Nishizawa, C. Freund, J. Li, G. Wagner, E. L. Reinherz, *P Natl Acad Sci USA* **1998**, *95*, 14897-14902.
[160] C. Freund, V. Dotsch, K. Nishizawa, E. L. Reinherz, G. Wagner, *Nat Struct Biol* **1999**, *6*, 656-660.
[161] O. Pornillos, S. L. Alam, D. R. Davis, W. I. Sundquist, *Nat Struct Biol* **2002**, *9*, 812-817.
[162] O. Pornillos, S. L. Alam, R. L. Rich, D. G. Myszka, D. R. Davis, W. I. Sundquist, *EMBO J.* **2002**, *21*, 2397-2406.
[163] N. M. Mahoney, P. A. Janmey, S. C. Almo, *Nat Struct Biol* **1997**, *4*, 953-960.
[164] C. E. Schutt, Myslik, J. C., Rozycki, M. D., Goonesekere, M. C. W., Lindberg, U., *Nature* **1993**, *365*, 810-816.
[165] B. Brodsky, N. K. Shah, *FASEB J.* **1995**, *9*, 1537-1546.
[166] J. Engel, H. P. Bachinger, *Top Curr Chem* **2005**, *247*, 7-33.
[167] A. Pepe, M. R. Armenante, B. Bochicchio, A. M. Tamburro, *Soft Matter* **2009**, *5*, 104-113.
[168] P. J. Ferris, J. P. Woessner, S. Waffenschmidt, S. Kilz, J. Drees, U. W. Goodenough, *Biochemistry-Us* **2001**, *40*, 2978-2987.
[169] M. R. Holt, A. Koffer, *Trends Cell Biol* **2001**, *11*, 38-46.
[170] Y. A. Nagel, M. Kuemin, H. Wennemers, *Chimia* **2011**, *65*, 264-267.
[171] M. Kumin, L. S. Sonntag, H. Wennemers, *J Am Chem Soc* **2007**, *129*, 466-467.
[172] V. V. Rostovtsev, L. G. Green, V. V. Fokin, K. B. Sharpless, *Angew Chem Int Edit* **2002**, *41*, 2596.
[173] R. S. Erdmann, H. Wennemers, *J Am Chem Soc* **2010**, *132*, 13957-13959.
[174] C. W. Tornoe, C. Christensen, M. Meldal, *J. Org. Chem.* **2002**, *67*, 3057-3064.
[175] R. S. Erdmann, M. Kumin, H. Wennemers, *Chimia* **2009**, *63*, 197-200.
[176] L. Stryer, R. P. Haugland, *P Natl Acad Sci USA* **1967**, *58*, 719-&.
[177] B. Schuler, E. A. Lipman, P. J. Steinbach, M. Kumke, W. A. Eaton, *P Natl Acad Sci USA* **2005**, *102*, 2754-2759.

[178] R. B. Best, K. A. Merchant, I. V. Gopich, B. Schuler, A. Bax, W. A. Eaton, *P Natl Acad Sci USA* **2007**, *104*, 18964-18969.
[179] K. E. Sapsford, L. Berti, I. L. Medintz, *Angew Chem Int Edit* **2006**, *45*, 4562-4588.
[180] Z. K. Majumdar, R. Hickerson, H. F. Noller, R. M. Clegg, *J. Mol. Biol.* **2005**, *354*, 504-504.
[181] M. Cordes, A. Kottgen, C. Jasper, O. Jacques, H. Boudebous, B. Giese, *Angew Chem Int Edit* **2008**, *47*, 3461-3463.
[182] B. Giese, M. Graber, M. Cordes, *Curr. Opin. Chem. Biol.* **2008**, *12*, 755-759.
[183] B. Giese, M. Wang, J. Gao, M. Stoltz, P. Muller, M. Graber, *J. Org. Chem.* **2009**, *74*, 3621-3625.
[184] S. A. Serron, W. S. Aldridge, C. N. Fleming, R. M. Danell, M. H. Baik, M. Sykora, D. M. Dattelbaum, T. J. Meyer, *J Am Chem Soc* **2004**, *126*, 14506-14514.
[185] D. R. Striplin, S. Y. Reece, D. G. McCafferty, C. G. Wall, D. A. Friesen, B. W. Erickson, T. J. Meyer, *J Am Chem Soc* **2004**, *126*, 5282-5291.
[186] K. M. Bonger, V. V. Kapoerchan, G. M. Grotenbreg, C. J. van Koppen, C. M. Timmers, G. A. van der Marel, H. S. Overkleeft, *Org Biomol Chem* **2010**, *8*, 1881-1884.
[187] C. Kroll, PhD thesis, University of Basel (Basel), **2012**.
[188] H. L. Liu, Y. J. Ye, J. Chen, D. Y. Lin, Z. Jiang, Z. J. Liu, B. Sun, L. B. Yang, J. H. Liu, *Chem-Eur J* **2012**, *18*, 8037-8041.
[189] V. W. M. Lee, H. B. Li, T. C. Lau, R. Guevremont, K. W. M. Siu, *J. Am. Soc. Mass. Spectrom.* **1998**, *9*, 760-766.
[190] E. Podstawka, Y. Ozaki, L. M. Proniewicz, *Appl. Spectrosc.* **2004**, *58*, 570-580.
[191] T. Shoeib, K. W. M. Siu, A. C. Hopkinson, *J. Phys. Chem. A* **2002**, *106*, 6121-6128.
[192] Y. N. Tan, J. Y. Lee, D. I. C. Wang, *J Am Chem Soc* **2010**, *132*, 5677-5686.
[193] B. R. Peelle, E. M. Krauland, K. D. Wittrup, A. M. Belcher, *Langmuir* **2005**, *21*, 6929-6933.
[194] S. K. Bhargava, J. M. Booth, S. Agrawal, P. Coloe, G. Kar, *Langmuir* **2005**, *21*, 5949-5956.
[195] C. E. Hoppe, M. Lazzari, I. Pardinas-Blanco, M. A. Lopez-Quintela, *Langmuir* **2006**, *22*, 7027-7034.
[196] D. A. Dougherty, *Acc. Chem. Res.* **2013**, *46*, 885-893.
[197] M. Kuemin, S. Schweizer, C. Ochsenfeld, H. Wennemers, *J Am Chem Soc* **2009**, *131*, 15474-15482.
[198] M. Kümin, Diploma thesis, University of Basel **2005**.
[199] L. S. Sonntag, S. Schweizer, C. Ochsenfeld, H. Wennemers, *J Am Chem Soc* **2006**, *128*, 14697-14703.
[200] R. S. Erdmann, H. Wennemers, *Angew Chem Int Edit* **2011**, *50*, 6835-6838.
[201] B. W. Chellgren, T. P. Creamer, *Biochemistry-Us* **2004**, *43*, 5864-5869.
[202] D. D. Jenness, C. Sprecher, W. C. Johnson, *Biopolymers* **1976**, *15*, 513-521.
[203] Greenfie.N, G. D. Fasman, *Biochemistry-Us* **1969**, *8*, 4108-&.
[204] R. K. Dukor, T. A. Keiderling, *Biopolymers* **1991**, *31*, 1747-1761.
[205] G. J. Lee, S. I. Shin, Y. C. Kim, S. G. Oh, *Mater. Chem. Phys.* **2004**, *84*, 197-204.
[206] C. Pfumbidzai, PhD Thesis thesis, University of Basel (Basel), **2011**.
[207] K. T. Sullivan, C. W. Wu, N. W. Piekiel, K. Gaskell, M. R. Zachariah, *Combust. Flame* **2013**, *160*, 438-446.
[208] H. N. Po, N. M. Senozan, *J. Chem. Educ.* **2001**, *78*, 1499-1503.
[209] T. Pal, S. De, N. R. Jana, N. Pradhan, R. Mandal, A. Pal, A. E. Beezer, J. C. Mitchell, *Langmuir* **1998**, *14*, 4724-4730.
[210] R. A. Alvarez-Puebla, R. F. Aroca, *Anal. Chem.* **2009**, *81*, 2280-2285.
[211] K. T. Nam, Y. J. Lee, E. M. Krauland, S. T. Kottmann, A. M. Belcher, *Acs Nano* **2008**, *2*, 1480-1486.

[212] Y. Y. Cui, Y. L. Wang, R. Liu, Z. P. Sun, Y. T. Wei, Y. L. Zhao, X. Y. Gao, *Acs Nano* **2011**, *5*, 8684-8689.
[213] B. Hu, S. B. Wang, K. Wang, M. Zhang, S. H. Yu, *J Phys Chem C* **2008**, *112*, 11169-11174.
[214] Y. Cui, Wang, Y., Liu, R., Sun, Z., Wei, Y., Zhao, Y., Gao, X., *Acs Nano* **2011**, *5*, 8684 - 8689.
[215] M. Lamani, R. S. Guralamata, K. R. Prabhu, *Chem. Commun.* **2012**, *48*, 6583-6585.
[216] T. Ishikawa, *Arkivoc* **2006**, 148-168.
[217] B. Hernandez, F. Pfluger, N. Derbel, J. De Coninck, M. Ghomi, *J. Phys. Chem. B* **2010**, *114*, 1077-1088.
[218] F. Pfluger, B. Hernandez, M. Ghomi, *J. Phys. Chem. B* **2010**, *114*, 9072-9083.
[219] Y. Shao, Y. D. Jin, S. J. Dong, *Chem. Commun.* **2004**, 1104-1105.
[220] J. Y. Chen, B. Lim, E. P. Lee, Y. N. Xia, *Nano Today* **2009**, *4*, 81-95.
[221] J. A. Zhang, M. R. Langille, C. A. Mirkin, *J Am Chem Soc* **2010**, *132*, 12502-12510.
[222] R. B. Merrifield, *J Am Chem Soc* **1963**, *85*, 2149-2154.
[223] E. Kaiser, Colescot.Rl, Bossinge.Cd, P. I. Cook, *Anal Biochem* **1970**, *34*, 595-&.
[224] T. Vojkovsky, *Peptide Res* **1995**, *8*, 236-237.
[225] W. S. Hancock, J. E. Battersby, *Anal. Biochem.* **1976**, *71*, 260-264.
[226] D. E. McRee, *Practical protein crystallography*, Second ed., Academic Press, San Diego, **1999**.
[227] G. Rhodes, *Crystallography made crystal clear a guide for users of macromolecular models*, 3rd ed., Elsevier, Amsterdam, **2006**.